

INVESTIGATION OF NOVEL SOLID FORMS OF ACTIVE PHARMACEUTICAL INGREDIENTS

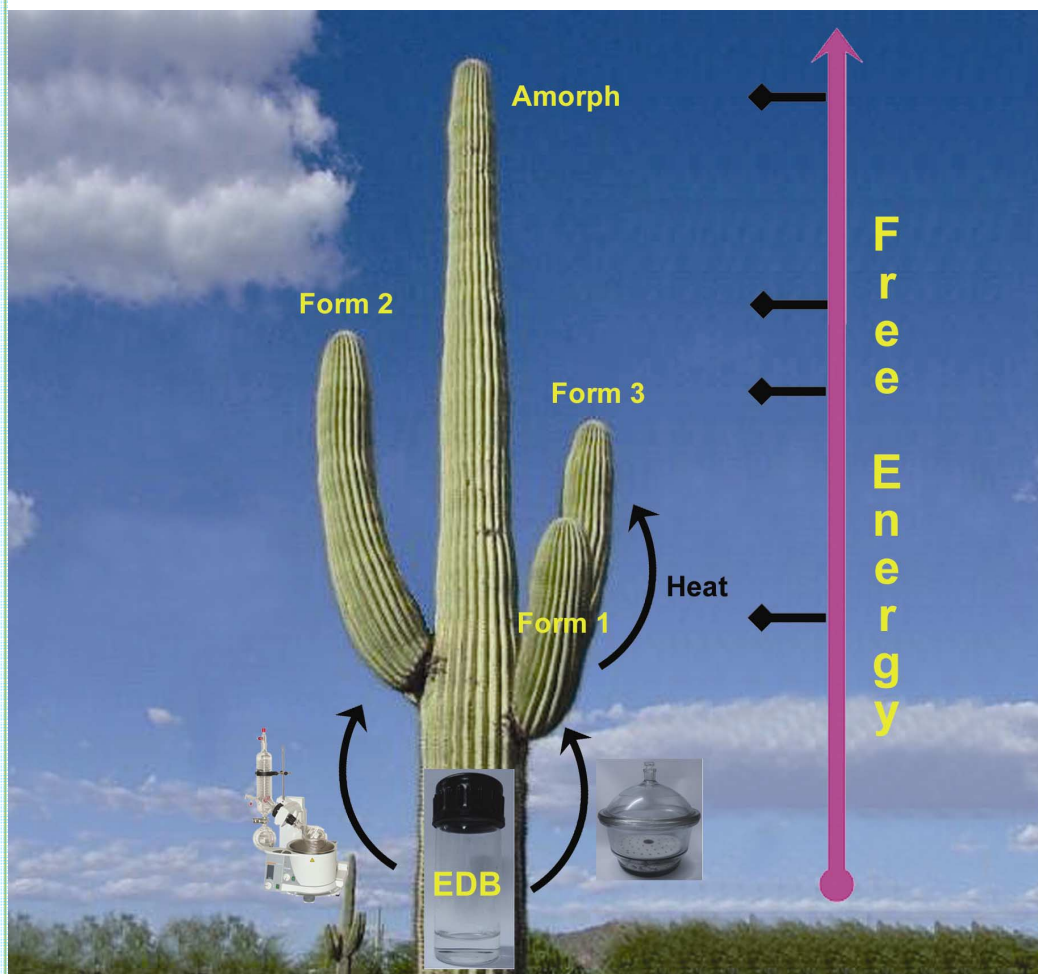
**A Thesis Submitted to the
University of Hyderabad in partial fulfillment of
the Award of PhD Degree in Chemistry**

By

Cherukuvada Suryanarayan



**School of Chemistry
University of Hyderabad
Hyderabad 500 046, Andhra Pradesh
India
September 2012**



The first example of polymorphic phase transformations in an API ionic liquid ethambutol dibenzoate (EDB) is depicted on a cactus plant. The dry conditions of crystallization are typical of the cactus habitat and its tips represent the energy levels of polymorphs.

S. Cherukuvada and A. Nangia,

CrystEngComm, 2012, DOI: 10.1039/C2CE25842K.

INVESTIGATION OF NOVEL SOLID FORMS OF ACTIVE PHARMACEUTICAL INGREDIENTS

**A Thesis Submitted to the University of Hyderabad in partial
fulfillment of the Award of PhD Degree in Chemistry**

By

Cherukuvada Suryanarayan



School of Chemistry

University of Hyderabad

Hyderabad 500046, Andhra Pradesh, India

September 2012

DEDICATION

To

Amma, Nanna & Tammu



CERTIFICATE

This is to certify that the thesis entitled **“Investigation of Novel Solid Forms of Active Pharmaceutical Ingredients”** submitted by **Cherukuvada Suryanarayan** bearing Regd. No. 07CHPH20 in partial fulfillment of the requirements for the award of Doctor of Philosophy in Chemistry is a bonafide work carried out by him under my supervision.

The thesis has not been submitted previously in part or in full to this or any other University or Institution for the award of any degree or diploma.

Prof. Ashwini Nangia
Thesis Supervisor

Dean
School of Chemistry

DECLARATION

I, **Cherukuvada Suryanarayan**, hereby declare that this thesis entitled **“Investigation of Novel Solid Forms of Active Pharmaceutical Ingredients”** submitted by me under the supervision of **Professor Ashwini Nangia** is a bonafide research work. I also declare that it has not been submitted previously in part or in full to this University or any other University or Institution for the award of any degree or diploma.

Hyderabad

Signature:

Date:

Name: **Cherukuvada Suryanarayan**

Regd. No. 07CHPH20

ACKNOWLEDGEMENTS

With a belief in the quote “*There is no such thing as a 'self-made' man...*” by George Matthews Adams, I wish to acknowledge all the people who have made a mark on my personality and career up to this stage in my life.

Firstly, I am delighted to express my gratitude and profound thanks to my PhD Supervisor **Prof. Ashwini Nangia** for his encouragement, guidance, appreciation and freedom throughout my PhD tenure. With a life sciences background, it would have been difficult for me to pursue research in chemistry without his cooperation and training. I learnt a lot from him in dealing things, directly and indirectly, and feel my association with him a rewarding experience.

I would like to thank Prof. M. V. Rajasekharan, Dean, School of Chemistry, and former Deans Prof. M. Periasamy and Prof. D. Basavaiah, and all Faculty Members of the School for their efforts in developing infrastructural facilities in the School which benefitted me in my research projects. Their approachability and cooperation on several occasions is laudable.

I take this opportunity to thank Prof. G. R. Desiraju for his inspiring lectures and motivation to excel. I am thankful to Prof. M. Durga Prasad for alerting me to improve my presentation and language skills during my SRF upgradation.

The cooperation and affection I got from the Non-Teaching Staff, especially V. M. Setty garu, Desbandhu ji, Dr. Raghaviah and Kumar, of the School is unforgettable. I would like to acknowledge several Faculty Members of other Schools and Staff of CIL, Administrative Section, Security etc. for their timely help on several occasions.

I am grateful to the Indian Council of Medical Research for providing Fellowship support and for a ‘Foreign Travel Grant’ to participate in the IUCr 2011 Conference held in Madrid, Spain, during August 22-30, 2011. I take this opportunity to thank the UGC, DST and CSIR for developing infrastructure and providing instrumentation facilities without which my research would not have taken place.

It gives me immense pleasure to thank my lab mates Dr. Saikat Roy, Mr. Sreekanth, Dr. Jagadeesh Babu, Dr. Bipul Sarma, Dr. Ranjit Thakuria, Dr. Naba Kamal Nath, Dr. Palash Sanphui, Rajesh, Kalyan, Maddileti, Sudalai, Geetha, Suresh, Swapna and Sudhir for their help and cooperation and making a cheerful atmosphere in the lab. My association with them is unforgettable and cherishable. I also like to thank Sreenu, Uday, Sumanth garu, Swarupa garu, Raghav, Srikanth and Chaitanya of TBI lab. Dr. Soumendra Rana and Mr. Satish deserve special thanks for their help in carrying out HPLC experiments and project students Venkat rao and Kanishka for their help in the research projects. Mr. Badrinath is thanked for his help in dissolution studies.

I wish to record my thanks to Dr. Pedireddi, Dr. Ram Jetti, Dr. Sreenivasulu, Dr. Bala krishna reddy, Dr. Yasser Azim, Dr. Prashant and Dr. Tejender for their help on various occasions. My stay on the campus has been pleasant with the association of many friends from different labs and to name a few, Gupta, Hari, Dinesh, Santosh, Seshadri, Venu, Madhu, Chary, Babu, Swamy, Dr. Srinivas, G. D. Prasad, Kishore, Bharat, Sridevi, Sanjeev, Tridib, Vikrant, Guru brahmam, Ganesh, Srinivas, Vanaja, Dr. Vijayender, Venkaih, Praveen, Kishore, Anand, Prabhu, Ramesh, Dr. Chaitanya, Dr. D. K. Srinivas, Satish, Viji, Chandrasekhar, Aanjaneyulu, Ramesh, and Satpal.

I take this opportunity to express my gratitude to my School Teachers Ramesh sir and Jagadeesh sir, B. Sc. Lecturers Ram mohan rao sir and Ramalingeswara rao sir, M. Sc. Lecturer Prof. Sreenivasulu sir and B. Ed. Principal Vincent Stephens sir for their inspiration and guidance.

I wish to acknowledge my School Friends Mallesh, Sai baba, Srivalli (5th Std.), Rajesh, Kishore, Madhuri, Venkatesh, Rama krishna, Balasubramanyam, Sarath Jain, Jyothi, Deepa, Rupa, Naga mahesh (6 to 9th Std.), M. S. V. Kumar, Sriram, Rajiv, Archana, Mythili, Kiran, Suresh (10th Std.), College Friends Satyanarayana (Inter), Satyanarayana, Deedi, Jyothi, Vijaya lakshmi, Anil, Mouli, Pradeep, Krishnamurthy, Kesav, Rama rao, Bobby (B. Sc.), Gopi (late), Dr. Nageswar rao, Habeeba, Dr. Ruxana, Satish, Srilatha, Suma, Surendra, Venkateswarlu, Kiran, Rambhupal and Vamsi (M. Sc.) for their affection and competitive spirit. I cherish my associations with several Friends like Mohan brothers (Hyderabad), Suri babu & Jami, Siva brothers, Kamesh & Co., Chary & Rajesh at PST International (Kakinada), Srinivas garu & Rama Rao (B. Ed.).

The help and affection of my brother's friends Siva, Kishore, Upendhar, G. Kishore, Satish, Anil, Srinivas and N. Kishore I got during my PhD tenure is worth special mention. Also the help and care from my relatives at different times deserves due acknowledgement.

A lot more people need to be thanked, but due to space constraints it is impossible to express my gratitude. I deeply regret if I overlook, miss or forget anyone and do not mean to undermine their contributions.

Last, but not the least, I feel immensely proud and fortunate to be born to **my parents Mrs. Ramalakshmi and Mr. Mahajan** (late), who taught me morals and values in life and made me what I am today, and as an elder brother to **my one and only brother Dr. Bhaskar**. My Mother is always consolatory to my failures, and my Father, who always wanted his both sons to become medical doctors, is behind my success. Without my brother, who is moral support and has taken care of all household things during the last five years, my research would not have taken a proper shape. They coped with all my frustrations and emotions. I owe everything to them. Dedicating this thesis to them is a minor recognition to their unconditional love and care.

... *Surya*

SYNOPSIS

The thesis entitled “**Investigation of Novel Solid Forms of Active Pharmaceutical Ingredients**” consists of eight chapters.

CHAPTER ONE

Introduction to Pharmaceutical Solids

Majority of the drugs are marketed as solid formulations (tablets, capsules and powders) because of several reasons such as ease of manufacture, administration, convenience to patients, storage etc. Solid state chemistry of drugs is thus of fundamental importance in pharmaceutical industry and also as the physical property management of pharmaceutical solids is a current challenge for their commercial utility. A pharmaceutical solid formulation contains the ‘Active Pharmaceutical Ingredient’ (API) as a polymorphic form/mixture, salt, hydrate/solvate, complex or an amorphous solid blended with excipients. Each of these solid forms exhibit different physico-chemical behavior/properties such as solubility, dissolution rate, stability and bioavailability which finally govern the therapeutic efficacy of the drug. Thus, optimization of a solid drug form is crucial not only in drug research and development but also for oral administration and usage.

Solids are broadly classified as ‘crystalline’ and ‘amorphous’ states based on the internal structure, order and degree of periodicity. Crystalline solids have long-range order but it is short-range in amorphous solids. Amorphous forms, though they impart solubility enhancement in a drug formulation for a poorly soluble API, tend to be unstable and hence not preferred in drug development unless there are clear-cut advantages over the crystalline forms. A pharmaceutical solid can be made up of a single component or two or more components. A multi-component solid made up of ions is called a ‘salt’ (wherein the components are held together by ionic interactions), a ‘hydrate/solvate’ when one of the components is water or a solvent and a ‘complex’ when it contains a metal. The family of multi-component solids also includes ‘cocrystals’, ‘solid solutions’ and ‘eutectics’ which are relatively less explored. A cocrystal is a stoichiometric multi-component crystalline solid wherein the components are held together by intermolecular interactions, particularly hydrogen bonds. A solid solution is a variable stoichiometry multi-component crystalline solid and a eutectic is a conglomerate of solid solutions. Cocrystals and eutectics have a fixed stoichiometry of components but the composition is variable for solid solutions. Polymorphism, a

phenomenon in which the same substance can exist in more than one crystalline state, is possible both in single and multi-component solids. Therefore, a single (API) solid material can give rise to a multitude of crystal forms upon solid form screening viz. polymorphs of the API itself; salts, hydrates/solvates, cocrystals, complexes – each of which can be polymorphic; solid solutions and eutectics. The inherent differences among these crystalline forms, by virtue of their uniqueness, result in their varied physico-chemical properties which in essence is important for optimal solid form selection and development for an API. Since there is no one-size-fits-all solution to the problems arising from the physico-chemical behavior (e.g. solubility and stability) of different solid forms of drugs (whether polymorphs, amorphs, salts, solvates, cocrystals, eutectics or any complexes) and the properties can vary case-to-case, each of these solid forms can be advantageous for specific applications in different systems. Hence, it is important to understand the nature and properties of various pharmaceutical solids both from fundamental and application points of view. This thesis deals with the discovery of different solid forms of drugs and their physical form behavior and properties.

CHAPTER TWO

Pyrazinamide Polymorphs

Pyrazinamide (abbreviated as PZA) is a frontline anti-tuberculosis drug administered with Rifampicin, Isoniazid and Ethambutol dihydrochloride in Fixed Dose Combination (FDC). It is a rare example of a conformationally rigid molecule with four polymorphs (namely, α , β , γ and δ forms) reported in the literature. Polymorph, according to McCrone, is “*a solid crystalline phase of a given compound resulting from the possibility of at least two different arrangements of the molecules of that compound in the solid state*”. Since the polymorphs are unique entities and exhibit different physico-chemical properties (e.g. melting point, solubility, stability, bioavailability etc.), a study of all polymorphs of a drug and establishing their stability relationships is considered as an obligatory step in solid form development. Since the polymorphs are at different levels on the ‘free energy’ scale, inter-conversions are quite possible which lead to changes in the properties of bulk drug material finally affecting its efficacy. Therefore, it is essential to gain adequate understanding of their properties so as to optimize the conditions to develop a desired polymorph for formulation and avoid potential transformations (polymorphic transformations, hydration etc.). Pyrazinamide is a highly soluble and stable drug, and as such there is little scope for improvement in its formulation from solubility/stability points of view. Yet, it is a model pharmaceutical system to study phase relationships among the four polymorphs.

All PZA polymorphs were obtained concomitantly by recrystallization from several solvents with α form as the major polymorph. α , β , and δ forms convert to γ form at high temperature which then melts around 190 °C. Thus, the three polymorphs are enantiotropically related to γ form with $\delta \rightarrow \gamma$ transition having highest heat of transition followed by $\alpha \rightarrow \gamma$ and then by $\beta \rightarrow \gamma$ transitions. The stability order of PZA polymorphs proposed by Castro et al. as $\delta < \alpha < \beta < \gamma$ (i.e. δ form has the lowest Gibbs free energy and hence the stable polymorph) was revised at ambient temperature in this work. Since the polymorphs are obtained as concomitant mixtures, they are isoenergetic and thus inter-conversions are possible among them. Polymorphic transformation experiments through grinding, seeding, and solvent-mediated crystallization resulted in the conversion of all polymorphs to α form (Figure 2.1a). These results, though in contrast to the stability order proposed by Castro et al., are rationalized by the relative stability of the polymorphs through a semi-quantitative free energy vs. temperature (E–T) diagram (Figure 2.1b). According to the E–T diagram, the stability order at absolute zero (–273 °C) is $\delta < \alpha < \beta < \gamma$, between 25–155 °C is $\alpha < \delta < \gamma < \beta$, whereas after 155 °C it is $\gamma < \alpha < \delta < \beta$, i.e. α form is the thermodynamic form at ambient temperature. Though δ form has low free energy in sub-zero temperatures, it becomes metastable at room temperature (i.e. attains high free energy through entropy component with increase in temperature) and therefore converts to α form since the latter has the lower free energy at ambient temperature. In all, this study highlights the importance of establishing the relative stability of drug polymorphs in the real world conditions typical of pharmaceutical processing (crystallization, milling etc.) and storage conditions (temperature and relative humidity around 25 °C and 50% respectively).

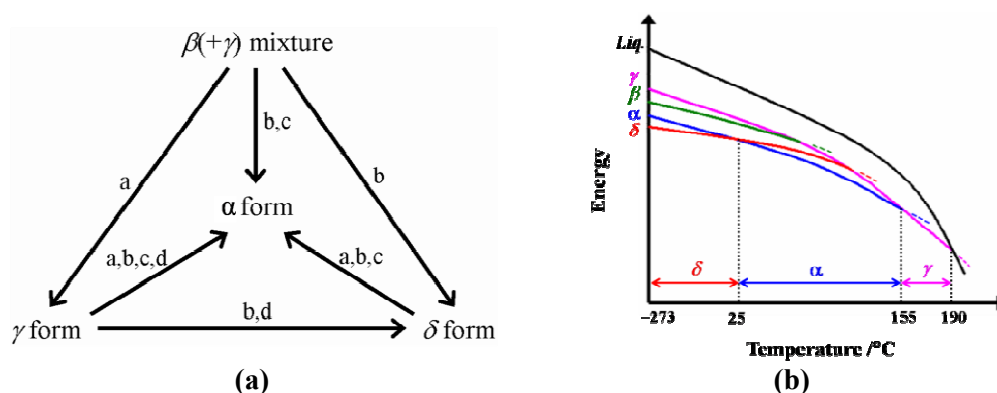


Figure 2.1 (a) Phase transformation experiments of PZA polymorphs: a - grinding of pure form; b - grinding together with the seeds of the final form; c - water assisted grinding of pure form; d - storage for 6 months. (b) Semi-quantitative E–T diagram to show the relative stability and polymorphic transformations of PZA polymorphs. At –273 °C δ is the stable form. Between 25–155 °C, α form has the lowest free energy; γ form is stable after 155 °C until it melts at 190 °C.

CHAPTER THREE

Salts and Ionic Liquids of Ethambutol

Ethambutol (abbreviated as EMB) is a frontline anti-tuberculosis drug administered with Rifampicin, Isoniazid and Pyrazinamide in Fixed Dose Combination (FDC). It is chiral basic drug with the S,S-enantiomer being therapeutically active whereas the R,R-form is inactive. It is administered as dihydrochloride salt (S,S-EDH) whose hygroscopicity is reported to result in instability and loss of potency of the FDC products upon storage. As a consequence, individual drugs of the FDC formulation are separately coated with polymers to avoid mutual interaction and water uptake and then blended to make up the final product formulation. S,S-EDH is tetramorphic but neither the X-ray crystal structure nor any polymorphs of the S,S-form of ethambutol base are reported so far. The reported crystal structures of EMB and its salts (dihydrochloride, dinitrate, dibromide, oxalate pentahydrate) in the Cambridge Structural Database (CSD) do not contain the Flack parameter and hence their absolute configuration is ambiguous. In this work, crystal structures of ethambutol and ethambutol dihydrochloride were redetermined and their absolute configuration is deduced as S,S-chirality.

Salt screen of EMB with the intent of obtaining salts with less hygroscopicity resulted in the formation of hygroscopic salts/ionic liquids. Ionic liquids (ILs) are salts with melting point below 100 °C and if they are liquids at room temperature (25 °C) then they are termed as ‘room temperature ionic liquids’ (RTILs). A total of twelve salts (including seven ionic liquids) were synthesized and all of them were found to be hygroscopic. Out of the five salts (sulfate, dimesylate, ditosylate, dibesylate and fumarate), only two gave diffraction quality single crystals and their X-ray structures were solved (dimesylate and fumarate hydrate). Among the seven ionic liquids, only two crystallized (dibenzoate and adipate) and the remaining five (dinicotinate, disalicylate, di-4-aminosalicylate, disaccharinate and succinate salts) never crystallized in the experimental conditions attempted. Ethambutol dibenzoate (abbreviated as EDB) crystallized as a trimorph and thus becomes the first example of an API ionic liquid exhibiting polymorphism.

Solution crystallization of ethambutol and benzoic acid in 1:2 stoichiometry in methanol or ethanol yielded a liquid product (Figure 3.1) whose water content was found to be 10.1% by Karl-Fischer titration. The difficult issue of classifying EDB as a hygroscopic salt or an ionic liquid was resolved by DSC. A heat-cool-reheat DSC run will evolve any water and give T_g (glass transition temperature) or T_m (melting temperature), thereby eliminating interferences from water evolution with thermal

transitions in DSC. Solid salts were obtained upon crystallizing alcoholic solution of EMB and benzoic acid (in 1:2 ratio) in a desiccator and rotavap separately. The DSCs of both these solid salts (chemical composition was confirmed by NMR) indicated that they are ionic liquids ($T_m = \text{ca. } 90\text{ }^\circ\text{C}$) and also polymorphs. The crystalline solid obtained in the desiccator is designated Form 1 and that from the rotavap as Form 2 (Figure 3.1). A high temperature polymorph (designated as Form 3) was obtained upon heating form 1 prior to melting temperature. Though diffraction quality single crystals could not be obtained to determine the X-ray crystal structures of the three polymorphs, their distinctive PXRD patterns, IR and Raman spectra, and DSC thermal behavior differences mean that they are polymorphs. The thermodynamic stability order of the three polymorphs was deduced from heat of fusion rule and phase transformation experiments: at room temperature form 1 (most stable) < form 3 < form 2 and at high temperature form 3 < form 1 < form 2 (least stable). Ionic liquids have been proposed as alternatives to solid forms of drugs for obviating contentious issues of intellectual property, polymorphism, and polymorphic transformations in APIs. This study shows that unless the ionic liquid is an RTIL, it may not be a substitute for solid forms free of polymorphism issues, since ILs in the temperature range 50-100 $^\circ\text{C}$ can exhibit polymorphism like API salts.

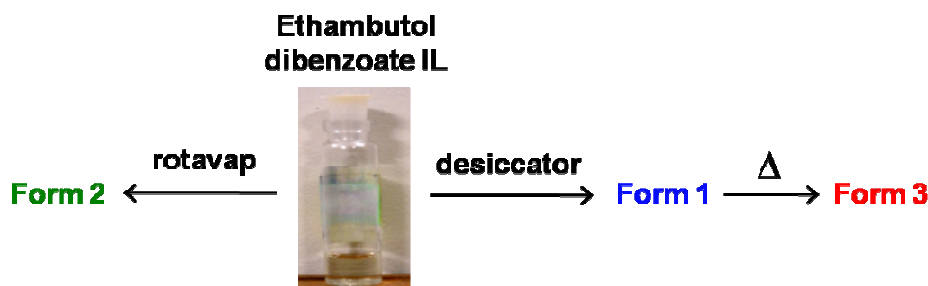


Figure 3.1 Ethambutol dibenzoate ionic liquid crystallized as trimorphs in different conditions. Form 2 and 3 converted to form 1 upon mechano-chemical grinding. The thermodynamic polymorph at room temperature is form 1 and at high temperature is form 3.

CHAPTER FOUR

Nitrofurantoin-*p*-Aminobenzoic Acid Cocrystal

Nitrofurantoin (abbreviated as NF) is an anti-bacterial drug used in the treatment of urinary tract infections. Polymorphism and pseudopolymorphism of NF are reported in the literature with two polymorphs of anhydrous Nitrofurantoin (α and β) and two polymorphs of Nitrofurantoin monohydrate (Form I and Form II). A side effect of NF is nausea and emesis upon oral administration and is due to its high absorption rate. It is

reported that larger crystals (150 μm mesh size) of lower surface area and slower absorption reduce emesis and still confer optimal therapeutic effect. The dissolution profile of the drug (marketed as stable β polymorph) is variable: after a high initial dissolution the drug is released slowly because it converts to the more stable monohydrate II in aqueous medium, and it is the latter form that has lower dissolution rate. A control over the dissolution rate can influence the absorption rate which in turn may regulate the side effects of the drug. With the intent of controlling the hydration and dissolution behavior of Nitrofurantoin, the cocrystallization approach was examined.

Two cocrystals NF-*p*-aminobenzoic acid and NF-urea, a salt NF-Arginine- H_2O and a solvate NF-MeOH were obtained in solid form screening experiments. Solubility and dissolution measurements on the compounds showed that the two cocrystals have comparative dissolution rate to the reference drug and the salt has higher dissolution rate. NF-PABA cocrystal was found to be stable to hydration in water and showed minimal transformation to NF monohydrate II in other media (0.1 N HCl and pH 6.8 buffer). Since the NF-PABA cocrystal was resistant to hydration, the effect of PABA as an additive in reducing the hydration of the drug in water was studied (Figure 4.1). With increase in the % of PABA to NF (from 5% to 60% by weight) in water slurry, a steady increase in the concentration of NF-PABA cocrystal and decrease in NF monohydrate II content in the residue was observed as analyzed by PXRD. At 57.6% of PABA-to-NF (molar proportion of components in the 1:1 cocrystal), there was no trace of NF monohydrate II in the residue and the material was entirely NF-PABA cocrystal (Figure 4.1). This shows that PABA was effective as a coformer in the 1:1 cocrystal composition to make NF stable to hydration and also as an additive in controlling its hydration. Thus, NF-PABA combination can be useful as a novel formulation that can control dissolution and hydration and consequently the absorption rate of the drug.

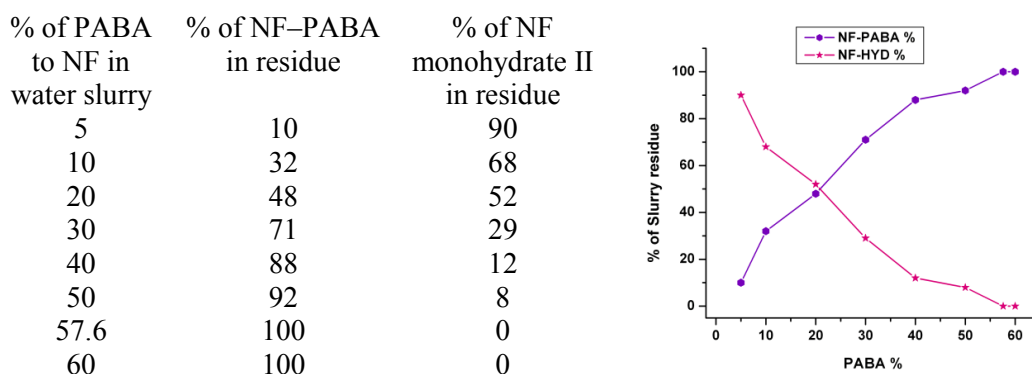


Figure 4.1 Variation in the composition of NF-PABA cocrystal and NF monohydrate II in the water slurry residue with increase of PABA concentration.

CHAPTER FIVE

Pyrazinamide and Isoniazid Cocrystals and Eutectics

Pyrazinamide (PZA) and Isoniazid (INH) are the first-line anti-tubercular drugs administered with Rifampicin and Ethambutol dihydrochloride in fixed dose combination (FDC). Multi-drug therapy is important to treat resistant strains of tuberculosis (TB), HIV and malaria. The classical approach of making combination drugs is to physically blend the drugs as a solid mixture. Covalent joining of the drugs through a labile linker is a synthetic modification in drug combinations. The non-covalent approach of combining the drugs PZA and INH was pursued to study the potential of cocrystallization in physical property enhancement for combination drugs. Attempts to make a binary cocrystal of PZA and INH by solution crystallization and grinding experiments were unsuccessful but led to a 1:1 binary eutectic, PZA–INH. Cocrystals of PZA and INH with GRAS (Generally Recognized As Safe) dicarboxylic acid cofomers, succinic acid (SA) and fumaric acid (FA) in 1:0.5 ratio respectively were obtained by mechano-chemical grinding. All four crystal structures of the composition PZA–(diacid)_{0.5} and INH–(diacid)_{0.5} are sustained by the strong carboxylic acid⋯pyridine heterosynthon (Figure 5.1a). Basing on these cocrystal structures, the possible role of dicarboxylic acids (SA and FA) as non-covalent linkers for PZA and INH to form ternary complexes via the acid–pyridine synthon was explored (Figure 5.1b).

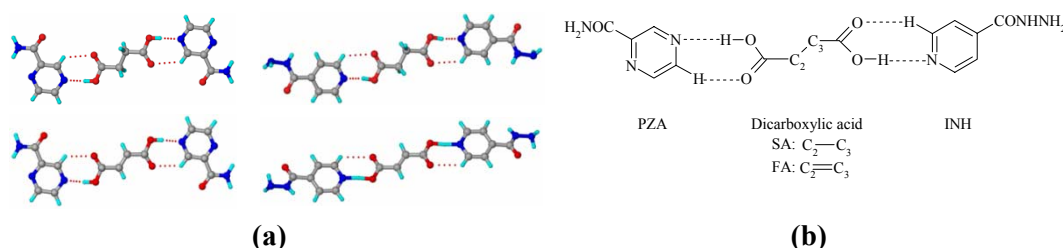


Figure 5.1 (a) Acid–pyridine synthon in PZA–(diacid)_{0.5} (left column) and INH–(diacid)_{0.5} (right column) cocrystal structures. (b) Proposed assembly of a ternary drug–drug complex through a non-covalent linker via the acid–pyridine synthon.

Solid-state grinding of PZA and INH with the diacid (SA or FA) in 1:1:1 molar stoichiometry did not result in a new cocrystal phase. Instead 1:1:1 ternary eutectics of PZA and INH with SA (PZA–SA–INH) and FA (PZA–FA–INH) were obtained and each phase was characterized by DSC, PXRD, ss-NMR and FT–IR. These three component solid phases of fixed stoichiometry were found to be eutectic composition of their respective binary cocrystals (i.e. PZA–SA–INH is composed of PZA–(SA)_{0.5} and INH–(SA)_{0.5} and PZA–FA–INH is composed of PZA–(FA)_{0.5} and INH–(FA)_{0.5}). These ternary eutectics are the first examples of cocrystals making novel eutectic phases.

Eutectics have excess thermodynamic functions (free energy, enthalpy and entropy) due to weak intermolecular interactions and thus can confer higher solubility and faster dissolution to a drug compared to other crystalline modifications. Equilibrium solubility measurements on the cocrystals and eutectics in water gave mixed results. The binary cocrystal PZA–SA and eutectics PZA–INH, PZA–SA–INH and PZA–FA–INH are incongruently dissolving systems (i.e. the solubility of one component is much higher than the other; PZA 22 mg/mL, SA 83 mg/mL, INH 125 mg/mL, FA 6 mg/mL) and thus dissociated in the aqueous slurry medium resulting in precipitation of the less soluble species. Though a solid drug form is unstable in the equilibrium solubility conditions (typically 24 h), nevertheless, the formulation is advantageous if it facilitates drug release within a desirable time-frame before it is destabilized. This evaluation whether the drug is sustained in the medium for the therapeutic retention time (usually 0.5–2–4–8 h) is achieved through a dissolution study. According to the WHO biowaiver dissolution criterion, an immediate release (IR) solid oral dosage form should exhibit ‘very rapid’ (no less than 85% of the drug must be dissolved in 15 minutes) or ‘rapid’ (no less than 85% of the drug must be dissolved in 30 minutes) *in vitro* dissolution kinetics. Dissolution testing of the compounds was carried out by the rotating disk intrinsic dissolution rate (DIDR) method in pH 1.2 aq. HCl medium at 37 °C using USP Apparatus II. The extent of solid form dissolved in 30 min was: INH–SA 94%, PZA–SA–INH 92%, INH 73%, PZA–INH 64%, INH–FA 62%, PZA–FA–INH 50%, PZA–SA 36%, PZA 25%, and PZA–FA 15% (Figure 5.2). INH–SA cocrystal and PZA–SA–INH eutectic qualify the criterion of ‘rapid’ dissolution, but the pure drug forms did not clear the bar in the tested conditions. The inclusion of high soluble succinic acid increased the dissolution rate for PZA and INH (in binary cocrystal) and PZA–INH (in ternary eutectic) and the less soluble fumaric acid gave the opposite effect of decreasing dissolution rates. Thus, a control over the solubility/dissolution of the drugs is achieved through cocrystals and eutectics in this study.

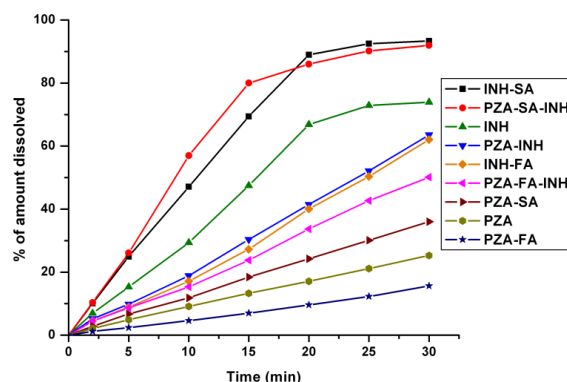


Figure 5.2 Dissolution curves of the compounds in pH 1.2 aq. HCl solution.

CHAPTER SIX

Ethambutol Dihydrochloride Eutectics

Ethambutol (EMB) is a frontline anti-tuberculosis drug administered as its dihydrochloride salt (EDH) in a Fixed Dose Combination (FDC) with Rifampicin, Isoniazid and Pyrazinamide. The hygroscopicity of EDH salt is reported to result in instability and loss of potency of the FDC products upon storage. To address the hygroscopicity problem of EDH, solid form screening to obtain cocrystals and eutectics was performed as they showed promising results in pharmaceutical property management for several drugs. The properties of partner molecules of cocrystals and eutectics play a vital role in affecting their properties e.g. high soluble coformer generally confers solubility/dissolution improvement to its cocrystal/eutectic. GRAS dicarboxylic acid coformers fumaric acid (FA), succinic acid (SA) and L-tartaric acid (TA) were selected based on the non-hygroscopic nature of FA and SA and hygroscopic stability improvement of Piracetam, a nootropic drug, by L-tartaric acid in a cocrystal. Mechano-chemical grinding method resulted in eutectics of EDH with all the three coformers (EDH-FA; EDH-SA; EDH-TA). The melting points of the EDH eutectics (Table 6.1) are proportional to coformer melting points (FA 287 °C, SA 188 °C, TA 169 °C) with fumaric acid eutectic having the highest melting point.

Hygroscopic stability testing of the EDH eutectics was conducted in accelerated stability testing conditions of 40 °C and 75% RH for two months and compared with EDH. Samples were analyzed for water uptake periodically at 15, 30 and 60 days through TGA and KF titration (Table 6.1). EDH salt became semisolid with 20% water uptake after 30 days and completely turned liquid after 60 days (Table 6.1 & Figure 6.1). EDH-TA eutectic was found to liquefy within 15 days (by visual inspection) and showed highest water uptake of 54% at the end of 60 days. EDH-SA eutectic turned semisolid with 14% water uptake by 60 days. EDH-FA eutectic did not show any significant water uptake in 60 days (Table 6.1 & Figure 6.1). In all, EDH-FA and EDH-SA eutectics showed hygroscopic stability compared to the reference drug and thus can become potential candidates for future anti-TB FDC formulations containing Ethambutol.

Table 6.1 Melting point and water uptake of the compounds in the hygroscopicity study.

Compound	Melting point (°C)	% water uptake							
		0 day		At 15 days		At 30 days		At 60 days	
		TGA	KF	TGA	KF	TGA	KF	TGA	KF
EDH	200	0.2	0.3	5.2	5.4	20.2	19.3	45.6	45.8
EDH-FA	174	0.2	0.2	0.2	0.2	0.5	0.4	2.9	3.0
EDH-SA	141	0.2	0.2	1.3	0.9	5.9	5.8	13.7	13.8
EDH-TA	109	0.2	0.2	19.5	19.3	38.5	38.6	54.5	54.6

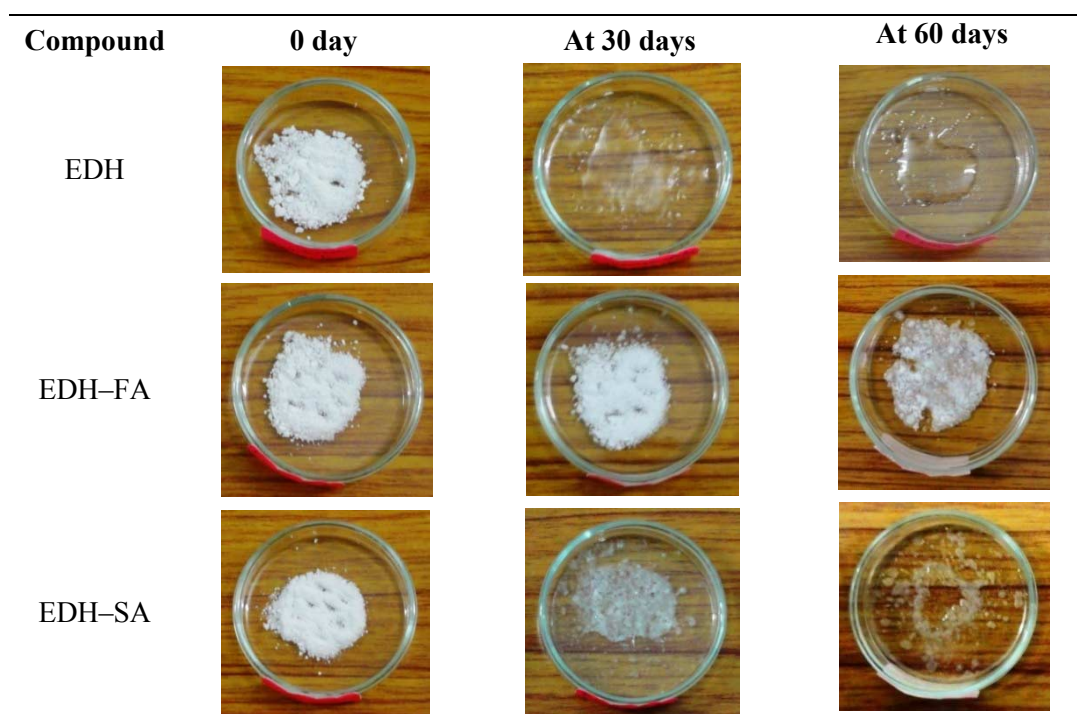


Figure 6.1 Snapshots to show relative hygroscopicity with EDH-FA eutectic showing higher stability towards the accelerated stability testing conditions of 40 °C and 75% RH for two months.

CHAPTER SEVEN

4-Aminosalicylic Acid Adducts

4-aminosalicylic acid, commonly known as *p*-aminosalicylic acid (PAS), is a second-line drug used in the treatment of multi-drug-resistant tuberculosis (MDR-TB). It is an amphoteric compound and exists in a unionized form ($4\text{-NH}_2\text{C}_6\text{H}_3(\text{OH})\text{COOH}$) in the solid state. It is found to exist as different ionic species in buffer solutions viz. (a) as a diprotic acid ($\text{NH}_3^+\text{C}_6\text{H}_3(\text{OH})\text{COOH}$) below its pK_{a1} ($=1.79$), (b) as a zwitterion ($\text{NH}_3^+\text{C}_6\text{H}_3(\text{OH})\text{COO}^-$) around its isoelectric point ($\text{pI} = 2.71$) and (c) as a diprotic base ($\text{NH}_2\text{C}_6\text{H}_3(\text{OH})\text{COO}^-$) above its pK_{a2} ($=3.63$). PAS is found to decarboxylate to 3-aminophenol through the zwitterionic state. About 13-25% of PAS is found to decompose in the pH range 1.3-4.2 in 24 h with the highest percentage of decomposition at its isoelectric point. No polymorphs of PAS have been reported so far but several salts (sodium, hydrochloride, sulfate, mesylate, ammonium etc.) and drug-drug cocrystals (with PZA, INH and Sulfadimidine) are reported by different groups. PAS of its rich functionalities (carboxylic acid, amine and phenol) can form a multitude of adducts (salts and cocrystals) with various coformers depending on the pK_{a} differences and thus becomes a model compound of study. The same solid form screening experiments may

result in the crystallization of its zwitterionic form which can be important as a novel form. A salt and a salt cocrystal with cytosine, a nicotinamide cocrystal, and anhydrate and hydrate sodium salts were obtained in this work. Attempts to crystallize the zwitterionic form of PAS were unsuccessful.

Solution crystallization of PAS and cytosine in 1:1 ratio in methanol resulted in two different stoichiometry adducts viz. a 1:1 salt and a 1:1:1:1 salt cocrystal hydrate from different batches. In the crystal structure of the salt ($\text{Cyto}^+-\text{PAS}^-$), PAS was found to donate its proton to the pyrimidine N that flanks the amino group of cytosine (Figure 7.1a). Thus, the PAS anions and cytosinium cations form heterodimers of carboxylate–aminopyrimidinium synthon. Crystal structure of the salt cocrystal ($\text{Cyto}^+-\text{PAS}^--\text{Cyto}-\text{H}_2\text{O}$) shows a PAS anion, a cytosinium cation and cytosine and water molecules in the asymmetric unit. Contrast to the salt structure, PAS anion makes a carboxylate–pyrimidinium synthon (Figure 7.1b). Generally, grinding technique (neat and/or liquid assisted) is employed to prepare macroscopic amounts of an adduct. The salt was reproduced upon grinding and but the salt cocrystal was not obtained. It is plausible that the crystallization of this salt cocrystal is a kinetic effect. The $\text{p}K_a$ difference between cytosine and PAS is less ($\Delta\text{p}K_a = 4.4$ (conjugate acid of pyrimidine base of cytosine) – 3.25 (PAS carboxylic acid) = 1.15) and hence both ionized and unionized species can exist in solution to finally result in the crystallization of two different adducts (a salt and a salt cocrystal). Similar to the cytosine case, the $\text{p}K_a$ difference between nicotinamide and PAS is less ($\Delta\text{p}K_a = 4.2$ (conjugate acid of pyridine base of nicotinamide) – 3.25 (PAS carboxylic acid) = 0.95) and hence formation of salt/cocrystal cannot be predicted. A 1:1:1 cocrystal hydrate of PAS and nicotinamide was obtained upon crystallization of a methanol solution. Thus, an ambiguity in the prediction of salt/cocrystal for the range $0 < \Delta\text{p}K_a < 3$ is observed in the cases of cytosine and nicotinamide adducts. Examples of this kind play a crucial role in the ongoing exercise on the classification of cocrystals recently sparked by the US-FDA draft guidance on pharmaceutical cocrystals and can result in an unambiguous classification of multi-component crystalline solids.

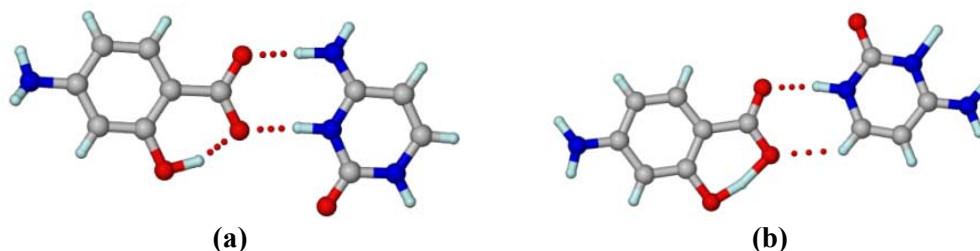


Figure 7.1 (a) Carboxylate–aminopyrimidinium synthon between PAS anion and cytosinium cation in the salt. (b) Carboxylate–pyrimidinium synthon between PAS anion and cytosine in the salt cocrystal.

CHAPTER EIGHT

Conclusions and Future Prospects

The study of the nature and properties of various pharmaceutical solids is central in pharmaceutical chemistry. The understanding of the phenomena that govern the physico-chemical behavior of pharmaceutical solids will avoid pit-falls in drug research and development and comprehend the quest for better medicines for affordable human health. Extensive studies on various solid forms such as polymorphs, salts, ionic liquids, cocrystals and eutectics of several APIs were carried out with the intent of understanding and addressing the problems associated with those APIs. In chapter 2, the importance of establishing the relative stability of drug polymorphs in the real world conditions is discussed through an anti-TB drug Pyrazinamide. The first case of polymorphism in an API ionic liquid (Ethambutol dibenzoate) is studied in chapter 3. A study on polymorphism in both single and multi-component APIs is covered in chapters 2 and 3. Additive/coformer effect of *p*-aminobenzoic acid in controlling the hydration tendency of an anti-bacterial drug Nitrofurantoin through their cocrystal formation is studied in chapter 4. The first examples of drug cocrystals forming eutectics and the importance of cocrystals and eutectics in modulating the solubility/dissolution of two anti-TB drugs Pyrazinamide and Isoniazid are discussed in chapter 5. The pharmaceutical formulation scope of the anti-TB drugs Pyrazinamide, Isoniazid and Ethambutol is broadened to cocrystals, eutectics and ionic liquids. A preliminary study on eutectics in controlling the hygroscopic nature of anti-TB drug Ethambutol dihydrochloride is discussed in chapter 6. Study on the effect of these eutectics in stabilizing the anti-TB FDC formulation of Rifampicin, Isoniazid and Pyrazinamide in accelerated stability testing conditions is ongoing. An understanding of the composition, structure and properties of a eutectic is attempted and its utility as a novel pharmaceutical solid is studied in Chapters 1, 5 and 6. In chapter 7, crystal structures of few adducts of the anti-TB drug 4-aminosalicylic acid are discussed. Since 4-aminosalicylic acid is found to partially decompose (to 3-aminophenol) in the pH range 1.3-4.2, a study on the effect of these adducts in controlling its decomposition can lead to a better formulation of the drug.

CONTENTS

Certificate	v
Declaration	vii
Acknowledgements	ix-x
Synopsis	xi - xxii

Chapter One

Introduction to Pharmaceutical Solids	1-37
1.1 Introduction.....	2
1.2 Solid State Chemistry.....	2
1.2.1 Eutectic microstructure.....	6
1.3 Solid State Chemistry of Drugs.....	10
1.3.1 Amorphous Forms.....	11
1.3.2 Polymorphism.....	12
1.3.2.1 Classification of Polymorphs.....	12
1.3.2.2 Polymorph Generation and Transformation.....	15
1.3.3 Pseudopolymorphism.....	18
1.3.4 Pharmaceutical Salts.....	20
1.3.5 Pharmaceutical Cocrystals.....	21
1.3.6 Relevance of Eutectic microstructure to Pharmaceutical Solid Design.....	25
1.4 Conclusions.....	29
1.5 References.....	30

Chapter Two

Pyrazinamide Polymorphs	39-64
2.1 Introduction	40
2.2 Crystallization of PZA Polymorphs.....	41
2.3 Crystal structure analysis of PZA Polymorphs.....	44
2.4 Spectroscopic analysis of PZA Polymorphs.....	47
2.5 Relative stability of PZA Polymorphs.....	49
2.6 Phase transformation experiments on PZA Polymorphs.....	52
2.6.1 Seeding and Grinding.....	52
2.6.2 Solvent-mediated phase transformation.....	52
2.6.3 Storage.....	54

2.7	Solubility and Dissolution study of PZA Polymorphs.....	54
2.8	Discussion.....	56
2.9	Conclusions.....	58
2.10	Experimental Section.....	58
2.11	References.....	61

Chapter Three

Salts and Ionic Liquids of Ethambutol 65-94

3.1	Introduction.....	66
3.2	Synthesis and Characterization of Salts and Ionic Liquids.....	67
3.2.1	X-ray Crystal structures.....	69
3.2.2	Spectroscopic and Thermal analysis.....	73
3.3	API Ionic Liquid Polymorphism.....	79
3.4	Conclusions.....	85
3.5	Experimental Section.....	86
3.6	References.....	91

Chapter Four

Nitrofurantoin-*p*-Aminobenzoic Acid Cocrystal 95-118

4.1	Introduction.....	96
4.2	Crystallization of the Adducts.....	97
4.2.1	Cocrystal of NF and PABA.....	100
4.2.2	Cocrystal of NF and Urea.....	101
4.2.3	Hydrate of NF and L-Arginine Salt.....	102
4.2.4	NF methanolate.....	104
4.3	Solubility and Dissolution study of the Adducts.....	106
4.4	Conclusions.....	113
4.5	Experimental Section.....	113
4.6	References.....	116

Chapter Five

Pyrazinamide and Isoniazid Cocrystals and Eutectics 119-153

5.1	Introduction.....	120
5.2	Crystal Structures of Binary Cocrystals.....	122
5.3	Characterization of Eutectics of PZA-INH combination.....	127
5.3.1	X-ray diffraction analysis.....	127

5.3.2	Thermal analysis.....	130
5.3.3	Spectroscopic analysis.....	133
5.4	Solubility and Dissolution study.....	141
5.5	Conclusions.....	143
5.6	Experimental Section.....	145
5.7	References.....	148

Chapter Six

Ethambutol Dihydrochloride Eutectics 155-172

6.1	Introduction.....	156
6.2	Solid form screening.....	157
6.3	Characterization of the EDH eutectics.....	158
6.4	Hygroscopicity study.....	162
6.5	Conclusions.....	166
6.6	Experimental Section.....	167
6.7	References.....	170

Chapter Seven

4-Aminosalicylic Acid Adducts 173-189

7.1	Introduction.....	174
7.2	Crystal Structures of the Adducts.....	175
7.3	Thermal analysis of the Adducts.....	183
7.4	Conclusions.....	185
7.5	Experimental Section.....	185
7.6	References.....	187

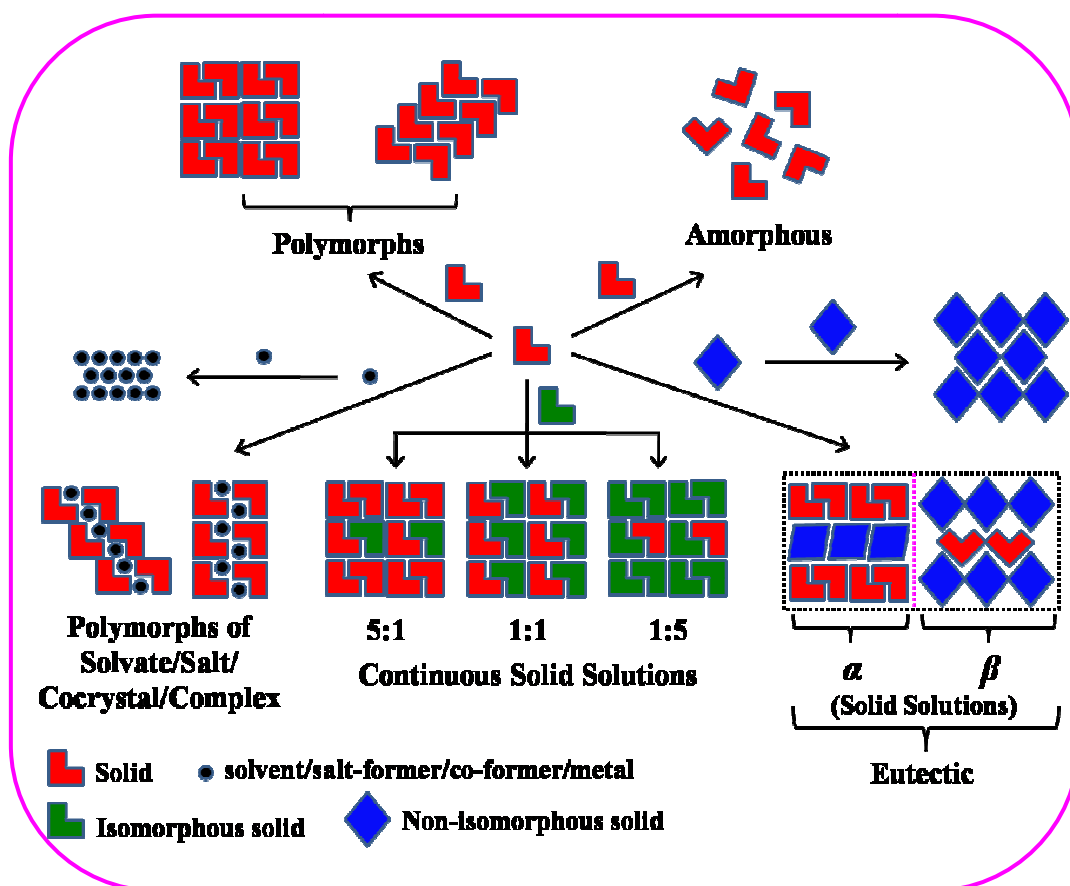
Chapter Eight

Conclusions and Future Prospects 191-193

About the Author.....	195
List of Publications.....	197
Participation in Symposia & Conferences.....	199

CHAPTER ONE

INTRODUCTION TO PHARMACEUTICAL SOLIDS



Schematic representation of various solid forms. A pharmaceutical solid formulation contains the 'Active Pharmaceutical Ingredient' (API) as a polymorphic form/mixture, salt, hydrate/solvate, complex, cocrystal, eutectic or an amorphous solid.

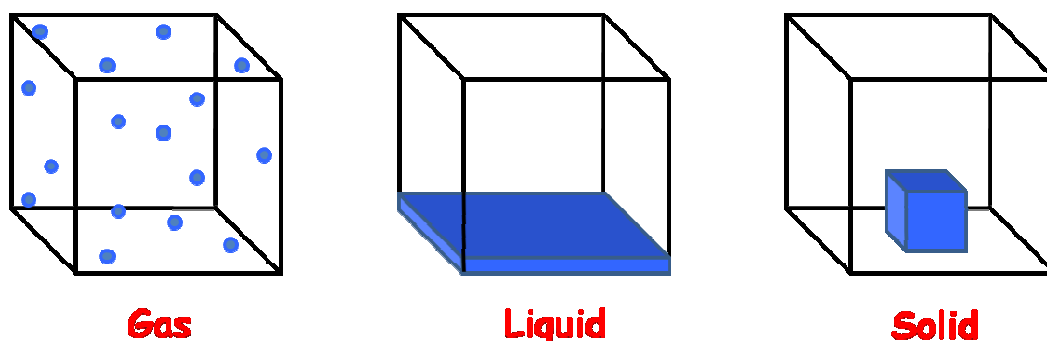
1.1 Introduction

Majority of the drugs are marketed as solid dosage formulations (tablets, capsules and powders) because of several reasons such as ease of manufacture, administration, convenience to patients, storage etc.¹ The study and understanding of the nature and properties of various pharmaceutical solids is, thus, central in pharmaceutical chemistry and therefore the subject '*Solid State Chemistry of Drugs*'² is of fundamental importance in drug industry. The current challenges of 'pharmaceutical form development' and 'intellectual property management' in drug research and development render these materials increasingly important in the pharmaceutical industry for commercial reasons as well as lifecycle management of the drug.^{1a,3} A pharmaceutical solid formulation contains the 'Active Pharmaceutical Ingredient' (abbreviated as 'API') as a polymorphic form/mixture, salt, hydrate/solvate, complex, eutectic or an amorphous solid blended with excipients.^{2,4} Each of these solid forms exhibit different physico-chemical properties such as flowability, compressibility, stability, solubility, dissolution rate and bioavailability which finally govern the therapeutic efficacy of the drug.^{1b,2,3a} Thus, optimization of the solid drug form is crucial not only in drug research and development but also for administration and usage as oral medicines. The understanding of the phenomena that govern the physico-chemical properties of pharmaceutical solids will avoid pit-falls in drug development and comprehend the quest for better medicines.^{1a,2,3a,5}

1.2 Solid State Chemistry

A fundamental understanding of the solid state is needed before studying various kinds of (pharmaceutical) solid materials and their structure and properties. '*Solid*' is one of the fundamental states of matter and is characterized as the '*state/phase*' wherein the particles, whether atoms, ions or molecules, are tightly bound to each other in space (Scheme 1.1).⁶ In the gas phase, the particles are far apart due to thermal energy and randomly interact with each other when brought into a container i.e. particles exist in a disordered state.⁶ When a material in gaseous state condenses to a solid, through or without a liquid phase in between, the collisions/vibrations of the particles get minimized due to the loss of thermal energy and the particles come closer and interact with each other. The forces of attraction that develop between the particles (or constituents) in a solid lead them to '*arrange*' in an '*orderly*' manner in accordance to the thermodynamic principles.^{6a,b} The ordered arrangement in a definite three dimensional space (or

geometry or framework) termed as '*lattice*' or '*space lattice*' is characteristic of the solid.^{6a,b} The lattice organization on the whole is called the '*structure*' or '*packing*' (in a broad sense) of the solid and is independent of gravity. Thus, the solid does not pack onto a container unlike liquids and gases and has its own shape and volume.⁶



Scheme 1.1 In the gas phase, since the forces of attraction between the particles (atoms, ions or molecules) are negligible due to thermal energy, they scatter and take both the shape and volume of the container. In the liquid phase, the thermal energy is less and so the particles come closer and interact. The forces of attraction between the particles are strong such that the liquid makes a fixed volume, but not strong enough to defy gravitational force and hence it takes the shape of the container under the influence of gravity. In the solid phase, the particles are held together by strong attractive forces such that the solid holds its shape and the volume is about the shape of the solid (Adapted from 'Phases of Matter' image of NASA's Glenn Research Centre).^{6c}

When the structural pattern or packing or order of the solid is '*regular*' and '*repeating*' in the three dimensional space, it is called '*periodic*' order.^{6a,b} Based on the degree of order (pattern) and periodicity (repeat) of its constituents in the atomic level, solids can be classified as '*crystalline*', '*quasicrystalline*' and '*amorphous*' states^{6,7} (Figure 1.1). A crystalline solid is characterized by long-range order and periodicity but the order is aperiodic in a quasicrystalline solid.^{6a,b,7} In an amorphous solid, which is considered as a super-cooled liquid, the order is restricted to short-range.^{6b,8} To simplify the situation, consider a group of molecules ordered or structured into a hexagon (Figure 1.1). If the propagation of hexagon is regular and repeating beyond the molecular scale (typically micron level), such an arrangement is characteristic of a crystalline solid. If the propagation (order) is limited to neighboring molecules i.e. nanometer range, it is typical of an amorphous state. In a quasicrystalline phase, the propagation of a particular pattern also goes beyond the molecular scale but the element of '*regularity of repetition*' is missing^{7a} (Figure 1.1). The three solid phases of matter can be distinguished by their diffraction behavior. The advent of X-ray diffraction has revolutionized the materials

chemistry, particularly solid state chemistry, by elucidating the structural integrity, and thus property, of solid materials.^{6,9} X-ray powder diffraction is used as a routine technique to characterize the solid state.⁹ The word ‘powder’ will be misleading in the early stages of the study of solid state phenomena. Any ‘crystal’ is imagined as macroscopic material (a 3D object) based on the everyday experience with sugar or salt crystals and an ‘amorphous’ material in powder morphology. But, a crystal retains its lattice order even if broken into pieces of microscopic scale. These microscopic crystals called ‘crystallites’ also assume powder morphology.⁹ Thus, crystalline solids can exist in powdered state as amorphous solids. An amorphous solid which is characterized by short-range order and randomness of molecules does not constructively diffract X-rays.⁸ Hence, the X-ray powder diffraction patterns of amorphous forms display broad and diffuse haloes^{8a} (Figure 1.2). Crystalline and quasicrystalline solids, of their long-range order, give rise to characteristic diffraction peaks (Figure 1.2) and therefore can be considered as true solids.

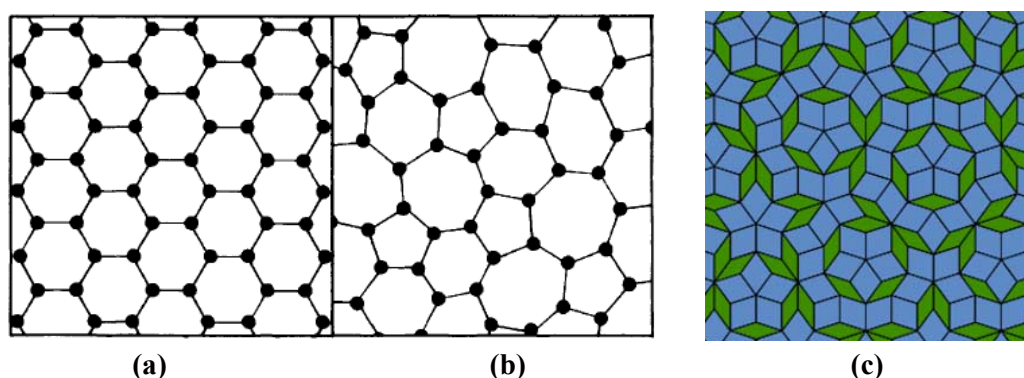


Figure 1.1 (a) A crystalline solid has periodic order of points (atoms, ions or molecules) in the space lattice but (b) an amorphous solid has a short-range order (Ref. 8c). (c) A quasicrystalline solid has aperiodic order in that the parallelogram pattern (cubical in 3D) of points does not repeat in a regular fashion i.e. patterns with repeats (Ref 7b).

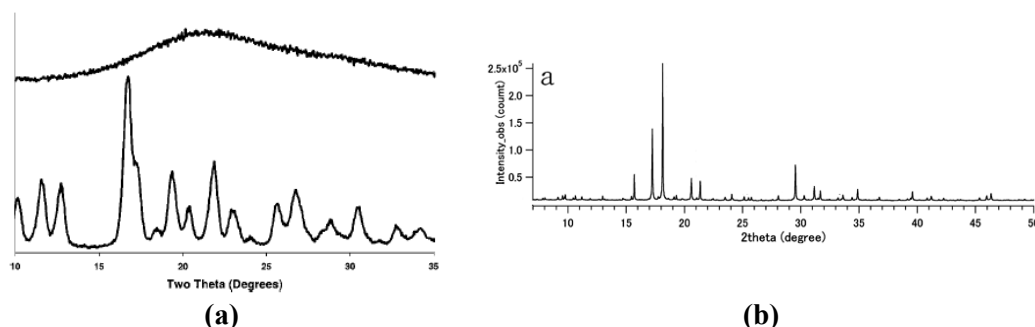
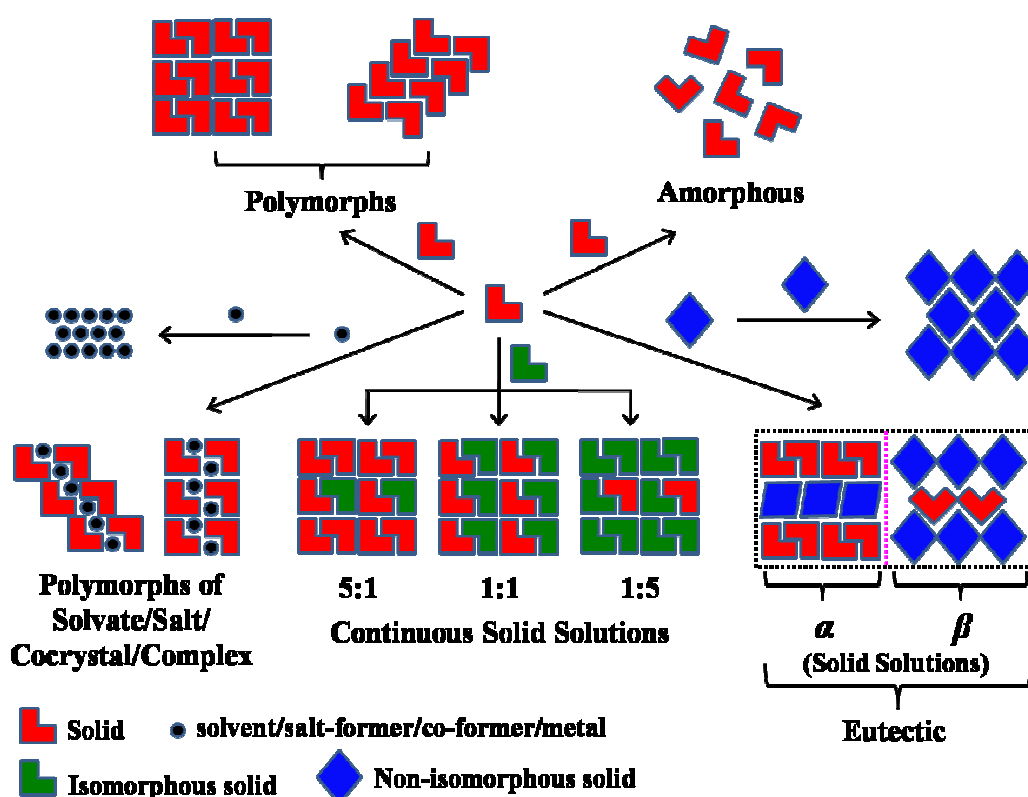


Figure 1.2 Powder X-ray diffraction pattern of (a) amorphous (top) and crystalline (bottom) Indomethacin (Ref. 8a) and (b) that of Zn-Mg-Ho quasicrystal (Adapted from Ref. 10).

A solid can be made up of a single component or two or more components. On the basis of composition, solids are classified into two types viz. (i) homogeneous solids and (ii) heterogeneous solids.^{6a} Elemental solids composed of all atoms of the same kind are homogeneous solids. Compound solids made up of different atoms/compositions of atoms are heterogeneous solids; they include alloys, intermetallic, ionic, molecular and coordination compounds. Both elemental and compound solids can exist in crystalline and amorphous states (e.g. carbon¹¹ and steel¹² respectively). The various forms possible for a solid material and their plausible structures are depicted in Scheme 1.2. Again both elemental and compound solids (except alloys) of the same chemical composition can exhibit different structures in the solid state and the phenomena are called ‘allotropism’ and ‘polymorphism’ respectively¹³ (Scheme 1.2). For e.g., elemental carbon exists in different allotropic forms such as diamond, graphite, fullerene etc.^{6b} Similarly, glycine,¹⁴ a small biomolecule, and calcium carbonate,¹⁵ a biomineral salt, exist in three polymorphic forms each. Quasicrystalline state is a relatively new finding compared to crystalline and amorphous states and is observed in some alloys.⁷ The discussion and illustrations on the solid state herein are not exhaustive. For the sake of convenience and understanding of the new definitions and analogies proposed next in a supramolecular sense, the discussion is focused to crystalline state of alloys and ionic/molecular solids.

An ‘alloy’ is a multi-component crystalline solid made up of different atoms or elements (e.g. steel).¹⁶ A multi-component crystalline solid made up of ions or molecular ions is called a ‘salt’ (e.g. sodium chloride and caffeine citrate),¹⁷ and a ‘coordination complex’ or simply ‘complex’ when it contains a metal (e.g. fosinopril sodium).^{3a} A ‘stoichiometric multi-component molecular crystal wherein the components are assembled by adhesive (heteromolecular) interactions’ is called a ‘cocrystal’ (e.g. carbamazepine–saccharin),¹⁸ a ‘hydrate/solvate’ when one of the components is water or a solvent (e.g. nitrofurantoin monohydrate).¹⁹ A ‘solid solution’ is a ‘variable stoichiometry multi-component crystalline solid formed by substitutional incorporation of a component (element or compound) in the lattice of another component (element or compound)’ (e.g. Copper-Nickel alloys).¹⁶ A ‘eutectic’ is a ‘conglomerate of solid solutions’ (e.g. Lead-Tin system).¹⁶ Thus, the solid solutions/eutectics retain their parent lattice structures and cohesive (homo or self) interactions and therefore have scarce adhesive interactions. Hence, alloys and certain compounds by virtue of their integrity of solid solutions and eutectics retain their parent crystal structures (Scheme 1.2). The other

multi-component crystalline solids (e.g. salts, cocrystals, complexes etc.) have unique crystal structures as they are manifested by adhesive interactions that direct the crystal structure and packing.^{1,2}



Scheme 1.2 Schematic representation of various forms possible for a solid when combined with the same solid or different phase which can be solid or liquid or gas. Both elemental and compound solids can be polymorphic and amorphous. When different elements/compounds combine where adhesive interactions dominate over cohesive interactions, a new compound with crystal structure different from that of the parent materials can form (e.g. salt and cocrystal). Elements/compounds with similar size and crystal structures can form ‘continuous solid solutions’ upon substitution with one another and the ones with mismatch and misfit can give rise to a ‘eutectic’. A ‘eutectic’ is a ‘conglomerate of solid solutions’ wherein the solid solution domains are held by weak interactions (dotted magenta line). Solid solutions/eutectics resemble crystal structures of their individual components.

1.2.1 Eutectic microstructure

Solid solutions and eutectics are well studied in inorganics where alloys are classified as (i) solid solution alloys and (ii) eutectic alloys.¹⁶ Traditionally both the materials are prepared by fusion of two or more solids in different ratios and are thus characterized by their melting behavior through a solid-liquid phase diagram.^{16,20} The typical phase diagrams of a solid solution and a eutectic are exemplified by Copper-Nickel solid

solution alloy and Lead-Tin eutectic alloy respectively (Figure 1.3).¹⁶ A solid solution, in general, exhibits a melting/freezing range and the temperature below which the material is solid is called ‘solidus’ and ‘liquidus’ is the temperature above which it is liquid (Figure 1.3a).¹⁶ Between solidus and liquidus, the solid and liquid phases of the material coexist. On the other hand, a eutectic exhibits characteristic lower melting point than its components (Figure 1.3b).¹⁶ Further, its melting point is sharp and not in a range unlike that of a solid solution i.e. its solidus and liquidus temperature is same. The word ‘eutectic’ is derived from the Greek word ‘*eutectos*’, which means ‘easily fused’.¹⁶ Several definitions of eutectic are available in the literature based on its characteristic lower melting point.^{20,21} It can be defined as ‘a specific composition of constituents in a mixture of elements or compounds which exhibits the lowest melting point than any other composition of the constituents’. Several compositions of the constituents can also exhibit lower melting points than the parent materials but they will be higher than the eutectic melting point (Figure 1.3b).

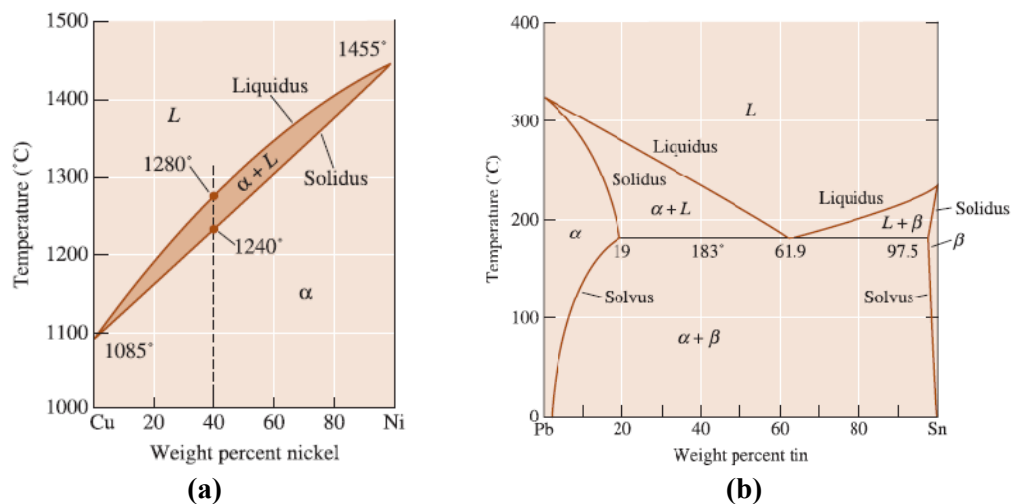


Figure 1.3 (a) Phase diagram of Copper-Nickel solid solution alloy. The 40% copper solid solution of nickel exhibits a melting range of 1240-1280 °C. Below the solidus temperature (1240 °C), the alloy is a homogeneous solid phase designated as ‘ α ’ and above the liquidus temperature (1280 °C) it is a liquid phase. **(b)** Phase diagram of Lead-Tin eutectic alloy. The 61.9:38.1 tin-lead composition exhibits characteristic lower melting point (183 °C) than its parent materials (Tin = 232 °C, Lead = 327 °C) and also other compositions. (Ref. 16)

A solid solution is made up of a major phase (solvent) and one or more minor phases (solutes)¹⁶ and can be formed by isomorphous crystals (crystals having same space group and unit cell dimensions)²² in accordance to the Hume-Rothery rules (same crystal structure and valence, and similar size and electronegativity).¹⁶ Conversely, non-

isomorphous crystals can give rise to a eutectic and is discussed next. When the components have similar size and crystal structures, they can have unlimited solubility and accommodate well (either substitutionally or interstitially) in the crystal lattice without disturbing the parent lattice structure and thus form ‘continuous solid solutions’ in 1:99 to 99:1 ratios (Scheme 1.2) as in case of Copper-Nickel system.^{16,23} When nickel (Ni, $Z = 28$) is added to copper (Cu, $Z = 29$), both having ‘*face-centered cubic (fcc)*’ crystal structure, or vice-versa, both of them mix in any amount and randomly distribute within the ‘*fcc*’ crystal structure. They form a homogeneous phase designated as ‘ α ’ (Figure 1.4) throughout the lattice, wherein no interface exists between the copper and nickel atoms (Figure 1.4).¹⁶

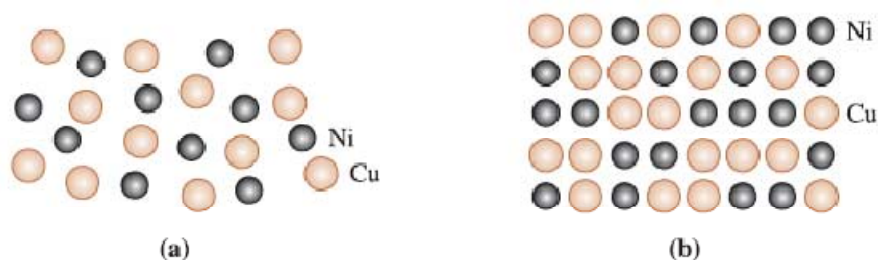


Figure 1.4 (a) Liquid copper and liquid nickel are completely soluble in each other. (b) Copper and nickel atoms occupy random lattice sites in the copper-nickel solid solution alloys (Ref. 16).

When the components have mismatch and asymmetry (in size, crystal structures and interacting groups), they have limited solubility and thus cannot fit beyond a threshold in the crystal lattice of one another, since it leads to strain and disorganization of their lattice structures. Such systems cannot form continuous solid solutions instead tend to form ‘eutectics’ exemplified by Lead-Tin system.¹⁶ When tin (Sn, $Z = 50$, tetragonal) is added to lead (Pb, $Z = 82$, cubic) or vice-versa, they form solid solution alloys just like copper-nickel system up to their solubility limits. Since, tin is smaller in size it has higher solubility in lead (0 to 19%) and lead because of its larger size has lower solubility (0 to 2.5% in Sn). This means up to 19% tin can be accommodated in the lattice structure of lead to form a homogeneous solid solution represented as ‘ α ’ (Figure 1.5), which retains the lattice structure of lead as it is the major component (81%). Similarly, 2.5% solid solution of lead in tin, represented as ‘ β ’, retains the crystal structure of tin as it is the major component (97.5%).¹⁶ When the percentage of either of the elements goes beyond their solubility, it leads to strain and disorganization of the solid solution lattice. To conciliate this, the system segregates and reorganizes into two

different phases (solid solutions - ' α ' and ' β ', each of which rich in a particular element and retains the parent lattice structure) to result in a eutectic upon solidification (Figure 1.5).¹⁶ Thus, a eutectic can be defined as 'a conglomerate of lattice structures of two or more components' or 'a conglomerate of solid solutions'. The eutectic microstructure is manifested by domains of solid solutions held together by incoherent inter-phase boundaries (Scheme 1.2 & Figure 1.5) along which atoms can diffuse and redistribute in the solid solutions.^{16,20} The inherent strain in the solid solution domains maximized by imperfect atomic arrangements and poor inter-phase bonding across the domain boundaries lead to excess thermodynamic functions (free energy, enthalpy and entropy)²⁴ of the eutectic, with the result that it exhibits characteristic lower melting point than the components.¹⁶ At 61.9% tin in lead or 38.1% lead in tin, the alloy has lowest melting point (183 °C) than its parent elements (Tin = 232 °C, Lead = 327 °C) and also other compositions (Figure 1.5) and displays the characteristic eutectic microstructure. Many eutectic systems manifest in a 'lamellar' or plate-like arrangement including the lead-tin system (Figure 1.6).¹⁶ From the phase diagram (Figure 1.5a), it can be noted that the other compositions can exhibit solidus-liquidus melting behavior typical of solid solutions or lower melting points than the parent elements but higher than the 'eutectic composition'. These compositions too can be composed of different amounts of solid solutions (as shown in Figure 1.5b) with varying degree of domain organization and inter-phase interactions in the crystal lattice.

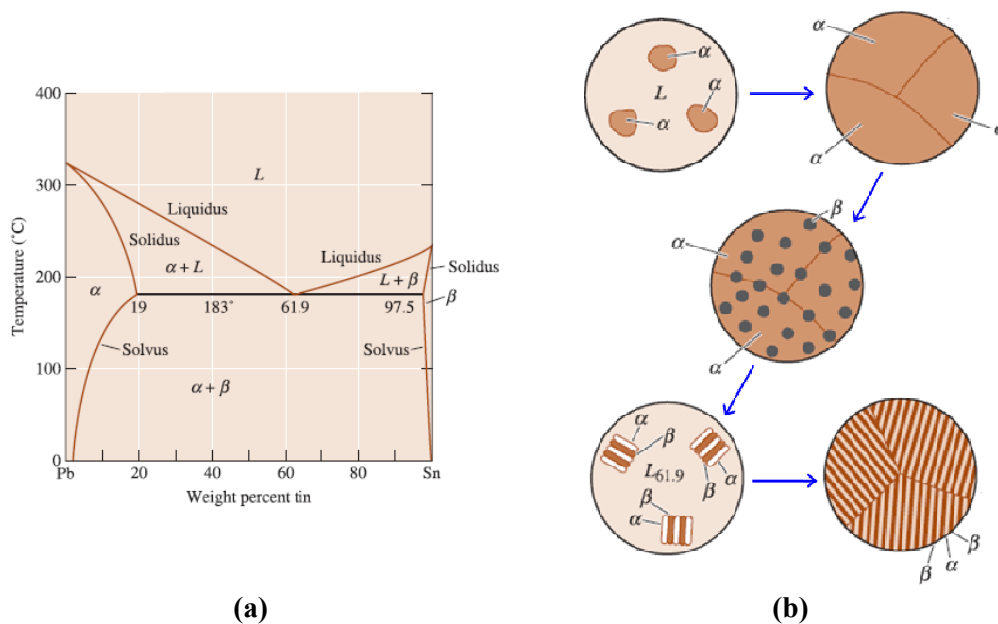


Figure 1.5 (a) Phase diagram and (b) microstructure of Lead-Tin eutectic alloy showing solidification and growth of solid solutions (Adapted from Ref. 16).

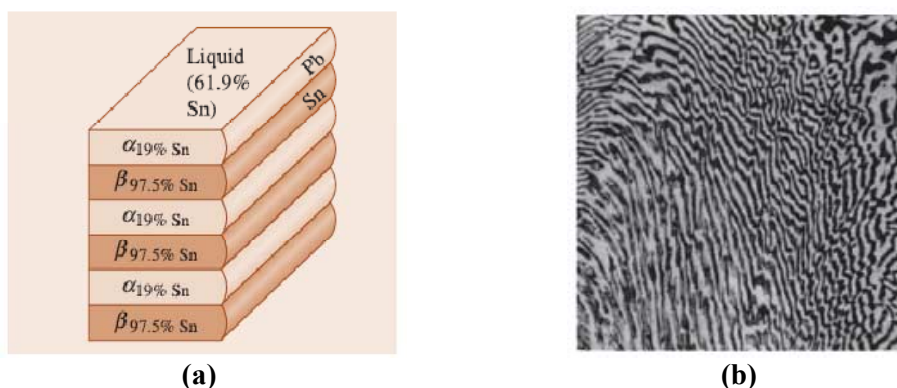


Figure 1.6 (a) Lamellar arrangement of lead-rich ' α ' and tin-rich ' β ' solid solutions in Lead-Tin eutectic alloy. Lead atoms from the liquid preferentially diffuse to the ' α ' plates, and tin atoms to the ' β ' plates. **(b)** Photomicrograph of Lead-Tin eutectic microconstituent (Ref. 16).

1.3 Solid State Chemistry of Drugs

Solubility/dissolution and stability are the prime issues in drug research and development as they influence bioavailability and therapeutic efficacy of a drug.^{1,2,25} The alarming increase in the number of hydrophobic drug molecules with the advent of 'High Throughput Combinatorial Medicinal Chemistry'²⁶ has become a formidable challenge to the popular solid oral dosage formulations (tablets and capsules).^{3a,c} The oral route of administration relies on the aqueous dissolution and absorption of the solid drug in the biological media before the drug reaches the site of action through systemic circulation. When a hydrophobic solid drug enters the gut upon oral administration, it will be partially or not at all absorbed by the aqueous medium which results in inadequate or loss of bioavailability, finally leading to ineffective therapeutic impact. Thus, the drug formulation will not be useful for patients. The subject '*Solid State Chemistry of Drugs*',² which primarily focused on solid state reactions of drugs and their stability issues, now widened its scope to 'pharmaceutical form development' and 'intellectual property management' of drugs to address and achieve the ultimate goal of modulation of physico-chemical properties of drugs in a desired way. Several phenomena, strategies and techniques are well pursued in the area of solid state chemistry of drugs which include polymorphism and amorphous state of the drugs, multi-component systems such as hydrates/solvates, salts, complexes and, more recently, cocrystals.^{1,2,3} Solid dispersions (dispersion of one or more components in a solid matrix),^{20,27} nanoparticles^{27c} etc. also come under the broad umbrella of the subject. This thesis deals with the formers as they are intimately related to each other with respect to their chemistry and the latter

are not discussed since they are more of a technology. The inherent features (structure and interactions) of these various solid forms result in their characteristic attributes (property) such that they can be assessed by different analytical techniques such as diffraction, spectroscopy etc.^{1,2} Each of these solid forms, by virtue of their uniqueness, exhibit different physico-chemical properties and thus are important for the optimization and development of a suitable solid drug formulation.

1.3.1 Amorphous Forms

Amorphous forms, characterized by the lack of lattice order, bear high thermodynamic functions and thus can facilitate enhancement of solubility/dissolution of a low soluble API.⁸ The antibiotic Novobiocin is poorly absorbed as its crystalline form and hence therapeutically ineffective. But, its amorphous form, which is 70 times more soluble than the crystalline form, is readily absorbed and thus is effective.^{2,28} Similarly, the amorphous form/solid dispersion of the anti-fungal drug Itraconazole (Figure 1.7) of its faster dissolution rate than the crystalline form (about 20 times) is understandably the marketed form (brand name ‘Sporanox’) of the drug.²⁹ Amorphous forms can be produced by several techniques such as melt quenching, spray- and freeze-drying, milling, wet granulation etc.^{8b} and recently, grinding³⁰ was shown to result in amorphous salts. On the other hand, though amorphous forms impart solubility/dissolution improvement in a drug formulation for a poorly soluble API, they tend to be unstable because of their high energy and can convert to the low energy crystalline form at any point of time.^{1,2,8} Hence, they are generally not preferred in drug development and formulation unless there are clear-cut advantages over the crystalline forms. Several excipients such as methyl cellulose, alginic acid, polyvinyl pyrrolidone (PVP), polyethylene glycol (PEG) etc.^{2,8} have been developed to stabilize the amorphous forms.

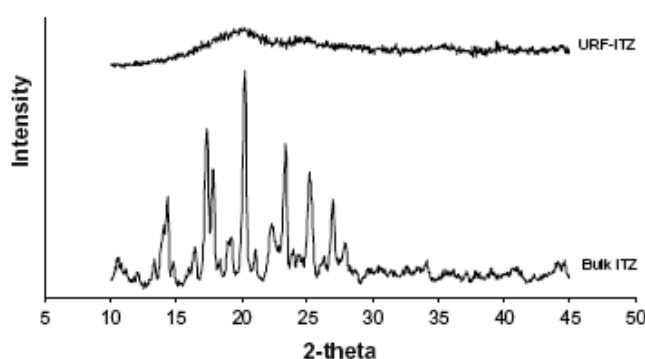


Figure 1.7 Powder X-ray diffraction patterns of amorphous (top) and crystalline (bottom) Itraconazole (Ref. 31).

1.3.2 Polymorphism

The word ‘*Polymorphism*’^{13,32,33} is encountered in various scientific streams such as biology, materials science, computer science etc.^{34,35} It is derived from Greek, *poly* = many + *morph* = form.¹³ In the area of materials science, the phenomenon of polymorphism pertains to crystalline solid state. Polymorphism can be defined as the ‘existence of the same chemical compound in different crystalline environments’ and ‘different crystal forms of the compound are called ‘polymorphs’. What is allotropism and allotropes for an element are polymorphism and polymorphs to a compound in a broad sense.¹³ Although the history of polymorphism can be traced to nineteenth century, its importance in the field in pharmaceuticals was brought to light by Walter McCrone who also gave the widely accepted definition of polymorph as: “*a solid crystalline phase of a given compound resulting from the possibility of at least two different arrangements of the molecules of that compound in the solid state*”.³² As per the structure-property relationship, different polymorphs exhibit different properties just as different compounds.³² In effect, polymorphs of an API by virtue of their difference in structures can display differences in physico-chemical properties, such as melting point, compressibility, stability, solubility, dissolution rate and bioavailability, which form important criterion for the selection of optimal solid form for formulation and usage.^{5,13}

1.3.2.1 Classification of Polymorphs

Polymorphs are synonymously called as ‘forms’, ‘modifications’ or ‘phases’ and represented as numerals (Arabic: 1, 2, 3 etc. and Roman: I, II, III etc) or alphabets (Greek: α , β , γ etc. and English: A, B, C etc) in the literature.¹³ From a structural point of view, polymorphs can be broadly classified into three categories viz. (i) conformational polymorphs, (ii) synthon polymorphs and (iii) packing polymorphs³⁶ (Figure 1.8). When the differences in molecular conformations lead to different crystal structures, it is called ‘conformational polymorphism’³⁷ e.g. dimorphs of anti-HIV drug Ritonavir³⁸ (discussed later). When the supramolecular synthon or non-covalent interactions are different in different crystal structures, it is called ‘synthon polymorphism’^{36,39} e.g. acid dimer and acid catemer in the dimorphs of Oxalic acid⁴⁰ (Figure 1.9). When the arrangement of molecules (whether conformationally flexible or rigid) varies in different crystal structures, it is called ‘packing polymorphism’.^{36,41} In general, all polymorphs arise from differences in molecular packing and so referring them as packing polymorphs is a gross

classification which does not give information about structural details. Though these classifications are subjective because of overlap possible between them and more than one can coexist in a given system, for e.g. conformational and synthon polymorphism (in the trimorphs of diuretic drug Furosemide, Figure 1.10)³⁶ or synthon and packing polymorphism (in the tetramorphs of anti-tuberculosis drug Pyrazinamide, Figure 1.11),⁴² the advantage of classifying polymorphs in the above categories is to facilitate understanding of the differences between polymorphs at the molecular level.

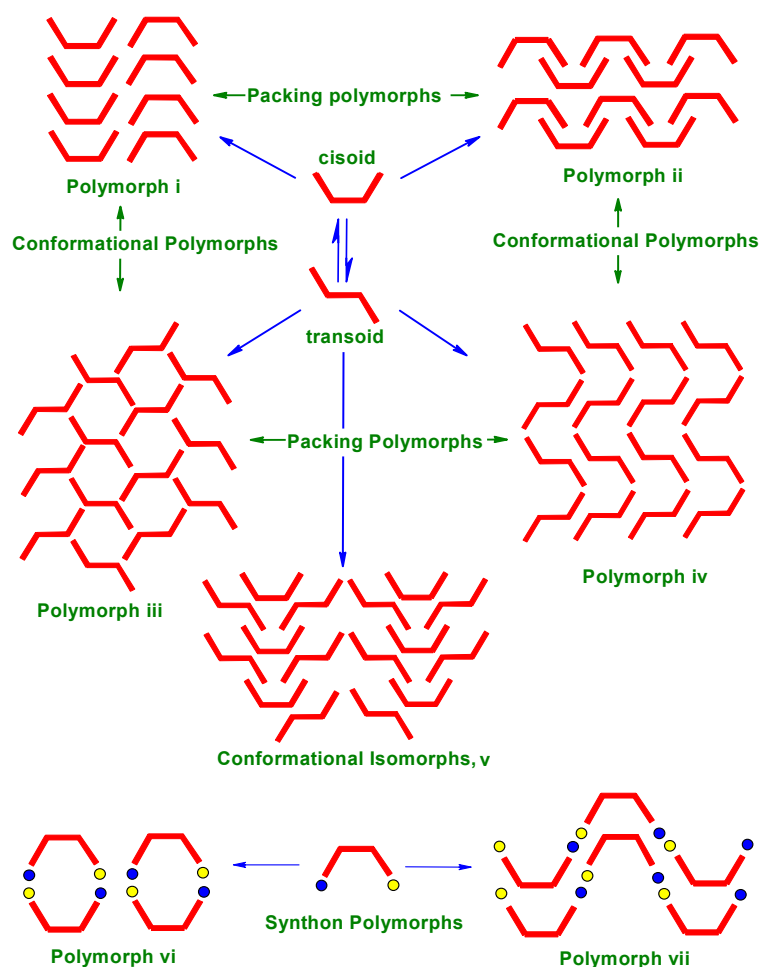


Figure 1.8 Schematic representation of different kinds of polymorphs (Adapted from Ref. 37a).

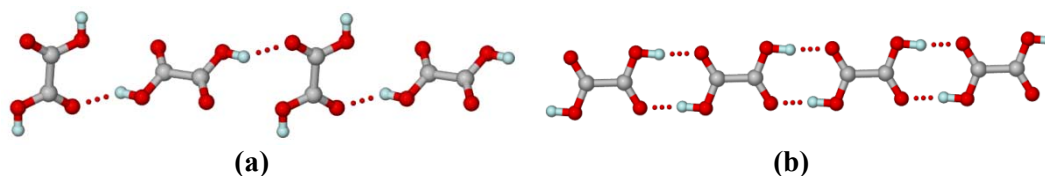


Figure 1.9 Synthon polymorphs of Oxalic acid. (a) α -form has acid catemer and (b) β -form has acid dimer in their crystal structures (Adapted from Ref. 40).

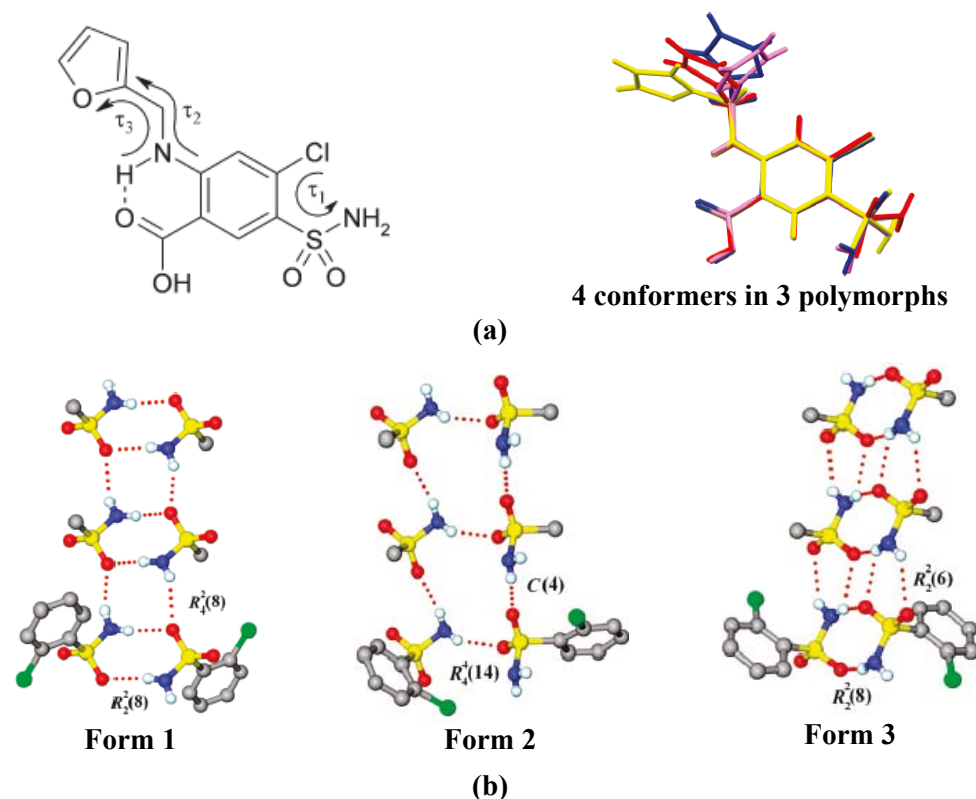


Figure 1.10 (a) Conformational polymorphism in Furosemide. The three torsion parameters in Furosemide: $\tau_1 = \text{C-C-S-N}$, $\tau_2 = \text{C-N-C-C}$, $\tau_3 = \text{N-C-C-O}$. The anthranilic acid moiety is conformationally locked by intramolecular hydrogen bond but conformational flexibility in the furan and sulfonamide moieties resulted in four conformers (red, blue, pink and yellow) manifested in three polymorphs. (b) Synthon polymorphism in Furosemide. $R_2^2(8)$ N-H \cdots O dimer and $R_4^2(8)$ motif in form 1, $C(4)$ catemer and $R_4^4(14)$ tetramer motif in form 2, $R_2^2(8)$ N-H \cdots O motif and $R_2^2(6)$ rings in skewed dimer of form 3 (Ref. 36).

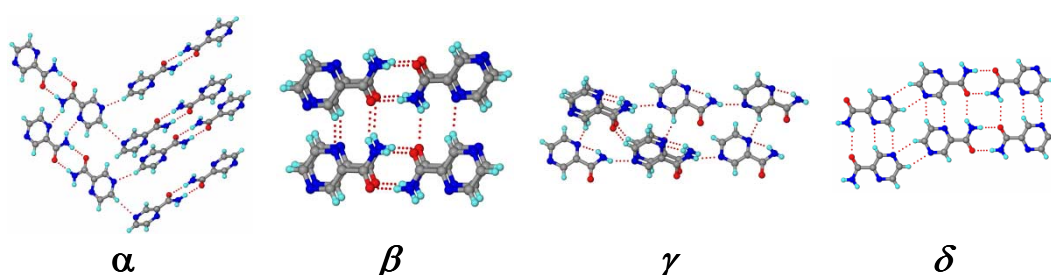


Figure 1.11 Synthon and packing polymorphism in Pyrazinamide. In α polymorph, zigzag tapes formed by $R_2^2(8)$ N-H \cdots O and $R_2^2(10)$ N-H \cdots N hydrogen bonds are connected orthogonally to 2_1 screw related tapes through C-H \cdots N interactions in a 3D arrangement. The β polymorph has non-planar $R_2^2(8)$ N-H \cdots O dimers that make a helix along the b -axis through anti N-H \cdots O and C-H \cdots N interactions. In γ polymorph, 1D tapes assembled via N-H \cdots N hydrogen bonds of $C(6)$ notation are connected through C-H \cdots O and C-H \cdots N interactions. In δ polymorph, carboxamide tapes formed by $R_2^2(8)$ dimer and $C(4)$ catemer N-H \cdots O synthons and $R_2^2(6)$ C-H \cdots N synthons make 2D sheets (Ref. 42).

1.3.2.2 Polymorph Generation and Transformation

Polymorph screening and generation is an essential component of pharmaceutical research.^{2,5} Apart from the conventional methods of evaporative crystallization in different solvents, varying temperature of crystallization, milling etc.,^{2,5} new techniques such as sublimation and melting,^{43a,b} crystallization with structurally related additives,⁴⁴ using polymers as heteronuclei,⁴⁵ laser induced nucleation,⁴⁶ crystallization in capillaries,⁴⁷ rotavaporization,⁴⁸ controlled desolvation^{5b,49} etc. are being employed for the generation of polymorphs. Of late, new polymorphs are being obtained during cocrystallization experiments.⁵⁰ Once a polymorph with desired properties is obtained, conditions need to be standardized for bulk manufacture and sustenance of the polymorph to prevent potential transformation to a more stable polymorph with time. This can happen because the polymorphs are at different levels on the ‘free energy’ surface and therefore inter-conversions are quite possible which lead to changes in the properties of bulk drug material finally affecting its efficacy^{5,32,38b} (discussed later). Therefore, it is essential to gain adequate understanding of their properties so as to optimize the conditions to develop a desired polymorph for formulation.

Polymorphism results from the interplay of thermodynamic functions (free energy, enthalpy and entropy) and kinetic factors (activation energy, temperature, supersaturation, rate of evaporation etc.) that govern the crystallization process.^{5,13} According to Ostwald’s rule of stages,⁵¹ a system reaches the low energy state and attains equilibrium from an initial high-energy state through minimal changes in free energy involving different intermediate forms at different stages (Figure 1.12). Thus, the form that crystallizes first is the one which has the lowest energy barrier (high energy, metastable form) from liquid to solid state. This form then transforms to the next lower energy polymorph on the energy diagram and the process continues until the crystallization of the thermodynamically stable form.⁵¹ The transformation of the metastable form to the stable form and number of intermediate forms manifesting during the process is dependent on free energy of activation, nucleation as well as time. On the other hand, as the energy difference between the polymorphs is typically within a 5 kcal mol⁻¹ window,^{37a} several polymorphs can crystallize simultaneously if their nucleation rates are equal. This phenomenon is called ‘*concomitant polymorphism*’^{13,52} wherein the polymorphs, both stable and metastable, crystallize under the same conditions and the same vessel. Concomitant polymorphs are generally ‘near-energetic’.⁵²

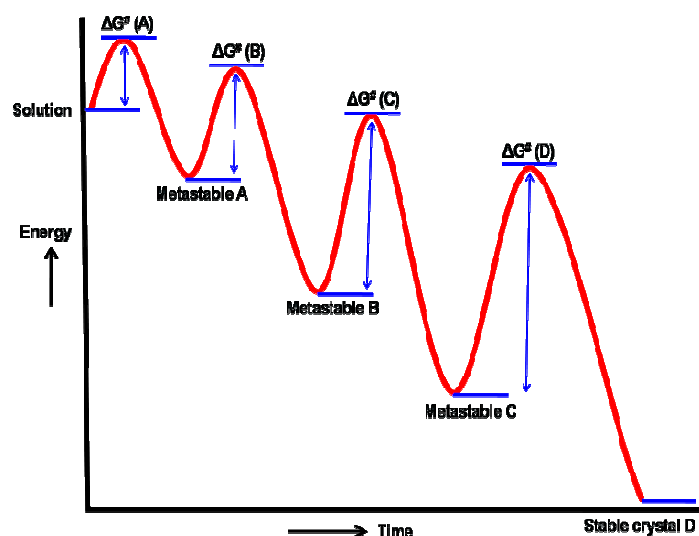


Figure 1.12 Ostwald's rule of stages to show the transformation of high energy (metastable) form to low energy (stable) form with time during crystallization. (Adapted from Ref. 51a)

Polymorphic transformations (solid-solid phase transformations) can happen during crystallization as above i.e. in solution, upon storage and with variation in temperature.^{1,2,5,36,42} The transformation or interconversion of polymorphs (whether from metastable to stable form or even stable to metastable form in a given set of conditions) depends on how the free energy of activation is achieved by the system for the nucleation of a polymorph and its consequent growth.^{1,2,53} The manufacturing processes such as granulation, milling, compression etc. can also facilitate transformation.^{1,2} Seeding also induces the formation of particular polymorphs since the process bypasses the rate-limiting nucleation step.⁵³ In all, the transformation is dependent on the inherent thermodynamic functions of the system with respect to temperature, which can also provide the activation energy for nucleation and transformation. The entropy and temperature components influence the free energy of a system and thus are crucial in establishing the relative thermodynamic stability relationships of polymorphs.^{13,42,54} They can shift the balance from one polymorph to another polymorph with respect to their stability depending on the conditions prevalent. Thus, thermodynamically, polymorphs are divided into monotropic and enantiotropic systems.^{13,32,55} Monotropism is the phenomenon in which only one polymorph is the stable form at any temperature and all other polymorphs convert to through exothermic phase transition. Enantiotropism is the phenomenon in which one polymorph is stable at one temperature and other at another temperature and the two are related by a reversible phase transition. An endothermic

phase transition at some temperature before melting is characteristic of an enantiotropic system. In general the situation of an enantiotropic system is like this: when a polymorph is heated, it transforms to another polymorph, by taking energy, at one particular temperature called ‘transition temperature’, above which the new polymorph is stable; this high temperature polymorph reversibly converts to the original polymorph, by losing energy, upon cooling beyond the transition temperature.^{13,55} Sometimes, if the conditions favor, the high temperature polymorph, though metastable at room temperature, can elude transformation.^{42,54b} The same is true for near-energetic polymorphs of a concomitant crystallization batch. If the conditions are such that the free energy of activation required for the transformation to the stable polymorph is high and the nucleation of stable polymorph is not favored, all these metastable polymorphs can sustain from days to many years.^{13,54b} But, once the conditions favoring the formation of stable form prevail, the metastable forms can convert to it at any time. Nevertheless, the metastable nature of such polymorphs can be translated as solubility advantage over stable polymorphs which have lower solubility, as per the inverse relationship of solubility and stability.^{2,5} Thus, this attribute of metastable polymorphs is taken advantage of for pharmaceutical formulation purposes. However, their potential transformation to the stable form is a serious concern and special care should be exercised to avoid the transformation and achieve the desired objective.

Ritonavir (brand name ‘Norvir’), a HIV protease inhibitor, developed by Abbott Laboratories is a popular example which drew a lot of attention both from academia and industry with respect to polymorphic transformations and control and their potential implications.^{38,56} After two years of its launch in the market (1996-98), a new stable but less soluble polymorph II (4 times less soluble than form I) of Ritonavir was detected in the drug formulations which led to inadequate activity/bioavailability. Abbott withdrew the drug from the market and re-entered the market after standardizing the procedures to obtain the original more soluble polymorph I. In this process, the company lost an estimated \$250 million in sales the year the drug was withdrawn.⁵⁶ Ritonavir polymorphs represent an example of conformational polymorphs and also polymorphism induced by an impurity. It is hypothesized that a carbamate impurity (hydrolytic product of Ritonavir), having *syn* conformation of amide moiety, in bulk drug, induced the crystallization of form II having amide in *syn* conformation from form I with amide in *anti* conformation (Figure 1.13).^{38a}

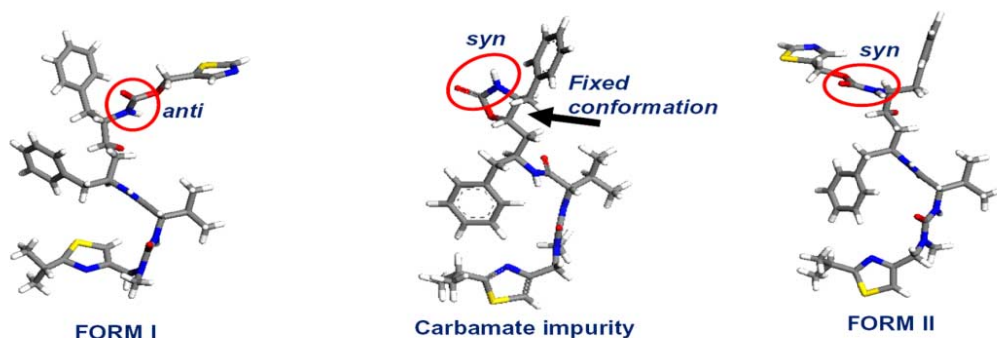


Figure 1.13 The *anti* and *syn* amide conformers of Ritonavir form I and II. The carbamate impurity with amide in *syn* conformation is speculated to induce the crystallization of form II (Adapted from Ref. 38a).

1.3.3 Pseudopolymorphism

Polymorphism is not reserved to single-component systems and is also widely encountered in multi-component systems such as hydrates/solvates, salts (including ionic liquids which are low melting salts), cocrystals etc.^{1,2,5,13,37b,57} The term ‘*pseudopolymorphism*’ used for solvate/hydrate systems was the subject of intense debate in literature and legal fields with regard to nomenclature and intellectual property (IP) issues surrounding polymorphism.^{33,58} It is defined as the phenomenon wherein ‘a compound is obtained in crystalline forms that differ in the nature or stoichiometry of included solvent molecules’⁵⁹ and the compounds are called ‘*pseudopolymorphs*’. Alternate terms ‘*solvate*’ and ‘*solvatomorphism*’ are also widely used in the literature.^{13,57a,58b} A solid can incorporate different ratios of the same solvent (e.g. antibiotic drug Norfloxacin forms a dihydrate, 1.25 hydrate and 1.125 hydrate)⁶⁰ or different solvents in its crystal lattice (e.g. antibacterial drug Nitrofurantoin forms solvates with water, DMF, DMSO, methanol etc.)¹⁹ or can form polymorphs of solvates (e.g. Nitrofurantoin monohydrate forms I and II) (Figure 1.14).¹⁹ For pharmaceutical purposes, understandably solvents with low toxicity need to be used and hence are classified based on decreasing toxicity, from Class I (should be avoided e.g. benzene, carbon tetrachloride etc.) to Class II (should be limited e.g. acetonitrile, methanol, pyridine etc.) to Class 3 (can be preferred because of their low toxicity e.g. ethanol, acetic acid, acetone etc.) solvents.⁶¹ Some solvents although present in the crystal lattice of the parent solid (in channels/voids) have no or little role on the integrity of the crystal structure and hence can be readily desolvated and resolvated for practical purposes (e.g.

cephalosporin solvates).^{2,62} But, some solvents upon controlled desolvation can produce new polymorphs of the parent material (e.g. caffeine form II from its hydrate)^{5b} and hence purposive solvation and desolvation experiments are a routine during polymorph screening of APIs and important for crystallization of a desired polymorph.⁴⁹ On the other hand, some solvents whether included in the lattice of the API or residually present in the bulk material influence the properties (such as solubility) and characteristic attributes (such as diffraction and spectroscopic patterns which are signatures) of the material and therefore a matter of concern.^{5b,63} Hydrates, in general, have low solubility and dissolution rate compared to their anhydrate API in water.⁶⁴ This is because they have less free energy available to bond with the aqueous medium as they already used some free energy for making API–water hydrogen bonds during crystallization. Nevertheless, for special requirements like slow/delayed release drug formulations, pharmaceutical hydrates are of good utility (e.g. Nitrofurantoin monohydrate form II, brand name ‘Macrobid’)^{19,65} and are also important in intellectual property and patent protection issues as illustrated in the case of anti-depressant drug Paroxetine hydrochloride.^{3b,58a} GlaxoSmithKline (GSK) patented a hemi-hydrate form of Paroxetine hydrochloride along with the anhydrate form (brand name ‘Paxil’) as a protection against generic competition after the expiry of patent on the anhydrate form of the drug. It was successful in demonstrating the presence of hemi-hydrate in the Apotex’s generic product and won the legal battle against Apotex with respect to its patent covering the hemi-hydrate form.^{3b} In all, hydrates/solvates are one of the important solid drug forms which have several applications in the pharmaceutical industry.

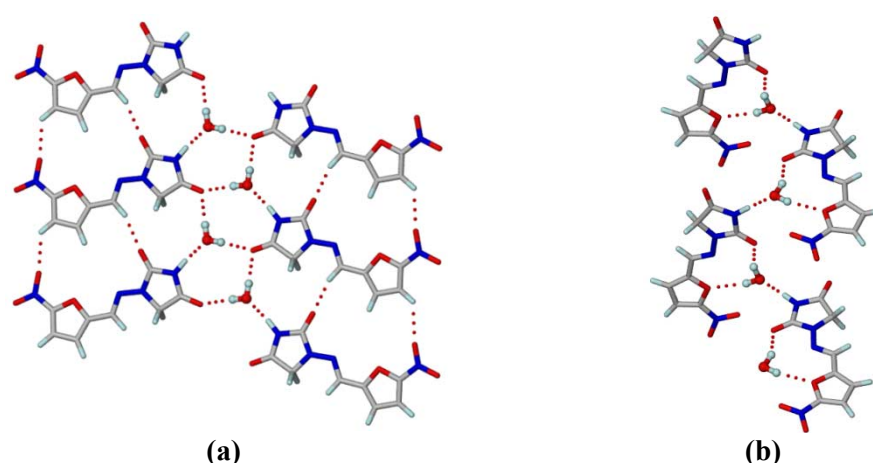


Figure 1.14 Pseudopolymorphs of Nitrofurantoin monohydrate. **(a)** In form I, tapes of translation related nitrofurantoin molecules are connected by water molecules through O–H...O and N–H...O hydrogen bonds. **(b)** In form II, discrete nitrofurantoin molecules form a zigzag tape through water molecules (Adapted from Ref. 19).

1.3.4 Pharmaceutical Salts

Traditionally, drugs are formulated as their salt forms to achieve higher solubility and stability.^{1a,b,2,3a,b,c,25b,66} Salts of their inherent strong ionic interactions tend to be stable and in general exhibit higher melting points than their parent APIs. Their ability to form electrostatic interactions and charge-assisted hydrogen bonds with water in the biological media confers higher solubility to the API salt formulation. Thus, salts offer dual advantages of solubility and stability.^{2,25b} The blockbuster drug Ranitidine hydrochloride (brand name ‘Zantac’)^{5a,56} used in the treatment of gastro-intestinal ulcers is one of the best examples of the case and is also another instance of commercial success through polymorphs as intellectual property. Ranitidine base is low water soluble (25 mg/mL)⁶⁷ and becomes unstable when exposed to light.⁶⁸ It also gives a sulfurous odor and has a low melting point of 70 °C. But, ranitidine hydrochloride salt has all the desirable attributes of high water solubility (1 g/mL),⁶⁹ higher melting point (136 °C), more stability and is almost odorless.⁶⁸ With regard to the IP issue of polymorphs, Glaxo patented two polymorphs of Ranitidine hydrochloride because of which it could sustain in the market even after patent expiry of the first polymorph.^{5a,56} This is because the generic companies have to make a formulation that should be free of the second polymorph, otherwise it would be infringement of reigning patent on the second polymorph. Thus, ranitidine hydrochloride is the illustrative example of ‘pharmaceutical form development’ and ‘intellectual property management’ i.e. two birds in one shot.

However, salts are not without any problems. The hygroscopic nature of salts, by virtue of their inherent affinity to water/moisture, is a serious problem in several cases.^{25b,66b,70} The hygroscopicity of the anti-tuberculosis drug Ethambutol dihydrochloride salt is reported to cause instability of the anti-TB fixed dose combination (FDC) drug formulations, thus leading to poor quality medicines which will not be useful for treatment (Figure 1.15).⁷¹ Moreover, for neutral and weakly ionizable APIs, salts cannot be made.^{3c,d} Of late, majority of the new drug candidates coming into the arena are hydrophobic and lack ionizable functional groups.²⁶ These issues warrant the need of novel solid forms that can circumvent these problems. Although, prodrugs, solid dispersions, nanoparticles, cyclodextrin inclusion complexes etc.^{3c,27c,72} were shown to be promising approaches, the ultimate goal of modulation of physico-chemical properties of drugs in a desired way warrants other strategies to achieve the objective.

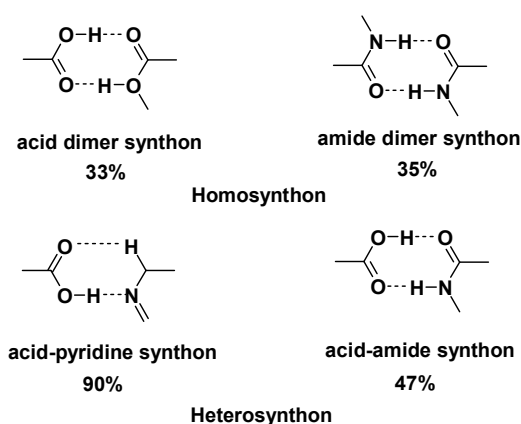


Figure 1.15 Marketed anti-TB FDC products in packed and unpacked state and their behavior when unpacked products are exposed to humidity and photostability chambers after 5 days. (a) Strip pack, packed control; (b) unpacked control; (c) exposed to 40 °C/75% RH; (d) exposed to 40 °C/75% RH/Light; (e) blister pack, packed control; (f) unpacked control; (g) exposed to 40 °C/75% RH; (h) exposed to 40 °C/75% RH/Light. RH = relative humidity (Ref. 71b).

1.3.5 Pharmaceutical Cocrystals

Crystal engineering,⁷³ the rational design of functional molecular solids, came out with a strategy in the form of ‘pharmaceutical cocrystal’ in early 2000s.^{3c,d,e,74} A cocrystal is a stoichiometric multi-component molecular crystal wherein the components are assembled by heteromolecular interactions, particularly hydrogen bonds, analogous to a salt with ionic interactions. Pharmaceutical cocrystals are a subclass of cocrystals that are formed between Active Pharmaceutical Ingredients (APIs) and Generally Recognized as Safe (GRAS) substances.^{3c,74a,b} The supramolecular synthon⁷⁵ approach of crystal engineering is the underlying principle in designing a cocrystal based on molecular recognition and binding (Scheme 1.3). Desiraju coined the term ‘supramolecular synthon’ and defined it as ‘*structural units within supermolecules which can be formed and/or assembled by known or conceivable intermolecular interactions.*’^{75a} In simple terms, it is the entity of the molecule(s) through which the crystal lattice grows. Depending on the type of functional groups involved in the interaction/assembly, it is categorized into two types by Zaworotko et al.⁷⁶ viz. homosynthon, wherein self-

complementary moieties (e.g. carboxylic acid-dimer) interact, and heterosynthon, in which two different groups (e.g. acid–amide dimer) associate. A detailed understanding of the supramolecular sense of the functional groups of the API in study is a prerequisite for designing cocrystals and is facilitated by Cambridge Structural Database.⁷⁷ The database contains over 2,00,000 crystal structures of organic solids which helps to identify the potential supramolecular synthons and/or non-covalent interactions that can be used in the synthesis of cocrystals. For example, if an API contains a carboxylic acid group one can choose a partner molecule, popularly called as ‘cocrystal former’ or simply ‘coformer’,^{3c,d,74a,b} with an acid/amide/pyridyl functionality to make a cocrystal.



Scheme 1.3 Few examples of supramolecular synthons with their probability of occurrence in the CSD.⁷⁷

Cocrystals can be synthesized by different methods wherein the components are mixed together and are subjected to solution crystallization, co-sublimation, co-melting, solid state grinding, liquid assisted grinding, slurry crystallization, reaction crystallization, spray drying etc.^{74,78} The properties of the coformers are found to play a vital role in influencing the properties of the parent materials through the formation of cocrystals, although crystal packing has its own influence on the properties of a cocrystal.^{3c,d,74j,79} In majority of the studies, the high melting coformers resulted in high melting cocrystals and the high solubility coformers in high solubility cocrystals and vice-versa.⁷⁹ Thus, cocrystals can impart stability and solubility/dissolution advantage to the materials/APIs. Recently, Nangia et al.^{3c} proposed a model to explain how a coformer can improve the solubility of cocrystals, based on ‘spring and parachute’ model of amorphous forms.⁸⁰ The model also applies to high solubility salts within the factors (electrostatic interactions, hydrogen bonding etc.) that regulate solubility of a salt. According to the model, a cocrystal containing a high soluble coformer can facilitate

faster dissolution of a low soluble component. This happens via the fast release of high soluble coformer into aqueous medium (because of its higher affinity to the latter) that results in the dissociation of cocrystal, thereby leaving behind the low soluble component in an amorphous/randomized state, which understandably leads to an increase in the free energy of the system, ultimately leading to an improvement of solubility/dissolution of the low soluble component (Figure 1.16).^{3c} This model conforms to the ‘coformer solubility rule’^{79b} in that high solubility cofomers will give rise to high solubility cocrystals and vice-versa. If the coformer has low water solubility, it does not dissociate from the lattice easily and in effect can control the solubility/dissolution of the drug. For example, the solubility of an anti lung cancer agent Hexamethylenebisacetamide was tuned through a series of its dicarboxylic acid cocrystals from low soluble to high soluble nature (Figure 1.17),^{74j} using dicarboxylic acids of different solubilities, rendering it to be formulated both as controlled release and immediate release formulations.

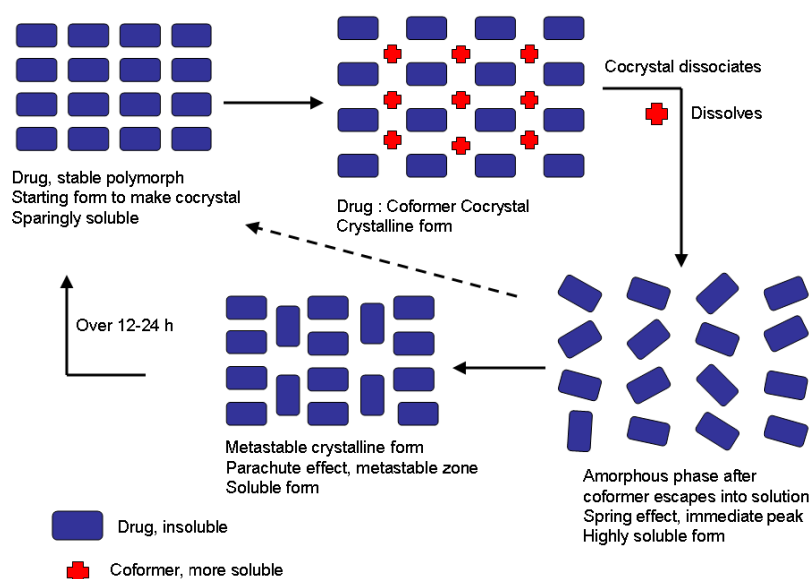


Figure 1.16 Babu and Nangia’s model of solubility enhancement of a drug through a pharmaceutical cocrystal.^{3c}

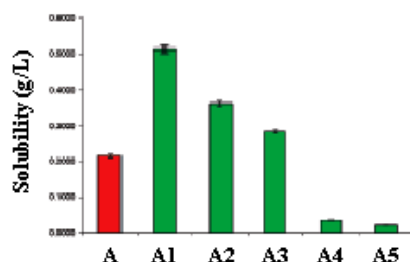


Figure 1.17 Aqueous equilibrium solubilities of Hexamethylenebisacetamide (A) and its cocrystals (A1 to A5) (Ref. 74j).

The advantages of pharmaceutical cocrystals over salt forms are viz. (i) there will be no alteration in the covalent bonds of the API, (ii) ease of making new solid forms of neutral and weakly ionizable APIs that would be incapable of forming salts, (iii) availability of over 3000 GRAS substances as partner molecules contrast to about 30 pharmaceutically acceptable counter-ions in case of salts and (iv) modulation of properties in a desirable way.^{3c,74j} As per conventional wisdom and literature studies, salts tend to improve the solubility of an API.^{25b} But, through cocrystals one can increase or decrease solubility of an API depending on the application as discussed earlier. On the other hand, cocrystals are found to match the properties for which amorphous forms and polymorphs are purposefully developed. The superior dissolution property of amorphous Itraconazole was also observed for its malic acid cocrystal such that it can be an alternative to the existing amorphous formulation.²⁹ The compression stability of the analgesic Paracetamol was achieved by its theophylline cocrystal.^{74e} In similar lines, Carbamazepine–Saccharin cocrystal was reported to have superior properties to the existing crystalline forms of Carbamazepine, an anti-epileptic drug, in terms of stability, dissolution, oral absorption profile etc.⁸¹ Also it is an example of a pharmaceutical cocrystal displaying polymorphism (Figure 1.18).¹⁸ All these attributes fulfill the criteria of ‘pharmaceutical form development’ and ‘intellectual property management’, as they showed promising results in modulating the physico-chemical properties of several APIs vis-a-vis polymorphs, amorphous forms and salts. The former aspect is thus established for cocrystals by now, and the latter aspect is under the purview of the US-FDA which recently published a ‘draft guidance on pharmaceutical cocrystals’⁸² and hopefully a cocrystal formulation of a drug will be a reality in the near future.

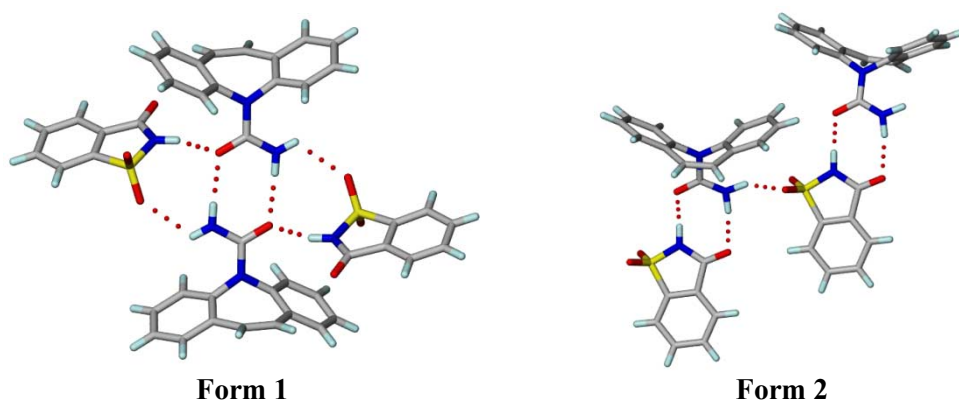


Figure 1.18 Polymorphic cocrystals of Carbamazepine–Saccharin. In form I, saccharin molecules are connected to the amide dimer of carbamazepine through N–H···O interactions. In form II, heterodimers of carbamazepine–saccharin are connected by N–H···O interactions (Adapted from Ref. 18)

1.3.6 Relevance of Eutectic microstructure to Pharmaceutical Solid Design

Eutectics are long known materials and have varied applications in different fields. From the classic sodium chloride-water eutectic mixture^{21a} used for refrigeration and snow removal on roads to more recent energy storage purposes,⁸³ from conventional soldering materials to novel materials in ceramic and glass industry,¹⁶ eutectics presence is felt in daily life and importantly in pharmaceuticals.^{20,27c} A eutectic composition of local anesthetics Lidocaine and Prilocaine (trade name 'EMLA') is used for the enhancement of topical drug delivery and transdermal permeation of lidocaine.⁸⁴ Eutectics are being utilized to enhance solubility of low soluble drugs.²⁰ This is because of the high thermodynamic functions of the eutectics similar to amorphous forms and solid dispersions.²⁰ It is hypothesized that many pharmaceutical solid formulations which undergo manufacturing process operations such as wet granulation and compression lead to unintentional eutectic formation between API and excipient, with the resultant that the material exhibits enhanced solubility.^{20,85} On the other hand, many solid dispersions of drugs exhibit eutectic nature and therefore lead to solubility improvement of drugs.^{20,27,86} Thus, eutectics whether formed intentionally or unintentionally are useful in pharmaceutical applications. But, unlike solid dispersions which are largely amorphous in nature,^{20,27} eutectics being crystalline have less free energy than amorphous materials and thus can confer stability advantage too. Further, some kind of design aspect appears to be there in the formation of eutectics just as cocrystals which are well established by crystal engineering principles. In addition, eutectics were observed to be intermediates on the way to the formation of some cocrystals.⁸⁷ Thus, there exists a relation between cocrystals and eutectics and there is no proper study on the structural aspects that relate these two crystalline solids.

Eutectics/solid solutions and cocrystals are closely related multi-component crystalline solids but with varying proportion of components and degree of interactions. A comparison of these materials was discussed in the earlier sections from which it can be understood that solids with stronger adhesive (hetero) interactions can form cocrystals and those having stronger cohesive (homo/self) interactions can result in solid solutions/eutectics. Eutectics are well studied in inorganic materials¹⁶ where asymmetry, mismatch and misfit between the components induce eutectic structures such that the components retain their lattice structures as solid solutions, which are accommodated in the lattice through weak and imperfect interactions. It should be noticed that a

salt/cocrystal can form between components of dissimilar size and crystal structures, provided the adhesive interactions can overcome the size and mismatch effects. In these cases, the adhesive interactions replace cohesive interactions and lead to distinct bonding interactions between the components and, thus, can direct the crystal packing such that their packing arrangement can be different from that of the parent components. Thus, these materials can exhibit characteristic diffraction and spectroscopic patterns.^{1,2} In contrast, a eutectic exhibits close diffraction and spectroscopic patterns to its component materials since it retains the lattice structure of its parent components as observed in the case of paracetamol–cloperastine hydrochloride drug-drug eutectic (Figure 1.19).⁸⁸

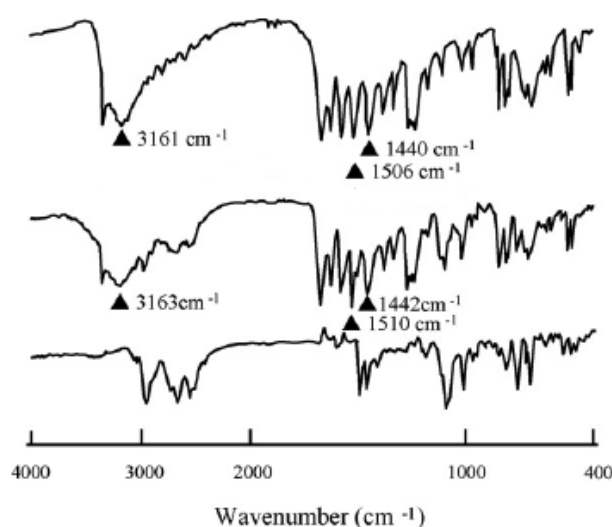


Figure 1.19 FT-IR spectrum of paracetamol–cloperastine hydrochloride eutectic (middle) compared to its parent drugs paracetamol (top) and cloperastine hydrochloride (bottom) shows no significant shift in vibrational frequencies (Adapted from Ref. 88).

Though superficially it appears that the design aspect is lacking in the synthesis of eutectics unlike cocrystals, careful analysis of the plausible supra/hetero molecular interactions will give some hint whether the materials can form eutectics. An illustrative case of cocrystal vs. eutectic formation is exemplified by benzamide–benzoic acid system.^{24b,89} In 2008, Singh et al.^{24b} reported that benzamide and benzoic acid form a eutectic system. Brittain,^{89a} in 2009, claimed the formation of a cocrystal between benzamide and benzoic acid based on slight changes in spectroscopic and diffraction patterns compared to the parent compounds. In 2011, Seaton et al.^{89b} observed that because of the lack of secondary/auxiliary interactions to support the primary interaction of amide⋯acid between benzamide and benzoic acid, growth of a cocrystal lattice is not possible, which supports benzamide–benzoic acid eutectic formation.^{24b} On the other

hand, benzamide forms cocrystals with several benzoic acid derivatives such as pentafluoro benzoic acid,^{89c} 3-nitrobenzoic acid, o-hydroxybenzoic acid (salicylic acid) etc.,^{89b} as evident from the single crystal X-ray diffraction data.⁷⁷ In these cases, the auxiliary interactions augment the primary amide-acid heterosynthons in the growth of the cocrystal lattice (Figure 1.20). Unless there is a single crystal X-diffraction data, it will not be convincing to ascertain cocrystal formation, exemplified by benzamide-benzoic acid system. The lack of strong adhesive interactions led to mismatch and misfit between benzamide and benzoic acid with the resultant that the system forms a eutectic.

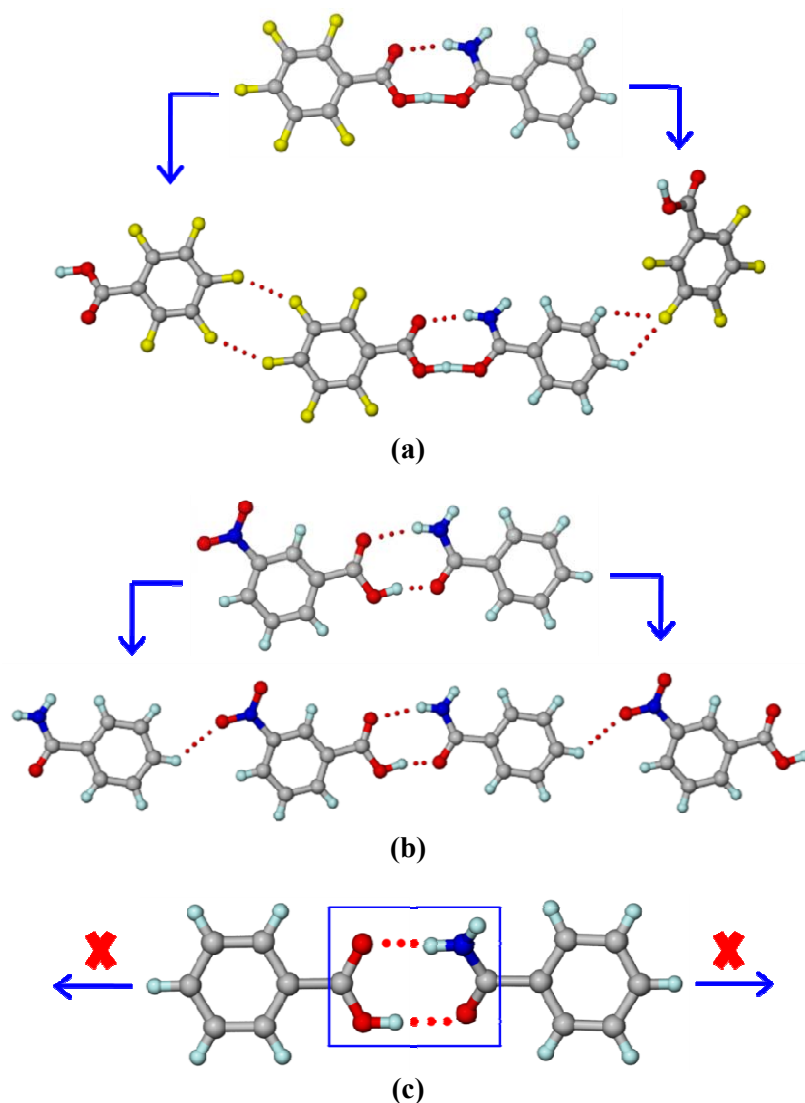


Figure 1.20 Lattice growth in (a) benzamide–pentafluoro benzoic acid and (b) benzamide–3-nitrobenzoic acid cocrystals sustained by amide–acid heterosynthons occurs through C–H \cdots F and F \cdots F interactions in the former and C–H \cdots O interactions in the latter. (c) In benzamide–benzoic acid system, due to the lack of auxiliary interactions that can augment the primary amide–acid interaction, a cocrystal lattice cannot develop and instead a eutectic is resulted (Adapted from Ref. 89).

In all, the benzamide-benzoic acid system elucidates two things with regard to eutectics, the first one is about the design and formation of a eutectic and the second is about its characterization: 1) in the absence of heteromolecular interactions to result in a cocrystal, the system can adjust such that the components are accommodated either substitutionally or interstitially in the crystalline lattice without affecting the overall lattice structure of parent materials to result in a eutectic, and 2) lack of analytical techniques, apart from melting point analysis, that can be used to characterize a eutectic unambiguously.

The understanding of supramolecular chemistry facilitates the rational selection of coformers for cocrystal/eutectic formation and will be useful in modulating the physico-chemical properties of a material, say a drug molecule, in a desirable way. The same cocrystallization experiment can result in the formation of cocrystals/eutectics depending on the interactions (adhesive or cohesive) that dominate.^{87b,89} Cocrystals and eutectics, being unique and novel solid forms, can have their own advantages and applications in different systems and therefore can be useful in ‘pharmaceutical form development’ and ‘intellectual property management’ in drug research and development.

Single crystal X-ray diffraction is the principal technique to characterize crystalline solids, more importantly multi component species since it reveals the identity and bonding interactions and structural organization of the components in the lattice. An adduct structure can be ascertained as being a salt, cocrystal or complex through it.^{1b,90} Even solid solutions can be assessed by the technique.^{22b,91} Generating diffraction quality single crystals is central in this technique. Eutectics are crystalline solids just as the other materials discussed above but are heterogeneous (composed of different solid solutions) unlike the others which are homogeneous. Though they originate via typical crystallization stages such as nucleation,⁹² Ostwald ripening etc.,^{92a} they do not tend to afford diffraction quality single crystals. This can be because of the heterogeneity of component solid solutions and inherent entropy/disorder between the solid solution domains. Even if single crystals of a eutectic can be generated, it will be a tough task to assign the components and their domains and solve the crystal structure. Apart from few inorganic materials (for e.g. Lead-Tin system),¹⁶ eutectic microstructure is poorly understood in organic materials. The lack of crystal structure of a eutectic, despite its long history, emphasizes the difficulty in generating single crystals or solving the crystal

structure of a eutectic, otherwise its lattice structure would have been determined just like other crystalline solids. Of late, the atomic pair distribution function (PDF) analysis, based on scattering and diffraction phenomena, which is known to appraise the local structure of crystalline and amorphous materials, has been proposed^{20,93} to be useful in understanding the eutectic microstructure. The current challenge is to dissect the organic eutectic materials into solid solutions and assess their domain structure as established for inorganic materials. Overall, techniques for the characterization of eutectics are not yet fully developed as quantitative analytical tools.

1.4 Conclusions

Solid state chemistry of drugs in the context of ‘pharmaceutical form development’ and ‘intellectual property management’ was studied. Several aspects of the solid state such as polymorphism, amorphous forms, salts, cocrystals and solid solutions/eutectics were pursued in relation to pharmaceuticals. New definitions are proposed for multi-component systems to correlate cocrystals with eutectics. The factors that influence the formation of cocrystals and eutectics were explored and their utility as novel pharmaceutical solids was investigated. The understanding of the nature and properties of these solids is important both from fundamental and application points of view. Such an understanding will be useful in the rational design of new materials including the pharmaceuticals and therefore to achieve the ultimate goal of modulating the function of materials in a desired way.

An API can give rise to a multitude of crystal forms upon solid form screening viz. polymorphs of the API itself; salts, hydrates/solvates, cocrystals and their polymorphs, solid solutions and eutectics. The inherent differences among these crystalline forms, by virtue of their uniqueness, result in their varied physico-chemical properties which in essence is important for optimal solid form selection and development. Since there is no one-size-fits-all solution to the problems arising from the physico-chemical behavior (e.g. solubility and stability) of different solid forms of drugs (whether polymorphs, amorphs, salts, solvates, cocrystals, eutectics or any complexes) and the properties can vary case-to-case, each of these solid forms can be advantageous for specific and desirable applications in different systems. This thesis deals with the discovery of different solid forms of drugs and their physical form behavior and properties and rationalization of structure-property relationships.

1.5 References

1. (a) S. L. Morrisette, Ö. Almarsson, M. L. Peterson, J. F. Remenar, M. J. Read, A. V. Lemmo, S. Ellis, M. J. Cima and C. R. Gardner, *Adv. Drug Deliv. Rev.*, 2004, **56**, 275; (b) J. Lu and S. Rohani, *Curr. Med. Chem.*, 2009, **16**, 884; (c) G. G. Z. Zhang, D. Law, E. A. Schmitt and Y. Qiu, *Adv. Drug Delivery Rev.*, 2004, **56**, 371.
2. S. R. Byrn, R. R. Pfeiffer and J. G. Stowell, *Solid-State Chemistry of Drugs*; SSCI, West Lafayette, IN, 1999.
3. (a) Y. Qiu; Y. Chen and G. G. Z. Zhang, Eds., *Developing Solid Oral Dosage Forms. Pharmaceutical Theory and Practice*, Academic Press, New York, 2009; (b) C. R. Gardner, C. T. Walsh and Ö. Almarsson, *Nat. Rev. Drug. Disc.*, 2004, **3**, 926; (c) N. J. Babu and A. Nangia, *Cryst. Growth Des.*, 2011, **11**, 2662; (d) N. Schultheiss and A. Newman, *Cryst. Growth Des.*, 2009, **9**, 2950; (e) A. V. Trask, *Mol. Pharmaceutics*, 2007, **4**, 301.
4. (a) D. C. Monkhouse, *Drug Dev. & Indus. Pharm.*, 1984, **10**, 1373; (b) S. R. Byrn, R. R. Pfeiffer, G. Stephenson, D. J. W. Grant and W. B. Gleason, *Chem. Mater.*, 1994, **6**, 1148.
5. (a) R. Hilfiker, Ed., *Polymorphism in the Pharmaceutical Industry*; Wiley-VCH, Weinheim, Germany, 2006; (b) H. G. Brittain, Ed., *Polymorphism in Pharmaceutical Solids*, Informa Healthcare USA Inc., New York, 2009.
6. (a) R. C. Ropp, *Solid State Chemistry*, Elsevier Science B. V., Amsterdam, The Netherlands, 2003; (b) B. B. Laird, *University Chemistry*, McGraw-Hill Companies Inc., New York, 2009; (c) <http://www.grc.nasa.gov/WWW/k-12/airplane/state.html>.
7. (a) B. E. Puckermann, Ed., *Quasicrystals: Types, Systems, and Techniques*, Nova Science Publishers Inc., New York, 2011; (b) <http://www.scientificamerican.com/article.cfm?id=the-2011-nobel-prize-in-chemistry>.
8. (a) L. R. Hilden and K. R. Morris, *J. Pharm. Sci.*, 2004, **93**, 3; (b) L. Yu, *Adv. Drug Deliv. Rev.*, 2001, **48**, 27; (c) R. Zallen, *Amorphous Solids*, John Wiley & Sons Inc., New York, 1983.
9. C. Hammond, *The Basics of Crystallography and Diffraction*, IUCr, Oxford University Press, Oxford, 2009.

10. T. Ishimasa, K. Oyamada, Y. Arichika, E. Nishibori, M. Takata, M. Sakata and K. Kato, *J. Non-Cryst. Solids*, 2004, **167**.
11. J. Robertson and E. P. O'Reilly, *Physical Review B*, 1987, **35**, 2946.
12. (a) http://www.ornl.gov/info/ornlreview/v38_1_05/article17.shtml; (b) <http://www.eurekamagazine.co.uk/article/20099/Amorphous-steel-transforms-electrical-efficiency-.aspx/>.
13. J. Bernstein, *Polymorphism in Molecular Crystals*; Clarendon, Oxford, U. K., 2002.
14. G. Han, P. S. Chow and R. B. H. Tan, *Cryst. Growth Des.*, 2012, **12**, 2213.
15. A. Sarkar and S. Mahapatra, *Cryst. Growth Des.*, 2010, **10**, 2129.
16. D. R. Askeland and P. P. Fulay, *Essentials of Materials Science and Engineering*, 2nd ed., Cengage Learning, 2009.
17. (a) WHO model list of Essential Medicines is available at http://www.who.int/selection_medicines/committees/expert/17/sixteenth_adult_list_en.pdf; (b) http://en.wikipedia.org/wiki/Caffeine_citrate.
18. W. W. Porter III, S. C. Elie and A. J. Matzger, *Cryst. Growth Des.*, 2008, **8**, 14.
19. M. R. Caira, E. W. Pienaar and A. P. Lötter, *Mol. Cryst. Liq. Cryst.*, 1996, **279**, 241.
20. M. D. Moore and P. L. D. Wildfong, *J. Pharm. Innov.*, 2009, **4**, 36.
21. (a) http://en.wikipedia.org/wiki/Eutectic_system;
 (b) <http://www.drugs.com/dict/eutectic.html>;
 (c) <http://oxforddictionaries.com/definition/english/eutectic>;
 (d) <http://www.thefreedictionary.com/eutectic>.
22. (a) http://reference.iucr.org/dictionary/Isomorphous_crystals; (b) N. K. Nath, B. K. Saha and A. Nangia, *New J. Chem.*, 2008, **32**, 1693.
23. http://www.copper.org/applications/cuni/txt_dki.html.
24. (a) S. S. Das, N. P. Singh, T. Agrawal, P. Gupta, S. N. Tiwari and N. B. Singh, *Mol. Cryst. Liq. Cryst.*, 2009, **501**, 107; (b) N. B. Singh, S. S. Das, N. P. Singh and T. Agrawal, *J. Cryst. Growth*, 2008, **310**, 2878; (c) N. B. Singh and P. Kumar, *J. Chem. Eng. Data*, 1989, **34**, 145.
25. (a) A. M. Thayer, *Chem. Eng. News*, 2010, **88**, 13; (b) P. H. Stahl and C. G. Wermuth, Eds., *Handbook of Pharmaceutical Salts, Properties, Selection and Use*, Wiley-VCH, 2002.

26. (a) G. Chessari and A. J. Woodhead, *Drug Disc. Today*, 2009, **14**, 668; (b) C. A. Lipinski, F. Lombardo, B. W. Dominy and P. J. Feeney, *Adv. Drug Deliv. Rev.*, 2001, **46**, 3.
27. (a) T. Vasconcelos, B. Sarmiento and P. Costa, *Drug Disc. Today*, 2007, **12**, 1068; (b) S. Janssens, C. Roberts, E. F. Smith and G. V. Mooter, *Int. J. Pharm.*, 2008, **355**, 100 (c) A. Fahr and X. Liu, *Expert Opin. Drug Deliv.*, 2007, **4**, 403.
28. J. D. Mullins and T. J. Macek, *J. Pharm. Sci.*, 1960, **49**, 245.
29. J. F. Remenar, S. L. Morrisette, M. L. Peterson, B. Moulton, J. M. MacPhee, H. R. Guzmán and Ö. Almarsson, *J. Am. Chem. Soc.*, 2003, **125**, 8456.
30. R. Thakuria and A. Nangia, *CrystEngComm*, 2011, **13**, 1759.
31. W. Yang, K. P. Johnston and R. O. Williams III, *Eur. J. Pharm. BioPharm.*, 2010, **75**, 33.
32. J. Halebian and W. McCrone, *J. Pharm. Sci.*, 1969, **58**, 911.
33. J. Bernstein, *Cryst. Growth Des.*, 2011, **11**, 632.
34. C. G. Wermuth, Ed., *The Practice of Medicinal Chemistry*, 3rd ed., Academic Press, Elsevier Ltd., USA, 2008.
35. (a) <http://oxforddictionaries.com/definition/english/polymorphism>;
(b) [http://en.wikipedia.org/wiki/Polymorphism_\(computer_science\)](http://en.wikipedia.org/wiki/Polymorphism_(computer_science)).
36. N. J. Babu, S. Cherukuvada, R. Thakuria and A. Nangia, *Cryst. Growth Des.*, 2010, **10**, 1979.
37. (a) A. Nangia, *Acc. Chem. Res.*, 2008, **41**, 595; (b) S. Aitipamula and A. Nangia, In *Supramolecular Chemistry: From Molecules to Nanomaterials*, P. A. Gale and J. W. Steed, Eds., John Wiley & Sons Ltd, West Sussex, U. K., 2012, pp. 2957–2974.
38. (a) J. Bauer, S. Spanton, R. Henry, J. Quick, W. Dziki, W. Porter and J. Morris, *Pharm. Res.*, 2001, **18**, 859; (b) S. R. Chemburkar, J. Bauer, K. Deming, H. Spiwek, K. Patel, J. Morris, R. Henry, S. Spanton, W. Dziki, W. Porter, J. Quick, P. Bauer, J. Donaubauer, B. A. Narayanan, M. Soldani, D. Riley, and K. McFarland, *Org. Process Res. Dev.*, 2000, **4**, 413.
39. (a) R. K. R. Jetti, R. Boese, J. A. R. P. Sarma, L. S. Reddy, P. Vishweshwar and G. R. Desiraju, *Angew. Chem., Int. Ed.*, 2003, **42**, 1963; (b) B. R. Sreekanth, P. Vishweshwar, K. Vyas, *Chem. Commun.*, 2007, 2375.
40. J. L. Derissen and P. H. Smit, *Acta Crystallogr.*, 1974, **B30**, 2240.

41. S. R. Vippagunta, H. G. Brittain, D. J. W. Grant, *Adv. Drug Delivery Rev.* **2001**, *48*, 3.
42. S. Cherukuvada, R. Thakuria and A. Nangia, *Cryst. Growth Des.*, 2010, **10**, 3931.
43. (a) B. Sarma, S. Roy and A. Nangia, *Chem. Commun.*, 2006, 4918; (b) N. K. Nath, H. Aggarwal and A. Nangia, *Cryst. Growth Des.*, 2011, **11**, 967.
44. (a) P. K. Thallapally, R. K. R. Jetti, A. K. Katz, H. L. Carrell, K. Singh, K. Lahiri, S. Kotha, R. Boese, G. R. Desiraju, *Angew. Chem. Int. Ed.*, 2004, **43**, 1149; (b) C. -H. Gu, K. Chatterjee, V. Young Jr, D. J. W. Grant, *J. Cryst. Growth*, 2002, **235**, 471.
45. (a) M. D. Lang, A. L. Grzesiak, A. J. Matzger, *J. Am. Chem. Soc.*, 2002, **124**, 14834; (b) C. P. Price, A. L. Grzesiak, A. J. Matzger, *J. Am. Chem. Soc.*, 2005, **127**, 5512.
46. X. Sun, B. A. Garetz, A. S. Myerson, *Cryst. Growth Des.*, 2006, **6**, 684.
47. J. L. Hilden, C. E. Reyes, M. J. Kelm, J. S. Tan, J. G. Stowell, K. R. Morris, *Cryst. Growth Des.*, 2003, **3**, 921.
48. (a) N. K. Nath, S. Nilapwar and A. Nangia, *Cryst. Growth Des.*, 2012, **12**, 1613; (b) P. P. Bag and C. M. Reddy, *Cryst. Growth Des.*, 2012, **12**, 2740.
49. (a) D. Martins, M. Sanselme, O. Houssin, V. Dupray, M. N. Petit, D. Pasquier, C. Diolez and G. Coquerel, *CrystEngComm*, 2012, **14**, 2507; (b) B. Samas, C. Seadeek, A. M. Campeta and B. P. Chekal, *J. Pharm. Sci.*, 2011, **100**, 186; (c) B. Nicolaï, P. Espeau, R. Céolin, M. -A. Perrin, L. Zaske, J. Giovannini and F. Leveiller, *J. Ther. Anal. Cal.*, 2007, **90**, 337.
50. (a) M. Karanam, S. Dev and A. R. Choudhury, *Cryst. Growth Des.*, 2012, **12**, 240; (b) N. K. Nath, S. S. Kumar and A. Nangia, *Cryst. Growth Des.*, 2011, **11**, 4594; (c) P. Sanphui, N. R. Goud, U. B. R. Khandavilli, S. Bhanoth and A. Nangia, *Chem. Commun.*, 2011, **47**, 5013; (d) N. J. Babu, L. S. Reddy, S. Aitipamula and A. Nangia, *Chem. Asian. J.*, 2008, **3**, 1122; (e) G. M. Day, A. V. Trask, W. D. S. Motherwell and W. Jones, *Chem. Commun.*, 2006, 54; (f) S. Ahn, F. Guo, B. M. Kariuki, K. D. M. Harris, *J. Am. Chem. Soc.*, 2006, **128**, 8441; (g) P. Vishweshwar, J. A. McMahon, M. Oliveira, M. L. Peterson and M. J. Zaworotko, *J. Am. Chem. Soc.*, 2005, **127**, 16802.
51. (a) W. F. Ostwald, *Z. Phys. Chem.* **1897**, *22*, 289; (b) J. Nývlt, *Cryst. Res. Technol.*, 1995, **30**, 443; (c) T. Threlfall, *Org. Pro. Res. Dev.*, 2003, **7**, 1017.

52. J. Bernstein, R. J. Davey and J. -O. Henck, *Angew. Chem., Int. Ed.*, 1999, **38**, 3440.
53. (a) R. J. Davey, N. Blagden, S. Righini, H. Alison and E. S. Ferrari, *J. Phys. Chem. B.*, 2002, **106**, 1954; (b) A. Y. Lee, D. Erdemir and A. S. Myerson, *Ann. Rev. Chem. Biomol. Eng.*, 2011, **2**, 259; (c) J. Lu, X. -J. Wang, X. Yang, C. -B. Chung, *Cryst. Growth Des.*, 2007, **7**, 1590; (d) W. Beckmann, *Org. Pro. Res. Dev.*, 2000, **4**, 372; (e) N. Doki, M. Yokota, K. Kido, S. Sasaki and N. Kubota, *Cryst. Growth. Des.*, 2004, **4**, 103.
54. (a) A. Grunenberg, J. -O. Henck and H. W. Siesler, *Int. J. Pharm.*, 1996, **129**, 147; (b) N. Zencirci, T. Gelbrich, D. C. Apperley, R. K. Harris, V. Kahlenberg and U. J. Griesser, *Cryst. Growth. Des.*, 2010, **10**, 302.
55. A. Burger and R. Ramberger, *Mikrochim. Acta II*, 1979, 273.
56. A. Goho, *Science News*, 2004, **166**, 122.
57. (a) H. G. Brittain, *J. Pharm. Sci.*, 2012, **101**, 464; (b) G. Laus, M. Hummel, D. M. Többens, T. Gelbrich, V. Kahlenberg, K. Wurst, U. J. Griesser and H. Schottenberger, *CrystEngComm*, 2011, **13**, 5439; (c) N. J. Babu, L. S. Reddy, S. Aitipamula and A. Nangia, *Chem. Asian J.*, 2008, **3**, 1122; (d) J. D. Holbrey, W. M. Reichert, M. Nieuwenhuyzen, S. Johnston, K. R. Seddon and R. D. Rogers, *Chem. Commun.*, 2003, 1636; (e) T. Endo, T. Morita and K. Nishikawa, *Chem. Phy. Lett.*, 2011, **517**, 162.
58. (a) A. Nangia, *Cryst. Growth. Des.*, 2006, **6**, 2; (b) J. Bernstein, *Cryst. Growth. Des.*, 2005, **5**, 1661; (c) K. R. Seddon, *Cryst. Growth. Des.*, 2004, **4**, 1087.
59. A. Nangia and G. R. Desiraju, *Chem. Commun.*, 1999, 605.
60. (a) S. Roy, N. R. Goud, N. J. Babu, J. Iqbal, A. K. Kruthiventi and A. Nangia, *Cryst. Growth. Des.*, 2008, **8**, 4343; (b) W. Chongcharoen, S. R. Byrn and N. Sutantavibul, *J. Pharm. Sci.*, 2008, **97**, 473; (c) C. Puigjaner, R. Barbas, A. Portell, M. Font-Bardia, X. Alcobe and R. Prohens, *Cryst. Growth. Des.*, 2010, **10**, 2948.
61. <http://www.ich.org/products/guidelines/quality/article/quality-guidelines.html>.
62. R. R. Pfeiffer, K. S. Yang and M. A. Tukker, *J. Pharm. Sci.*, 1970, **59**, 1809.
63. (a) C. Witschi and E. Doelker, *Eur. J. Pharm. Biopharm.*, 1997, **43**, 215; (b) K. Kachrimanis, K. Fucke, M. Noisternig, B. Siebenhaar and U. J. Griesser, *Pharm. Res.*, 2008, **25**, 1440.

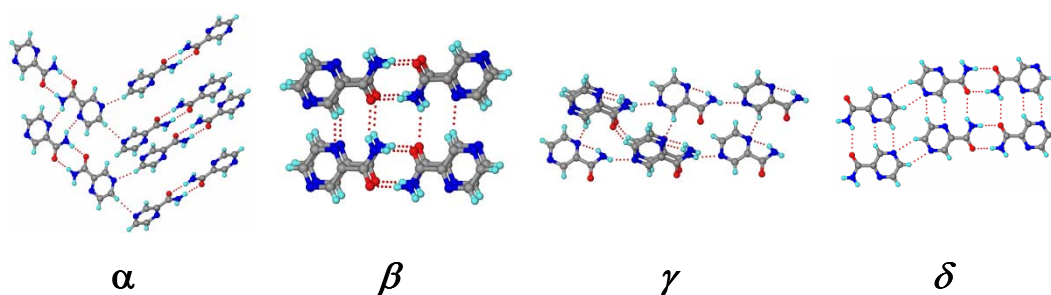
64. (a) R. K. Khankari and D. J. W. Grant, *Thermochim. Acta*, 1995, **248**, 61; (b) E. Shefter and T. Higuchi, *J. Pharm. Sci.*, 1963, **52**, 781.
65. http://www.accessdata.fda.gov/drugsatfda_docs/label/2009/020064s019lbl.pdf.
66. (a) S. M. Berge, L. D. Bighley and D. C. Monkhouse, *J. Pharm. Sci.*, 1977, **66**, 2; (b) R. J. Bastin, M. J. Bowker and B. J. Slater, *Org. Pro. Res. Dev.*, 2000, **4**, 427; (c) G. F. Paulekuhn, J. B. Dressman and C. Saal, *J. Med. Chem.*, 2007, **50**, 6665; (d) A. T. M. Serajuddin, *Adv. Drug Deliv. Rev.*, 2007, **59**, 603.
67. <http://www.chemspider.com/Chemical-Structure.571454.html>.
68. M. Mirmehrabi, S. Rohani, K. S. K. Murthy and B. Radatus, *Int. J. Pharm.*, 2004, **282**, 73.
69. N. A. Kasim, M. Whitehouse, C. Ramachandran, M. Bermejo, H. Lennernäs, H. E. Junginger, S. A. Stavchansky, K. K. Midha, V. P. Shah and G. L. Amidon, *Mol. Pharm.*, 2004, **1**, 85.
70. P. L. Gould, *Int. J. Pharm.*, 1986, **33**, 201.
71. (a) H. Bhutani, S. Singh, K. C. Jindal and A. K. Chakraborti, *J. Pharm. Biomed. Anal.*, 2005, **39**, 892; (b) S. Singh and B. Mohan, *Int. J. Tuberc. Lung Dis.*, 2003, **7**, 298.
72. (a) V. J. Stella and K. W. Nti-Addae, *Adv. Drug Deliv. Rev.*, 2007, **59**, 677; (b) H. Matsumoto, T. Hamawaki, H. Ota, T. Kimura, T. Goto, K. Sano, Y. Hayashi and Y. Kiso, *Bioorg. Med. Chem. Let.*, 2000, **10**, 1227.
73. (a) G. R. Desiraju, *Crystal Engineering: The Design of Organic Solids*, Elsevier, Amsterdam, 1989; (b) G. R. Desiraju, *J. Chem. Sci.*, 2010, **122**, 667.
74. (a) P. Vishweshwar, J. A. McMahon, J. A. Bis and M. J. Zaworotko, *J. Pharm. Sci.*, 2006, **95**, 499; (b) N. Shan and M. J. Zaworotko, *Drug Discov. Today*, 2008, **13**, 440; (c) N. Blagden, M. de Matas, P. T. Gavan and P. York, *Adv. Drug Deliv. Rev.*, 2007, **59**, 617; (d) M. K. Stanton, R. C. Kelly, A. Colletti, Y.-H. Kiang, M. Langley, E. J. Munson, M. L. Peterson, J. Roberts and M. Wells, *J. Pharm. Sci.*, 2010, **99**, 3769; (e) S. Karki, T. Frišćić, L. Fábián, P. R. Laity, G. M. Day and W. Jones, *Adv. Mater.*, 2009, **21**, 3905; (f) D. P. McNamara, S. L. Childs, J. Giordano, A. Iarriccio, J. Cassidy, M. S. Shet, R. Mannion, E. O'Donnell and A. Park, *Pharm. Res.*, 2006, **23**, 1888; (g) S. L. Childs, L. J. Chyall, J. T. Dunlap, V. N. Smolenskaya, B. C. Stahly and G. P. Stahly, *J. Am. Chem. Soc.*, 2004, **126**, 13335; (h) S. L. Childs, N. Rodríguez-Hornedo, L. S. Reddy, A. Jayasankar, C. Maheshwari, L. McCausland, R. Shipplett and B. C.

- Stahly, *CrystEngComm*, 2008, **10**, 856; (i) K. Guo, G. Sadiq, C. Seaton, R. Davey and Q. Yin, *Cryst. Growth Des.*, 2010, **10**, 268; (j) C. B. Aakeröy, S. Forbes and J. Desper, *J. Am. Chem. Soc.*, 2009, **132**, 17048.
75. (a) G. R. Desiraju, *Angew. Chem. Int. Ed.*, 1995, **34**, 2311; (b) A. Nangia and G. R. Desiraju, *Top. Curr. Chem.*, 1998, **198**, 57.
76. R. D. B. Walsh, M. W. Bradner, S. Fleischman, L. A. Morales, B. Moulton, N. Rodríguez-Hornedo and M. J. Zaworotko, *Chem. Commun.*, 2003, 186.
77. Cambridge Structural Database, ver. 5.33, ConQuest 1.14, November 2011 release, May 2012 update; www.ccdc.cam.ac.uk.
78. A. Alhalaweh and S. P. Velaga, *Cryst. Growth Des.*, 2010, **10**, 3302.
79. (a) M. K. Stanton and A. Bak, *Cryst. Growth Des.*, 2008, **8**, 3856; (b) D. J. Good and N. Rodríguez-Hornedo, *Cryst. Growth Des.*, 2009, **9**, 2252.
80. H. R. Guzmán, M. Tawa, Z. Zhang, P. Ratanabanangkoon, P. Shaw, C. R. Gardner, H. Chen, J. -P. Moreau, Ö. Almarsson, J. F. Remenar, *J. Pharm. Sci.*, 2007, **96**, 2686.
81. M. B. Hickey, M. L. Peterson, L. A. Scoppettuolo, S. L. Morrisette, A. Vetter, H. Guzmán, J. F. Remenar, Z. Zhang, M. D. Tawa, S. Haley, M. J. Zaworotko and Ö. Almarsson, *Eur. J. Pharm. Biopharm.*, 2007, **67**, 112.
82. <http://www.fda.gov/downloads/Drugs/.../Guidances/UCM281764.pdf>.
83. (a) A. Karaipekli and A. Sari, *J. Indus. Engi. Chem.*, 2010, **16**, 767; (b) L. Shilei, Z. Neng and F. Guohui, *Ener. Build.*, 2006, **38**, 708.
84. B. F. J. Broberg, H. C. A. Evers, *US Pat.*, 4529601, 1985.
85. M. Bi, S. -J. Hwang and K. R. Morris, *Ther. Acta*, 2003, **404**, 213.
86. S. R. Vippagunta, Z. Wang, S. Hornung and S. L. Krill, *J. Pharm. Sci.*, 2007, **96**, 294.
87. (a) K. Chadwick, R. Davey and W. Cross, *CrystEngComm*, 2007, **9**, 732; (b) E. Lu, N. Rodríguez-Hornedo and R. Suryanarayanan, *CrystEngComm*, 2008, **10**, 665; (c) T. Frišćić and W. Jones, *Cryst. Growth Des.*, 2009, **9**, 1621.
88. Y. Sakata, E. Tanabe, T. Sumikawa, S. Shiraishi, Y. Tokudome and M. Otsuka, *Int. J. Pharm.*, 2007, **335**, 12.
89. (a) H. G. Brittain, *Cryst. Growth Des.*, 2009, **9**, 2942; (b) C. C. Seaton and A. Parkin, *Cryst. Growth Des.*, 2011, **11**, 1502; (c) L. S. Reddy, P. M. Bhatt, R. Banerjee, A. Nangia and G. J. Kruger, *Chem. Asian J.*, 2007, **2**, 505.

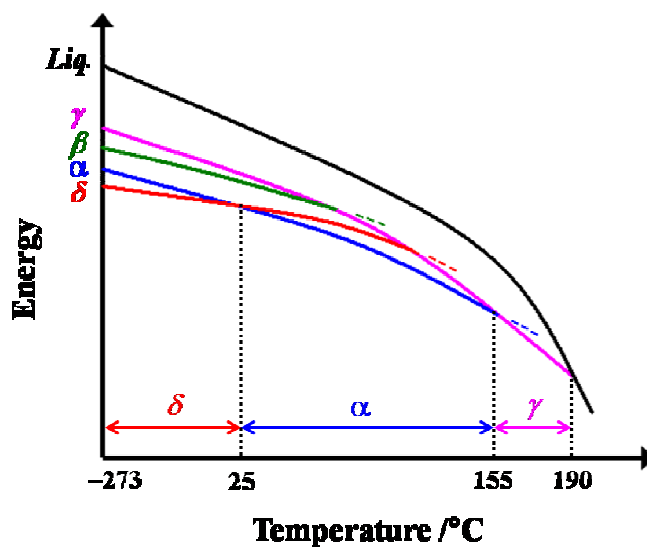
90. (a) S. L. Childs, G. P. Stahly and A. Park, *Mol. Pharmaceutics*, 2007, **4**, 323; (b) B. R. Bhogala, S. Basavoju and A. Nangia, *CrystEngComm*, 2005, **7**, 551.
91. (a) A. A. Bredikhin, Z. A. Bredikhina, D. V. Zakharychev, A. T. Gubaidullin and R. B. Fayzullin, *CrystEngComm*, 2012, **14**, 648; (b) S. K. Chandran, R. Thakuria and A. Nangia, *CrystEngComm*, 2008, **10**, 1891; (c) A. Anthony, M. Jaskolski, A. Nangia and G. R. Desiraju, *Chem. Commun.*, 1998, 2537.
92. (a) S. A. Kukushkin and D. A. Grigoriev, *J. Phy. Chem. Solids*, 2000, **61**, 1337; (b) D. I. Popov, L. L. Regel and W. R. Wilcox, *Cryst. Growth Des.*, 2001, **1**, 313.
93. (a) T. Proffen, K. L. Page, S. E. McLain, B. Clausen, T. W. Darling, J. A. TenCate, S. -Y. Lee and E. Ustundag, *Z. Kristallogr.*, 2005, **220**, 1002; (b) V. Petkov, M. Gateshki, J. Choi, E. G. Gillan and Y. Ren, *J. Mater. Chem.*, 2005, **15**, 4654.

CHAPTER TWO

PYRAZINAMIDE POLYMORPHS



Synthon and Packing Polymorphs



Semi-quantitative free energy vs. temperature diagram to show the polymorphic transformations and relative stability of PZA polymorphs. ‘ δ ’ polymorph is the stable polymorph at -273 °C. ‘ α ’ polymorph has the lowest free energy between 25 - 155 °C; ‘ γ ’ polymorph is stable after 155 °C until it melts at 190 °C.

2.1 Introduction

Pyrazinamide (pyrazine-2-carboxamide, abbreviated as PZA; Figure 2.1) is a frontline anti-tuberculosis drug¹ and is on the WHO Model List of Essential Medicines.² It is administered with Rifampicin, Isoniazid and Ethambutol dihydrochloride in a Fixed Dose Combination (FDC).^{1b,c} Pyrazinamide is a rare example of a conformationally rigid molecule with four polymorphs (namely α , β , γ and δ) reported in literature.³ Theoretically, two possible conformers of PZA have been predicted to exist (Figure 2.1), one with the NH₂ group in the *cis* orientation to the ring nitrogen atom *ortho* to the amide substituent (*E* conformer) and the other one with the NH₂ group in the *trans* orientation (*Z* conformer).⁴ The *E* conformer stabilized by two intramolecular hydrogen bonds adopts a planar structure and renders the molecule rigid (Figure 2.1). It is predicted to be 30 kJ mol⁻¹ lower in energy than the twisted *Z* conformer⁴ and is thus, unsurprisingly, present in all the polymorphs of PZA in the solid state.

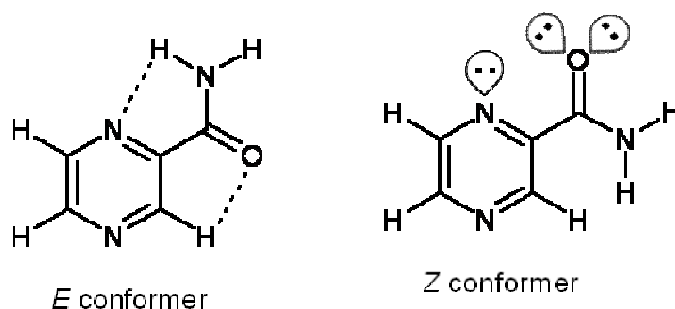


Figure 2.1 Molecular structures of pyrazinamide (PZA) conformers. The planar *E* conformer stabilized by intramolecular hydrogen bonds is found in all the polymorphs of PZA. The amide group in the high energy *Z* conformer is twisted out of the aromatic plane to minimize O–N and H–H repulsions.

Polymorphism was noted in PZA much before this phenomenon became important to the pharmaceutical industry, which is usually taken as the 1990s decade,⁵ when litigation took place surrounding polymorphs 1 and 2 of anti-ulcer drug Ranitidine hydrochloride^{5a-c} and the accidental appearance of a stable, less soluble polymorph II of anti-HIV drug Ritonavir,^{5a-d} which were discussed in Chapter 1. As the polymorphs are unique crystalline entities and exhibit different physico-chemical properties (e.g. melting point, solubility, stability, bioavailability etc.),⁵ a study of all polymorphs of a drug and establishing their stability relationships is as an obligatory step in solid form development.^{5,6} Since polymorphs occur at different levels on the ‘free energy’ surface, inter-conversions are possible and lead to changes in bulk drug properties which in turn

will affect drug efficacy.⁵ Therefore, it is essential to gain adequate understanding of their properties so as to optimize conditions for a desired polymorph and avoid accidental transformations (polymorphic transformations, hydration etc.).⁵ Surprisingly, barring the crystal structures, which date back to the 1960s and 1970s,^{3a-d} there are no studies on PZA polymorphs. Spectroscopic information (IR,^{4a,7} Raman^{4a,7b,8} and ¹³C SSNMR⁹) limited to one polymorph (α polymorph) and bending behavior of two polymorphs (α and δ polymorphs)¹⁰ of PZA are reported. PZA is a highly soluble¹¹ and stable¹² drug, and as such there is no need to improve in its formulation from solubility point of view. Yet, it is a model pharmaceutical system to study phase relationships among the four polymorphs. Recently, Castro et al.¹³ described thermal/stability relationships of PZA polymorphs as $\delta < \alpha < \beta < \gamma$ (i.e. δ polymorph has the lowest Gibbs free energy and hence the stable polymorph) and Borba et al.¹⁴ observed $\alpha \rightarrow \delta$ transformation through an amorphous phase in sub-zero temperatures.

The paper of Castro et al.¹³ appeared when this study was in its final stages. The results obtained in this study suggested a different stability order to that proposed by Castro et al.¹³ Based on the phase transformation studies of PZA polymorphs under different conditions such as polymorphic seeds, mechanical stress (grinding), solvent, storage and temperature, the relative stability order of PZA polymorphs was deduced to be: at absolute zero $\delta < \alpha < \beta < \gamma$, at ambient temperature $\alpha < \delta < \gamma < \beta$, whereas at high temperature $\gamma < \alpha < \delta < \beta$.¹⁵ Apart from this, PZA polymorphs were characterized as belonging to synthon and packing polymorphs by X-ray crystal structure analysis. Furthermore, during solubility study of PZA polymorphs, it was noted that the molar absorptivities (or molar extinction coefficients) of polymorphs differ from each other just as other physico-chemical properties.¹⁵

2.2 Crystallization of PZA Polymorphs

Commercial pyrazinamide (Merck) is in the α polymorphic modification (PXRD pattern match in Figure 2.2) and the material was used for all experiments of this study. All PZA polymorphs except β polymorph were reproduced in macroscopic amounts in pure state as confirmed by their experimental PXRD profile match with that of the calculated lines from the X-ray crystal structures (Figure 2.2); β polymorph in bulk was always contaminated with the γ polymorph in 80:20 ratio (from PXRD profiling, Figure 2.3) and

is represented as $\beta(+\gamma)$ form or mixture.¹⁵ α polymorph was obtained as needles exclusively from water, acetonitrile and nitromethane. β polymorph was obtained in less quantity as $\beta(+\gamma)$ mixture of plate morphology concomitantly with α and δ polymorphs from dioxane and toluene–chloroform solvent mixture (in 1:1 v/v). Crystals of β , γ and δ polymorphs, all with plate morphology, could be separated based on their size and extinction under polarized light. HSM snapshots to depict the differences are shown in Figure 2.9 discussed later. Crystals of β polymorph have better extinction and of γ polymorph were small sized and formed on the surface of β crystals. γ polymorph, which could be obtained exclusively by sublimation and melt crystallization, was also crystallized during attempted co-crystallization of PZA with pyrazinoic acid in water, along with the α polymorph.¹⁵ The crystallization of several/new polymorphs of one of the components in a co-crystallization experiment is not uncommon.¹⁶ δ polymorph was obtained as plates exclusively from benzene and toluene. A summary of the crystallization experiments performed to obtain the polymorphs is given in Table 2.1. In all, the PZA polymorphs were obtained both exclusively and also concomitantly by recrystallization from several solvents with α polymorph as the major polymorph (Table 2.1). Thus, PZA was found to exhibit concomitant polymorphism.^{5e}

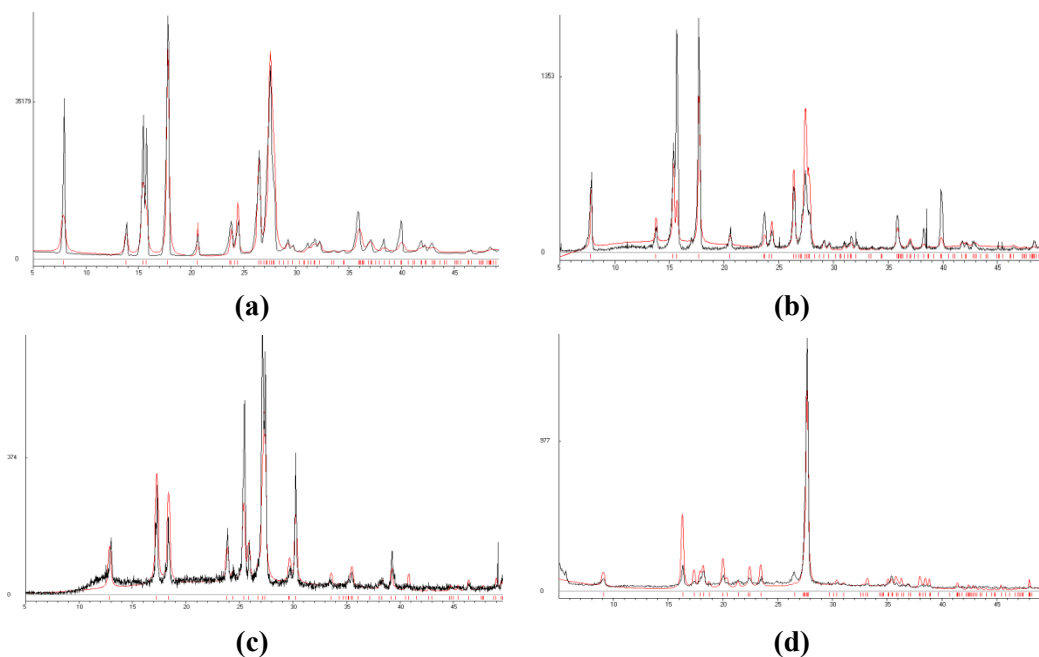


Figure 2.2 Overlay of the calculated lines from X-ray crystal structures (red) and experimental PXRD patterns (black) of PZA polymorphs show peak-to-peak match. α polymorph is the commercial material (a) and crystallized from water (b). γ polymorph (c) crystallized from melt and δ polymorph (d) crystallized from toluene.

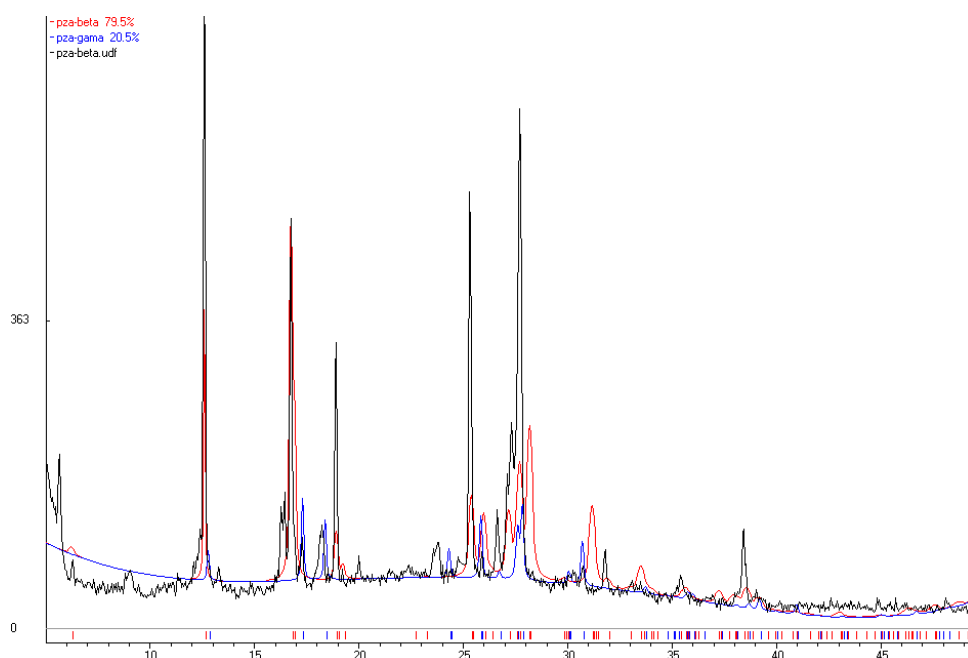


Figure 2.3 Overlay of the calculated X-ray crystal structures of β (red) and γ (blue) polymorphs on the PXRD pattern of the crystalline mixture (black) isolated from dioxane shows 80:20 composition of polymorphs by Rietveld refinement ($R_p = 0.30$).

Table 2.1 Summary of crystallization conditions of PZA polymorphs.

Condition	α	β	γ	δ
water, acetonitrile, nitromethane	√	×	×	×
ethanol	√	√ (only once)	×	√
ethanol (0 °C)	√	×	×	×
methanol	√	×	×	√ (only once)
1-propanol, 2-propanol, n-butanol	√	×	×	×
acetic acid	√	×	×	√
DMF	√	×	×	×
DMSO	√	×	×	×
dichloromethane	√	√ (only once)	×	√
dioxane	√	√	√	√
THF	√	×	×	√
EtOAc	√	×	×	√
chloroform	√	×	×	√
benzene, toluene	×	×	√ (metastable crystallites)*	√
toluene + chloroform	√	√	√	×
sublimation and melt	×	×	√	×
Co-crystallization with pyrazinoic acid	√	×	√	×

* precipitate and redissolve to form plates of δ polymorph upon solvent evaporation.

2.3 Crystal structure analysis of PZA polymorphs

Crystal structures of PZA polymorphs were reported by several groups^{3,13} since 1960s and Nangia et al.^{3g} obtained high quality structures of α and δ polymorphs. The reported crystal structures of γ polymorph have no 3D coordinates for all atoms.^{3b,f} Recently, Castro et al. obtained 3D coordinates of γ polymorph but the structure solved with a high R -factor of 0.1066.¹³ Careful analysis of this structure showed residual electron density of 0.88 eÅ⁻³ which is due to disorder in the structure that was not modeled. In this study, crystal structures of β and γ polymorphs were redetermined and solved to a higher accuracy.¹⁵ The disorder in γ polymorph was solved using both unmodeled and modeled methods (detailed in Experimental Section) which led to an improvement in the R -factor to 0.0796 and 0.0392 respectively. Crystallographic parameters are given in Table 2.2. In the modeled structure, disorder was modeled into two parts with s.o.f. (site occupancy factor) of 0.87 and 0.13. The structural analysis and hydrogen bonding of γ polymorph discussed next deals with the major 87% site occupancy of atoms of the structure.

Table 2.2 Crystallographic parameters.

Polymorph	β	γ (disorder modeled)	γ (disorder unmodeled)
chemical formula	C ₅ H ₅ N ₃ O	C ₅ H ₅ N ₃ O	C ₅ H ₅ N ₃ O
formula weight	123.12	123.12	123.12
crystal system	monoclinic	monoclinic	monoclinic
space group	$P2_1/c$	Pc	Pc
T/K	100(2)	100(2)	100(2)
$a/\text{\AA}$	14.315(2)	7.1756(14)	7.170(3)
$b/\text{\AA}$	3.6238(5)	3.6508(7)	3.6477(15)
$c/\text{\AA}$	10.6158(15)	10.663(2)	10.648(4)
$\alpha/^\circ$	90	90	90
$\beta/^\circ$	101.119(2)	106.337(3)	106.350(6)
$\gamma/^\circ$	90	90	90
Z	4	2	2
$V/\text{\AA}^3$	540.34(13)	268.05(9)	267.21(19)
$D_{\text{calc}}/\text{g cm}^{-3}$	1.513	1.525	1.530
μ/mm^{-1}	0.112	0.113	0.114
reflns. collected	5047	961	2116
unique reflns.	1062	684	960
observed reflns.	1026	681	926
$R_1 [I > 2\sigma(I)]$	0.0340	0.0392	0.0796
$wR_2 [\text{all}]$	0.0880	0.0960	0.2145
goodness-of-fit	1.121	1.116	1.072
CCDC Refcode*	PYZIN18	PYZIN19	PYZIN20

* Ref. 15

All PZA polymorphs have a three-dimensional packing except δ polymorph which is a layered structure (Figure 2.4).¹⁵ α polymorph is a crisscross structure, β is a helical structure and γ polymorph has a corrugated sheet structure. There is π - π stacking in all crystal structures with varying degree of offset (β , three-fourth ring $>$ γ , half ring $>$ α , one-third ring $>$ δ , double bonds overlap) and perpendicular distance between the ring planes (δ , 3.01 $<$ β , 3.22 $<$ γ , 3.33 $<$ α , 3.39 Å). In general, all polymorphs arise from a difference in molecular packing and so referring them as packing polymorphs¹⁷ is a gross classification which does not yield structural details.^{17b} Conformational polymorphism^{5,18} is ruled out in PZA because it is conformationally locked by intramolecular hydrogen bonds (Figure 2.1). Even though the same *E* conformer is manifested in all polymorphs, nevertheless, due to the presence of carboxamide and pyrazine functionalities, variable hydrogen bonding possible between PZA molecules leads to synthon polymorphism.¹⁹

Accordingly, the crystal structures of PZA polymorphs are analyzed in terms of supramolecular synthons.²⁰ At the primary level, the cyclic carboxamide N-H \cdots O dimer synthon is present in α , β and δ polymorphs compared to N-H \cdots N tape in γ polymorph (Figure 2.4). The weak C-H \cdots N and C-H \cdots O interactions are different at the secondary level. Whereas the carboxamide syn NH makes the dimer synthon in α , β and δ polymorphs, these polymorphs differ in their anti NH hydrogen bonding. The α polymorph has N-H \cdots N dimer, the β polymorph has N-H \cdots O hydrogen bond, the γ polymorph has a relatively short intramolecular anti N-H \cdots N bond (with syn N-H \cdots N intermolecular bond), and finally in the δ polymorph the anti NH makes a catemer synthon through long N-H \cdots O contact of 2.62 Å. Hydrogen bond metrics are given in Table 2.3. The centrosymmetric carboxamide N-H \cdots O dimer present in α , β and δ polymorphs has $R_2^2(8)$ graph set notation,²¹ while the carboxamide tape in δ polymorph is a $C(4)R_4^2(8)$ motif (the tape repeat distance is 5.7 Å instead of the usual 5.1 Å).²² The N-H \cdots N cyclic synthon in the α polymorph makes $R_2^2(10)$ ring and the C-H \cdots N cyclic synthon in the δ polymorph makes $R_2^2(6)$ ring. The γ polymorph has an N-H \cdots N tape of $C(6)$ notation. These synthon differences, associated hydrogen bonding, graph set patterns, and different molecular packing arrangements (as shown in Figure 2.4) in the four polymorphs of PZA imply their more accurate classification as synthon and packing polymorphs.¹⁵

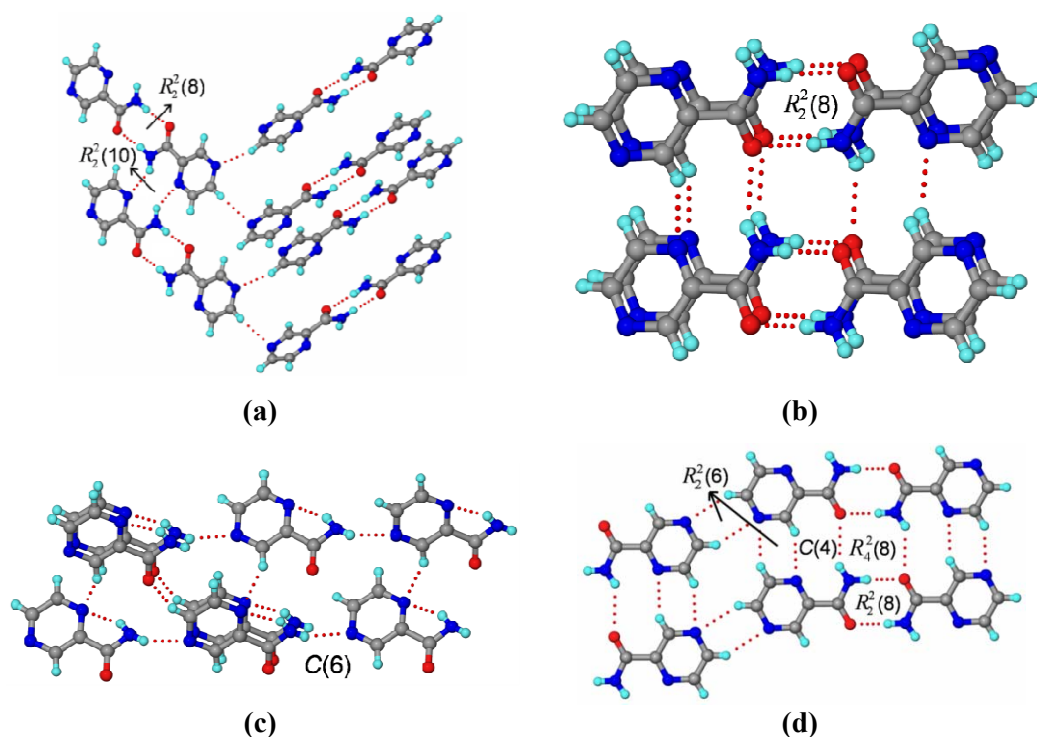


Figure 2.4 (a) In α polymorph, zigzag tapes formed by $R_2^2(8)$ N-H \cdots O and $R_2^2(10)$ N-H \cdots N hydrogen bonds are connected orthogonally to 2_1 screw related tapes through C-H \cdots N interactions in a 3D arrangement. (b) The β polymorph has non-planar $R_2^2(8)$ N-H \cdots O dimers that make a helix along the b -axis through anti N-H \cdots O and C-H \cdots N interactions. (c) In γ polymorph, 1D tapes assembled via N-H \cdots N hydrogen bonds of C(6) notation are connected through C-H \cdots O and C-H \cdots N interactions. (d) Carboxamide tapes formed by $R_2^2(8)$ dimer and C(4) catemer N-H \cdots O synthons and $R_2^2(6)$ C-H \cdots N synthons make 2D sheets that give a layered structure to δ polymorph.

Table 2.3 Hydrogen bonds in crystal structures of PZA polymorphs.^a

Interaction	H \cdots A/Å	D \cdots A/Å	\angle D-H \cdots A/ $^\circ$	Symmetry code
α form^b				
N1-H4 \cdots O1	1.87	2.875(2)	175.9	$1-x, 2-y, -z$ _c
N1-H5 \cdots N2	2.32	2.731(2)	103.2	
N1-H5 \cdots N2	2.29	3.074(2)	133.1	$2-x, 1-y, -z$
C2-H1 \cdots N3	2.52	3.543(2)	157.8	$5/2-x, -1/2+y, 1/2-z$ _c
C3-H3 \cdots O1	2.50	2.809(2)	94.7	
C5-H2 \cdots O1	2.29	3.338(2)	162.0	$1+x, -1+y, z$
β form^d				
N3-H1 \cdots O1	2.35	3.193(2)	140.6	$x, 1/2-y, 1/2+z$ _c
N3-H1 \cdots N1	2.32	2.731(2)	102.8	
N3-H2 \cdots O1	1.89	2.902(2)	175.5	$1-x, -y, 1-z$ _c
C2-H1 \cdots O1	2.46	2.793(1)	95.8	
C3-H3 \cdots N1	2.35	3.334(2)	150.7	$x, 1/2-y, -1/2+z$
C4-H4 \cdots N2	2.48	3.451(2)	149.3	$-x, 1/2+y, 1/2-z$
C5-H5 \cdots N2	2.33	3.326(2)	151.4	$x, 3/2-y, 1/2+z$

		γ form^d		
N3–H3A...N2	2.11	3.051(7)	154.3	$-1+x, 1-y, -1/2+z$
N3–H5...N1	1.79	2.680(7)	144.9	c
C2–H2...N1	2.38	3.372(7)	152.0	$x, 1-y, 1/2+z$
C3–H3...O1	2.35	3.288(7)	143.8	$1+x, -1+y, z$
C4–H2...O1	2.45	2.777(6)	95.7	c
C4–H4...N2	2.37	3.374(7)	153.4	$x, -y, -1/2+z$
		δ form^e		
N1–H5...O1	1.87	2.879(2)	177.6	$3-x, 2-y, -z$
N1–H4...N2	2.30	2.715(2)	103.2	c
N1–H4...O1	2.62	3.460(2)	140.5	$x, 1+y, z$
C2–H1...O1	2.48	2.811(2)	95.8	c
C2–H1...N2	2.41	3.363(2)	146.1	$x, 1+y, z$
C4–H3...N3	2.41	3.363(2)	145.9	$x, -1+y, z$
C3–H2...N3	2.51	3.450(2)	144.6	$1-x, 2-y, 1-z$

^a O–H, N–H and C–H distances are neutron-normalized to 0.983, 1.009 and 1.083 Å respectively; ^b A. Nangia and A. Srinivasulu, CCDC no. PYRZIN15, 2005 (Ref. 3g); ^c Intramolecular hydrogen bond; ^d This work (Ref. 15); ^e A. Nangia and A. Srinivasulu, CCDC no. PYRZIN16, 2005 (Ref. 3g).

2.4 Spectroscopic analysis of PZA polymorphs

All four forms of PZA exhibit distinct N–H and C=O stretching vibrations in FT-IR spectra (Figure 2.5) and N–H first overtone and C=O second overtone bands in FT-NIR spectra (Figure 2.6) and thus can be readily distinguished by their characteristic patterns. The overtones are in concurrence with the fundamental frequencies (Table 2.4). α form has lower stretching frequencies compared to other forms (Table 2.4) which means it has stronger intermolecular hydrogen bonds. Thus, according to the ‘infrared rule’,²³ the structure with higher frequency in bond stretching modes may be assumed to have larger entropy, and so the α form can be assigned as the lower entropy form. Raman spectra of PZA polymorphs are also quite distinct such that the polymorphs can be easily distinguished by their signature peaks (Figure 2.7, Table 2.4).

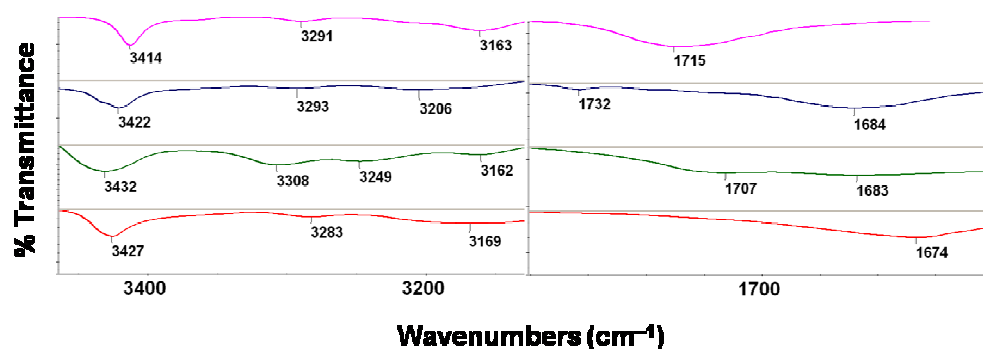


Figure 2.5 FT-IR spectra of α (magenta), β (+ γ) (blue), γ (green) and δ (red) forms show marked differences in the N–H and C=O stretching vibrations.

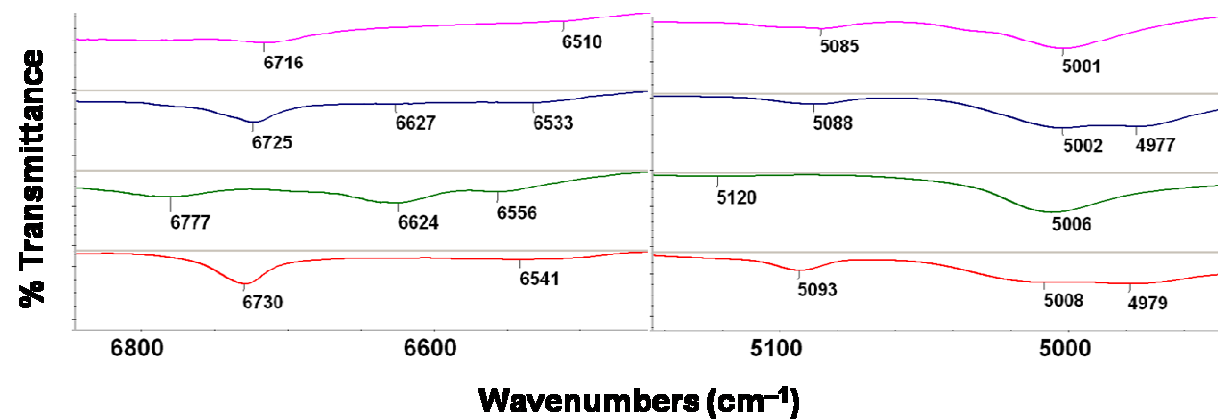


Figure 2.6 FT-NIR spectra of α (magenta), $\beta(+\gamma)$ (blue), γ (green) and δ (red) forms show marked differences in the N–H first overtone and C=O second overtone bands.

Table 2.4 FT-IR (KBr pellet), NIR (KBr pellet), and Raman (neat solid) Spectral Bands of PZA Polymorphs.

Form	IR absorption bands (cm^{-1})		NIR absorption bands (cm^{-1})		Raman scattering bands (cm^{-1})		
	N–H stretch	C=O stretch	N–H stretch 1 st overtone	C=O stretch 2 nd overtone and CONH ₂ combination band	aromatic C–H stretching vibrations	aromatic skeletal vibrations	lattice vibrations
α	3414, 3291, 3163	1715	6716, 6510	5085, 5001	3066, 3053	1489, 1453, 1381	178, 117
$\beta(+\gamma)$	3422, 3293, 3206	1732, 1684	6725, 6627, 6533	5088, 5002, 4977	3059	1479, 1447, 1430, 1389, 1369	182
γ	3432, 3308, 3249, 3162	1707, 1683	6777, 6624, 6556	5120, 5006	3065	1481, 1445, 1392, 1371	180, 138, 122
δ	3427, 3283, 3169	1674	6730, 6541	5093, 5008, 4979	3065	1482, 1444, 1395	180, 140, 123

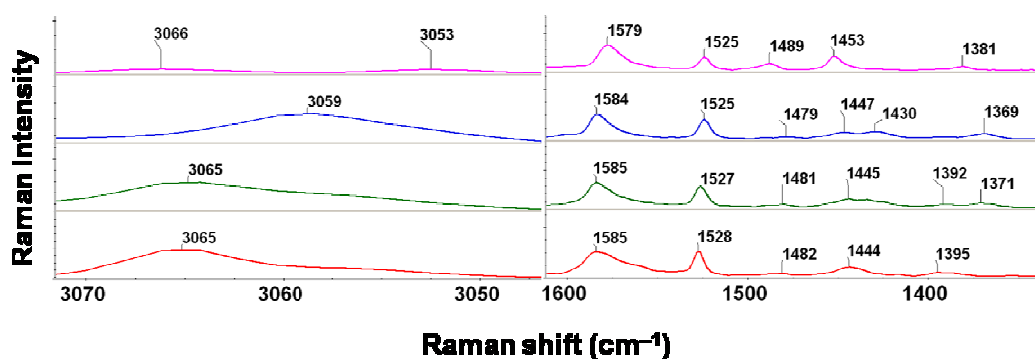


Figure 2.7 FT-Raman spectra of α (magenta), $\beta(+\gamma)$ (blue), γ (green) and δ (red) forms show marked differences in the aromatic C–H and skeletal vibration bands.

2.5 Relative stability of PZA polymorphs

All PZA polymorphs were obtained as concomitant mixtures from several solvents (Table 2.1) and thus they are near-energetic^{5e} and so inter-conversions are possible among them. α , β and δ forms independently convert to γ form through an endothermic phase transition at high temperature, which then melts around 190 °C (Figure 2.8, Table 2.5).^{13,15} The solid-solid phase transformation of α , β and δ forms to γ form and sublimation of γ form was monitored by HSM (Figure 2.9). The three polymorphs are enantiotropically related to γ form with $\delta \rightarrow \gamma$ transition having highest heat of transition followed by $\alpha \rightarrow \gamma$ and then by $\beta \rightarrow \gamma$ transitions (Table 2.5). The stability order proposed by Castro et al., based on the ‘heat of transition rule’,²³ is $\delta < \alpha < \beta < \gamma$, i.e. δ form has the lowest Gibbs free energy and hence the stable polymorph.¹³ Subsequently, Borba et al. observed $\alpha \rightarrow \delta$ transformation through an amorphous phase in sub-zero temperatures and quoted δ form as the stable form of PZA by citing Castro’s paper.¹³ Crystal density²³ and packing fraction of α , β , γ , δ forms ($D_c = 1.496, 1.513, 1.530, 1.521 \text{ g cm}^{-3}$; $C_k = 73.3, 73.8, 74.1, 74.2\%$) also indicate that the δ form is the most stable polymorph. But, the phase transformation occurs at a higher temperature for $\alpha \rightarrow \gamma$ (155 °C) compared to $\delta \rightarrow \gamma$ transition (130 °C), which shows that α form has greater stability than δ form in the 25–155 °C temperature range (Figure 2.8, Table 2.5). The ‘infrared rule’ (discussed earlier) and the crystal lattice energy (U_{latt}) values calculated in Cerius² ($\alpha - 24.88, \beta - 24.20, \gamma - 23.75$ and $\delta - 23.47 \text{ kcal mol}^{-1}$) favor α form to be the most stable polymorph. In general, the stable form is commercialized, unless for special purposes and conditions,^{5b,d,e} to avoid transformations that can take place from production to

consumption. Thus, the existence of commercial PZA in the α form (Figure 2.2) supports it to be the most stable polymorph. In addition, α form crystallized exclusively from several solvents and is the major polymorph of concomitant mixtures (Table 2.1). On the other hand, the transformation of α , β and δ forms to γ form upon heating (sublimation) is not reversible upon cooling (Figure 2.8) and the γ form was found to be stable for 6 months during this study. In essence, α , γ and δ forms each have adequate features to be established as the most stable polymorph. Since the lattice energies of four polymorphs are very close (within 1-2 kcal mol⁻¹), inter-conversions are quite possible among them. Therefore, thermal transformations and thumb rules are not sufficient to establish the stability order of polymorphs. Moreover, the stability profile of polymorphs is temperature-dependent as entropy varies with temperature and thus modify the free energy of the system.^{5e,24} Therefore, the relative stability order of polymorphs at different temperatures should be established, more importantly in the temperature regime and conditions close to real world conditions. In this background, the relative stability of PZA polymorphs is studied in this work.

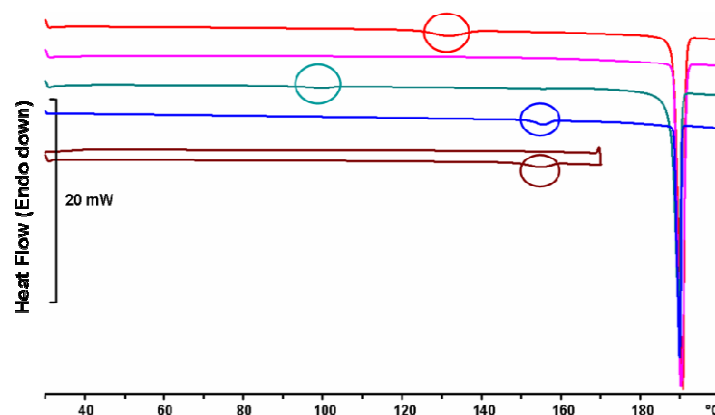


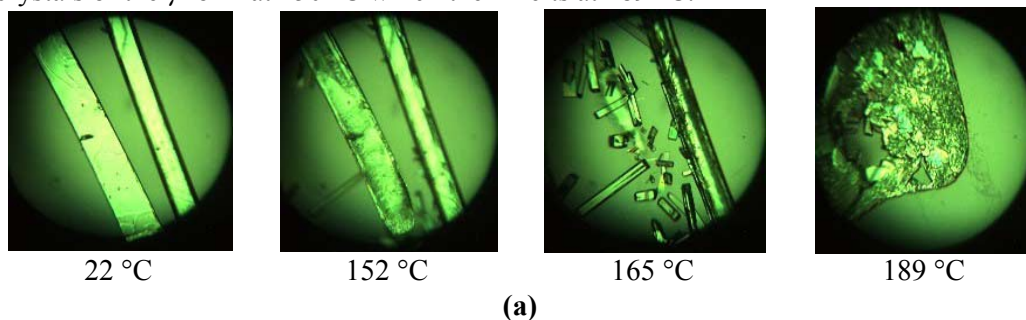
Figure 2.8 DSC of α (blue), $\beta(+\gamma)$ (green), δ (red) to show endothermic phase transition at 155, 99, 131 °C respectively to the γ form. Heat-cool cycle of the α form (brown) shows no reversible transition upon cooling. The high temperature γ phase (magenta) has no phase transition and sharply melts around 189 °C.

Table 2.5 Thermal data on PZA polymorphs.

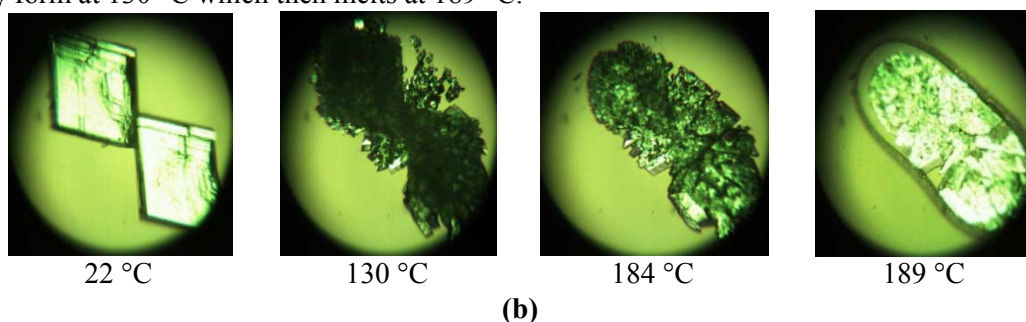
Form	$T_{\text{trs}}/^{\circ}\text{C}$		$\Delta H_{\text{trs}} (\text{kJ mol}^{-1})$		$T_{\text{m}}/^{\circ}\text{C}$		$\Delta H_{\text{fus}} (\text{kJ mol}^{-1})$	
	Reported ^a	This work ^b	Reported ^a	This work ^b	Reported ^a	This work ^b	Reported ^a	This work ^b
α	146.9	155.1	1.63	1.30	188.3	188.5	28.1	26.1
$\beta(+\gamma)$	~95	99.4	^c	0.78	^c	188.6	^c	26.6
γ	^d	^d	^d	^d	187.9	188.5	28.1	26.5
δ	131.6	131.2	2.1	1.66	188.4	188.8	28.0	26.9

^a Ref. 13; ^b Ref. 15; ^c Not reported; ^d Does not transform upon heating.

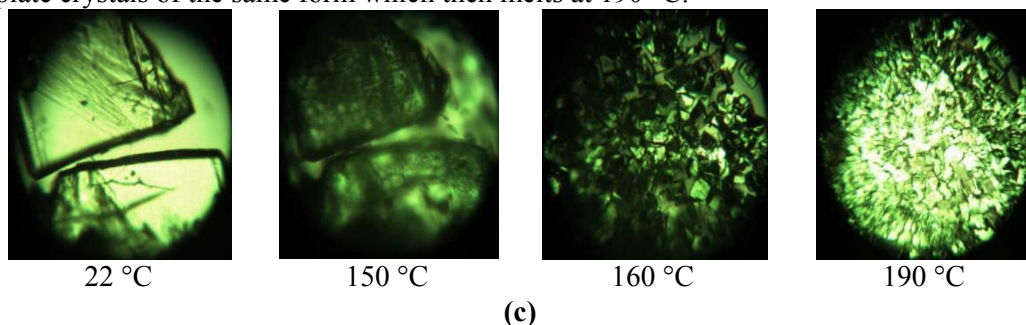
α form – The big needle crystals of the α form give rise to small needle to plate shaped crystals of the γ form at 150 °C which then melts at 189 °C.



β form – The plate crystals of the β form give rise to smaller plate shaped crystals of the γ form at 130 °C which then melts at 189 °C.



γ form – The big plate crystals of the γ form start to sublime at 150 °C and give small plate crystals of the same form which then melts at 190 °C.



δ form – The plate crystals of the δ form give rise to smaller plate shaped crystals of the γ form at 135 °C which then melts at 188 °C.

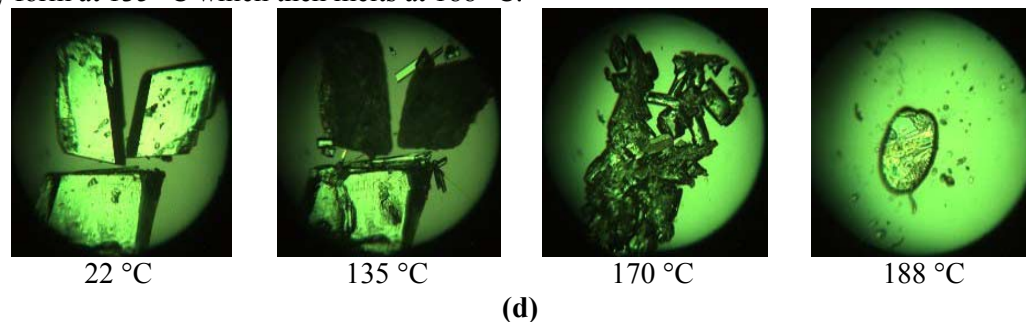


Figure 2.9 HSM snapshots of (a) α , (b) β , (c) γ and (d) δ forms to show the morphology of the polymorphs, solid-solid phase transformation of α , β and δ forms to high temperature γ form, and sublimation of γ form.

2.6 Phase transformation experiments on PZA polymorphs

All PZA polymorphs were subjected to conditions typical of pharmaceutical processing viz. seeding, grinding, solvent and crystallization, and storage at ambient temperature and humidity for one year, each of which are known to bring about polymorphic transformations.^{5,6} Since β form was not obtained in macroscopic amounts (as discussed in Section 2.2), only few experiments were performed on $\beta(+\gamma)$ form/mixture.

2.6.1 Seeding and Grinding

Seeding technique is widely used in drug industry to control nucleation process and also for selective crystallization purposes.²⁵ Intentional seeding is employed for preferential crystallization of desired polymorphs, whether stable or metastable.^{5d,26} On the other hand, unintentional seeding of a polymorph, which is not uncommon and can happen during process conditions and handling, may induce polymorphic transformations in the bulk material.⁵ Milling or grinding is also accounted to induce polymorphic transformations.^{6,27} At first, all four polymorphs of PZA were subjected to solid state grinding (also called neat grinding)^{27c} using a mortar-pestle together with seeds of another form, and the ground material was analyzed by PXRD. Polymorphic mixtures of $\beta(+\gamma)$, γ and δ forms with the α form converted to the α polymorph within 5 min. Polymorphic mixtures of $\beta(+\gamma)$ and γ with the δ form converted to the δ form within 5 min. When pure γ and δ forms were subjected to manual grinding, each polymorph converted to the α form in 45 min. Pure $\beta(+\gamma)$ form converted to the γ form after 5 min of manual grinding which then gave the α form after 45 min. However, the pure α form, when subjected to either manual or mechanical grinding, was found to be stable after 1 h.

2.6.2 Solvent-mediated phase transformation

Solvent or solution-mediated phase transformation is well known to infer stability relationships among polymorphs.²⁸ Liquid-assisted grinding^{27c,29} of the pure forms was carried out using three solvents of different polarity, viz. water, acetonitrile and toluene. This is to see any preferential solvent effect towards the crystallization of a particular polymorph^{27c} as α form crystallized exclusively from water and acetonitrile and δ form from toluene (Table 2.1). Pure $\beta(+\gamma)$, γ and δ forms respectively were taken in mortar-pestle, a few drops of water were added and each form was subjected to grinding separately. Transformation to the α form was complete within 5 min for all cases.

Similarly, pure γ and δ forms when subjected to acetonitrile-assisted grinding converted to the α form in 5 and 30 min respectively. Transformation to the α form by toluene-assisted grinding occurred in 5 min for the γ form and 15 min for the δ form as the starting material. $\beta(+\gamma)$ form could not be analyzed due to insufficient material. α form was found to be stable towards grinding in water, acetonitrile and toluene.

Water is the biological and manufacturing process medium and present as moisture in the air, and hence the correct solvent to study transformation and stability of drug polymorphs. A suspension of each of the pure α , γ and δ forms was stirred in water at 25 °C, the suspensions were filtered at 5 min intervals, and the residue was analyzed by FT-IR. γ form converted to the α form within 20 min of stirring in water (Figure 2.10a). δ form converted to the α form after 30 min of stirring (Figure 2.10b). α form was stable in the aqueous medium for 3 days. Again, $\beta(+\gamma)$ mixture could not be analyzed because of insufficient material. It can be safely assumed that it too would have converted to the α form during slurry crystallization in water because it converted to the α form upon water assisted grinding (as discussed earlier). Solution crystallization experiments in water further confirmed the transformation of each of the $\beta(+\gamma)$, γ and δ forms to the α form. When a saturated aqueous solution of each of $\beta(+\gamma)$, γ and δ forms was allowed to crystallize, the α form was obtained in all cases. These results demonstrate the α form¹⁵ as the most stable polymorph compared to other forms including the δ form, which was ascribed the most stable form by Castro et al.¹³

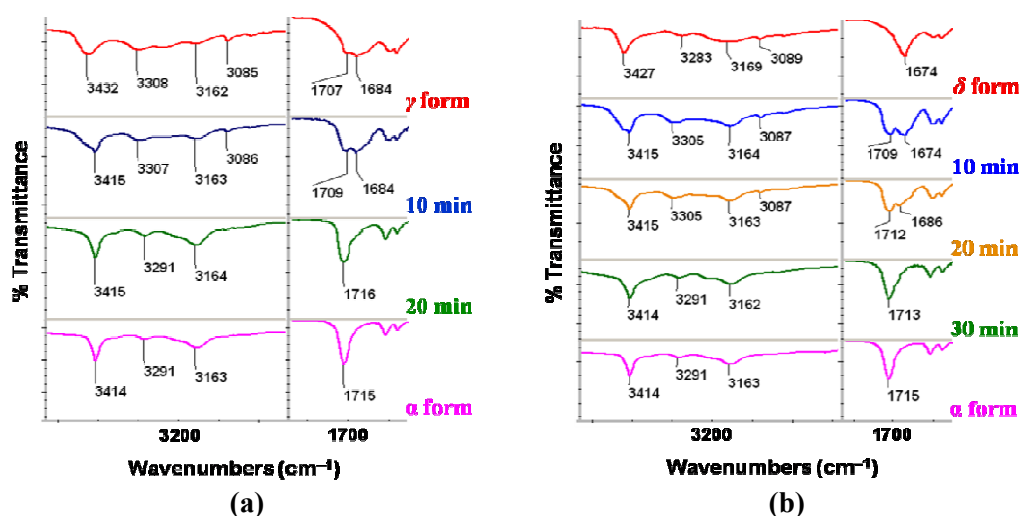


Figure 2.10 Phase transformation of (a) γ and (b) δ forms to α form upon slurry crystallization in water monitored by FT-IR spectroscopy.

2.6.3 Storage

All four forms were stored for a year at ambient temperature (varying between 15–40 °C) and relative humidity (varying between 30–70% RH) and PXRD of the polymorphs was recorded periodically to detect any transformations. α , $\beta(+\gamma)$ and δ forms were found to be stable but γ form which was stable up to 6 months converted to α form upon prolonged storage. A saturated solution of PZA in benzene or toluene yielded a visible precipitate within 2 h of crystallization which disappeared into solution when left undisturbed and formed plate-shaped crystals after complete evaporation of the solvent (Table 2.1). The precipitated material was found to be the γ form by PXRD and the crystals are of the δ form. The precipitated material (γ form) obtained in the above experiment converted to the δ form after 6 months storage at ambient conditions, but not to the α form. A plausible reason for this transformation could be due to the seeds of the δ form formed during the primary nucleation in solution which facilitated the transformation upon storage. Thus, the γ form converted to α and δ forms after a long time in independent experiments.

2.7 Solubility and Dissolution study of PZA polymorphs

PZA is a highly water soluble drug (22 mg ml⁻¹)¹¹ but solubility values are not reported for its polymorphs. Equilibrium solubility experiments (detailed in Experimental Section) on γ and δ forms in water led to their transformation to α form independently (same procedure as discussed above in the context of water-mediated phase transformation) and hence their solubilities could not be evaluated. Only the solubility of α form, which is stable to equilibrium solubility conditions (high supersaturation, agitation, long duration, typically 24 h), was measured and the value matched with the reported one (22 mg ml⁻¹). For metastable forms like γ and δ forms, a calculated parameter called ‘apparent solubility’^{16c,30} is used to estimate the solubility difference between stable and metastable forms. Apparent solubility is distinct from equilibrium solubility which is reached at infinite time and is deduced from intrinsic dissolution rates (IDRs) of stable and metastable forms as follows.

$$\text{Solubility}_{\text{metastable}} = \text{Solubility}_{\text{stable}} (\text{IDR}_{\text{metastable}} / \text{IDR}_{\text{stable}})^{30}$$

Dissolution testing of α , γ and δ forms was carried out by the rotating disk intrinsic dissolution rate (DIDR) method³¹ in water at 37 °C using USP Apparatus II

(detailed in Experimental Section). About 57% of the α form, 75% of the γ form and 56% of the δ form were dissolved in one hour and their intrinsic dissolution rates (IDRs) are 2.07, 2.78 and 2.05 $\text{mg cm}^{-2} \text{min}^{-1}$ respectively (Figure 2.11). Based on the IDRs, the apparent solubility of γ and δ forms is calculated to be 29.5 and 21.8 mg ml^{-1} respectively. Thus, the metastable γ form is 1.3 times more soluble than the stable α form and the δ form is almost same as the α form. There was partial conversion of δ and complete conversion of γ to the α form when the undissolved material was analyzed by PXRD after the dissolution experiment.

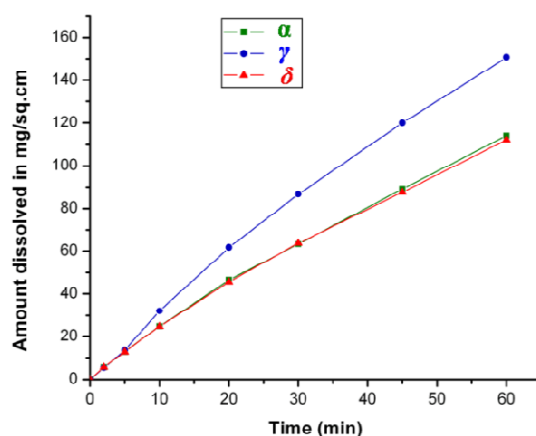


Figure 2.11 Dissolution curves of PZA polymorphs in water.

During the making of calibration curves of the PZA polymorphs for solubility/dissolution study, it was noted that the molar absorptivities (or molar extinction coefficients, designated as ' ϵ ') of polymorphs differ from each other just as other physico-chemical properties.¹⁵ α , γ and δ forms have the same λ_{max} of 269 nm but their ' ϵ ' values are different (Table 2.6). The calibration solutions of the three forms were incubated separately for 24 hours and ' ϵ ' values were determined at different intervals to observe any changes in line with the phase transformation of polymorphs. The molar absorptivities were found to be quite constant within the error limits. Molar absorptivities of a compound are known to vary with change in λ values, solvent and solute.³² But, with respect to polymorphs of a compound, there is no proper study on this phenomenon. Since, molar absorptivity is a solution property and as other solution properties such as solubility and dissolution behaviors of polymorphs vary,⁵ it is not unusual that polymorphs can exhibit different molar absorptivities. The variation of ' ϵ ' between polymorphs can be due to differences in hydrogen bonding/solvation motifs of the polymorphs in solution.

Table 2.6 Molar extinction coefficients (ϵ , mL mg⁻¹ cm⁻¹) of PZA polymorphs.

Polymorph	0 h	1 h	2 h	3 h	24 h	ϵ_{av}^*
α	67.18	67.34	67.12	67.06	67.27	67.19
γ	71.75	71.55	72.04	71.5	71.05	71.45
δ	66.35	66.63	66.29	66.62	66.31	66.44

* Average value was taken for calculation of solubility and IDR.

2.8 Discussion

α form was found to be the most stable of the four polymorphs of PZA in the real world conditions.¹⁵ Transformation of all polymorphs to the stable α form occurred with the transformation being accelerated by seeds and solvent. A summary of the phase transformation experiments executed was depicted in Figure 2.12. Though the δ form has higher enthalpy of transformation (Table 2.5), higher density and packing fraction than the α form, it converted to the latter when subjected to conditions commonplace in pharmaceutical processing. The conversion of δ form to α form is rationalized by their closeness in lattice energy and the layered structure of δ form transforming to the 3D packing of α form. Second, both $\beta(+\gamma)$ and γ forms transform to the δ form but only in the presence of the latter polymorph as seeds. Otherwise they convert to the α form. The transformation of δ to α form is slow compared to that of other forms demonstrating that the δ form is the next stable form at ambient conditions. Surprisingly, the $\beta(+\gamma)$ mixture converts to the metastable γ form upon grinding, which in turn converts to the stable α form on further grinding. There was no effect of the γ form on the stability of the $\beta(+\gamma)$ mixture at ambient conditions, but transformation to the γ form upon grinding suggests that it is an intermediate on the way to the stable α form. Unless there is no activation (by grinding or heating), $\beta(+\gamma)$ mixture remains stable since the bulk of it is β form.

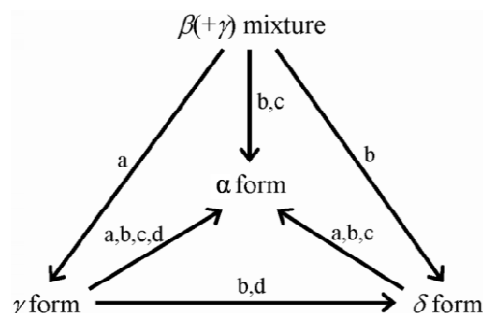


Figure 2.12 Phase transformation experiments of PZA polymorphs: a – grinding of pure form; b – grinding together with the seeds of the final form; c – water assisted grinding of pure form; d – storage for 6 months.

A semi-quantitative free energy vs. temperature (E–T) diagram^{5e,24} consistent with the transformations of polymorphs is shown in Figure 2.13. According to the E–T diagram, the relative phase energy ranking at absolute zero (–273 °C) is $\delta < \alpha < \beta < \gamma$, between 25–155 °C is $\alpha < \delta < \gamma < \beta$, whereas after 155 °C it is $\gamma < \alpha < \delta < \beta$, i.e. α form is the thermodynamic form in real world conditions.¹⁵ The E–T diagram establishes the δ form as the stable polymorph at absolute zero temperature consistent with Castro’s report (based on ‘heat of transition rule’),¹³ ‘density rule’²³ and also Borba’s report¹⁴ on the crystallization of the δ form from α under cryogenic conditions. But, it becomes metastable at room temperature (i.e. attains high free energy through entropy component with increase in temperature) and therefore converts to α form since the latter has lower free energy at ambient temperature. Since β and γ forms are at higher level on the free energy scale (Figure 2.13), it is unsurprising that they convert to α and δ forms independently. The stability of $\beta(+\gamma)$ mixture in storage but its conversion to the γ form upon grinding is rationalized by their close energy at 25 °C. The conversion of α , β , and δ forms to the high enthalpic γ form is also due to entropy effect at high temperature where the γ form becomes the low energy form as per the E–T diagram.

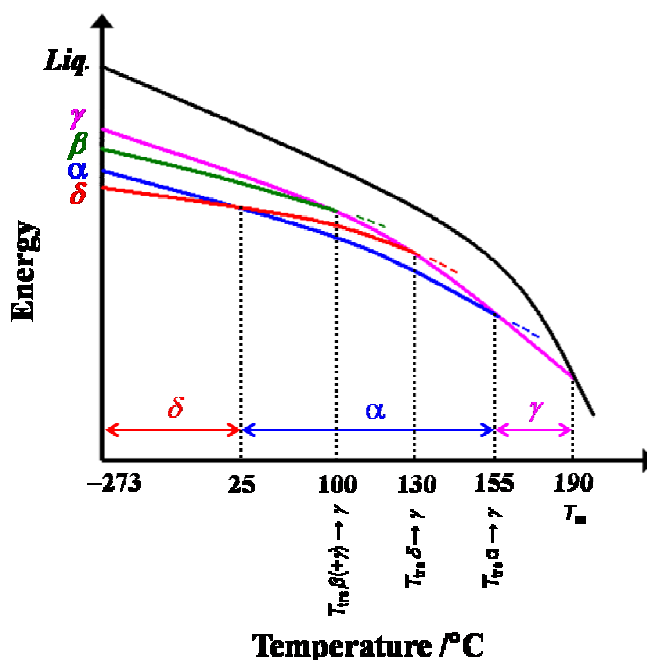


Figure 2.13 Semi-quantitative energy vs. temperature diagram shows the relative stability and polymorphic transformations of PZA polymorphs. At –273 °C δ has the lowest free energy. Between 25–155 °C, α form is the stable form; all other forms convert to it under laboratory experiments of grinding and slurry transformation. γ form is stable after 155 °C until it melts at 190 °C.

2.9 Conclusions

The relative stability of pyrazinamide polymorphs is studied and a control over polymorph crystallization is achieved through seeding, grinding and solvent-mediated processes.¹⁵ PZA is an interesting example wherein the ‘heat of transition and density rules’²³ indicate one form (δ form) and the ‘infrared rule’²³ infers another form (α form) as the most stable polymorph. Grinding and solvent-mediated phase transformation experiments establish α form as the most stable polymorph of PZA under ambient conditions. The high transition temperature (155 °C for $\alpha \rightarrow \gamma$ compared to 130 °C of $\delta \rightarrow \gamma$ transition), commercial occurrence and wide crystallization rationalize the thermodynamic nature of α form at 25 °C. Whereas the transformation of α to δ form was shown to occur in sub-zero temperatures,¹⁴ the reverse phenomenon, namely, conversion of δ to α form is the transformation in the real world conditions.¹⁵ This study shows that thermal transformations and thumb rules alone are not sufficient to establish the complete stability profile of polymorphs. The entropy component plays a crucial role in changing the free energy of a system and thus can shift the balance from one polymorph to another polymorph with respect to temperature.^{5c,24} This work highlights the importance of establishing the relative stability of drug polymorphs in the real world conditions typical of pharmaceutical processing (seeding, grinding, crystallization etc.) and storage conditions (normal temperature and relative humidity of 25 °C and 50% respectively), through a classic example.

2.10 Experimental Section

Materials and Methods: Commercially available Pyrazinamide (Merck) and Pyrazinoic acid (Acros) were used without further purification. All other chemicals were of analytical or chromatographic grade. Water filtered through a double deionized purification system (Milli Q Plus Water System from Millipore Co., USA) was used for experiments.

Preparation of Polymorphs: Polymorphs were obtained upon evaporative crystallization in various solvents at different temperatures as given in Table 2.1. Typically, 50 mg saturated solutions of PZA were made, warmed and left for slow evaporation and the resulting polymorphs were physically isolated from several batches and thus macroscopic amounts were obtained. Co-crystallization of pyrazinamide (50

mg) with pyrazinoic acid (50 mg) in 1:1 ratio was done in 6 mL water. γ form was isolated by filtration of precipitate formed from saturated benzene/toluene solutions.

Polymorphic Transformation Experiments: Grinding experiments were done on 50 mg scale. 10% polymorph was used in seeding experiments. A Wig-L-Bug type mixer mill equipped with a 5 mL stainless steel grinding jar and SS balls of 4 mm diameter was used for mechanical grinding. Slurry experiments were carried out on 200 mg of the polymorph in 5 mL water (aqueous solubility of PZA is 22 mg mL⁻¹).¹¹ 100 mg of each polymorph was stored in a tightly capped glass bottle in the dark for periodic stability testing at ambient conditions.

X-ray Crystallography: X-ray reflections on β and γ polymorphs were collected at 100 K on Bruker SMART-APEX CCD diffractometer equipped with a graphite monochromator and Mo-K α ($\lambda = 0.71073$ Å) fine-focus sealed tube. Data reduction was performed using Bruker SAINT software.³³ Intensities were corrected for absorption using SADABS.³⁴ The β structure was solved and refined using SHELX-97³⁵ with anisotropic displacement parameters for non-H atoms. Hydrogen atoms on O and N were experimentally located in difference electron density maps. All C–H atoms were fixed geometrically using HFIX command in SHELX-TL.³⁶ The disorder in the γ structure was solved and refined using both unmodeled and modeled methods. In the unmodeled structure, the site occupancy of all the atoms was 100% with anisotropic displacement parameters for non-H atoms, but in the modeled structure the disorder was modeled for all the heavy atoms with isotropic displacement parameters using the PART command and assigning s.o.f. (site occupancy factor) of 0.87 and 0.13 for the two parts using the FVAR command.³⁴ DFIX, DANG and FLAT commands³⁵ were used to stabilize the disorder. All hydrogen atoms were geometrically fixed and have same the s.o.f. with respect to the heavy atoms connected. The final CIF files and hydrogen bond geometries were validated in PLATON.³⁷ X-Seed³⁸ was used to prepare packing diagrams.

Powder X-ray Diffraction: Powder X-ray diffraction of all the samples were recorded on PANalytical 1830 (Philips Analytical) diffractometer using Cu-K α X-radiation ($\lambda = 1.54056$ Å) at 35 kV and 25 mA. Diffraction patterns were collected over 2θ range of 5–50° at a scan rate of 1° min⁻¹. Powder Cell 2.4 was used for Rietveld refinement.³⁹

Vibrational Spectroscopy: Nicolet 6700 FT-IR spectrometer with an NXR FT-Raman Module was used to record IR, NIR and Raman spectra. IR and NIR spectra were

recorded on samples dispersed in KBr pellets. Raman spectra were recorded on solid samples contained in standard NMR diameter tubes or on compressed samples contained in a gold-coated sample holder.

Thermal Analysis: DSC was performed on Mettler Toledo DSC 822e module. Samples were placed in crimped but vented aluminum sample pans. The typical sample size is 3-4 mg, temperature range is 30-200 °C @ 5 °C min⁻¹. Samples were purged by a stream of dry nitrogen flowing at 150 mL min⁻¹. HSM was performed on a Wagner & Munz PolythermA Hot Stage and Heiztisch microscope. A Moticam 1000 (1.3 MP) camera supported by Motic Image Plus 2.0 ML software is used to record images.

Computations: Lattice energies were computed in Cerius² using the COMPASS force field.⁴⁰ Crystal structures were minimized (U_{latt}) by allowing small variations in the cell parameters but not gross differences between the calculated and experimental crystal lattice.

Equilibrium solubility and Intrinsic dissolution measurements: Prior to solubility and dissolution measurements, calibration curves of each of the polymorphs were obtained and their molar extinction coefficients were determined spectrophotometrically on a Thermo Scientific Evolution 300 UV-Vis spectrometer based on the absorbance at 269 nm (Table 2.6). The respective molar extinction coefficients of the polymorphs were used to estimate solubility and dissolution values. Equilibrium solubility was determined in water at 25 °C using the shake-flask method.⁴¹ 200 mg of the powdered polymorph was added to 5 mL water and the resulting suspension was stirred at 25 °C for 24 h. The suspension was equilibrated for one hour and then filtered through 2.5 µm Whatman filter paper. The concentration of the solution thus obtained was determined spectrophotometrically after appropriate dilution using the respective molar extinction coefficients. IDR measurements were carried on a USP certified Electrolab TDT-08L Dissolution Tester. 100 mg of the polymorph was taken in the intrinsic attachment and compressed to a 0.5 cm² disk (also called tablet or pellet) using a hydraulic press at a pressure of 2.5 ton inch⁻² for 5 min. The intrinsic attachment was placed in a jar of 900 mL water at 37 °C and rotated at 50 rpm. Aliquots of 5 mL were collected at specific time intervals and concentration of the aliquots was determined spectrophotometrically. The linear region of the dissolution profile (regression >0.99) was used to determine the IDR of the polymorph as [slope of the amount dissolved ÷ surface area of the disk] per unit time. There is no polymorphic transformation upon compression.

2.11 References

1. (a) M. -T. Gutierrez-Lugo and C. A. Bewley, *J. Med. Chem.*, 2008, **51**, 2606; (b) E. Catalani, *Int. J. Tuberc. Lung Dis.*, 1999, **3**, S289; (c) Y. Zhang and D. Mitchison, *Int. J. Tuberc. Lung Dis.*, 2003, **7**, 6.
2. WHO model list of Essential Medicines is available at http://www.who.int/selection_medicines/committees/expert/17/sixteenth_adult_list_en.pdf.
3. (a) Y. Takaki, Y. Sasada and T. Watanabe, *Acta Crystallogr.*, 1960, **13**, 693 (α form: CCDC no. PYRZIN); (b) C. Tamura, Y. Sasada, H. Kuwano, *Acta Crystallogr.*, 1961, **14**, 693 (γ form: CCDC no. PYRZIN03); (c) G. Ro and H. Sorum, *Acta Crystallogr.*, 1972, **B28**, 991 (β form: CCDC no. PYRZIN01); (d) G. Ro and H. Sorum, *Acta Crystallogr.*, 1972, **B28**, 1677 (δ form: CCDC no. PYRZIN02); (e) R. K. Tiwari, T. C. Patel and T. P. Singh, *Indian J. Phys.*, 1982, **A56**, 413 (α form: CCDC no. PYRZIN14); (f) K. Nakata and Y. Takaki, *Mem. Osaka Kyoiku Univ. Ser. III*, 1987, **36**, 93 (γ form: CCDC no. PYRZIN05); (g) A. Nangia and A. Srinivasulu, *Private Communication*, **2005** (α form - CCDC no. PYRZIN15; δ form - CCDC no. PYRZIN16).
4. (a) V. Chis, A. Pirnau, T. Jurca, M. Vasilescu, S. Simon, O. Cozar and L. David, *Chem. Phys.*, 2005, **316**, 153. (b) O. Cozar, V. Chis, L. David and M. Baias, *J. Optoelectron. Adv. Mater.*, 2006, **8**, 164.
5. (a) A. Nangia, *J. Ind. Inst. Sci.*, 2007, **87**, 133; (b) R. Hilfiker, Ed. *Polymorphism in the Pharmaceutical Industry*; Wiley-VCH, Weinheim, Germany, 2006; (c) A. Goho, *Science News*, 2004, **166**, 122; (d) S. R. Chemburkar, J. Bauer, K. Deming, H. Spiwek, K. Patel, J. Morris, R. Henry, S. Spanton, W. Dziki, W. Porter, J. Quick, P. Bauer, J. Donaubauer, B. A. Narayanan, M. Soldani, D. Riley, and K. McFarland, *Org. Process Res. Dev.*, 2000, **4**, 413; (e) J. Bernstein, *Polymorphism in Molecular Crystals*; Clarendon, Oxford, U. K., 2002. (f) S. Aitipamula and A. Nangia, In *Supramolecular Chemistry: From Molecules to Nanomaterials*, P. A. Gale and J. W. Steed, Eds., John Wiley & Sons Ltd, West Sussex, U. K., 2012, pp. 2957–2974.
6. (a) S. R. Byrn, R. R. Pfeiffer and J. G. Stowell, *Solid-State Chemistry of Drugs*; SSCI, West Lafayette, IN, 1999; (b) G. G. Z. Zhang, D. Law, E. A. Schmitt and Y. Qiu, *Adv. Drug Delivery Rev.*, 2004, **56**, 371.

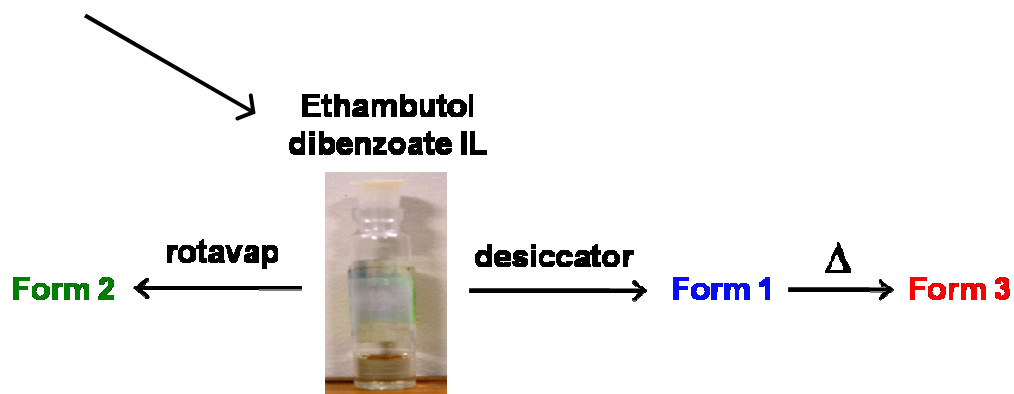
7. (a) S. Yoshida, *Chem. Pharm. Bull.*, 1963, **11**, 628; (b) M. J. M. Delgado, F. Marquez, M. I. Suero and J. I. Marcos, *Spectrosc. Lett.*, 1988, **21**, 841; (c) A. K. Kalkar, N. M. Bhosekar and S. T. Kshirsagar, *Spectrochim. Acta Part A*, 1989, **45**, 635; (d) S. J. Akyuz, *J. Mol. Struct.*, 2003, **651**, 541; (e) A. Favila, M. Gallo and D. Glossman-Mitnik, *J. Mol. Modeling*, 2007, **13**, 505; (f) S. Gunasekaran, E. Sailatha, *Indian J. Pure Appl. Phys.*, 2009, **47**, 259.
8. M. A. S. Goher and F. A. Mautner, *Polyhedron*, 2000, **19**, 601.
9. D. H. Barich, J. S. Clawson, D. Stueber, M. Strohmeier, R. J. Pugmire and D. M. Grant, *J. Phys. Chem. A*, 2000, **106**, 11375.
10. C. M. Reddy, K. A. Padmanabhan, G. R. Desiraju, *Cryst. Growth Des.*, 2006, **6**, 2720.
11. C. Becker, J. B. Dressman, G. L. Amidon, H. E. Junginger, S. Kopp, K. K. Midha, V.P. Shah, S. Stavchansky and D. M. Barends, *J. Pharm. Sci.*, 2008, **97**, 3709.
12. G. G. Gallo and P. Radaelli, In *Analytical Profiles of Drug Substances*, K. Florey, Ed., Academic Press, London, 1976, pp. 467–513.
13. R. A. E. Castro, T. M. R. Maria, A. O. L. Évora, J. C. Feiteira, M. R. Silva, A. M. Beja, J. Canotilho and M. E. S. Eusébio, *Cryst. Growth Des.*, 2010, **10**, 274 (γ form: CCDC no. 754512).
14. A. Borba, M. Albrecht, A. Gomez-Zavaglia, M. A. Suhm and R. Fausto, *J. Phys. Chem. A*, 2010, **114**, 151.
15. S. Cherukuvada, R. Thakuria and A. Nangia, *Cryst. Growth Des.*, 2010, **10**, 3931.
16. (a) M. Karanam, S. Dev and A. R. Choudhury, *Cryst. Growth Des.*, 2012, **12**, 240; (b) N. K. Nath, S. S. Kumar and A. Nangia, *Cryst. Growth Des.*, 2011, **11**, 4594; (c) P. Sanphui, N. R. Goud, U. B. R. Khandavilli, S. Bhanoth and A. Nangia, *Chem. Commun.*, 2011, **47**, 5013; (d) N. J. Babu, L. S. Reddy, S. Aitipamula and A. Nangia, *Chem. Asian. J.*, 2008, **3**, 1122; (e) G. M. Day, A. V. Trask, W. D. S. Motherwell and W. Jones, *Chem. Commun.*, 2006, 54; (f) S. Ahn, F. Guo, B. M. Kariuki, K. D. M. Harris, *J. Am. Chem. Soc.*, 2006, **128**, 8441; (g) P. Vishweshwar, J. A. McMahon, M. Oliveira, M. L. Peterson and M. J. Zaworotko, *J. Am. Chem. Soc.*, 2005, **127**, 16802.

17. (a) S. R. Vippagunta, H. G. Brittain, D. J. W. Grant, *Adv. Drug Delivery Rev.* **2001**, *48*, 3; (b) N. J. Babu, S. Cherukuvada, R. Thakuria and A. Nangia, *Cryst. Growth Des.*, 2010, **10**, 1979.
18. A. Nangia, *Acc. Chem. Res.*, 2008, **41**, 595.
19. (a) R. K. R. Jetti, R. Boese, J. A. R. P. Sarma, L. S. Reddy, P. Vishweshwar and G. R. Desiraju, *Angew. Chem., Int. Ed.*, 2003, **42**, 1963; (b) B. R. Sreekanth, P. Vishweshwar, K. Vyas, *Chem. Commun.*, 2007, 2375.
20. (a) G. R. Desiraju, *Angew. Chem., Int. Ed. Engl.*, 1995, **34**, 2311; (b) A. Nangia and G. R. Desiraju, *Top. Curr. Chem.*, 1998, **198**, 57.
21. (a) M. C. Etter, J. C. MacDonald and J. Bernstein, *Acta Crystallogr.*, 1990, **B46**, 256. (b) J. Bernstein, R. E. Davis, L. Shimon, N.-L. Chang, *Angew. Chem., Int. Ed.*, 1995, **34**, 1555.
22. (a) L. Leiserowitz and A. T. Hagler, *Proc. R. Soc. Lond.*, 1983, **388**, 133. (b) S. S. Kuduva, D. Bläser, R. Boese and G. R. Desiraju, *J. Org. Chem.*, 2001, **66**, 1621.
23. A. Burger and R. Ramberger, *Mikrochim. Acta II*, 1979, 273.
24. (a) A. Grunenberg, J. -O. Henck and H. W. Siesler, *Int. J. Pharm.*, 1996, **129**, 147; (b) N. Zencirci, T. Gelbrich, D. C. Apperley, R. K. Harris, V. Kahlenberg and U. J. Griesser, *Cryst. Growth. Des.*, 2010, **10**, 302.
25. (a) S. K. Heffels and M. Kind, Seeding Technology – An Underestimated Critical Success Factor for Crystallisation. *Proceedings of the 14th International Symposium on Industrial Crystallisation*; Cambridge, 1999; (b) W. Beckmann, K. Nickisch and U. Budde, *Org. Pro. Res. & Dev.*, 1998, **2**, 298.
26. (a) W. Beckmann, *Org. Pro. Res. & Dev.*, 2000, **4**, 372; (b) W. Beckmann, W. Otto and U. Budde, *Org. Pro. Res. & Dev.*, 2001, **5**, 387; (c) H. Miura, T. Ushio, K. Nagai, D. Fujimoto, Z. Lepp, H. Takahashi and R. Tamura, *Cryst. Growth. Des.*, 2003, **3**, 959; (d) N. Doki, M. Yokota, K. Kido, S. Sasaki and N. Kubota, *Cryst. Growth. Des.*, 2004, **4**, 103; (e) N. Zencirci, T. Gelbrich, V. Kahlenberg and U. J. Griesser, *Cryst. Growth. Des.*, 2009, **9**, 3444.
27. (a) N. Chieng, Z. Zujovic, G. Bowmaker, T. Rades and D. Saville, *Int. J. Pharm.*, 2006, **327**, 36. (b) S. -Yang Lin, C. -Hung Hsu and W. -Ting Ke, *Int. J. Pharm.*, 2010, **396**, 83. (c) A. V. Trask, N. Shan, W. D. S. Motherwell, W. Jones, S. Feng,; R. B. H. Tan and K. J. Carpenter, *Chem. Commun.*, 2005, 880.

28. (a) P. T. Cardew and R. J. Davey, *Proc. R. Soc. Lond. A*, 1985, **398**, 415; (b) N. R. Hornedo and D. Murphy, *J. Pharm. Sci.*, 1999, **88**, 651; (c) C. -H. Gu, V. Young Jr., D. J. W. Grant, *J. Pharm. Sci.*, 2001, **90**, 1878; (d) R. J. Davey, N. Blagden, S. Righini, H. Alison and E. S. Ferrari, *J. Phys. Chem. B*, 2002, **106**, 1954; (e) E. S. Ferrari, R. J. Davey, *Cryst. Growth Des.*, 2004, **4**, 1061.
29. A. V. Trask W. D. S. Motherwell and W. Jones, *Chem. Commun.*, 2004, 890.
30. (a) N. J. Babu and A. Nangia, *Cryst. Growth Des.*, 2011, **17**, 2662; (b) V. M. Rao, R. Sanghvi and H. (Jim) Zhu, In *Developing Solid Oral Dosage Forms. Pharmaceutical Theory and Practice*, Y. Qiu; Y. Chen and G. G. Z. Zhang, Eds., Academic Press, New York, 2009, pp. 319–340; (c) R. K. Khankari and D. J. W. Grant, *Thermo. Acta*, 1995, **248**, 61; (d) M. Otsuka, R. Teraoka and Y. Matsuda, *Chem. Pharm. Bull.*, 1991, **39**, 2667.
31. L. X. Yu, S. Carlin, G. L. Amidon and A. S. Hussain, *Int. J. Pharmaceutics*, 2004, **270**, 221.
32. K. A. Connors, *Binding Constants: The Measurement of Molecular Complex Stability*, John Wiley & Sons Inc., New York, 1987.
33. SAINT-Plus, version 6.45, Bruker AXS Inc.: Madison, Wisconsin, 2003.
34. G. M. Sheldrick, SADABS, Program for Empirical Absorption Correction of Area Detector Data, University of Göttingen, Göttingen, Germany, 1997.
35. G. M. Sheldrick, SHELX-97, University of Göttingen, Göttingen, Germany, 1997.
36. SMART (Version 5.625) and SHELX-TL (Version 6.12), Bruker AXS Inc.: Madison, Wisconsin, 2000.
37. A. L. Spek, PLATON, A Multipurpose Crystallographic Tool, Utrecht University, Utrecht, Netherlands, 2002.
38. L. J. Barbour, X-Seed, Graphical Interface to SHELX-97 and POV-Ray, University of Missouri-Columbia, USA, 1999.
39. PowderCell, Program for structure visualization, powder pattern calculation and profile fitting, <http://www.ccp14.ac.uk/index.html>.
40. Cerius2, Ver. 4, <http://accelrys.com/>.
41. A. Glomme, J. März and J. B. Dressman, *J. Pharm. Sci.*, 2005, **94**, 1.

CHAPTER THREE

SALTS AND IONIC LIQUIDS OF ETHAMBUTOL



Salt screen of Ethambutol resulted in the formation of both hygroscopic salts and ionic liquids. Ethambutol dibenzoate (EDB) ionic liquid crystallized as trimorphs in different conditions. EDB form 2 and 3 converted to form 1 upon mechano-chemical grinding. The thermodynamic polymorph at room temperature is form 1 and at high temperature is form 3.

3.1 Introduction

Ethambutol (abbreviated as EMB; Figure 3.1) is a frontline anti-tuberculosis drug administered with Rifampicin, Isoniazid and Pyrazinamide in Fixed Dose Combination (FDC).¹ It is a chiral basic drug (Figure 3.1) with the S,S-enantiomer therapeutically active whereas R,R-form is inactive.² It is administered as a dihydrochloride salt (S,S-EDH) in the drug formulation which is synonymously used to represent the drug.^{1,3} Anti-TB FDC products are reported to be unstable due to drug-drug interactions between the component drugs.³ The hygroscopicity of ethambutol dihydrochloride catalyzes the degradation of rifampicin and isoniazid in the FDC formulation, resulting in the instability and loss of potency of the FDC products upon storage.^{1a,3} As a consequence, individual drugs of the FDC formulation are separately coated with polymers to avoid mutual interaction and water uptake and then blended to make up the final product formulation.⁴ Several salts of ethambutol base (dinitrate,⁵ dihydrobromide,⁶ oxalate pentahydrate⁷ and metal salts⁸) including a drug-drug methane sulfonic acid salt with isoniazid⁹ are reported but with no property studies. The dihydrochloride salt was reported to be tetramorphic,¹⁰ but neither the X-ray crystal structure nor any polymorphs of the S,S-form of ethambutol base are reported so far. The reported crystal structures of EMB and its salts (dihydrochloride, dinitrate, dibromide, oxalate pentahydrate) in the Cambridge Structural Database (CSD)¹¹ have no mention of the 'Flack parameter'¹² and hence their absolute configuration is ambiguous. In this work, crystal structures of ethambutol and ethambutol dihydrochloride were redetermined and their absolute configuration is deduced as S,S-chirality.

In addition, salt screen of EMB with different salt formers (Figure 3.1) was undertaken in this study with the intent of obtaining less hygroscopic salts and thus provide alternatives to the existing hydrochloride salt formulation. But, the study resulted in the formation of several salts and ionic liquids all of which were found to be hygroscopic. Ionic liquids (ILs) are salts with a melting point below 100 °C¹³ and if they are liquids at room temperature (m.p. \leq 25 °C) then they are termed as 'room temperature ionic liquids' (RTILs).¹⁴ A total of twelve salts, including seven ionic liquids, were obtained and their hygroscopicity was assessed by visual inspection for some cases and Karl Fischer (KF) titration for other cases. Out of the five salts (sulfate, dimesylate, ditosylate, dibesylate and fumarate), only two gave diffraction quality single crystals and their X-ray structures were determined (dimesylate and fumarate hydrate).

Among the seven ionic liquids, only two crystallized (dibenzoate and adipate) and the remaining five (dinicotinate, disalicylate, di-4-aminosalicylate, disaccharinate and succinate salts) never crystallized in the experimental conditions studied. Ethambutol dibenzoate (abbreviated as EDB) was crystallized as trimorphs in different conditions and characterized by DSC, PXRD and spectroscopy.¹⁵ Although few ionic liquids are reported to be polymorphic, this is the first example of an API ionic liquid exhibiting polymorphism.¹⁵

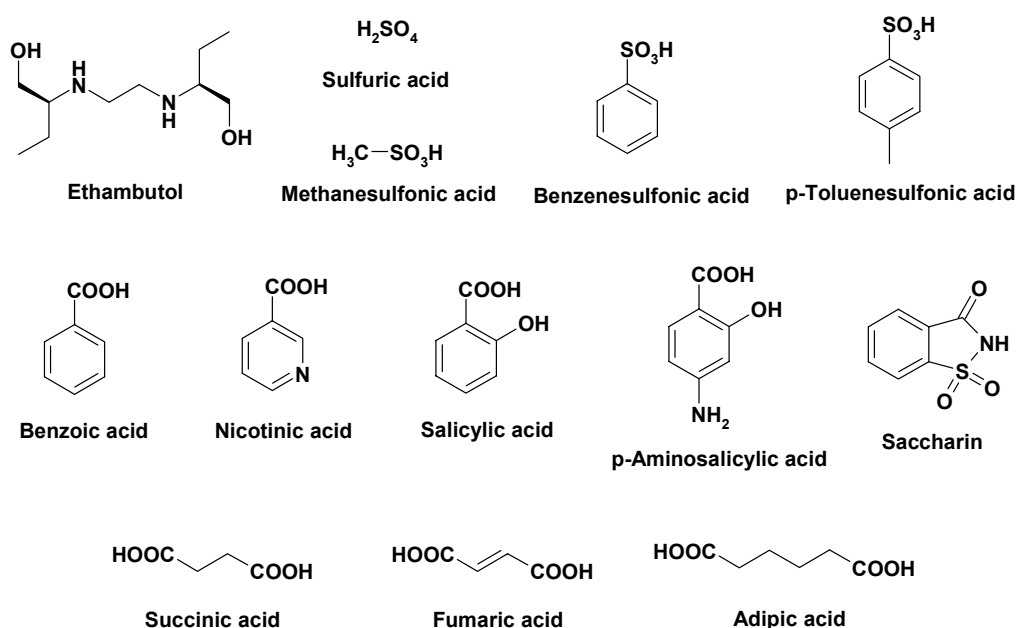


Figure 3.1 Molecular structures of ethambutol and salt formers used in this study.

3.2 Synthesis and Characterization of Salts and Ionic Liquids

Salts were prepared by different methods such as (i) direct reaction of base (EMB) and acid (salt former) in a suitable solvent, (ii) co-grinding,¹⁶ (iii) co-melting, (iv) solution crystallization etc. A summary of the experiments carried out to obtain the salts is given in Table 3.1 and the details are provided in Experimental Section. Both solid and liquid products were obtained from these experiments (Table 3.1). A total of twelve salts were obtained, of which seven are ionic liquids (dibenzoate,¹⁵ adipate, dinicotinate, disalicylate, di-4-aminosalicylate, disaccharinate and succinate) and five are high melting salts (sulfate, dimesylate, ditosylate, dibesylate and fumarate). All of them were found to be hygroscopic and hence few salts/ionic liquids were obtained in liquid state. In all, four salts viz. dimesylate, ditosylate, dibesylate and fumarate were obtained in solid form in majority of the experiments; sulfate, adipate and dibenzoate (trimorphs)¹⁵ salts were

Table 3.1 Summary of salt screening experiments.

S. No.	Salt	Synthesis by direct reaction of base and acid	Solution crystallization in MeOH/ EtOH	Crystallization in desiccator	Crystallization in rotavapor	Co-grinding	Co-melting	Storage of physical mixture
1	Ethambutol sulfate	solid product ^a	viscous liquid	viscous liquid	semisolid	viscous liquid ^b	^c	^c
2	Ethambutol dimesylate	solid product ^d	solid ^d ; single crystals at -20 °C	solid ^d	solid ^d	slight sticky solid ^b	-do-	-do-
3	Ethambutol dibesylate	-do-	solid ^d	-do-	liquid extract	viscous liquid ^e	semisolid	semisolid
4	Ethambutol ditosylate	-do-	-do-	-do-	solid ^d	-do-	-do-	-do-
5	Ethambutol dibenzoate ^f	no product	viscous liquid	crystallized to form 1 ^f	crystallized to form 2 ^f	-do-	form 1 ^f	-do-
6	Ethambutol dinicotinate	-do-	-do-	semisolid	liquid extract	-do-	^g	-do-
7	Ethambutol disalicylate	-do-	-do-	viscous liquid	-do-	-do-	semisolid	-do-
8	Ethambutol di-4-aminosalicylate	-do-	-do-	-do-	-do-	-do-	^h	-do-
9	Ethambutol disaccharinate	-do-	-do-	semisolid	-do-	-do-	semisolid	-do-
10	Ethambutol succinate	semisolid product	-do-	-do-	-do-	-do-	-do-	-do-
11	Ethambutol fumarate (hydrate)	-do-	solid ^d	single crystals	semisolid	-do-	^h	-do-
12	Ethambutol adipate	solid product ^a	viscous liquid	semisolid	-do-	-do-	semisolid	-do-

^a tends to liquefy during extraction upon concomitant exposure to atmospheric moisture, crystalline solid by PXRD; ^b acetone assisted grinding;

^c not feasible as the acid component is liquid; ^d crystalline solid by PXRD; ^e neat grinding and concomitant exposure to atmospheric moisture; ^f Ref 15;

^g decomposed solid melt; ^h not done since the acid component decomposes upon melting.

crystallized in few conditions; whereas dinicotinate, disalicylate, di-4-aminosalicylate, disaccharinate and succinate did not crystallize (Table 3.1). Among the crystallized salts/ionic liquids, only two gave diffraction quality single crystals and their X-ray structures were determined (dimesylate and fumarate hydrate). Thermal (DSC & TGA), spectroscopic (FT-IR and ss-NMR) and PXRD analysis established the integrity of other salts/ionic liquids and also the trimorphic dibenzoate ionic liquid¹⁵ (discussed later).

3.2.1 X-ray Crystal structures

Since ethambutol is a chiral molecule (Figure 3.1), absolute structure determination with a reliable 'Flack parameter' is necessary to ascertain its chirality.¹² The reported crystal structures of EMB and its salts (dihydrochloride, dinitrate, dibromide, oxalate pentahydrate) in the CSD have no mention of the Flack parameter.¹¹ It seems that the absolute configuration of the enantiomers is inferred from the known configuration of their respective starting materials. In this study, the absolute structures of EMB and few salts were deduced through reliable Flack parameter values. When the Flack parameter of a crystal structure is close to '0', it means the absolute configuration of the structure is properly assigned, and when it is close to '1', then the opposite enantiomer is solved.^{12,17} In this work, the starting material is commercial ethambutol dihydrochloride (EDH) salt from which base (EMB) was extracted and used for all the experiments. There is no information on the stereochemistry of the salt on the commercial package label. Hence, at first, single crystals of the salt were grown (from a methanol solution at -20 °C) to determine its chirality. The dihydrochloride salt structure solved in S,S configuration with a Flack parameter value of 0.09(17) and its structural features are same as the reported structures^{10,18} (CCDC Refcodes – CURJEE02 & CURJEE)¹¹ (Figure 3.2). X-ray crystallographic parameters are listed in Table 3.2 and hydrogen bonds in Table 3.3. The extracted base from commercial dihydrochloride salt was used to prepare ethambutol dimesylate salt. A methanolic solution of dimesylate salt kept at -20 °C afforded single crystals and its X-ray crystal structure was determined. It also solved in S,S configuration with a Flack parameter value of -0.04(16). Armed with knowledge of absolute structure of the two salts, single crystals of EMB were grown. Though the structure solved with an unreliable Flack parameter of -0.4(3), the absolute configuration was inferred to be S,S enantiomer based on the S,S configuration of the dihydrochloride and dimesylate salts. The EMB structure is same as the reported structure¹⁹ (CCDC Refcode – GEJHOT)¹¹ (Figure 3.3). Since EMB base is an intermediate product between

the parent material (S,S-dihydrochloride salt) and the end-product (S,S-dimesylate salt) in the experiments, it is unlikely that its absolute configuration changes during the course. Additionally, the chirality of the base and the dihydrochloride salt were confirmed through matching of their specific rotation values with the reported ones ($[\alpha]_D^{25}$, ethambutol = +13.7°, ethambutol dihydrochloride = +7.6°).²⁰

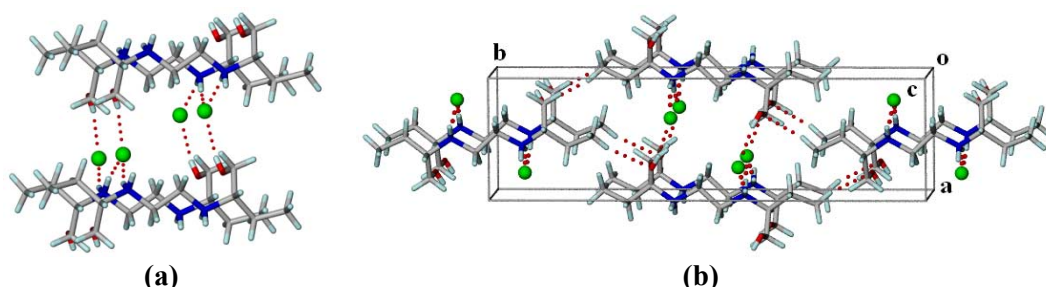


Figure 3.2 (a) N-H⁺...Cl⁻ and O-H...Cl⁻ interactions connect translation related molecules along the *c*-axis in S,S-EDH. (b) Screw related molecules form zigzag tapes through C-H...O interactions along the *b*-axis which further extend into 2D sheets.

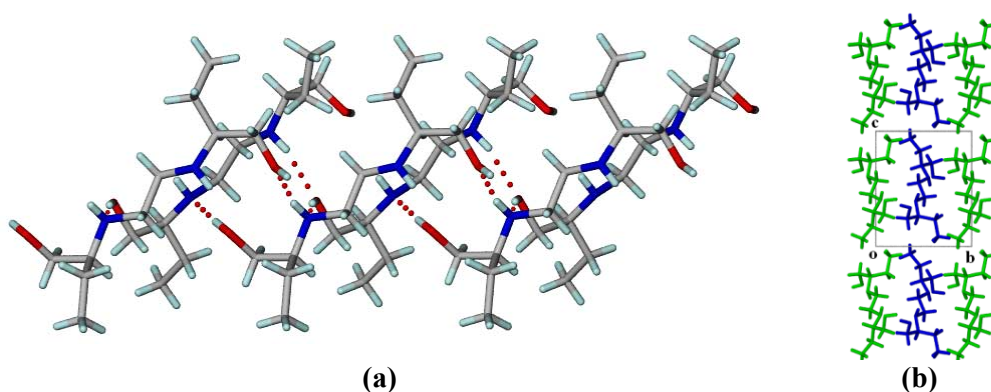


Figure 3.3 (a) Translation related molecules form a tape through N-H...O bonds in S,S-EMB. Screw related molecules through O-H...N bonds make parallel tapes which extend into (b) 2D sheets (shown in different color) along the *c*-axis through close pack.

[S,S]-Ethambutol dimesylate: A salt of ethambutol and methanesulfonic acid in 1:2 ratio was obtained upon crystallization of a methanol solution at -20 °C (Table 3.1). In the X-ray crystal structure, both the secondary amine NHs of ethambutol molecule are protonated by the sulfonic acid groups of two methanesulfonic acid moieties. Linear tapes of translation-related ethambutol molecules and screw-related mesylate molecules along the *b*-axis are formed through N⁺-H...O⁻, O-H...O and C-H...O hydrogen bonds (Figure 3.4a). These tapes make alternate 2D sheets of ethambutol and mesylate molecules along the *a*-axis (Figure 3.4b). Overall, ethambutol molecules are not directly connected to each other but come together through strong heteromolecular interactions with mesylate ions.

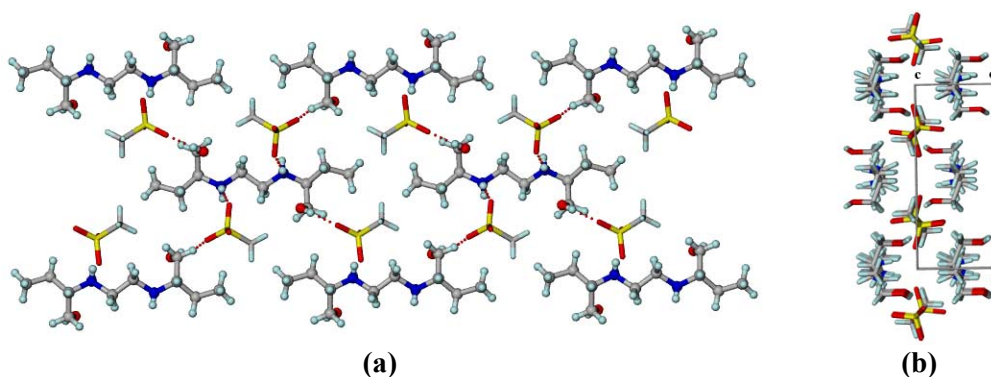


Figure 3.4 (a) Linear tapes of translation-related ethambutol molecules and screw-related mesylate molecules are connected by $\text{N}^+-\text{H}\cdots\text{O}^-$, $\text{O}-\text{H}\cdots\text{O}$ and $\text{C}-\text{H}\cdots\text{O}$ interactions. (b) Alternate sheets of ethambutol and mesylate molecules along the *a*-axis.

[S,S]-Ethambutol fumarate hydrate (2:2:1.145): A salt hydrate was obtained when ethambutol and fumaric acid in 1:1 ratio were crystallized from methanol in a desiccator. The same salt hydrate also crystallized at $-20\text{ }^\circ\text{C}$ (Table 3.1). The X-ray crystal structure shows two molecules of ethambutol and fumarate each, a water molecule and another water molecule of 0.145 site occupancy in the asymmetric unit. The structure was satisfactorily solved and refined to a good *R*-factor of 0.0326. Each crystallographic unique fumaric acid molecule donates protons to each of the two unique ethambutol molecules lying above and below it (Figure 3.5). These ethambutol molecules form parallel tapes along the *b*-axis through $\text{N}^+-\text{H}\cdots\text{O}^-$, $\text{O}-\text{H}\cdots\text{O}$ and $\text{C}-\text{H}\cdots\text{O}$ bonds. Water molecules lie along the tapes through $\text{O}-\text{H}\cdots\text{O}^-$ and $\text{C}-\text{H}\cdots\text{O}$ interactions with fumarate and ethambutol molecules respectively and make channels parallel to the *c*-axis.

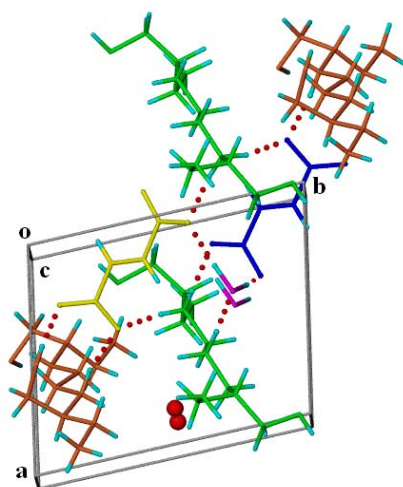


Figure 3.5 Linear tapes of ethambutol and fumarate crystallographic unique molecules (shown in different color) along the *b*-axis propagate through $\text{N}^+-\text{H}\cdots\text{O}^-$, $\text{O}-\text{H}\cdots\text{O}$ and $\text{C}-\text{H}\cdots\text{O}$ interactions. Water molecules (magenta and red) lying along the tapes form channels parallel to the *c*-axis.

Table 3.2 Crystallographic parameters.

Compound	Ethambutol dihydrochloride	Ethambutol	Ethambutol dimesylate	Ethambutol fumarate hydrate
empirical formula	C ₁₀ H ₂₆ Cl ₂ N ₂ O ₂	C ₁₀ H ₂₄ N ₂ O ₂	C ₁₂ H ₃₂ N ₂ O ₈ S ₂	C ₂₈ H ₅₈ N ₄ O ₁₃
formula weight	277.23	204.31	396.52	658.78
crystal system	orthorhombic	monoclinic	orthorhombic	triclinic
space group	<i>P</i> 2 ₁ 2 ₁ 2	<i>P</i> 2 ₁	<i>P</i> 2 ₁ 2 ₁ 2	<i>P</i> 1
<i>Z</i> *	6	2	6	5
<i>T</i> /K	100(2)	298(2)	100(2)	100(2)
<i>a</i> /Å	6.432(2)	7.1428(3)	12.239(3)	8.5813(6)
<i>b</i> /Å	22.966(9)	8.4149(3)	15.151(3)	10.5252(8)
<i>c</i> /Å	5.0934(19)	10.1973(4)	5.2980(11)	10.9210(8)
α /°	90	90	90	70.6260(10)
β /°	90	95.633(4)	90	68.8720(10)
γ /°	90	90	90	73.8670(10)
<i>V</i> /Å ³	752.4(5)	609.96(4)	982.4(3)	853.82(11)
<i>D</i> _{calc} /g cm ⁻³	1.224	1.112	1.340	1.281
μ /mm ⁻¹	0.423	0.613	0.310	0.101
reflns. collected	2891	3541	10263	8775
unique reflns.	1445	2201	1951	6434
observed reflns.	1282	2157	1763	6382
<i>R</i> ₁ [<i>I</i> > 2σ(<i>I</i>)]	0.0588	0.0506	0.0646	0.0326
<i>wR</i> ₂ [all]	0.1378	0.1438	0.1242	0.0859
goodness-of-fit	1.032	1.075	1.156	1.041
flack parameter	0.09(17)	−0.4(3)	−0.04(16)	0.1(5)
diffractometer	Bruker Smart-Apex	Oxford Xcalibur Gemini	Bruker Smart-Apex	Bruker Smart-Apex

* *Z* = *Z*' (no. of crystallographically non-equivalent molecules of any type in the asymmetric unit)²¹ × no. of independent general positions of the space group.

Table 3.3 Hydrogen bonds in the crystal structures.

Interaction	H...A/Å	D...A/Å	∠D–H...A/°	Symmetry code
Ethambutol dihydrochloride				
N1–H1A...Cl1	2.20(5)	3.046(4)	161(4)	*
N1–H1B...Cl1	2.35(5)	3.134(4)	159(4)	x, y, −1+z
O1–H1...Cl1	2.32(7)	3.055(3)	169(7)	−1+x, y, −1+z
C3–H3...O1	2.27(5)	3.234(5)	160(4)	x, y, 1+z
C1–H1D...O1	2.69	3.652(5)	165	−1/2+x, 1/2+y, −z
Ethambutol				
N2–H2...O1	2.22(2)	3.00(2)	156(2)	1+x, y, z
O1–H1D...N2	1.79(4)	2.763(2)	168(3)	1−x, 1/2+y, 1−z
O2–H2C...N1	1.98(3)	2.874(2)	176(3)	2−x, 1/2+y, 1−z
Ethambutol dimesylate				
N1–H1A...O2	1.92(4)	2.744(4)	159(3)	*
N1–H1B...O2	2.48(3)	3.060(4)	128(3)	x, y, −1+z

N1–H1B···O3	2.06(4)	2.864(4)	168(3)	x, y, -1+z
O1–H1···O4	1.98(5)	2.733(4)	176(4)	1/2+x, 1/2-y, 2-z
C5–H5A···O3	2.53	3.457(5)	155	1/2+x, 1/2-y, 2-z
C1–H1C···O3	2.64	3.621(6)	177	1/2-x, -1/2+y, 2-z
C6–H6B···O3	2.55	3.450(5)	152	1/2+x, 1/2-y, 1-z
C6–H6C···O1	2.69	3.543(5)	145	1-x, -y, z
Ethambutol fumarate hydrate				
N1–H1A···O3	1.87(3)	2.688(2)	158(2)	*
N1–H1B···O9	2.07(2)	2.881(2)	155(2)	*
N2–H2A···O11	1.80(3)	2.693(2)	167(2)	x, 1+y, z
N2–H2B···O5	1.90(3)	2.845(3)	166(3)	x, 1+y, z
N3–H3A···O9	1.82(3)	2.742(2)	166(2)	*
N3–H3B···O12	1.82(2)	2.701(2)	172(2)	1+x, y, z
N4–H4C···O4	1.84(2)	2.689(2)	168(2)	x, 1+y, z
N4–H4D···O5	1.77(3)	2.686(2)	164(2)	1+x, 1+y, z
O1–H1···O6	1.78(4)	2.692(2)	169(3)	x, 1+y, z
O2–H2···O10	1.82(2)	2.648(2)	175(2)	1+x, -1+y, z
O7–H7A···O10	1.88(3)	2.684(2)	173(3)	*
O8–H8···O7	1.90(3)	2.782(2)	177(2)	x, y, 1+z
O13–H13A···O11	1.82(3)	2.897(2)	169(2)	x, y, 1+z
O13–H13B···O4	1.59(4)	2.744(2)	173(4)	x, y, 1+z
C1–H1D···O13	2.63	3.136(3)	112	*
C5–H5A···O14	2.70	3.650(1)	159	x, y, 1+z
C6–H6A···O4	2.55	3.348(2)	138	*
C6–H6B···O9	2.42	3.225(2)	138	*
C9–H9C···O14	2.54	3.153(9)	121	x, y, -1+z
C18–H18B···O2	2.42	3.347(2)	156	x, 1+y, 2+z
C19–H19A···O13	2.46	3.362(2)	151	x, 1+y, 2+z
C23–H23A···O7	2.67	3.471(3)	139	x, y, 1+z
C26–H26···O6	2.59	3.251(2)	127	x, 1+y, z

* Molecules/ions in the same asymmetric unit.

3.2.2 Spectroscopic and Thermal analysis

Salt screen on EMB gave both solid and liquid products (Table 3.1). The products were analyzed as salts through ATR-IR spectroscopy. IR spectroscopy is generally used as a first-hand tool to characterize hydrogen bonded adducts.²² Shifts in the vibrational frequencies with respect to the starting materials indicate the formation of an adduct. For example, in case of EMB carboxylic acid salts, the characteristic C=O absorption peak of -COOH group which appears around 1700 cm⁻¹ disappeared and gave two peaks in the salt spectra around 1600 and 1400 cm⁻¹ characteristic of the asymmetric and symmetric stretch of -COO⁻ group.²² The representative spectra are shown for ethambutol dibenzoate liquid product in Figure 3.6. Similarly, solid state NMR spectroscopy, particularly ¹⁵N spectrum, is characteristic in establishing the formation of an adduct²³

(here salt) and was recorded on all seven salts that crystallized. Since proton is accepted by base (from acid proton to 2° amine of ethambutol to result in protonated amine NH_2^+ in the salt), characteristic upfield shift takes place in the salt due to an increase in electron density on the nitrogen.^{23a} As such, an upfield shift of about 60 ppm was observed in all the salts and the spectra for six salts are depicted in Figure 3.7 and that of ethambutol dibenzoate is discussed later. The 2° amines of S,S-EMB are non-equivalent since one NH acts both as a hydrogen bond donor and acceptor and the other only as an acceptor (known from its X-ray crystal structure) and thus showed two peaks in the spectrum. In case of S,S-ethambutol dihydrochloride and dimesylate salts, the amines are protonated and are equivalent (known from their X-ray crystal structures) and hence gave only one peak which is upfield compared to that of EMB (Figure 3.7a). Similarly, the occurrence of upfield shift in other cases confirms their salt integrity (Figure 3.7b). PXRD on these seven salts (except dibenzoate which is shown later) confirmed their crystalline nature (Figure 3.8). DSC of these salts (except dibenzoate and adipate which are discussed later) showed endothermic phase transitions before melting in two cases, sulfate and ditosylate (Figure 3.9). These transitions are attributed to polymorphic transformation of the salts at high temperature because there is no weight loss in the phase transition temperature range in the TGA (Figure 3.10).

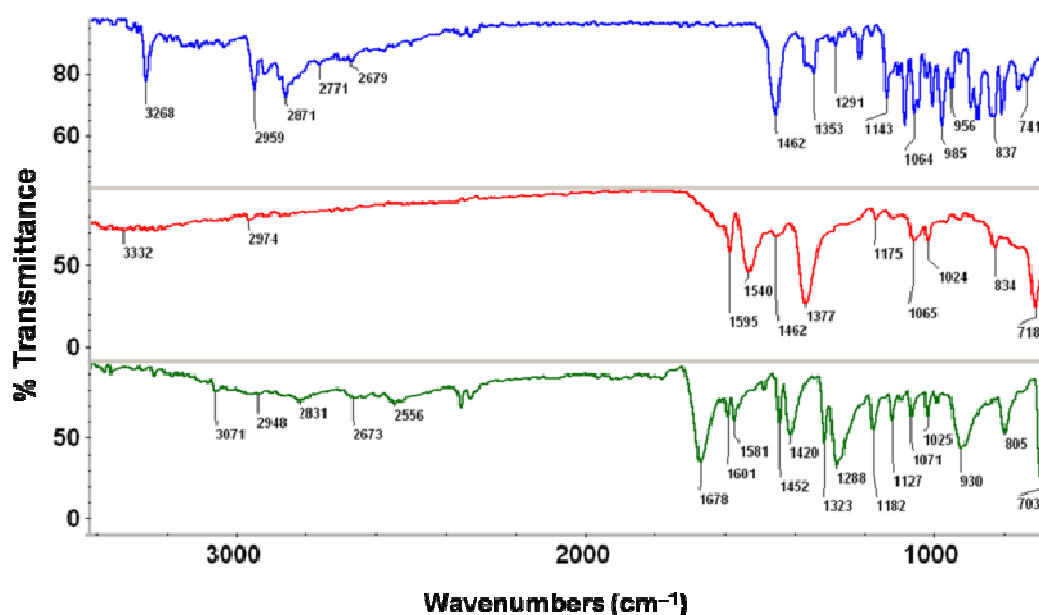


Figure 3.6 Ethambutol dibenzoate liquid product (red) exhibits distinct ATR FT-IR spectrum compared to its parent compounds ethambutol (blue) and benzoic acid (green) with respect to C=O, N–H, O–H and C–H bands.

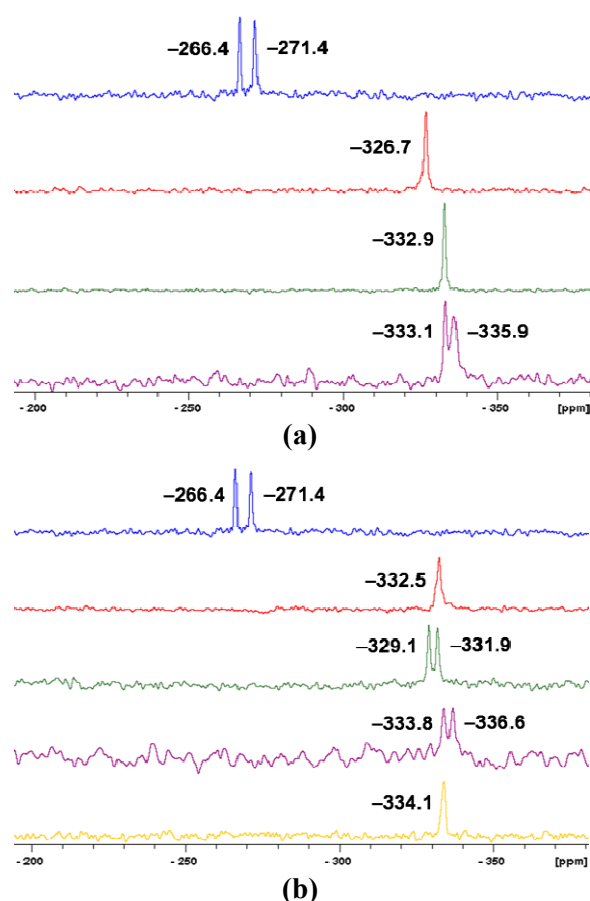


Figure 3.7 ^{15}N ss-NMR spectra of S,S-EMB (blue) and its salts **(a)** EDH (red), dimesylate (green) and fumarate hydrate (purple), and **(b)** sulfate (red), dibesylate (green), ditosylate (purple) and adipate (yellow) to show characteristic upfield shift of 2° amine group in the salts.

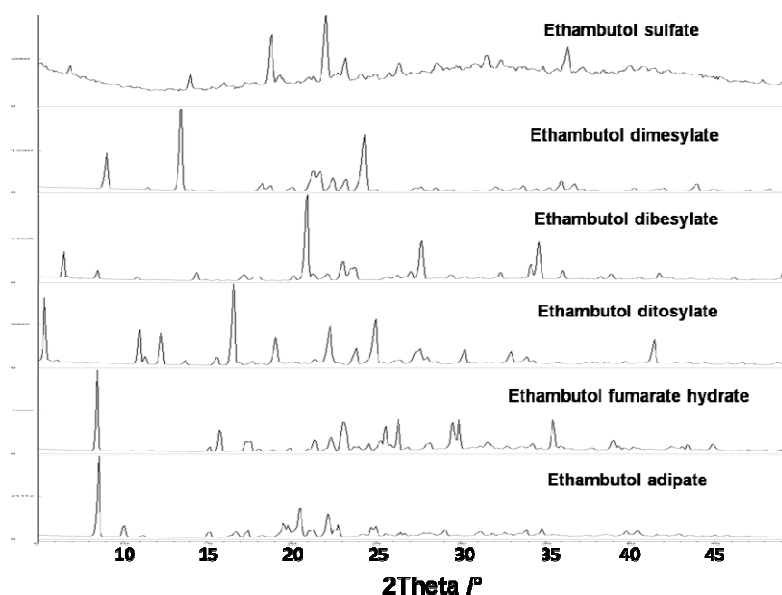


Figure 3.8 Experimental PXRD patterns of ethambutol salts.

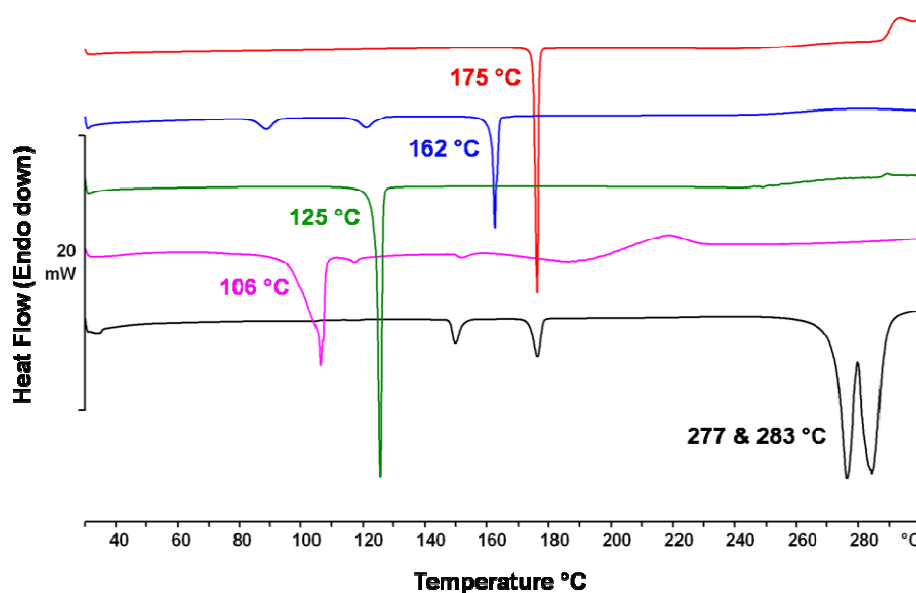


Figure 3.9 DSC of ethambutol sulfate (black), fumarate hydrate (magenta), dibesylate (green), ditosylate (blue) and dimesylate (red) salts.

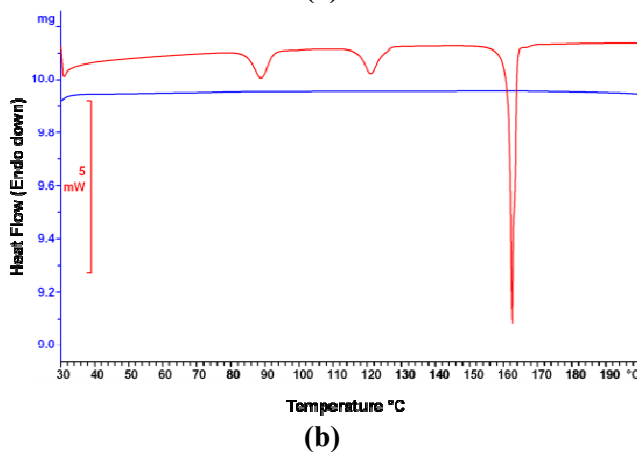
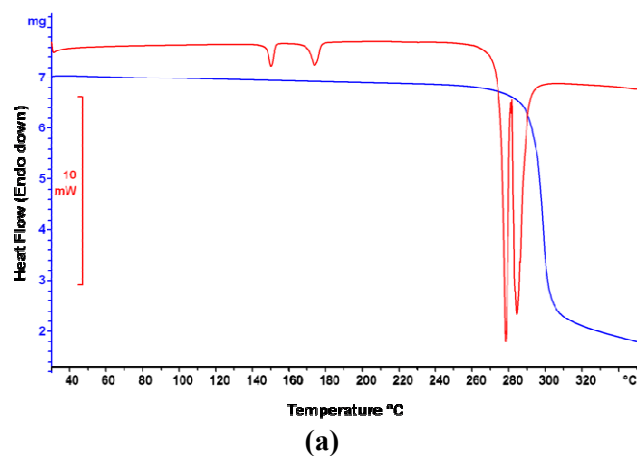


Figure 3.10 DSC (red) and TGA (blue) of **(a)** ethambutol sulfate and **(b)** ethambutol tosylate indicate polymorphic transformation of the salts at high temperature prior to melting as evident by no weight loss in the phase transition temperature range.

Of the seven salts that were obtained in liquid state, only two crystallized (dibenzoate and adipate) in moisture-free conditions (Table 3.1). The ambiguity in characterizing the remaining five liquid products as hygroscopic salts or ionic liquids was resolved by DSC. A hygroscopic salt can exist in the liquid state at room temperature due to deliquescence and the same is true for an ionic liquid even though it is not an RTIL. If the melting point of a hygroscopic salt is less than 100 °C, the solid residue upon water loss may not be visually observed if water loss and melting are concomitant upon heating. Thus, a hygroscopic salt of m.p. < 100 °C may be confused for an RTIL. A heat-cool-reheat DSC run will evolve any water and give T_g (glass transition temperature) or T_m (melting temperature) of the sample,^{13b} thereby eliminating interferences from water evolution with thermal transitions in the DSC. The typical thermal transitions of the liquid products in the DSC were shown for ethambutol dibenzoate¹⁵ sample (10.1% water content by KF titration) in Figure 3.11. The thermal transitions suggested that (i) water is lost corresponding to the broad endotherm between 60-100 °C in the heat run, (ii) the anhydrous liquid solidified during the broad exotherm between 0-40 °C in the cool run, and (iii) finally the solidified mass which is an amorphous/glassy phase goes into a rubbery phase through glass transition (T_g = ca. 0 °C, first endotherm in the reheat run), then crystallized (T_c = ca. 40 °C, exotherm) and finally melted at 88 °C (second endotherm) (Figure 3.11). These observations were substantiated by the DSC of ethambutol dibenzoate salts¹⁵ (discussed later).

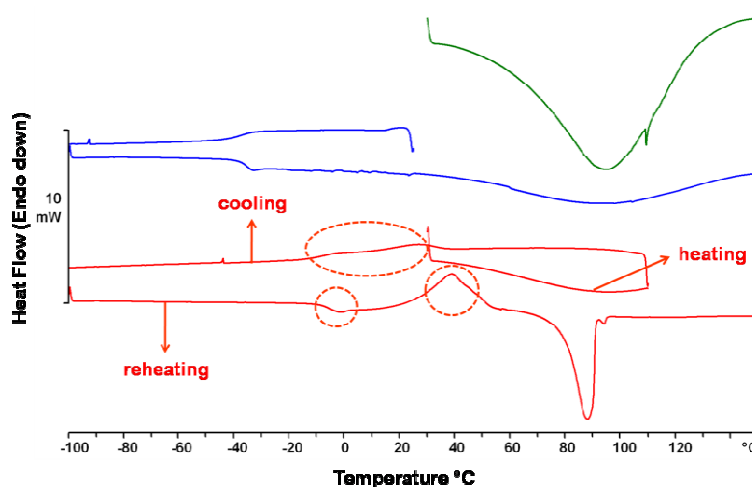


Figure 3.11 DSC of ethambutol dibenzoate hygroscopic liquid product. (a) Direct heating of the sample (green) in the temperature range 30-150 °C shows a broad endotherm around 100 °C corresponding to dehydration. (b) Cool-heat DSC (blue) also shows a broad endotherm at about the same temperature due to water vapor evolution. (c) Heat-cool-reheat DSC (red) reveals the thermal transitions of the typical solid phase obtained after dehydration of the liquid sample.

Similar thermal transitions were observed in case of ethambutol adipate liquid product (38.6% water content by KF titration) also and were confirmed by the DSC of its solid salt (Table 3.1) (Figure 3.12). Similar correlations were not obtained for the remaining five salts viz. dinicotinate, disalicylate, di-4-aminosalicylate, disaccharinate and succinate which always gave liquids (water content was estimated to be 44.5%, 48.4%, 30.3%, 15.9% and 19.3% respectively by KF titration) and never crystallized in different conditions tried (Table 3.1) and even in the inert DSC environment, up to 150 °C, unlike dibenzoate and adipate cases. This can be because of supercooling or glass formation in these cases which is not uncommon in ionic liquids.²⁴ The pictures of these liquid salts are shown in Figure 3.13. They showed T_g between -25 and +20 °C in the DSC heat-cool-reheat cycle and did not exhibit melting (Figure 3.14). In all, the seven salts exhibited T_g or T_m below 100 °C, and therefore can be stated as ionic liquids.¹³

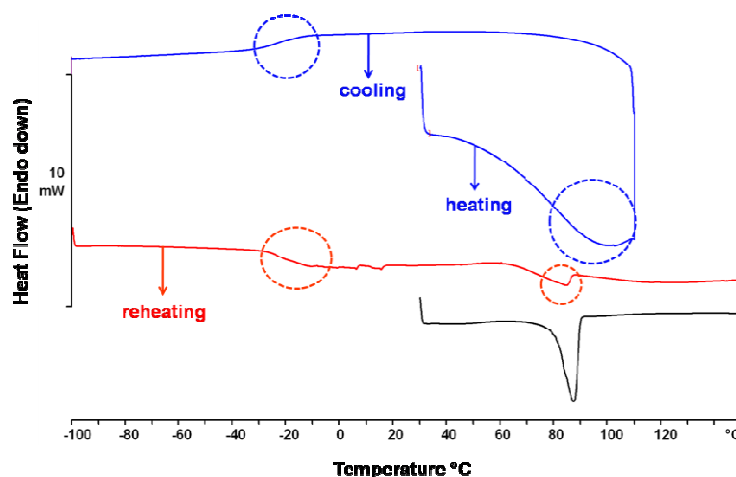


Figure 3.12 DSC of ethambutol adipate. (a) Heating and cooling of the hygroscopic liquid sample (blue trace) shows a broad endotherm around 100 °C indicative of water loss and a broad exotherm around -20 °C indicative of solidification, respectively. Reheating run (red trace) shows glass transition around -20 °C and melting at 85 °C. Crystalline sample (black trace) shows a single melting endotherm at 87 °C.



Figure 3.13 Snapshots of the hygroscopic ionic liquids (codes 1 to 7: dibenzoate, adipate, dinicotinate, disalicylate, di-4-aminosalicylate, disaccharinate and succinate) taken after 6 months of storage at ambient temperature and humidity. Only dibenzoate and adipate salts crystallized in moisture-free conditions (Table 3.1).

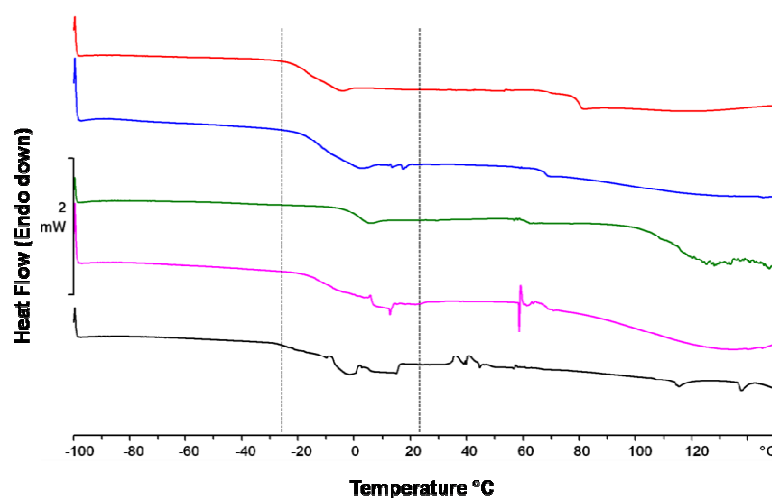


Figure 3.14 DSC (reheat segment) of ethambutol ionic liquids viz. dinicotinate (red), disalicylate (blue), di-4-aminosalicylate (green), disaccharinate (magenta) and succinate (black) show T_g between -25 and $+20$ °C. The samples also show weak transitions beyond the T_g .

3.3 API Ionic Liquid Polymorphism

Ionic liquids are essentially solids below 100 °C¹³ and hence can exhibit polymorphism just like high melting salts. In spite of few reports on polymorphism of ILs,²⁵ surprisingly, they have been proposed as alternatives to the solid forms of drugs for obviating contentious issues of intellectual property surrounding crystal structure polymorphism and polymorphic transformations in APIs.¹³ The name ‘ionic liquid’ seems to be misleading as it sounds that the material is a liquid and hence free of polymorphism issues. In this work, ethambutol dibenzoate ionic liquid crystallized as a trimorph and, thus, this first report of API ionic liquid polymorphism¹⁵ will alert the pharmaceutical community about potential pitfalls to simply assuming that polymorphism issues in drugs can be easily circumvented through ILs.¹³

Ethambutol dibenzoate (EDB), at first, was obtained as a viscous liquid (10.1% water content by KF titration) from routine solution crystallization (detailed in Experimental Section) at room temperature (Table 3.1). The salt nature of the EDB liquid was confirmed by ATR-IR spectroscopy¹⁵ as discussed earlier (Figure 3.6). Then, the difficult issue of classifying EDB as a hygroscopic salt or an ionic liquid came up. When the liquid sample was heated on a hot stage (Fisher-Johns melting point apparatus), neither evaporation of water (as small bubbles) nor a solid residue after possible water loss was observed. It appeared that EDB is an RTIL. But, when the

hygroscopic sample was subjected to a heat-cool-reheat cycle on the DSC (Figures 3.11 & 3.15), it showed a broad endotherm between 60-100 °C during heating indicating dehydration (blue trace, Figure 3.15) and a broad exotherm between 0-40 °C upon cooling which corresponds to solidification. The endo-exo-endo peaks in the reheat run from -100 to +150 °C (green trace, Figure 3.15) is characteristic of a typical amorphous solid showing glass transition (T_g = ca. 0 °C) followed by crystallization (T_c = ca. 40 °C) and finally melting (T_m = 88 °C) respectively. The validity of these thermal transitions in the DSC was confirmed by the DSC results of EDB solid salts obtained in moisture-free conditions of desiccator and rotavap¹⁵ (Figure 3.15).

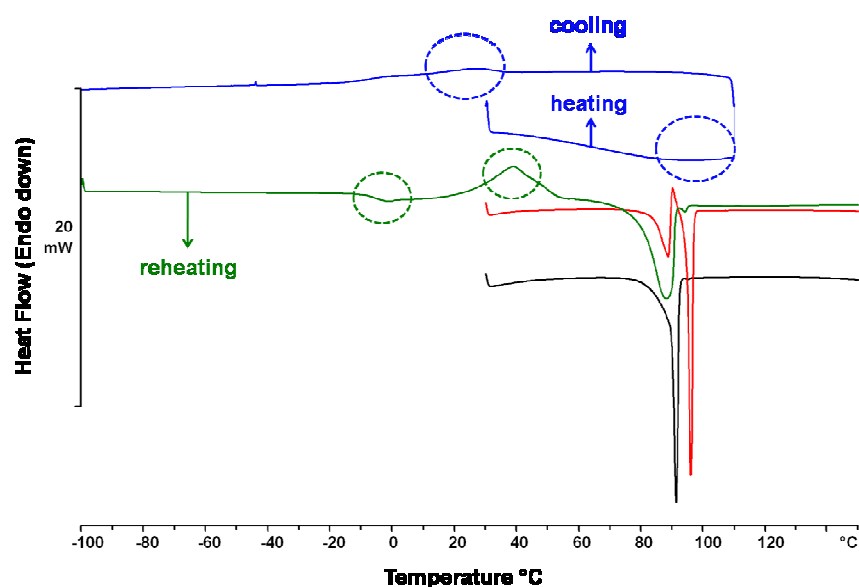


Figure 3.15 DSC of EDB salt. (a) Heating and cooling of the hygroscopic liquid sample (blue trace) shows a broad endotherm around 100 °C, indicative of water loss, and a broad exotherm around 20 °C, indicative of solidification, respectively. The reheating run (green trace) shows the glass transition around 0 °C, crystallization at around 40 °C and melting at 88 °C. (b) Crystalline salts obtained from desiccator (red) and rotavap (black) are two different polymorphs (forms 1 and 2 respectively) and show melting endotherms close to that of the liquid sample after dehydration. Form 1 (red) shows an endo-exo peak (between 88-92 °C) before melting at 95 °C. Form 2 (black) has a single melting endotherm at 90 °C, which is more close to that of the liquid sample.

Crystallization of ethambutol and benzoic acid in 1:2 ratio from alcohol in a desiccator chamber afforded a solid precipitate after complete evaporation of solvent. When the alcoholic solution was subjected to rotavaporization, a solid residue was obtained. The DSCs of both these solid salts (the chemical composition was confirmed by NMR, Experimental Section) indicated that they are polymorphs. The crystalline solid obtained in the desiccator is designated form 1 and that from the rotavap as form 2.¹⁵ Co-

melting the components gave a molten mass which upon solidification was identified as form 1. The melting endotherms of the two polymorphs are very close to the liquid sample (Figure 3.15). EDB is thus a hygroscopic salt (heat-cool-reheat DSC cycle) and an ionic liquid ($T_m = \text{ca. } 90\text{ }^{\circ}\text{C}$).¹⁵ The inert atmosphere of the DSC sample chamber and the moisture free conditions of desiccator/rotavap resulted in the solidification of this hygroscopic ionic liquid. DSC of form 1 shows an endo-exo peak (between 88-92 $^{\circ}\text{C}$) before the melting endotherm at 95 $^{\circ}\text{C}$ (Figure 3.15). The DSC of form 2 exhibited a single endotherm for melting at 90 $^{\circ}\text{C}$, which is close to the melting point of the crystalline material that was obtained from the liquid sample through an amorphous phase (Figure 3.15). A heat-cool-reheat DSC on form 1 (blue trace, Figure 3.16) indicated polymorphic transformation to a high temperature form (designated ‘form 3’)¹⁵ which exhibited sharp melting at 95 $^{\circ}\text{C}$ in the reheat cycle (red trace, Figure 3.16). The melting peak for pure form 1 (93 $^{\circ}\text{C}$) was observed at a high heating rate of 50 $^{\circ}\text{C min}^{-1}$, which minimizes polymorphic transformations typically observed at slow heating rates (of about 5 $^{\circ}\text{C min}^{-1}$). Variable temperature PXRD experiment on form 1 confirmed its transformation to form 3 at 88-90 $^{\circ}\text{C}$ (Figure 3.17). Though diffraction quality single crystals were not obtained to solve X-ray crystal structures of the three polymorphs, their distinctive PXRD patterns with signature peaks (Figure 3.18), IR and Raman spectra (Figures 3.19 & 3.20), and DSC thermal behavior differences mean that they are polymorphs. Thus, EDB ionic liquid makes a trimorphic system.¹⁵ Solid-state ^{15}N NMR spectra of form 1 and 2 (form 3 could not be recorded due to insufficient material) add support to the polymorphism of EDB (Figure 3.21).

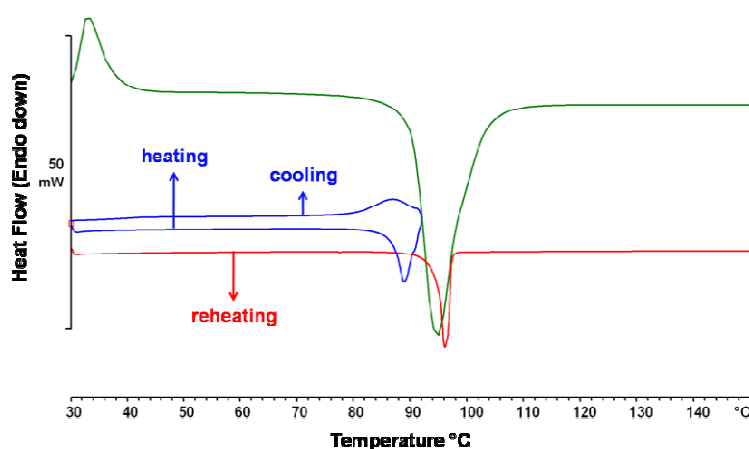


Figure 3.16 Heat-cool-reheat DSC of EDB form 1 (blue and red traces) shows transformation (pertaining to endo-exo peak in Figure 3.15) to a high temperature polymorph (designated as form 3) that melts at 95 $^{\circ}\text{C}$. Heating form 1 at the rate of 50 $^{\circ}\text{C min}^{-1}$ (green) resulted in melting endotherm at 93 $^{\circ}\text{C}$ for pure form 1.

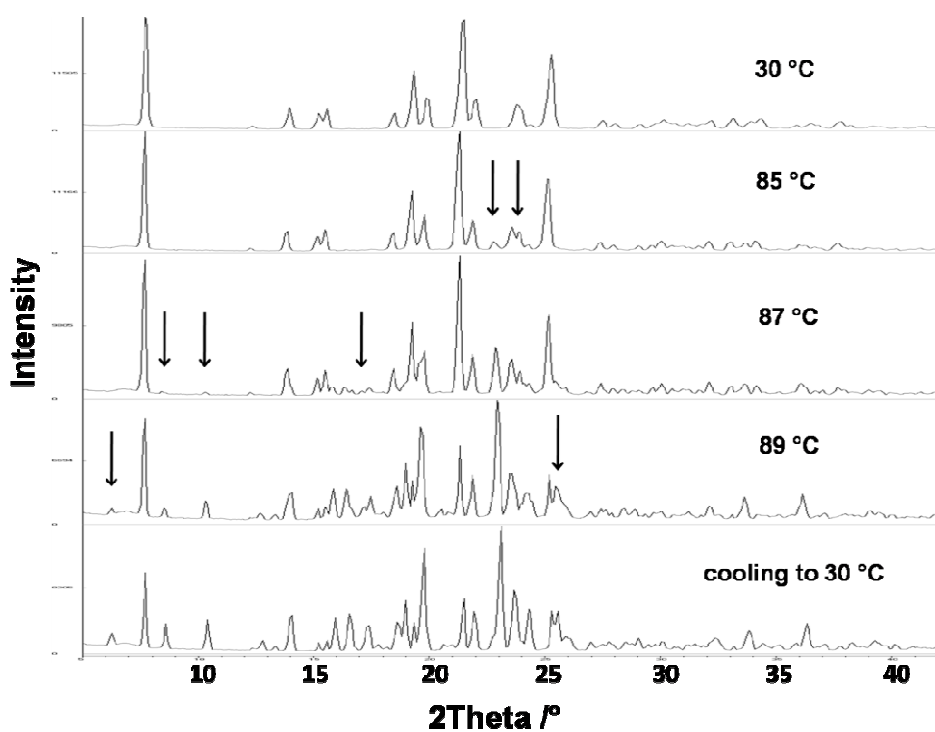


Figure 3.17 VT-PXRD of ethambutol dibenzoate form 1 (top) to show transformation to form 3 (bottom) upon heating.

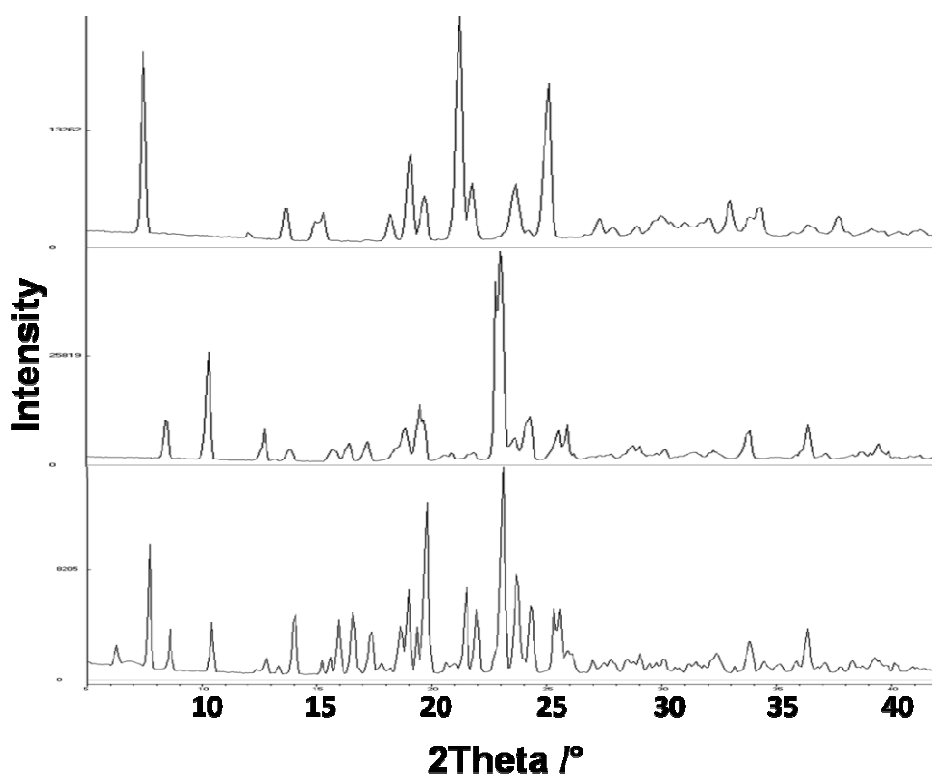


Figure 3.18 PXRD patterns of EDB form 1 (top), form 2 (middle), and form 3 (bottom) show characteristic diffraction peaks for each polymorph.

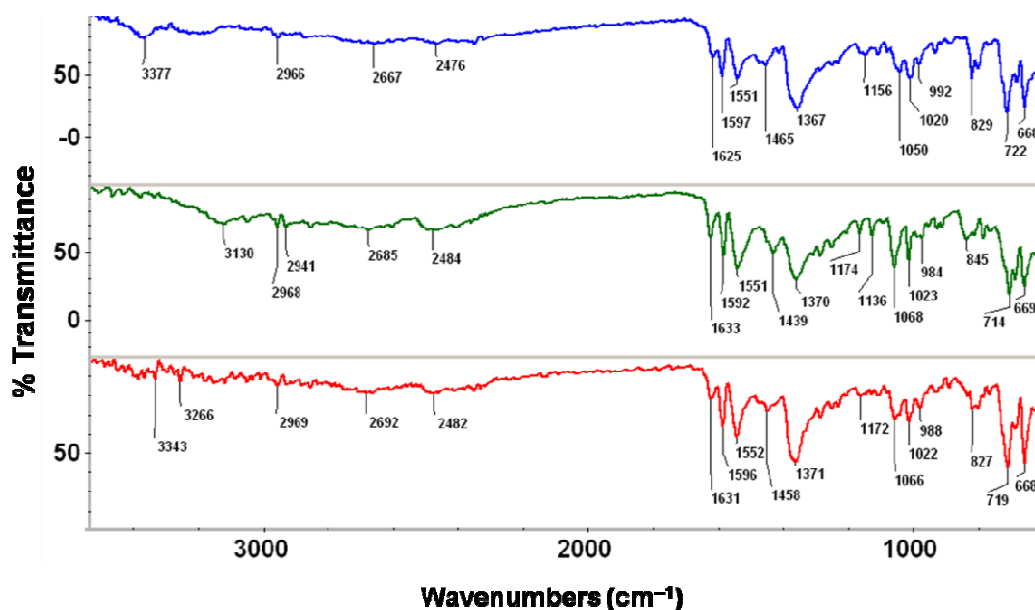


Figure 3.19 ATR-IR spectra of ethambutol dibenzoate forms 1 (blue), 2 (green) and 3 (red) show differences in their C=O, N-H, O-H and C-H bands.

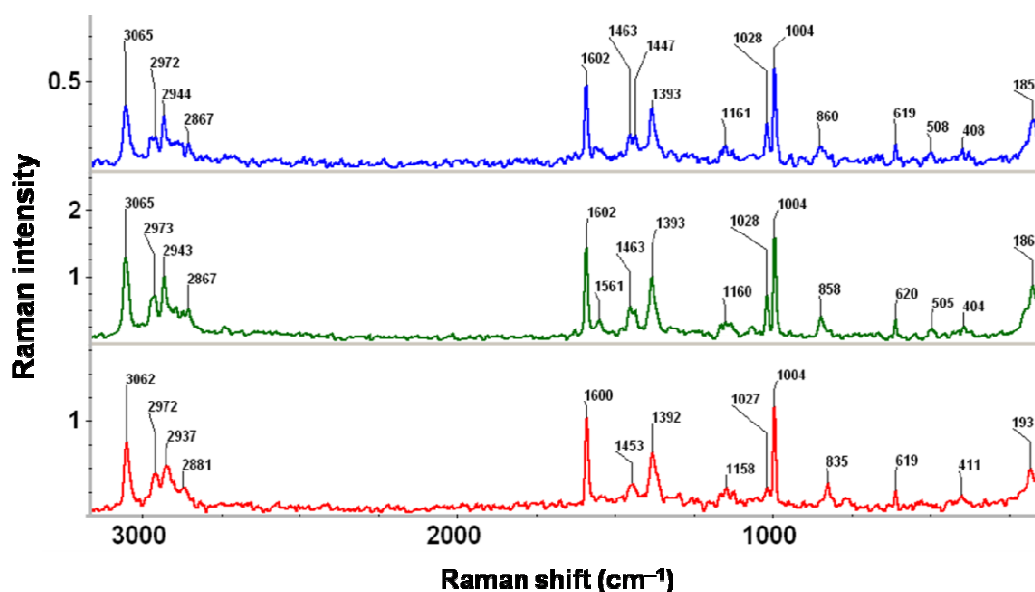


Figure 3.20 Raman spectra of ethambutol dibenzoate forms 1 (blue), 2 (green) and 3 (red) show differences in their C-H and C-C vibrations.

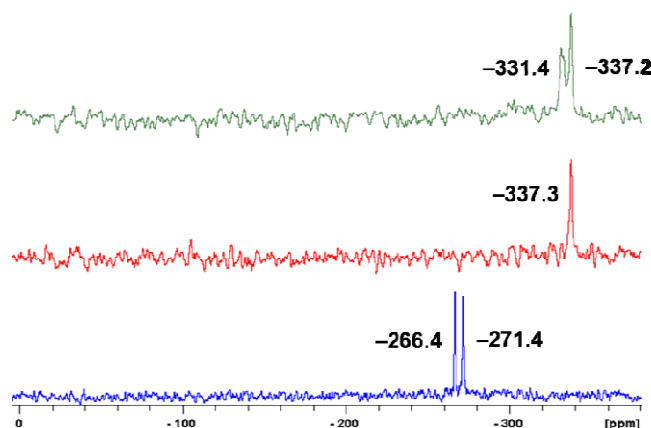


Figure 3.21 ^{15}N ss-NMR spectra of ethambutol dibenzoate forms 1 (red) and 2 (green) and ethambutol (blue). The singlet of form 1 and the doublet of form 2 demonstrate that their crystalline environments are different implying them to be polymorphs.

The stability order of the three EDB polymorphs was deduced from heat of fusion rule²⁶ and phase transformation experiments.¹⁵ Form 3 has the highest melting temperature followed by form 1 and 2 (Figures 3.15 & 3.16, Table 3.4). The high melting form 3 has lower heat of fusion than the low melting form 1 (Table 3.4), and hence they are enantiotropically related.²⁶ Form 2 has a lower heat of fusion and is thus monotropically related²⁶ to form 1 and form 3 as separate pairs (Table 3.4). Mechanochemical grinding-induced polymorphic transformations give an idea about stability order of polymorphs.²⁷ Form 1 and 2 were obtained reproducibly in macroscopic amounts and form 3 was obtained from form 1 material in a VT-PXRD experiment (detailed in Experimental Section). Each of the pure polymorphs was subjected to neat grinding using a mortar-pestle and the ground material was analyzed by PXRD. Form 2 and 3 converted to form 1 within 10 minutes. A polymorphic mixture of form 2 and 3 subjected to grinding also gave form 1. Polymorphic mixtures can exhibit different inter-conversions compared to pure crystalline forms because of seeds and impurities. Form 1 was stable for about 20 minutes after which it started to become pasty due to hygroscopic nature of the ionic liquid. The thermodynamic stability order of EDB polymorphs was established, based on the thermal data and polymorphic transformations, through a semi-quantitative free energy vs. temperature (E–T) diagram²⁸ (Figure 3.22), as: at room temperature, (25 °C) form 1 (lowest free energy and thus most stable) < form 3 < form 2 (highest free energy and thus least stable), and at high temperature, (90 °C) form 3 (most stable) < form 1 < form 2 (least stable).¹⁵ The E–T diagram is consistent with the transformation of form 2 and 3 to form 1 upon grinding and of form 1 to form 3 upon

heating, on the basis lower free energy for the polymorph at that temperature. It also follows the Ostwald's rule of stages²⁹ in that the amorphous phase crystallized to metastable form 2 in the DSC of the liquid sample (Figures 3.11 & 3.15) which then converted to the stable form 1 upon grinding at ambient temperature¹⁵ (Figure 3.22).

Table 3.4 Thermal data of the EDB polymorphs.

Polymorph	T_m (°C)	ΔH_{fus} (kJ mol ⁻¹)
1	93.4	55.9
2	90.8	46.8
3	95.5	50.9

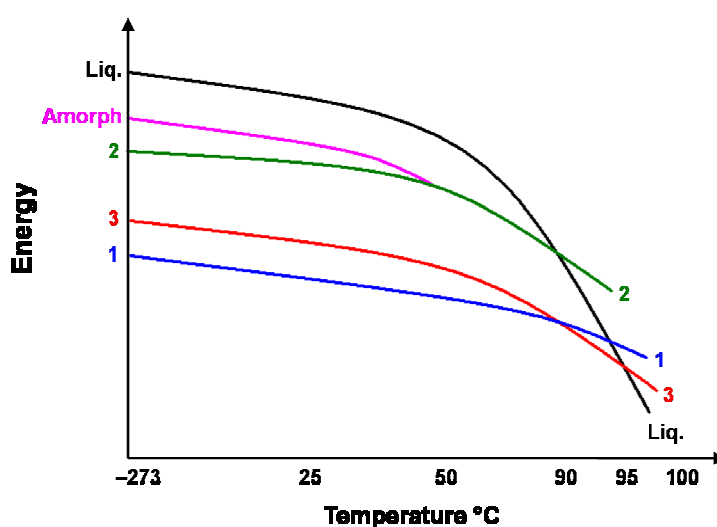


Figure 3.22 Semi-quantitative Energy vs. Temperature (E-T) diagram to show the relative free energy and phase transformation of EDB polymorphs. At 25 °C, form 1 (blue) has the lowest free energy and hence all other polymorphs convert to it upon mechano-chemical grinding. At 50 °C, amorphous form (observed in DSC run, Figure 3.15) crystallizes to form 2 (green) which melts at 90 °C. Form 1 transforms to form 3 (red) at 90 °C upon slow heating which then melts at 95 °C. Upon fast heating, form 1 (blue) directly melts at 93 °C (shown in the DSC, Figure 3.16).

3.4 Conclusions

Salt screening of ethambutol base with different salt formers (sulfonic acids, aromatic carboxylic acids, aliphatic dicarboxylic acids), most of which are non-toxic and approved chemicals,³⁰ was carried out with the intent of addressing the hygroscopicity problem of the drug. Both high melting and low melting salts (ionic liquids) all of which are hygroscopic were obtained. Molecular asymmetry and lack of strong heteromolecular interactions between the components seem to have resulted in ionic liquids.^{13a,31} Ethambutol di-4-aminosalicylate is a drug-drug ionic liquid but its utility as a novel

liquid formulation of the two drugs (both being anti-TB drugs) is thwarted by partial decomposition of 4-aminosalicylate component (which is known to undergo decarboxylation to 3-aminophenol)³² upon storage. Ethambutol disaccharinate ionic liquid can be useful as an oral sweet liquid formulation of the drug provided the water uptake upon storage is controlled. The first example of polymorphism in an API ionic liquid is reported for ethambutol dibenzoate.¹⁵ The room temperature stable EDB form 1 was obtained by slow (in a desiccator) and fast (by co-melting) crystallization, whereas metastable form 2 was crystallized by fast evaporation (by rotavaporization). New crystalline polymorphs of several compounds obtained by fast crystallization in a rotavap were recently reported.³³ In all, this study shows that unless the ionic liquid is an RTIL, it may not be a substitute for solid dosage forms free of polymorphism issues, since ILs in the temperature range 30-100 °C can exhibit polymorphism just like high melting salts. Further studies on the crystallization and characterization of ILs and RTILs will create new opportunities for pharmaceutical formulation. On the other hand, the classic problem of hygroscopicity of salts/ILs^{13,34} suggests that explorations of other solid forms of drugs such as cocrystals,³⁵ eutectics,³⁶ and solid dispersions^{36c,37} are equally important. A preliminary study on eutectics in controlling the hygroscopic nature of ethambutol dihydrochloride is discussed in chapter 6.

3.5 Experimental Section

Materials and Methods: Ethambutol dihydrochloride (Lot#090M0189V) and 4-aminosalicylic acid (Lot#S44855-419) were purchased from Sigma Aldrich and used without further purification. All other chemicals were of analytical or chromatographic grade. Water purified from a deionizer cum mixed bed purification system was used for experiments.

Preparation and Crystallization of Ethambutol base: The free base of ethambutol was prepared as per the method reported by Bhutani et al.^{1a} Ethambutol dihydrochloride (2 g) was added to 5N aqueous NaOH (20 ml). The mixture was stirred for 10-15 minutes and extracted with methylene chloride (25 ml). The organic extract was dried (Na₂SO₄) and left for evaporation at ambient temperature to afford big block crystals of ethambutol in a day. The product crystals are characterized by DSC (m.p. 88 °C), NMR and XRD. Recrystallization from acetone resulted in diffraction quality plate crystals but they showed twinning. Several crystals were checked for unchanging unit cell parameters

during X-ray cell check and the crystal which did not showed doubling of the unit cell was continued for data collection.

Ethambutol dihydrochloride ($C_{10}H_{26}Cl_2N_2O_2$): Colorless plate crystals of the salt, suitable for single crystal X-ray diffraction, were obtained from a methanolic solution, kept at $-20\text{ }^{\circ}\text{C}$, upon complete evaporation of the solvent.

^1H NMR (DMSO- d_6): δ 0.92 (3H, t, J 8), 1.68 (2H, m), 3.06 (1H, m), 3.71 (2H, m), 5.40 (1H, s), 9.29 (2H, d, J 80 (N–H coupling)). Protons of $-\text{CH}_2$ group (attached to $-\text{NH}_2^+$ group) merged with dissolved water peak of DMSO- d_6 .

^{13}C NMR (DMSO- d_6): δ 10.24, 20.78, 41.27, 57.99, 60.74.

Ethambutol ($C_{10}H_{24}N_2O_2$):

^1H NMR (DMSO- d_6): δ 0.82 (3H, t, J 8), 1.31 (2H, m), 2.32 (1H, m), 2.55 (2H, s), 3.27 (2H, m). NHs and OHs exchange in solvent.

^{13}C NMR (DMSO- d_6): δ 10.51, 24.22, 47.31, 60.72, 63.07.

Salt synthesis experiments

a. Synthesis by direct reaction of base and acid: Ethambutol and acid (in 1:1 molar ratio for diacids and 1:2 molar ratio for monoacids) were separately dissolved in acetone and kept at $-20\text{ }^{\circ}\text{C}$ for 10 minutes. After incubation, the two solutions were mixed and stirred for 5-10 minutes in an ice cold bath. Salt obtained as white precipitate in solution was filtered on a $2.5\text{ }\mu\text{m}$ Whatman filter paper and washed with acetone and dried.

b. Solution Crystallization: Ethambutol and acid (in 1:1 molar ratio for diacids and 1:2 molar ratio for monoacids) were directly dissolved in methanol/ethanol. The solutions were kept for slow crystallization at (i) room temperature, in (ii) a $-20\text{ }^{\circ}\text{C}$ refrigerator and (iii) a desiccator separately. For fast crystallization of salts, the alcoholic solutions were subjected to rotavaporization.

c. Co-grinding: Ethambutol and acid (in 1:1 molar ratio for diacids and 1:2 molar ratio for monoacids) were subjected to neat grinding using a mortar-pestle for 1-2 minutes.

d. Co-melting: Ethambutol and acid (in 1:1 molar ratio for diacids and 1:2 molar ratio for monoacids) were taken together in a sublimation tube and heated in an oil/salt bath beyond the melting point of the higher melting compound. The tube was held until a uniform liquid with no trace of solid material is formed and then kept aside for ambient cooling.

e. Physical mixtures: Ethambutol and acid (in 1:1 molar ratio for diacids and 1:2 molar ratio for monoacids) were mixed together with a glass rod on a glass plate and the material was transferred to a glass vial for storage at ambient temperature.

Ethambutol sulfate ($C_{10}H_{26}N_2O_6S$):

1H NMR (D_2O): δ 0.94 (3H, t, J 8), 1.70 (2H, m), 3.25 (1H, m), 3.48 (2H, s), 3.73 (2H, m). NHs and OHs exchange in solvent.

^{13}C NMR (D_2O): δ 9.00, 20.37, 40.82, 57.86, 61.40.

Ethambutol dimesylate ($C_{12}H_{32}N_2O_8S_2$):

1H NMR ($DMSO-d_6$): δ 0.90 (3H, t, J 8), 1.60 (2H, m), 2.39 (2H, s), 3.09 (1H, m), 3.42 (2H, m). Protons of $-CH_3$ group (attached to $-SO_3^-$ group) merged with dissolved water peak of $DMSO-d_6$. NHs and OHs exchange in solvent.

^{13}C NMR ($DMSO-d_6$): δ 10.14, 20.64, 39.10, 40.99, 57.99, 60.73.

Ethambutol dibesylate ($C_{22}H_{36}N_2O_8S_2$):

1H NMR ($DMSO-d_6$): δ 0.86 (3H, t, J 8), 1.57 (2H, m), 3.07 (1H, m), 3.30 (2H, s), 7.35 (2H, d, J 4), 7.64 (2H, d, J 4), 8.55 (1H, s). Protons of $-CH_2$ group (attached to $-NH_2^+$ group) merged with dissolved water peak of $DMSO-d_6$. NHs and OHs exchange in solvent.

^{13}C NMR ($DMSO-d_6$): δ 10.07 (2C), 20.60 (2C), 41.02 (2C), 57.95 (2C), 60.79 (2C), 125.89 (4C), 128.43 (4C), 129.65 (2C), 147.32 (2C).

Ethambutol ditosylate ($C_{24}H_{40}N_2O_8S_2$):

1H NMR ($DMSO-d_6$): δ 0.86 (3H, t, J 8), 1.57 (2H, m), 2.27 (3H, s), 3.05 (1H, m), 3.29 (2H, s), 7.14 (2H, d, J 8), 7.51 (2H, d, J 8). Protons of $-CH_2$ group (attached to $-NH_2^+$ group) merged with dissolved water peak of $DMSO-d_6$. NHs and OHs exchange in solvent.

^{13}C NMR ($DMSO-d_6$): δ 10.09 (2C), 20.63 (2C), 21.23 (2C), 41.06 (2C), 57.99 (2C), 60.77 (2C), 125.92 (4C), 128.82 (4C), 139.05 (2C), 144.73 (2C).

Ethambutol dibenzoate ($C_{24}H_{36}N_2O_6$):¹⁵ Solution crystallization of an alcoholic (MeOH or EtOH) solution of ethambutol and benzoic acid in 1:2 molar ratio in a desiccator resulted in form 1. When the solution was subjected to rotavaporization, form 2 was obtained. Form 3 was obtained from form 1 material subjected to VT-PXRD up to 90 °C, the phase transition temperature in DSC. The product from two VT-PXRD experiments on form 1 was combined and used for characterization and experiments. All

three polymorphs showed close chemical shifts and integration in both ^1H and ^{13}C NMR spectra.

^1H NMR (DMSO- d_6): δ 0.86 (3H, t, J 8), 1.47 (2H, m), 2.65 (1H, m), 2.90 (2H, s), 3.39 (2H, m), 7.39 (2H, d, J 8), 7.47 (1H, d, J 8), 7.90 (2H, d, J 8). NHs and OHs exchange in solvent.

^{13}C NMR (DMSO- d_6): δ 10.52 (2C), 22.65 (2C), 44.22 (2C), 60.51 (2C), 60.96 (2C), 128.43 (4C), 129.59 (4C), 131.64 (2C), 135.07 (2C), 169.31 (2C).

Ethambutol dinicotinate ($\text{C}_{22}\text{H}_{34}\text{N}_4\text{O}_6$):

^1H NMR (DMSO- d_6): δ 0.88 (3H, t, J 8), 1.52 (2H, m), 2.77 (1H, m), 3.06 (2H, s), 3.43 (2H, m), 7.40 (1H, dd, J 8, 4), 8.17 (1H, d, J 8), 8.60 (1H, d, J 4), 9.00 (1H, s). NHs and OHs exchange in solvent.

^{13}C NMR (DMSO- d_6): δ 10.44, 22.08, 43.34, 60.20, 60.54, 123.64, 131.67, 137.02, 150.81, 151.64, 168.54.

Ethambutol disalicylate ($\text{C}_{24}\text{H}_{36}\text{N}_2\text{O}_8$):

^1H NMR (DMSO- d_6): δ 0.93 (3H, t, J 8), 1.61 (2H, m), 3.02 (1H, m), 3.31 (2H, s), 6.67 (1H, d, J 4), 6.70 (1H, d, J 8), 7.21 (1H, t, J 8), 7.70 (1H, d, J 8). Protons of $-\text{CH}_2$ group (attached to $-\text{NH}_2^+$ group) merged with dissolved water peak of DMSO- d_6 . NHs and OHs exchange in solvent.

^{13}C NMR (DMSO- d_6): δ 10.29, 21.24, 41.99, 59.01, 60.60, 116.47, 117.38, 119.41, 130.65, 132.79, 162.50, 172.98.

Ethambutol di-4-aminosalicylate ($\text{C}_{24}\text{H}_{38}\text{N}_4\text{O}_8$):

^1H NMR (DMSO- d_6): δ 0.86 (3H, t, J 8), 1.51 (2H, m), 2.77 (1H, m), 3.03 (2H, s), 5.85 (1H, s), 5.93 (1H, d, J 8), 7.36 (1H, d, J 8). Protons of $-\text{CH}_2$ group (attached to $-\text{NH}_2^+$ group) merged with dissolved water peak of DMSO- d_6 . NHs and OHs exchange in solvent.

^{13}C NMR (DMSO- d_6): δ 10.44, 22.07, 43.22, 60.15, 60.42, 95.55, 105.14, 106.53, 131.73, 153.88, 163.93, 173.69.

Ethambutol disaccharinate ($\text{C}_{24}\text{H}_{34}\text{N}_4\text{O}_8\text{S}_2$):

^1H NMR (DMSO- d_6): δ 0.90 (3H, t, J 8), 1.61 (2H, m), 3.13 (1H, m), 3.31 (2H, s), 3.69 (2H, m), 7.60 (1H, m), 7.62 (2H, m), 7.68 (1H, m). NHs and OHs exchange in solvent.

^{13}C NMR (DMSO- d_6): δ 10.18, 20.69, 41.01, 58.04, 60.65, 119.77, 123.14, 131.87, 132.33, 134.70, 145.35, 168.38.

Ethambutol succinate (C₁₄H₃₀N₂O₆):

¹H NMR (DMSO-d₆): δ 0.85 (3H, t, *J* 8), 1.44 (2H, m), 2.26 (2H, s), 2.61 (1H, m), 2.82 (2H, s), 3.34 (2H, m). NHs and OHs exchange in solvent.

¹³C NMR (DMSO-d₆): δ 10.50, 22.77, 32.36, 44.32, 60.35, 61.06, 175.90.

Ethambutol fumarate (C₁₄H₂₈N₂O₆):

¹H NMR (DMSO-d₆): δ 0.86 (3H, t, *J* 8), 1.47 (2H, m), 2.69 (1H, m), 2.92 (2H, s), 3.39 (2H, m), 6.42 (1H, s). NHs and OHs exchange in solvent.

¹³C NMR (DMSO-d₆): δ 10.47, 22.30, 43.58, 60.39, 60.45, 135.88, 169.28.

Ethambutol adipate (C₁₆H₃₄N₂O₆):

¹H NMR (DMSO-d₆): δ 0.83 (3H, t, *J* 8), 1.39 (2H, m), 1.43 (2H, d, *J* 4), 2.08 (2H, d, *J* 4), 2.73 (1H, m), 3.15 (2H, s), 3.36 (2H, m). NHs and OHs exchange in solvent.

¹³C NMR (DMSO-d₆): δ 10.51, 24.11, 35.29, 45.05, 49.05, 60.45, 61.55, 176.15.

X-ray Crystallography: X-ray reflections for EDH, ethambutol dimesylate and ethambutol fumarate hydrate were collected at 100 K on Bruker SMART-APEX CCD diffractometer equipped with a graphite monochromator and Mo-Kα fine-focus sealed tube (λ = 0.71073 Å). Data reduction was performed using Bruker SAINT software.³⁸ Intensities were corrected for absorption using SADABS.³⁹ Structures were solved and refined using SHELX-97.⁴⁰ X-ray reflections for ethambutol were collected at 298 K on an Oxford Xcalibur Gemini Eos CCD diffractometer using Cu-Kα radiation (λ = 1.5418 Å). Data reduction was performed using CrysAlisPro (version 1.171.33.55)⁴¹ and OLEX2-1.0⁴² was used to solve and refine the structure. All non-hydrogen atoms were refined anisotropically. Hydrogen atoms on heteroatoms were located from difference electron density maps and all C–H hydrogens were fixed geometrically. Flack parameter¹² was obtained upon solving and refinement of the X-ray data. The final CIF files and hydrogen bond geometries were validated in PLATON.⁴³ X-Seed⁴⁴ was used to prepare packing diagrams.

Powder X-ray Diffraction: PXRD were recorded on Bruker D8 Advance diffractometer using Cu-Kα X-radiation (λ = 1.5406 Å) at 40 kV and 30 mA. Diffraction patterns were collected over 2θ range of 5–50° at scan rate of 1° min^{−1}. VT-PXRD was performed on the same instrument equipped with a variable temperature stage (TTK450 chamber, working temperature range −190 °C to 450 °C). The sample was packed in a Cr-plated copper holder and heated from 30 °C to 90 °C at 5 °C/min. Scans were taken at selected

temperatures over 2θ range of 5–42°, using a step size of 0.08° 2θ and time per step of 1 sec. Powder cell 2.4⁴⁵ was used to plot the diffraction patterns.

Spectroscopy: Nicolet 6700 FT-IR spectrometer equipped with a single bounce ATR and an NXR FT-Raman module was used to record IR and Raman spectra. IR spectra were recorded on samples placed on Zn-Se crystal. Raman spectra were recorded on compressed samples contained in a gold-coated sample holder. Solution and solid state NMR spectra were recorded on a Bruker Avance spectrometer at 400 MHz. SS-NMR spectra were recorded on a Bruker 4 mm double resonance CP-MAS probe in zirconia rotors at 5.0 kHz with a cross-polarization contact time of 2.5 ms and a recycle delay of 8 s. ¹⁵N CP-MAS spectra were recorded at 40 MHz and referenced to glycine N atom, and then the chemical shifts were recalibrated to nitromethane N ($\delta_{\text{glycine}} = -347.6$ ppm). Additionally the identity and stoichiometry of the components of the salts were established through solution ¹H NMR integration and ¹³C NMR spectra.

Thermal analysis: DSC was performed on a Mettler Toledo DSC 1 module calibrated with indium ($T_m = 156.60$ °C; $\Delta H_f = 28.45$ J g⁻¹) and zinc ($T_m = 419.50$ °C; $\Delta H_f = 107.50$ J g⁻¹) as per the manufacturer's specifications. TGA was performed on a Mettler Toledo TGA/SDTA 851e module calibrated with indium ($T_m = 156.60$ °C) and aluminium ($T_m = 660.30$ °C). The temperature range used for solid samples in both DSC and TGA is 30–400 °C at 5 °C min⁻¹. For liquid samples, a heat-cool-reheat DSC cycle through liquid nitrogen cooling in the temperature range –100 to +150 °C at 5 °C min⁻¹ was employed. The typical sample size is 5–10 mg for DSC and 10–15 mg for TGA. Samples were placed in crimped but vented aluminium pans for DSC and open alumina pans for TGA and were purged by a stream of dry nitrogen flowing at 50 mL min⁻¹.

Karl Fischer (KF) titration: Water content of the samples was determined using a Spectralab volumetric MA 101 C Karl Fischer titrator with KF reagent (single solution) as the titrant and anhydrous methanol as the solvent.

3.6 References

1. (a) H. Bhutani, S. Singh, K. C. Jindal and A. K. Chakraborti, *J. Pharm. Biomed. Anal.*, 2005, **39**, 892. (b) B. Blomberg, S. Spinachi, B. Fourie and R. Laing, *Bull. World Health Organ.*, 2001, **79**, 61.

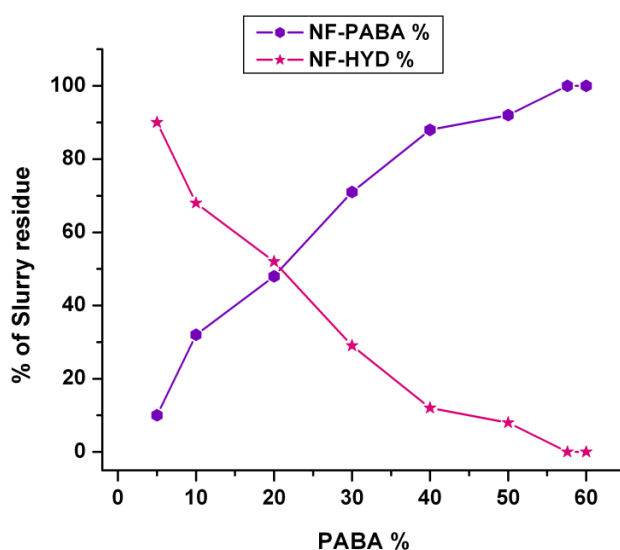
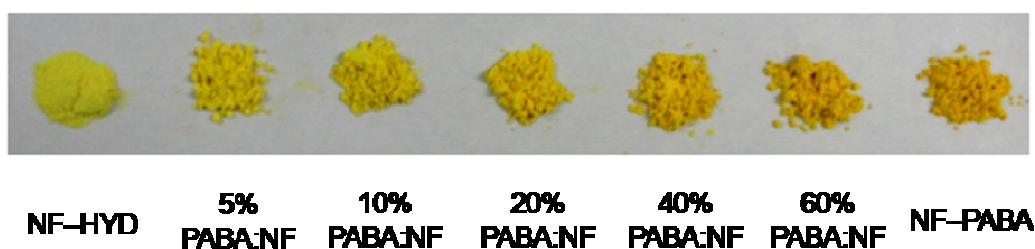
2. R. G. Wilkinson, R. G. Shepherd, J. P. Thomas and C. Baughn, *J. Amer. Chem. Soc.*, 1961, **83**, 2212.
3. S. Singh and B. Mohan, *Int. J. Tuberc. Lung Dis.*, 2003, **7**, 298.
4. <http://apps.who.int/prequal/whopar/whoparproducts/TB168Part6v1.pdf>.
5. G. -Y. Bai, H. -S. Ning, Y. -C. Zhang, T. Zeng and J. -S. Li, *Acta Crystallogr.*, 2006, **E62**, o3364.
6. R. Godfrey, R. Hargreaves and P. B. Hitchcock, *Acta Crystallogr.*, 1992, **C48**, 79.
7. G. -Y. Bai, H. -S. Ning, J. Simpson, X. -Y. Kin and N. Li, *Acta Crystallogr.*, 2006, **E62**, o4567.
8. Mitsui Toatsu Inc. And Mitsui Pharmaceuticals Inc. *GB Pat.*, 1365473A, 1973.
9. S. -W. Park, Korean Advanced Institute of Science and Technology, *US Pat.*, 4450274, 1984.
10. J. M. Rubin-Preminger, J. Bernstein, R. K. Harris, I. R. Evans and P. Y. Ghi, *Cryst. Growth Des.*, 2004, **4**, 431. (CCDC Refcode – CURJEE02)
11. Cambridge Structural Database, ver. 5.33, ConQuest 1.14, November 2011 release, May 2012 update; www.ccdc.cam.ac.uk.
12. (a) H. D. Flack and G. Bernardinelli, *Acta Crystallogr.*, 1999, **A55**, 908; (b) H. D. Flack and G. Bernardinelli, *J. Appl. Cryst.*, 2000, **33**, 1143.
13. (a) J. Stoimenovski, D. R. McFarlane, K. Bica and R. D. Rogers, *Pharm. Res.*, 2010, **27**, 521; (b) K. Bica and R. D. Rogers, *Chem. Commun.*, 2010, **46**, 1215.
14. D. S. Silvester and R. G. Compton, *Z. Phys. Chem.*, 2006, **220**, 1247.
15. S. Cherukuvada and A. Nangia, *CrystEngComm*, 2012, DOI: 10.1039/c2ce25842k.
16. A. V. Trask, D. A. Haynes, W. D. S. Motherwell and W. Jones, *Chem. Commun.*, 2006, 51.
17. P. M. Bhatt and G. R. Desiraju, *CrystEngComm*, 2008, **10**, 1747.
18. R. Hamalainen, M. Lehtinen and M. Ahlgren, *Arch. Pharm.*, 1985, **318**, 26. (CCDC Refcode – CURJEE)
19. G. -Y. Bai, C. -F. Zhang, Y. -C. Zhang, T. Zeng and J. -S. Li, *Acta Crystallogr.*, 2006, **E62**, o2173 & 2007, **E63**, e2.
20. The Merck Index, *An Encyclopedia of Chemicals, Drugs, and Biologicals*, Fourteenth Ed., Merck Research Laboratories, 2006.
21. B. P. van Eijck and J. Kroon, *Acta Crystallogr.*, 2000, **B56**, 535.

22. R. M. Silverstein, F. X. Webster and D. J. Kiemle, *Spectrometric Identification of Organic Compounds*, John Wiley & Sons, NJ, 2005.
23. (a) Z. J. Li, Y. Abramov, J. Bordner, J. Leonard, A. Medek and A. V. Trask, *J. Am. Chem. Soc.*, 2006, **128**, 8199; (b) F. G. Vogt, J. S. Clawson, M. Strohmeier, A. J. Edwards, T. N. Pham and S. A. Watson, *Cryst. Growth Des.*, 2009, **9**, 921.
24. J. G. Huddleston, A. E. Visser, W. M. Riechert, H. D. Willauer, G. A. Broker and R. D. Rogers, *Green Chem.*, 2001, **3**, 156; (b) E. W. Castner, Jr., J. F. Wishart, *J. Chem. Phys.*, 2010, **132**, 120901; (c) P. M. Dean, J. Turanjanin, M. Y.- Fujita, D. R. MacFarlane and J. L. Scott, *Cryst. Growth Des.*, 2009, **9**, 1137.
25. (a) J. D. Holbrey, W. M. Reichert, M. Nieuwenhuyzen, S. Johnston, K. R. Seddon and R. D. Rogers, *Chem. Commun.*, 2003, 1636; (b) S. Hayashi, R. Ozawa and H. Hamaguchi, *Chem. Lett.*, 2003, **32**, 498; (c) T. Endo, T. Morita and K. Nishikawa, *Chem. Phy. Lett.*, 2011, **517**, 162.
26. A. Burger and R. Ramberger, *Mikrochim. Acta*, 1979, **72**, 259.
27. (a) S. R. Byrn, R. R. Pfeiffer and J. G. Stowell, *Solid-State Chemistry of Drugs*, SSCI, IN, 1999; (b) S. Cherukuvada, R. Thakuria and A. Nangia, *Cryst. Growth Des.*, 2010, **10**, 3931.
28. (a) A. Grunenberg, J. -O. Henck and H. W. Siesler, *Int. J. Pharm.*, 1996, **129**, 147; (b) J. Bernstein, *Polymorphism in Molecular Crystals*; Clarendon, Oxford, U. K., 2002.
29. J. Nývlt, *Cryst. Res. Technol.*, 1995, **30**, 443.
30. (a) G. F. Paulekuhn, J. B. Dressman and C. Saal, *J. Med. Chem.*, 2007, **50**, 6665; (b) R. J. Bastin, M. J. Bowker and B. J. Slater, *Org. Pro. Res. Dev.*, 2000, **4**, 427; (c) GRAS (Generally Recognized As Safe)/EAFUS (Everything Added to Food in the United States) substances list is available through: <http://www.fda.gov/Food/FoodIngredientsPackaging/ucml15326.htm>.
31. (a) E. W. Castner, Jr. and J. F. Wishart, *J. Chem. Phys.*, 2010, **132**, 120901; (b) P. M. Dean, J. Turanjanin, M. Y.- Fujita, D. R. MacFarlane and J. L. Scott, *Cryst. Growth Des.*, 2009, **9**, 1137.
32. (a) R. F. Rekker and W. Th. Nauta, *J. Med. Pharm. Chem.*, 1960, **2**, 281; (b) M. K. Rotich, B. D. Glass and M. E. Brown, *J. Ther. Anal. Calor.*, 2001, **64**, 681.
33. (a) N. K. Nath, S. Nilapwar and A. Nangia, *Cryst. Growth Des.*, 2012, **12**, 1613; (b) P. P. Bag and C. M. Reddy, *Cryst. Growth Des.*, 2012, **12**, 2740.

34. (a) R. J. Bastin, M. J. Bowker and B. J. Slater, *Org. Pro. Res. Dev.*, 2000, **4**, 427;
(b) P. L. Gould, *Int. J. Pharm.*, 1986, **33**, 201.
35. (a) N. Schultheiss and A. Newman, *Cryst. Growth Des.*, 2009, **9**, 2950; (b) N. J. Babu and A. Nangia, *Cryst. Growth Des.*, 2011, **11**, 2662.
36. (a) A. Górniak, A. Wojakowska, B. Karolewicz and J. Pluta, *J. Ther. Anal. Calorim.*, 2011, **104**, 1195; (b) S. Cherukuvada and A. Nangia, *CrystEngComm*, 2012, **14**, 2579; (c) M. D. Moore and P. L. D. Wildfong, *J. Pharm. Innov.*, 2009, **4**, 36.
37. (a) T. Vasconcelos, B. Sarmiento and P. Costa, *Drug Disc. Today*, 2007, **12**, 1068; (b) S. Janssens, C. Roberts, E. F. Smith and G. V. Mooter, *Int. J. Pharm.*, 2008, **355**, 100.
38. SAINT-Plus, version 6.45, 2003, Bruker AXS Inc.: Madison, Wisconsin, USA.
39. SADABS, Program for Empirical Absorption Correction of Area Detector Data, **1997**, Sheldrick, G.M. University of Göttingen, Göttingen, Germany.
40. (a) SMART, version 5.625 and SHELX-TL, version 6.12, **2000**, Bruker AXS Inc., Madison, Wisconsin, USA. (b) SHELXS-97 and SHELXL-97, **1997**, Sheldrick, G.M. University of Göttingen, Göttingen, Germany.
41. CrysAlis CCD and CrysAlis RED, versions 1.171.33.55, **2008**, Oxford Diffraction Ltd, Yarnton, Oxfordshire, UK.
42. Dolomanov, O. V.; Blake, A. J.; Champness, N. R.; Schröder, M. *J. Appl. Crystallogr.* **2003**, *36*, 1283.
43. A. L. Spek, PLATON, A Multipurpose Crystallographic Tool, Utrecht University, Utrecht, Netherland, 2002
44. L. J. Barbour, X-Seed, Graphical Interface to SHELX-97 and POV-Ray, University of Missouri-Columbia, USA, 1999.
45. PowderCell, Program for structure visualization, powder pattern calculation and profile fitting, <http://www.ccp14.ac.uk/index.html>.

CHAPTER FOUR

NITROFURANTOIN-*p*-AMINOBENZOIC ACID COCRYSTAL



*Activity of *p*-Aminobenzoic acid (PABA) on the hydration of Nitrofurantoin (NF) in aqueous medium. PABA controls hydration of NF as an additive (from 5 to 50% weight of NF) and renders NF stable to hydration as a coformer (57.6% of NF) by forming a 1:1 NF-PABA cocrystal.*

4.1 Introduction

Nitrofurantoin (abbreviated as NF; Figure 4.1) is an anti-bacterial drug used in the treatment of urinary tract infections¹ and is on the WHO Model List of Essential Medicines.² Polymorphism and pseudopolymorphism of NF are reported in the literature.³ Caira et al. reported two polymorphs of anhydrous Nitrofurantoin (α and β) and two polymorphs of Nitrofurantoin monohydrate (Form I and Form II).⁴ NF β polymorph and monohydrate II are the stable anhydrate and monohydrate forms and exist in the marketed formulations.^{4a,5} The former has higher dissolution rate than the latter^{3b,4a} which is in accordance to the general observation that anhydrides tend to have higher dissolution rates than hydrates.⁶ The transformation of NF anhydrides to monohydrate II was observed during dissolution,^{3b,4a} pelletization⁷ and granulation.⁸ The transformation of anhydrate β polymorph is slower compared to α polymorph with the latter showing comparable dissolution rate to that of the monohydrate II.^{4a} NF is a Class IV drug according to the Biopharmaceutics Classification System i.e. it has low solubility and low permeability (and bioavailability).⁹ A side effect of NF is nausea and emesis upon oral administration and is due to its high absorption rate.¹⁰ The same study¹⁰ reported that larger crystals (150 μm mesh size) of lower surface area and slower absorption reduced emesis but still conferred optimal therapeutic effect. The rapid initial dissolution rate of the stable β polymorph has been linked to the side effects of the drug by Caira et al.^{4a} Though it appears unlikely that a stable polymorph has a higher dissolution rate, the slower transformation of β polymorph to monohydrate II compared to metastable α polymorph (which transforms faster to slow dissolving monohydrate II) renders it unimpeded during dissolution, thus leading to faster dissolution.^{4a} Considering these transformations, the drug is marketed as two different formulations to control fast dissolution/absorption and for sustained release purposes: macrocrystalline NF (brand name 'Macroclatin')^{1,11} and combination of macrocrystalline NF and NF monohydrate (brand name 'Macrobid').¹²

Dehydration kinetics of NF monohydrate II¹³ and solution behavior of anhydrate β polymorph and monohydrate II has been studied.¹⁴ Several NF salts such as sodium and potassium,¹⁵ and L-arginine, L-lysine, L-histidine, L-ornithine and glycine¹⁶ were reported in the patent literature, but there is no study on the control of hydration and dissolution of the drug. A control over the dissolution rate can influence the absorption

rate which in turn may regulate the side effects of the drug. With the intent of controlling the hydration and dissolution behavior of Nitrofurantoin, the cocrystallization approach was undertaken in this study. Based on the potential heterosynthons¹⁷ possible with coformers containing complementary functional groups to those of NF, cocrystallization with *p*-aminobenzoic acid (PABA), urea and L-arginine was executed (Figure 4.1). Two 1:1 cocrystals (NF–PABA and NF–urea), a 1:1:1 salt hydrate (NF–L-arginine–H₂O) and a 1:1 methanol solvate (NF–MeOH) were obtained and their crystal structures were determined in this work.¹⁸ The hydration stability and dissolution rate of the adducts were compared with that of NF β polymorph and monohydrate II. NF–PABA cocrystal was found to be superior among the adducts in terms of minimal transformation to NF hydrate and comparable dissolution rate to the reference drug.¹⁸ Pseudopolymorphs and cocrystals of Nitrofurantoin were recently reported by other groups as well.¹⁹

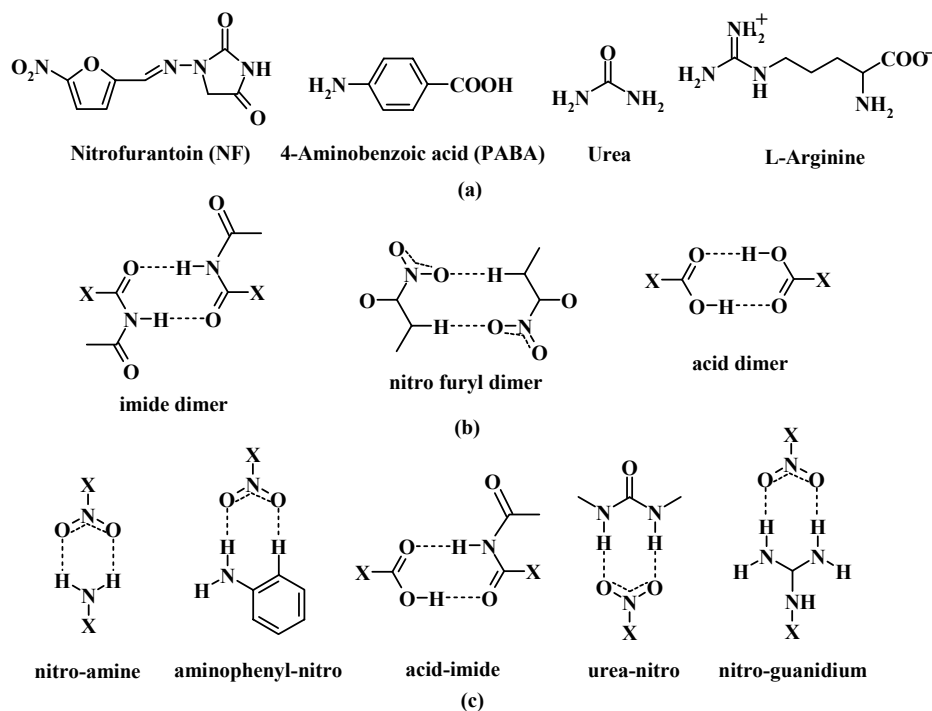


Figure 4.1 (a) Molecular structures of Nitrofurantoin and coformers used in this study. (b) Some possible homosynthons and (c) heterosynthons between the molecular components in the adducts.

4.2 Crystallization of the Adducts

Commercial NF (Alfa Aesar) matches with β polymorphic modification (PXRD profile match in Figure 4.2) and the material was used for all experiments of this study. NF monohydrate form II was obtained upon grinding the material by adding few drops of

water (PXRD profile match in Figure 4.3a). Evaporative crystallization of NF with PABA, urea and L-arginine respectively in equimolar stoichiometry resulted in single crystals of the corresponding adducts (detailed in Experimental Section). A methanol solvate of NF was crystallized from methanol. X-ray crystallographic parameters are shown in Table 4.1 and hydrogen bonds in Table 4.2. Macroscopic amounts of the adducts were obtained upon solid state grinding (also called neat grinding)²⁰ in case of cocrystals (NF–PABA and NF–urea) and water-assisted grinding for the L-arginine salt hydrate (PXRD profile match in Figure 4.3b-d).

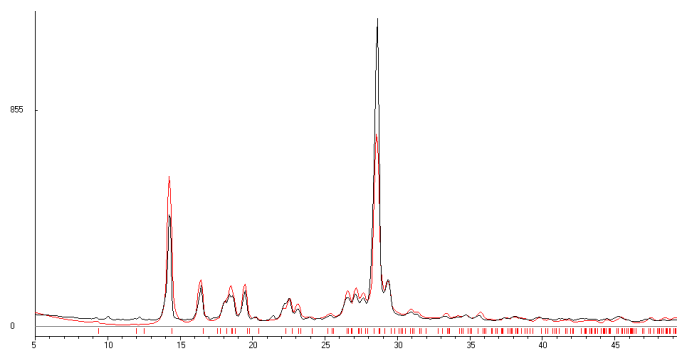


Figure 4.2 Overlay of the calculated lines from X-ray crystal structure (red) of NF β polymorph and the experimental PXRD pattern (black) of the commercial material shows peak-to-peak match.

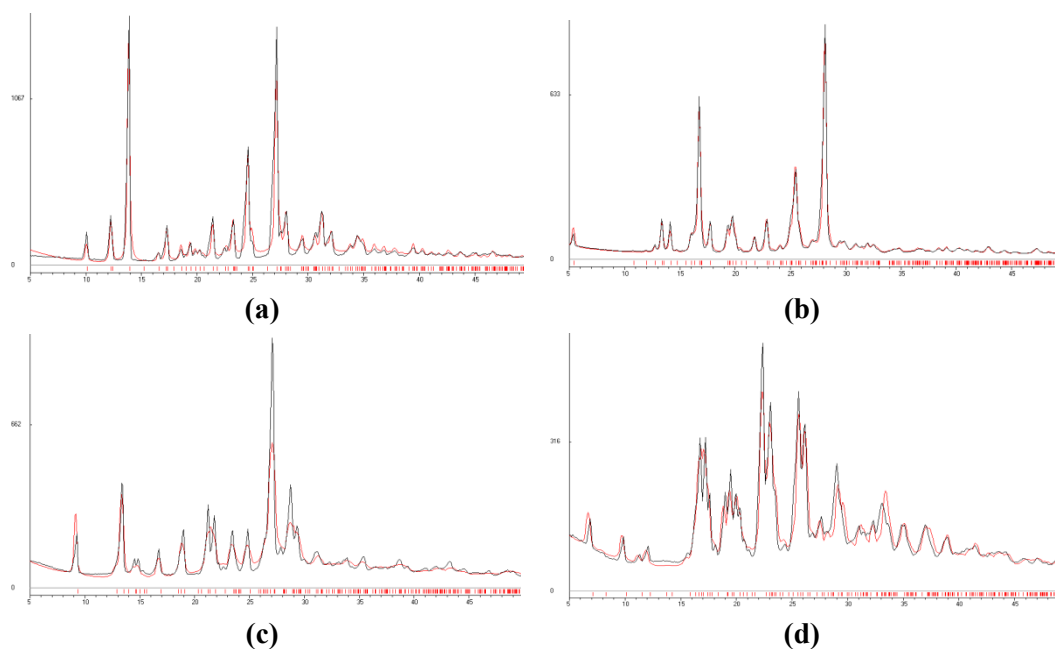


Figure 4.3 Overlay of the calculated lines from X-ray crystal structures (red) and experimental PXRD patterns (black) show peak-to-peak match. **(a)** NF monohydrate form II obtained upon water-assisted grinding²⁰ of NF. **(b)** NF–PABA and **(c)** NF–urea cocrystals and **(d)** NF–L-Arg–H₂O salt hydrate obtained upon neat grinding and water-assisted grinding of the respective components in equimolar stoichiometry.

Table 4.1 Crystallographic parameters.

Molecular adduct	NF-PABA	NF-Urea	NF-L-Arg-H ₂ O	NF-MeOH
empirical formula	C ₈ H ₆ N ₄ O ₅ – C ₇ H ₇ NO ₂	C ₈ H ₆ N ₄ O ₅ – CH ₄ N ₂ O	C ₈ H ₆ N ₄ O ₅ – C ₆ H ₁₅ N ₄ O ₂ – H ₂ O	C ₈ H ₆ N ₄ O ₅ – CH ₄ O
formula weight	375.30	298.23	430.40	270.21
crystal system	triclinic	monoclinic	orthorhombic	monoclinic
space group	<i>P</i> $\bar{1}$	<i>P</i> 2 ₁ / <i>n</i>	<i>P</i> 2 ₁ 2 ₁ 2 ₁	<i>P</i> 2 ₁ / <i>c</i>
<i>Z</i> ^a	4	8	12	8
<i>T</i> /K	298(2)	100(2)	100(2)	298(2)
<i>a</i> /Å	6.7239(11)	6.681(3)	5.7872(6)	6.4279(17)
<i>b</i> /Å	7.5460(12)	13.653(6)	15.3731(16)	6.7824(18)
<i>c</i> /Å	16.316(3)	13.189(6)	21.173(2)	26.841(7)
α /°	93.827(2)	90	90	90
β /°	92.538(2)	97.460(7)	90	92.149(4)
γ /°	101.659(2)	90	90	90
<i>V</i> /Å ³	807.5(2)	1192.9(9)	1883.7(3)	1169.4(5)
<i>D</i> _{calc} /g cm ^{–3}	1.543	1.661	1.518	1.535
μ /mm ^{–1}	0.125	0.142	0.126	0.131
reflns. collected	8466	10368	19511	11753
unique reflns.	3191	2130	3679	2335
observed reflns.	2722	1821	3476	1897
<i>R</i> ₁ [<i>I</i> > 2σ(<i>I</i>)]	0.0382	0.0539	0.0336	0.0429
<i>wR</i> ₂ [all]	0.0985	0.1430	0.0789	0.1134
goodness-of-fit	1.054	1.049	1.047	1.039
CCDC Refcode ^b	ORUXOP	ORUXUV	ORUXEF	ULECAQ01

^a *Z* = *Z*' (no. of crystallographically non-equivalent molecules of any type in the asymmetric unit)²¹ × no. of independent general positions of the space group; ^b Ref. 18.

Table 4.2 Hydrogen bonds in crystal structures of the adducts.*

Interaction	H...A/Å	D...A/Å	∠D–H...A/°	Symmetry code
NF-PABA				
N4–H4...O5	1.83	2.827(2)	165.3	–x, 1–y, 1–z
N5–H5A...O4	2.44	3.204(2)	131.5	1+x, y, z
N5–H5B...O3	2.25	3.265(2)	176.3	1–x, 2–y, 2–z
N5–H5A...O2	2.70	3.424(2)	128.9	1–x, 1–y, 1–z
O7–H7...O6	1.60	2.589(2)	178.4	–x, –y, 1–z
C3–H3...O4	2.50	3.263(2)	126.3	1+x, y, z
C3–H5...O4	2.30	3.157(2)	134.1	1+x, y, z
C14–H14...O2	2.35	3.381(2)	158.1	1–x, 2–y, 2–z
C8–H8B...O6	2.61	3.615(2)	153.2	1–x, 1–y, 1–z
NF-Urea				
N4–H4...O6	1.74	2.724(3)	163.1	1/2–x, 1/2+y, 1/2–z
N5–H5A...O3	2.23	3.144(3)	148.9	x, y, 1+z
N5–H5B...O4	2.15	3.062(3)	148.5	x, y, 1+z
N5–H5B...N2	2.49	3.308(3)	137.1	x, y, 1+z

N6–H6A···O6	1.95	2.960(3)	178.4	–x, 1–y, 1–z
N6–H6B···O4	2.19	3.071(3)	144.1	x, y, 1+z
N6–H6B···O5	2.50	3.023(3)	111.1	–1/2+x, 3/2–y, 1/2+z
N5–H5A···O1	2.59	3.188(3)	117.4	x, y, –1+z
C2–H2···O2	2.39	3.264(3)	136.4	–x, –y, –z
C3–H3···O5	2.35	3.355(3)	152.9	1/2–x, –1/2+y, 1/2–z
C5–H5···O3	2.52	3.181(3)	118.2	1/2+x, 1/2–y, 1/2+z
C5–H5···O2	2.60	3.668(3)	167.4	1/2+x, 1/2–y, 1/2+z
C3–H3···O3	2.62	3.216(3)	113.7	1/2+x, 1/2–y, 1/2+z
C8–H8···O4	2.70	3.650(3)	146.1	1–x, 1–y, –z
NF–L-Arg–H₂O				
N5–H5A···O5	1.78	2.775(2)	167.7	x, –1+y, z
N5–H5B···O8	2.01	2.880(2)	141.7	x, –1+y, –1+z
N5–H5C···O6	1.66	2.670(2)	176.1	1+x, y, z
N6–H6···N4	2.03	3.030(2)	167.7	–x, –1/2+y, 1/2–z
N7–H7A···O5	1.87	2.874(2)	169.4	–x, –1/2+y, 1/2–z
N7–H7B···O4	1.75	2.755(2)	172.4	1/2+x, 1/2–y, 1–z
N8–H9A···O3	2.06	3.062(2)	167.4	1/2+x, 1/2–y, 1–z
N8–H9B···N2	2.35	3.342(2)	164.1	1/2+x, 1/2–y, 1–z
O8–H15A···O7	1.86	2.836(2)	167.2	1+x, 1+y, 1+z
O8–H15B···O7	1.86	2.830(2)	164.5	1/2+x, 1/2–y, 1–z
C3–H3···O6	2.49	3.075(2)	112.2	3/2+x, 1/2–y, –z
C12–H12B···O6	2.50	3.281(2)	128.0	1+x, y, z
C2–H2···O2	2.51	3.589(2)	169.6	1/2+x, 1/2–y, –z
C2–H2···O3	2.57	3.340(2)	127.0	1/2+x, 1/2–y, 1–z
C13–H13B···O2	2.67	3.582(2)	141.5	1+x, y, z
C3–H3···O7	2.49	3.525(2)	158.5	3/2+x, 1/2–y, –z
C5–H5···O8	2.47	3.429(2)	146.0	1/2+x, 3/2–y, 1–z
C8–H8A···O7	2.64	3.636(2)	152.2	1/2+x, 1/2–y, –z
C11–H11A···O4	2.65	3.203(2)	110.7	–x, 1/2+y, 1/2–z
C11–H11A···O4	2.58	3.323(2)	124.8	x, –1+y, z
NF–MeOH				
N4–H4···O6	1.77	2.777(2)	172.7	–x, 1/2+y, 3/2–z
O6–H6···O5	1.83	2.809(2)	174.0	1–x, –1/2+y, 3/2–z
C2–H2···O3	2.35	3.230(2)	137.1	1+x, y, z
C5–H5···O4	2.11	3.171(2)	164.5	1+x, y, z
C8–H8B···O6	2.60	3.656(2)	165.7	1+x, y, z
C9–H9A···O4	2.71	3.501(2)	129.2	1+x, y, z

* O–H, N–H and C–H distances are neutron-normalized to 0.983, 1.009 and 1.083 Å respectively.

4.2.1 Cocrystal of NF and PABA

The crystal structure solved in the space group $P\bar{1}$ and contains each of the NF and PABA molecules in the asymmetric unit. NF molecules are hydrogen-bonded via the imide dimer and PABA molecules are connected via the acid dimer homosynthons (Figure 4.4). Such dimeric units are connected via the N–H···O + C–H···O two-point

aminophenyl–nitro motif into zigzag tapes which extend into 2D sheets through N–H \cdots O and bifurcated C–H \cdots O interactions (Figure 4.4). The 2D sheets are sustained by auxiliary C–H \cdots O interactions and lie at an interplanar separation of 3.6 Å. An alternative crystal structure (polymorph) of this cocrystal was anticipated with acid–imide heterosynthon (Figure 4.1) between NF and PABA, but such a structure was not realized experimentally. Solid state grinding^{20,22} of the components in equimolar stoichiometry resulted in the same cocrystal. This cocrystal was found to be stable to slurry crystallization in water suggesting that it is a stable form (discussed later).

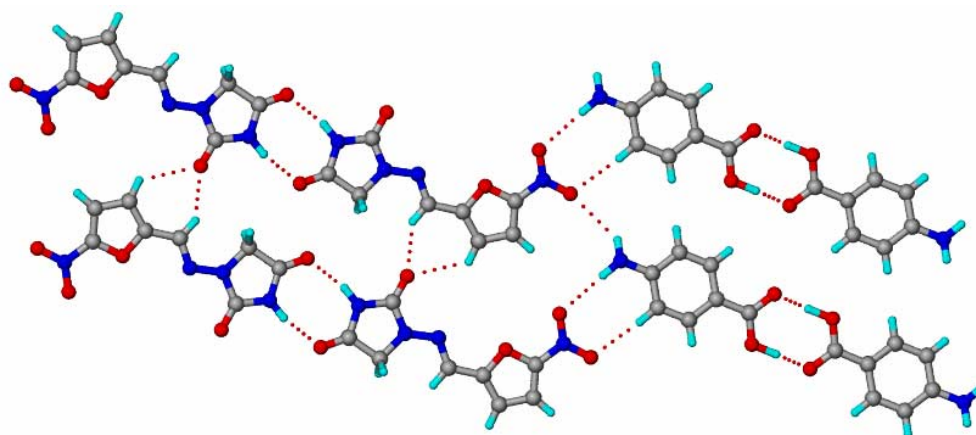
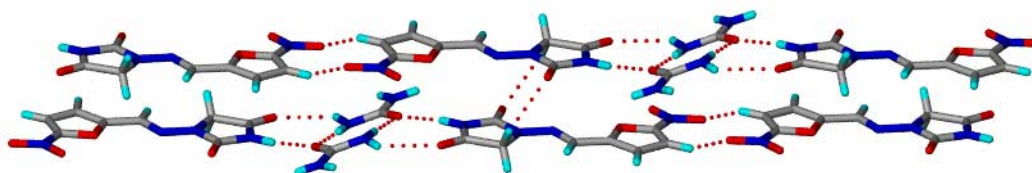


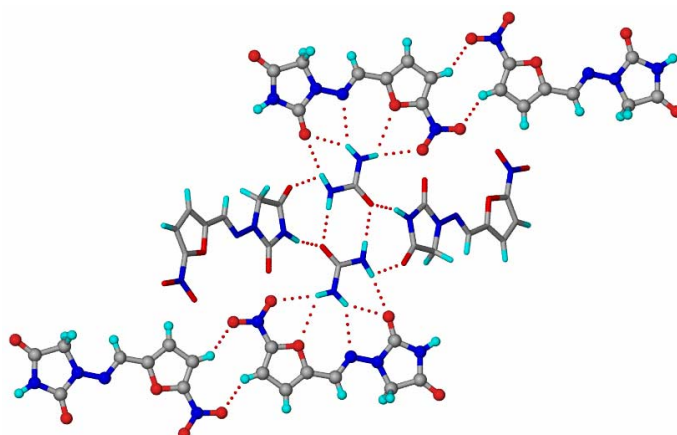
Figure 4.4 NF and PABA molecules are hydrogen-bonded via imide dimer and acid dimer homosynthon, which are in turn connected by aminophenyl-nitro N–H \cdots O and C–H \cdots O bonds to form zigzag tapes that extend into a sheet structure through N–H \cdots O and bifurcated C–H \cdots O interactions.

4.2.2 Cocrystal of NF and Urea

The crystal structure solved in the space group $P2_1/n$ and contains each of the NF and urea molecules in the asymmetric unit. There is no two-point urea-nitro synthon (Figure 4.1) in this crystal structure. A linear tape of nitrofuryl C–H \cdots O dimers of NF molecules is connected through N–H \cdots O hydrogen bonds to the urea dimer (Figure 4.5a). Such parallel tapes form offset stacks along the a -axis through C–H \cdots O interactions (Figure 4.5a). The non-planar consecutive tapes along the c -axis make an angle of 28.2° with each other and are connected through auxiliary interactions in 3D (Figure 4.5b).



(a)

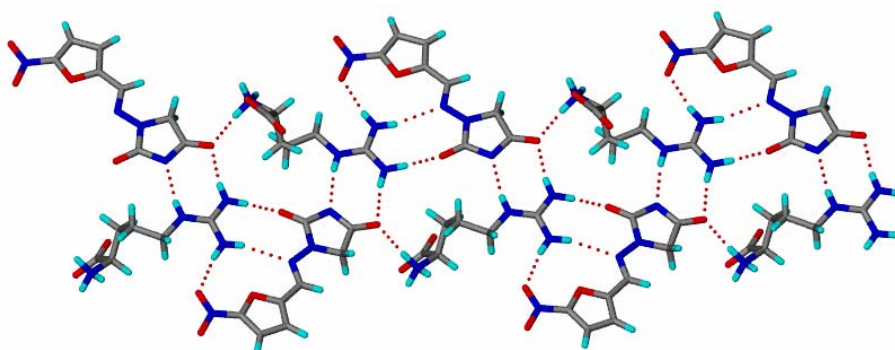


(b)

Figure 4.5 (a) Linear tapes of nitrofuryl C–H···O dimers of NF molecules are connected through N–H···O bonds to the urea dimer. The parallel offset tapes are connected via C–H···O interactions. (b) Adjacent tapes (shown as ball-stick and capped-stick models for clarity) along *c*-axis make an angle of 28.2° with each other.

4.2.3 Hydrate of NF and L-Arginine Salt

A salt of Nitrofurantoin and L-arginine with a solvent of crystallization was reported in a patent but without any X-ray crystal structure details.¹⁶ When an equimolar mixture of NF and L-arginine was crystallized in acetonitrile–isopropanol solvent mixture (in 1:1 v/v), a 1:1:1 NF–L-Arg–H₂O salt crystal was obtained.¹⁸ It solved in the space group *P*2₁2₁2₁ and contains each of the NF, L-arginine and water molecules in the asymmetric unit. The imine proton of NF is transferred to the α-amino group of L-arginine. There is no two-point nitro-guanidium synthon (Figure 4.1) between NF and L-arginine molecules, instead N–H···O and N–H···N hydrogen bonds between imide and guanidium groups connect the molecules and form a tape along [106] axis (Figure 4.6a). The tapes are arranged in a herringbone T-motif which makes channels for water inclusion along the *a*-axis (Figure 4.6b).



(a)

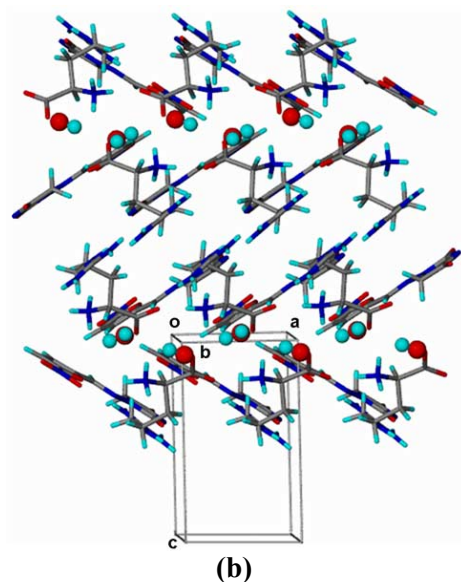


Figure 4.6 (a) A tape of NF and L-arginine molecules connected by N–H···O and N–H···N two-point motif. **(b)** Screw-related water molecules reside in channels parallel to the *a*-axis in the herringbone structure.

Solid state grinding of the components (to avoid contact with water) did not afford an anhydrous salt as monitored by PXRD. Attempts to dehydrate the salt hydrate did not succeed as the material decomposed abruptly around 180 °C as monitored by DSC (exotherm) and TGA (weight loss) (Figure 4.7). The measured weight loss of 27% in TGA corresponds to the theoretical loss of four volatile components from the salt hydrate – CO₂, H₂O, NH₃ and NO₂ (calculated 29.04%). The elemental analysis of the decomposed material showed C 51.12%, H 5.82%, N 27.35%, and O 15.71% (remaining), which matches with the empirical formula C₁₃H₁₈N₆O₃ that can be obtained by the loss of the above volatile components. This shows that the molecular adduct is stable with a water of crystallization in the lattice.

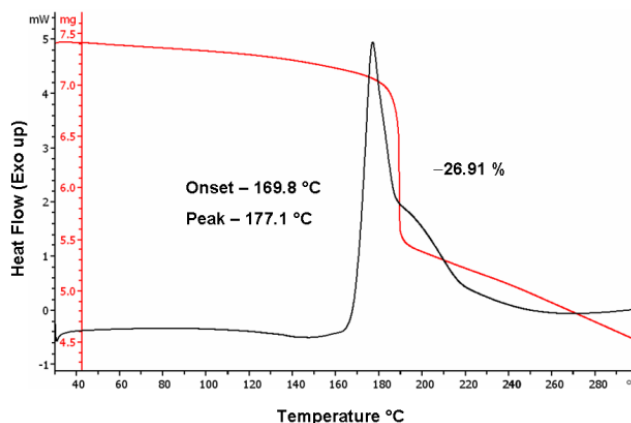


Figure 4.7 DSC (black) and TGA (red) of NF–L-arginine–H₂O.

4.2.4 NF methanolate

A 1:1 methanol solvate (NF–MeOH) was crystallized from methanol (detailed in Experimental Section). In the crystal structure, a tape of NF molecules assembled via C–H \cdots O interactions connects to methanol molecules through O_{MeOH}–H \cdots O_{NF} hydrogen bond. The tapes of Nitrofurantoin molecules form a herringbone motif, which makes channels of methanol molecules parallel to the *b*-axis (Figure 4.8).

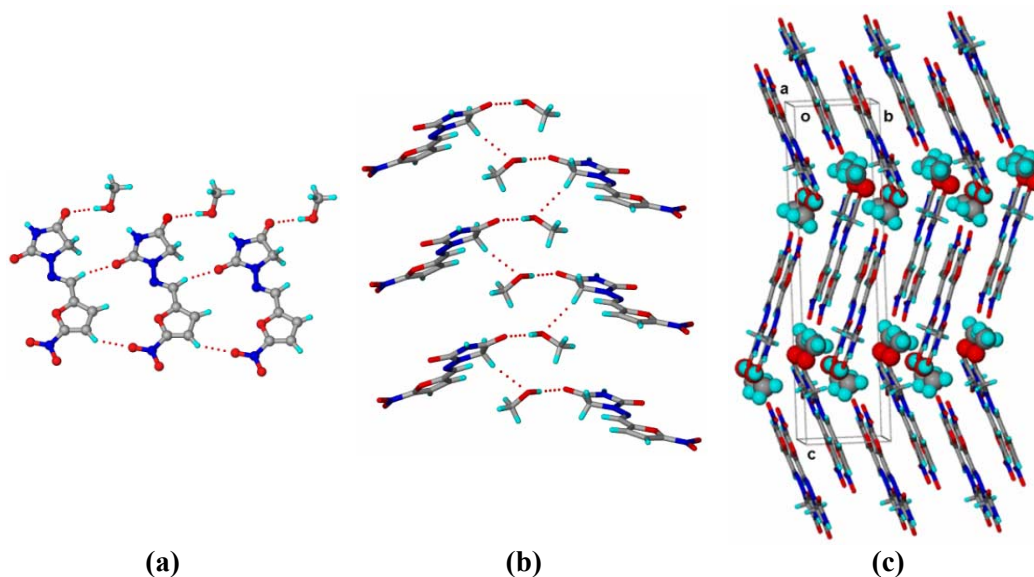


Figure 4.8 (a and b) A tape of NF molecules formed by C–H \cdots O interactions connects the channel of solvent methanol through O_{MeOH}–H \cdots O_{NF} hydrogen bonds along the *a*-axis. (c) Screw related methanol molecules reside in channels parallel to the *b*-axis and the overall crystal structure has a herringbone motif.

The methanolate crystals turned opaque after complete evaporation of the solvent and slowly converted to NF monohydrate form II at ambient temperature and humidity as monitored by PXRD (Figure 4.9). Guest exchange of NF methanolate with water was instant as the crystals opaqued immediately when suspended in water and converted to monohydrate II. The channel structure of NF methanolate could be a reason for its low stability and facile transformation to the hydrate form. Though there are no apparent similarities between the methanolate and hydrate II crystal structures, except that the guest molecules reside in channel/ cavity along the *b*-axis in the structures, presence of atmospheric moisture and the higher stability of the latter seem to favor the transformation instantly. DSC of NF methanolate showed an endotherm at 105 °C prior to melting and decomposition (270 °C) which is due to desolvation of methanol as observed from the weight loss of the material in TGA at the corresponding temperature

(experimental 11.83% and calculated 11.85% for 1 mole of MeOH) (Figure 4.10). Desolvation of solvates is known result in new polymorphs²³ and accordingly NF methanolate was subjected to controlled desolvation at 125 °C for 1 h. The resultant powdery material was found to be the stable NF β polymorph by PXRD profile match (with reference to Figure 4.2).

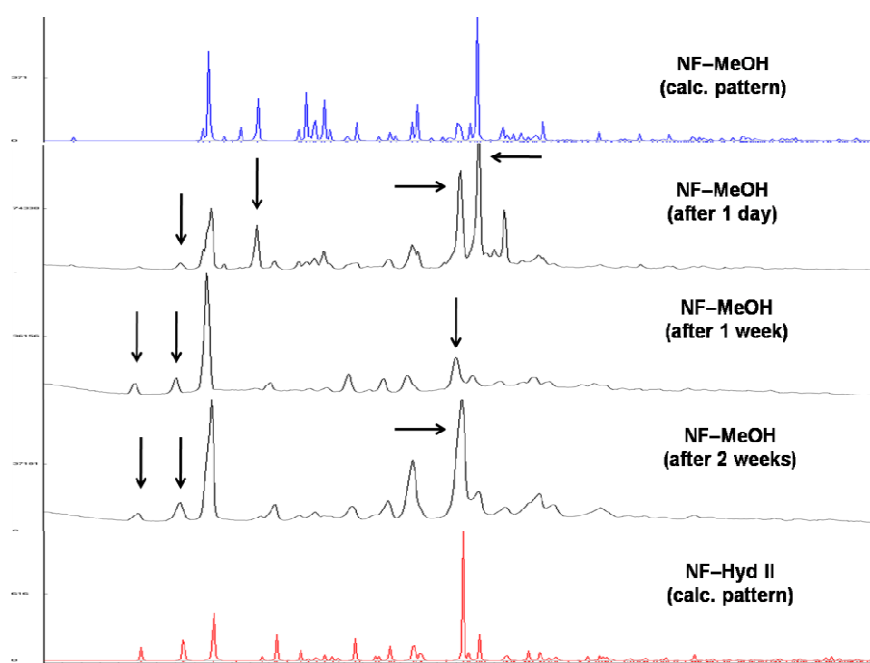


Figure 4.9 Transformation of NF methanolate to NF monohydrate II with time monitored by PXRD.

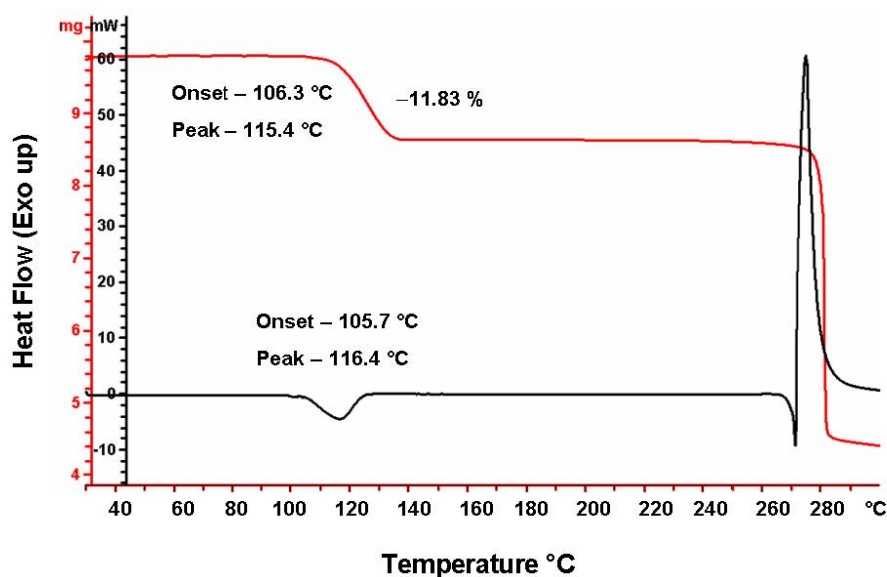


Figure 4.10 DSC (black) and TGA (red) of NF methanolate. The weight loss in TGA is consistent with one mole of MeOH in the solvate structure.

4.3 Solubility and Dissolution study of the Adducts

Solubility and dissolution are important physico-chemical parameters that influence the bioavailability of drugs.²⁴ Solubility is the concentration of the substance at equilibrium between the solution and the undissolved solid. The rate at which this equilibrium state is reached is the dissolution rate. The former is a thermodynamic parameter while the latter is a kinetic indicator.²⁴ The extent of drug dissolved in a particular time period is measured by the dissolution rate. During equilibrium solubility conditions (high supersaturation, agitation, long duration, typically 24 h), a solid drug form may dissociate or transform due to polymorphic change, hydrate formation, precipitation etc.^{24,25} Nevertheless, the formulation is advantageous if it facilitates drug release (in solution for absorption and consequent pharmacological action) within a desirable time-frame before it is destabilized. This evaluation whether the drug is sustained in the medium for the therapeutic retention time (usually 0.5–8 h) is achieved through a dissolution study.^{24,26}

Nitrofurantoin is a BCS Class IV drug with low water solubility.⁹ The reported aqueous solubility values of NF are quite far apart, 80 mg/L^{4a} and 190 mg/L¹⁶ at 25 °C. In this study, equilibrium solubility value obtained for NF (82 mg/L) at ambient temperature matched with the lower number.¹⁸ Cairra et al.^{4a} suggested that as anhydrous Nitrofurantoin (commercial NF β polymorph of this study) transforms to monohydrate II during solubility testing, the measured solubility of the drug actually corresponds to NF monohydrate II. The above transformation was confirmed by PXRD of the undissolved drug after the solubility experiment in this work. The transformation demonstrates higher stability of NF monohydrate II than the anhydrate β polymorph at ambient temperature and humidity. Similarly, equilibrium solubility experiments were done on NF–PABA, NF–urea and NF–L-Arg–H₂O in water at 25 °C. Only the solubility of NF–PABA cocrystal could be determined (216 mg/L is the molar equivalent solubility of NF in the cocrystal) because the other two adducts transformed to NF monohydrate II within one hour of the solubility experiment (analyzed by PXRD of the undissolved residue). NF–PABA cocrystal did not show any transformation to any of the NF forms (polymorph, hydrate) and was quite stable even after 3 days in the equilibrium solubility conditions.¹⁸ The solubility of NF–PABA cocrystal follows the ‘coformer solubility rule’²⁷ i.e. high solubility coformer (PABA aqueous solubility 5.8 g/L)²⁸ led to high solubility cocrystal. From a different perspective, this also means that low solubility NF resulted in even less

soluble NF–PABA cocrystal with respect to PABA. Thus, the compensation of solubility of NF (low) and PABA (high) resulted in intermediate solubility for the cocrystal.

As the NF–PABA cocrystal was found to be resistant to hydration, the effect of PABA as an additive in reducing the hydration of the drug in water was studied.¹⁸ With increase in the % of PABA to NF (from 5% to 60% by weight) in water slurry medium, a steady increase in the concentration of NF–PABA cocrystal and decrease in NF monohydrate II content in the residue (Figure 4.11) was observed as analyzed by PXRD (Table 4.3). This shows that PABA reacted with NF to form stable NF–PABA cocrystal in solution. Complexation between NF and PABA was observed as a visible color change of the solution from yellow to orange (NF/ NF–H₂O II is yellow, PABA is white and NF–PABA is orange), while the excess NF transformed to the monohydrate. The gradual change in the color of the residue (from yellow to orange) with increase in the concentration of NF–PABA cocrystal is shown in Figure 4.12. At 57.6% of PABA-to-NF (molar proportion of components in the 1:1 cocrystal), there was no trace of NF monohydrate II in the residue and the material was entirely NF–PABA cocrystal (with reference to PXRD pattern in Figure 4.3b). This shows that PABA was effective as a coformer in the 1:1 cocrystal composition to make NF stable to hydration and also as an additive in reducing its hydration.

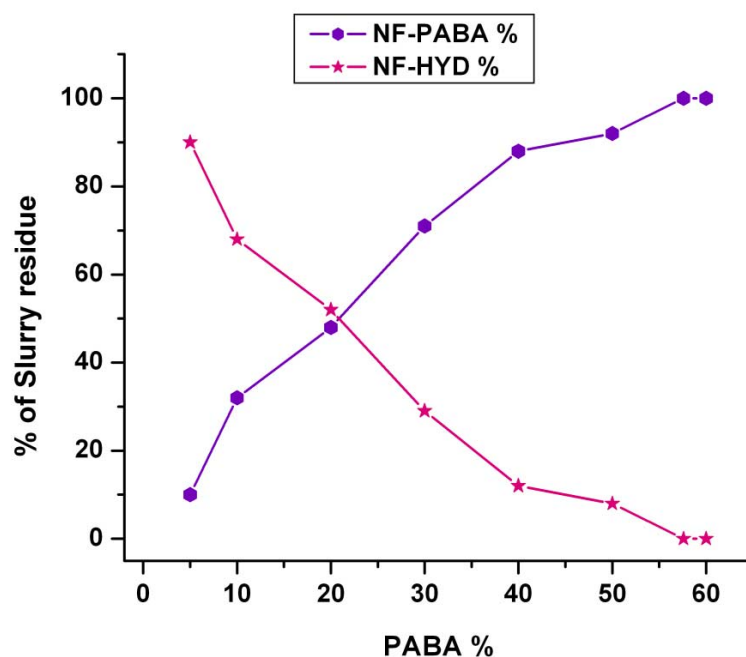
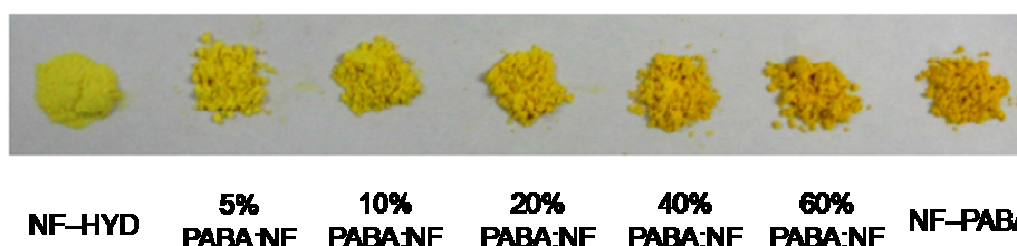


Figure 4.11 Variation in the composition of NF–PABA cocrystal and NF monohydrate II in the water slurry residue with increase of PABA concentration.

Table 4.3 Activity of PABA on NF in water slurry medium.

% of PABA to NF in water slurry	% of NF-PABA in residue	% of NF monohydrate II in residue	R_p from PXRD
5	10	90	0.27
10	32	68	0.26
20	48	52	0.22
30	71	29	0.25
40	88	12	0.33
50	92	8	0.26
57.6	100	0	0.15
60	100	0	0.16

**Figure 4.12** Color change of water slurry residue from yellow to orange with increase in the concentration of NF-PABA cocrystal.

Nitrofurantoin is a typical drug whose rapid initial dissolution and consequent faster absorption leads to side effects of nausea and emesis after oral administration,¹⁰ though being a BCS Class IV drug (low solubility and low permeability).⁹ The dissolution profile of the drug is variable: after a high initial dissolution the drug is released (dissolved) slowly because it converts to the more stable hydrate in aqueous medium (anhydrate β with faster dissolution rate \rightarrow monohydrate II with slower dissolution rate).^{4a} Hence, the drug is administered as macrocrystalline NF¹¹ and a combination of macrocrystalline NF and NF monohydrate¹² to facilitate slower dissolution and reduce the side effects due to faster absorption. Therefore, a drug formulation which can regulate the dissolution and hydration of NF is desirable. In this context, dissolution behavior of the adducts (NF-PABA, NF-urea and NF-L-Arg-H₂O) was compared with that of NF β polymorph and NF monohydrate II, in three different media viz. pure water (pH 6.4), 0.1 N HCl (pH 1.2) and disodium hydrogen phosphate buffer (pH 6.8) at 37 °C.¹⁸ The intrinsic dissolution rates (IDRs) of the compounds were estimated based on their individual molar extinction coefficients in the respective medium (Table 4.4). The IDR of the compounds was found to be higher for the first 30 min of the dissolution experiment and the value decreased with time except in a few

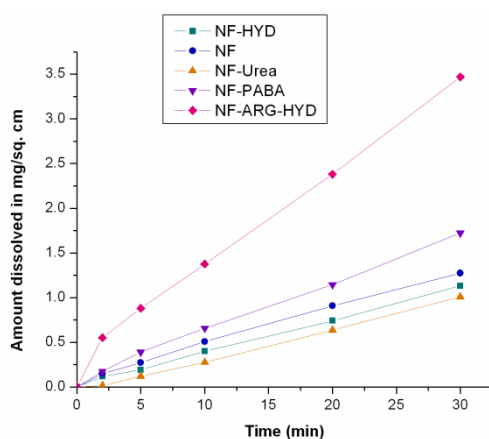
cases (Table 4.5). The IDR in water followed the order: NF-L-Arg-H₂O > NF-PABA > NF β > NF hydrate II > NF-urea for the first 30 min and NF-L-Arg-H₂O > NF-PABA > NF β > NF-urea > NF hydrate II for 4 h (Table 4.5 & Figure 4.13). In 0.1 N HCl the order is NF-L-Arg-H₂O > NF-PABA > NF-urea > NF β > NF hydrate II and the same trend is observed in pH 6.8 buffer (Table 4.5 & Figure 4.13).

Table 4.4 Molar extinction coefficients of the compounds in different media.

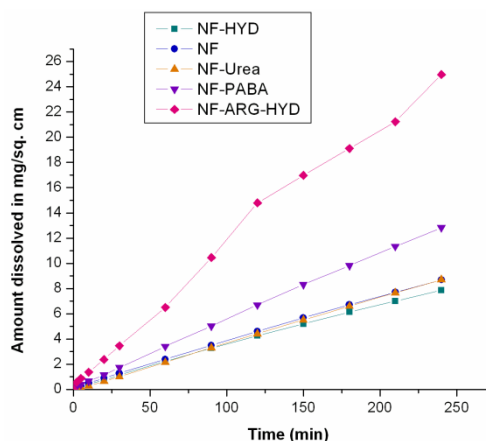
Molar extinction coefficient, mL mg ⁻¹ cm ⁻¹	NF β	NF monohydrate II	NF-Urea	NF-PABA	NF-L-Arg-H ₂ O
Water	73.69	68.31	58.41	46.10	43.56
0.1 N HCl	68.73	61.04	51.02	43.91	37.04
pH 6.8 buffer	71.61	66.70	57.24	44.80	40.85

Table 4.5 IDRs of the compounds in different media.

Compound	Water		0.1 N HCl		pH 6.8 buffer	
	IDR in $\mu\text{g cm}^{-2} \text{ min}^{-1}$ (for 30 min)	IDR in $\mu\text{g cm}^{-2} \text{ min}^{-1}$ (for 4 h)	IDR in $\mu\text{g cm}^{-2} \text{ min}^{-1}$ (for 30 min)	IDR in $\mu\text{g cm}^{-2} \text{ min}^{-1}$ (for 4 h)	IDR in $\mu\text{g cm}^{-2} \text{ min}^{-1}$ (for 30 min)	IDR in $\mu\text{g cm}^{-2} \text{ min}^{-1}$ (for 4 h)
NF β	44.2	37.1	39.7	30.8	48.5	43.4
NF monohydrate II	37.8	33.9	27.3	25.8	47.1	41.3
NF-Urea	32.5	36.5	39.9	35.8	51.5	52.2
NF-PABA	58.5	54.4	50.3	44.1	72.2	68.9
NF-L-Arg-H ₂ O	119.6	107.1	75.9	52.6	138.5	165.5



(a)



(b)

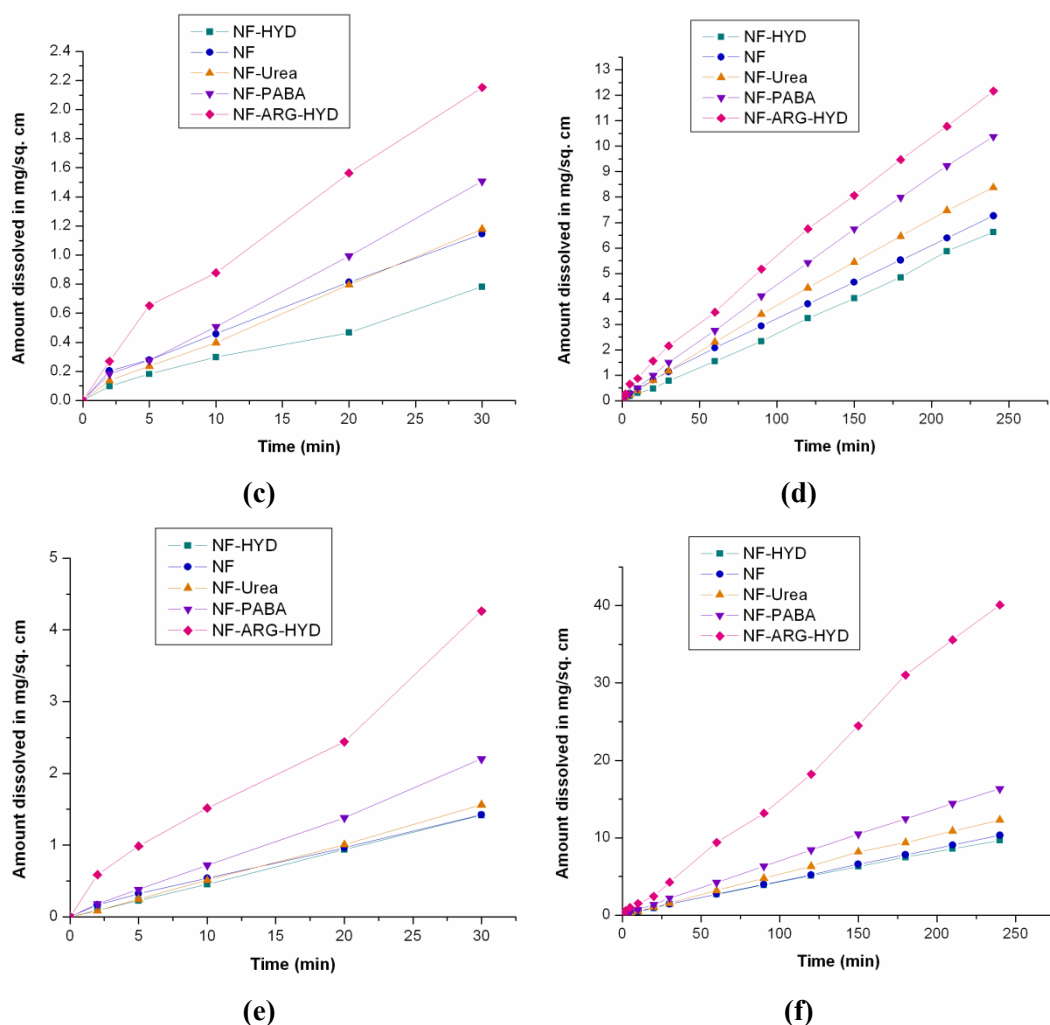


Figure 4.13 Dissolution profiles of NF and its adducts in water (a & b), 0.1 N HCl (c & d) and (e & f) pH 6.8 buffer.

The IDR of NF solid forms was higher in phosphate buffer compared to pure water and least in acidic medium (Table 4.5), indicating the role of pH in drug dissolution. The higher dissolution rate of NF β polymorph than NF monohydrate II is consistent with previous reports.^{3b,4a} The IDR of NF-urea cocrystal is closer to both NF β polymorph and NF monohydrate II in the three media (Table 4.5). The lower IDR of NF-urea cocrystal is attributed to its faster dissociation and consequent transformation of unbound NF on the exposed surface of the dissolution tablet (also called disk or pellet) to NF monohydrate II. Earlier, Caira et al.^{4a} reasoned the closeness of dissolution rates of NF α polymorph and NF monohydrate II as due to the transformation of the former to the latter such that the dissolution rate actually measured was that of the growing layer of

NF monohydrate II on the tablet surface exposed to aqueous medium, and confirmed it through DSC analysis of tablet surface. Similar to the case, the PXRD analysis of undissolved material of the NF–urea cocrystal (recovered after dissolution experiment) revealed NF monohydrate II content (about 25% in 0.1 N HCl and 30% in pH 6.8 buffer media) demonstrating partial transformation of the former to the latter (Figure 4.14). The NF–PABA cocrystal which is stable to hydration in water (in equilibrium solubility conditions) was also stable in water as the dissolution medium, but partially converted to NF monohydrate II in 0.1 N HCl (22% NF monohydrate II content by PXRD analysis, Figure 4.15) and pH 6.8 buffer media (14% NF monohydrate II content). This variation in the physicochemical behavior of NF–PABA cocrystal can be due to change in the ionization state of PABA (having two ionizable groups – carboxylic acid and amine) at different acidity levels, resulting in cocrystal dissociation and causing unbound NF to hydrate. The higher IDR of NF–PABA cocrystal compared to that of the NF–urea (Table 4.5) is attributed to its slower transformation to NF monohydrate II as observed from its higher content in the undissolved material at the end of dissolution experiments. Thus, the dissolution behavior of NF–PABA cocrystal is similar to that of NF β polymorph, which was known to exhibit higher IDR and slower transformation.^{4a}

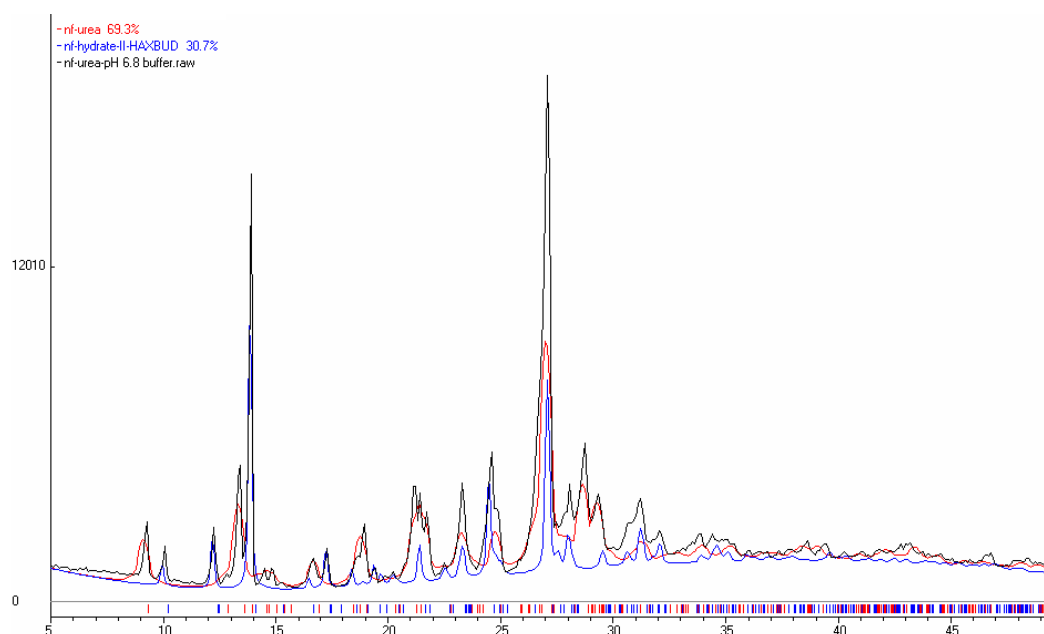


Figure 4.14 Overlay of the calculated X-ray crystal structures of NF–urea (red) and NF monohydrate II (blue) on the PXRD pattern of NF–urea cocrystal subjected to dissolution in pH 6.8 buffer medium (black) shows 70:30 composition by Rietveld refinement ($R_p = 0.15$).

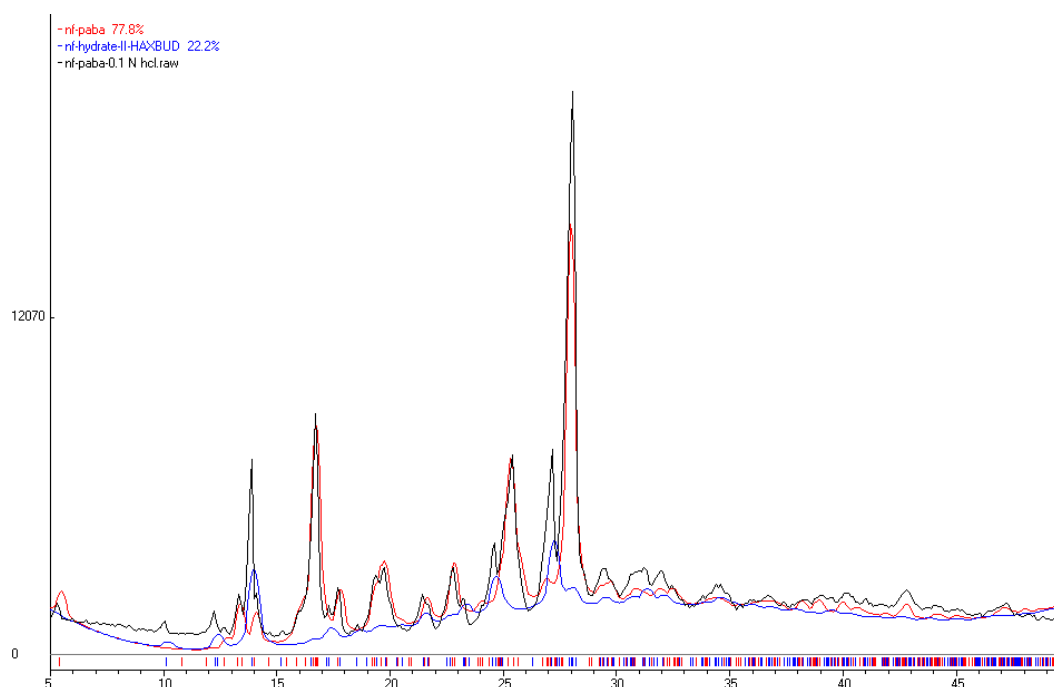


Figure 4.15 Overlay of the calculated X-ray crystal structures of NF–PABA (red) and NF monohydrate II (blue) on the PXRD pattern of NF–PABA cocrystal subjected to dissolution in 0.1 N HCl medium (black) shows 78:22 composition by Rietveld refinement ($R_p = 0.17$).

In contrast, NF–L–Arg–H₂O salt exhibited highest IDR of all compounds (Table 4.5) even though it completely transformed to NF monohydrate II in all the three media (analyzed by PXRD with reference to Figure 4.3a). The dissolution behavior of this salt conforms to Nangia’s model of cocrystal solubility.²⁹ According to the model, a cocrystal (or salt) containing a high soluble coformer (or salt former) can facilitate faster dissolution of a low soluble component. This happens via the fast release of high soluble coformer into aqueous medium (because of its higher affinity to the latter) that results in the dissociation of cocrystal, thereby leaving behind the low soluble component in an amorphous/randomized state, which understandably leads to an increase in the solubility/dissolution of the low soluble component.²⁹ In this case, before the unbound NF (formed upon release of L-arginine from the lattice) hydrates, it is believed that much of it actually dissolves in the medium thus giving rise to higher IDR values. The same behavior (high IDR despite transformation to slow dissolving monohydrate II) was not observed for the NF–urea cocrystal which showed low IDR values close to that of the monohydrate II upon transformation (Table 4.5). This anomalous behavior of NF–urea cocrystal, despite greater aqueous solubility of urea (1.21 g/mL)³⁰ than L-arginine (0.18

g/mL),³¹ could be due to relative differences between solute-solute (NF and urea/L-arginine) interactions and solute-solvent interactions which govern dissolution kinetics. In all, both NF-PABA and NF-urea cocrystals are more stable and exhibited desirable low IDRs compared to NF-L-Arg-H₂O salt in the aqueous dissolution experiments.¹⁸ The significance and take home point of these findings is that it runs contrary to the popular belief that salts are more preferable to cocrystals for drug formulation.

4.4 Conclusions

Cocrystallization with a few coformers was evaluated as a pharmaceutical development methodology to control the hydration and dissolution behavior of Nitrofurantoin.¹⁸ All the adducts except NF methanolate were found to be stable at ambient temperature and humidity conditions. Crystal structure analysis of the cocrystals NF-PABA and NF-urea suggest a possibility of polymorphs for the cocrystals based on the lack of expected supramolecular synthons in the manifested structures. Both the cocrystals come under the category of pharmaceutical cocrystals^{29,32} because of the GRAS (Generally Recognized as Safe) status of the coformers.³³ The two cocrystals showed desirable physicochemical properties viz. hydration stability (NF-PABA) and lower dissolution rate (NF-urea) compared to NF-L-Arg-H₂O salt. Among the three adducts, NF-PABA cocrystal is least susceptible to transformation to NF monohydrate II in the three media of different pHs. PABA was found to control hydration of NF both as an additive (from 5 to 50% of NF) and a coformer (57.6% of NF) by forming NF-PABA cocrystal. Thus, NF-PABA combination can be useful as a novel/alternate formulation that can control hydration and dissolution and consequently the absorption rate of the drug.¹⁸ The amount of actual drug absorbed can be adjusted by modifying PABA content in the NF drug formulation. This limited study suggests that, in some cases, the relatively new cocrystals methodology can be advantageous than the conventional salt forms for controlling the physicochemical properties of drugs.

4.5 Experimental Section

Materials and Methods: Commercially available Nitrofurantoin (Alfa Aesar) was used without further purification. All other chemicals were of analytical or chromatographic grade. Water filtered through a double deionized purification system (Milli Q Plus Water System from Millipore Co., USA) was used for experiments.

Crystallization of the molecular adducts

NF–PABA: NF (23.8 mg, 0.1 mmol) and PABA (13.7 mg, 0.1 mmol) were dissolved in 5 mL hot acetonitrile and left for slow evaporation at room temperature. Brownish red crystals were formed after a few days upon solvent evaporation. The cocrystal has no definite melting point and started to decompose from 210 °C (m.p. of NF 263 °C, m.p. of PABA 186 °C).

NF–Urea: A powdered mixture of NF (46.8 mg, 0.2 mmol) and urea (12 mg, 0.2 mmol) was dissolved in 4 mL hot DMF–dioxane solvent mixture (1:1 v/v) and left for slow evaporation at room temperature. Yellow crystals were formed after few days upon solvent evaporation. The cocrystal has no definite melting point and started to decompose at 160 °C (m.p. of urea 133 °C).

NF–L-Arg–H₂O: A powdered mixture of NF (23.8 mg, 0.1 mmol) and L-arginine (17.4 mg, 0.1 mmol) was dissolved in 6 mL of hot 1:1 acetonitrile–isopropanol solvent mixture (1:1 v/v). Brown crystals of 1:1:1 NF–L-Arg–H₂O were formed after a few days upon solvent evaporation at room temperature. The salt has no definite melting point and started to decompose at 170 °C (m.p. of L-arginine 222 °C).

NF–MeOH: 50 mg NF was dissolved in 15 mL hot methanol and left for slow evaporation at room temperature. Yellow crystals in equilibrium with the mother liquor formed after one day were filtered and used for characterization and experiments.

Grinding: The cocrystals were prepared in bulk quantity by neat grinding and the hydrates (salt hydrate and NF monohydrate II) by water-assisted grinding. About 200 mg of the components, combined together as per the stoichiometric ratio in the crystal structure, was ground for 15-20 min using a mortar-pestle. 8-10 drops water was added during grinding in case of water-assisted grinding. PXRD and melting point of the ground material was recorded to confirm complete reaction of starting materials and formation of a new crystalline phase.

X-ray Crystallography: X-ray reflections were collected on Bruker SMART-APEX CCD diffractometer equipped with a graphite monochromator and Mo-K α ($\lambda = 0.71073$ Å) fine-focus sealed tube. Data reduction was performed using Bruker SAINT software. Intensities were corrected for absorption using SADABS. Structures were solved and refined using SHELX-97 with anisotropic displacement parameters for non-H atoms. Hydrogen atoms on O and N were experimentally located in difference electron density

maps. All C–H atoms were fixed geometrically using HFIX command in SHELX-TL. The final CIF files and hydrogen bond geometries were validated in PLATON. X-Seed was used to prepare packing diagrams.

Powder X-ray Diffraction: Powder X-ray diffraction of the samples were recorded on Bruker D8 Advance diffractometer using Cu-K α X-radiation ($\lambda = 1.5406 \text{ \AA}$) at 40 kV and 30 mA. Diffraction patterns were collected over 2θ range of $5\text{--}50^\circ$ at scan rate of 1° min^{-1} . Powder Cell 2.4 was used for Rietveld refinement.

Thermal Analysis: DSC was performed on a Mettler Toledo DSC 822e module and TGA on a Mettler Toledo TGA/SDTA 851e module. The typical sample size is 3–5 mg for DSC and 8–12 mg for TGA. Samples were placed in sealed pin-pricked aluminum pans for DSC experiments and alumina pans for TGA experiments. A heating rate of $5^\circ \text{ C min}^{-1}$ in the temperature range $30\text{--}300^\circ \text{ C}$ was applied. Samples were purged by a stream of dry nitrogen flowing at 80 mL min^{-1} for DSC and 50 mL min^{-1} for TGA.

CHN Analysis: Microanalysis was performed on ThermoFinnigan/EA 1112 CHNS analyzer on a 5 mg sample.

Equilibrium solubility and Intrinsic dissolution measurements: Prior to solubility and dissolution measurements, calibration curves of each of the compounds in all the three media (water, 0.1 N HCl and pH 6.8 buffer) were obtained and their molar extinction coefficients were determined spectrophotometrically (Table 4.5) on a Thermo Scientific Evolution 300 UV-Vis spectrometer based on the absorbance at 368 nm (λ_{max} of Nitrofurantoin devoid of interference from other compounds). The respective molar extinction coefficients of the compounds were used to estimate solubility and dissolution values. Equilibrium solubility was determined in water using the shake-flask method.³⁴ 100 mg of powdered compound was added to 5 mL water and the resulting suspension was stirred at 25° C for 24 h. The suspension was equilibrated for one hour and then filtered through $2.5 \mu\text{m}$ Whatman filter paper. The concentration of the solution thus obtained was determined spectrophotometrically after appropriate dilution using the molar extinction coefficients of the respective compounds. IDR experiments in water, 0.1 N HCl and pH 6.8 buffer were carried on a USP certified Electrolab TDT-08L Dissolution Tester for 4 hours by the disk intrinsic dissolution rate (DIDR) method.³⁵ The pH 6.8 buffer was prepared as per the International Pharmacopoeia (3rd edition, 2003).³⁶ For IDR testing, 100 mg of the compound was taken in the intrinsic attachment

and compressed to a 0.5 cm² disk using a hydraulic press at a pressure of 2.5 ton inch⁻² for 5 min. The intrinsic attachment was placed in a jar of 500 mL medium preheated to 37 °C and rotated at 150 rpm. Aliquots of 5 mL were collected at specific time intervals and concentration of the aliquots was determined spectrophotometrically using the molar extinction coefficients of the respective compounds. The linear region of the dissolution profile (regression >0.99) was used to determine the IDR of the compound as (slope of the amount dissolved ÷ surface area of the disk) per unit time. The identity of the undissolved materials after solubility and dissolution experiments was established through PXRD. There is no transformation of the compounds upon compression.

4.6 References

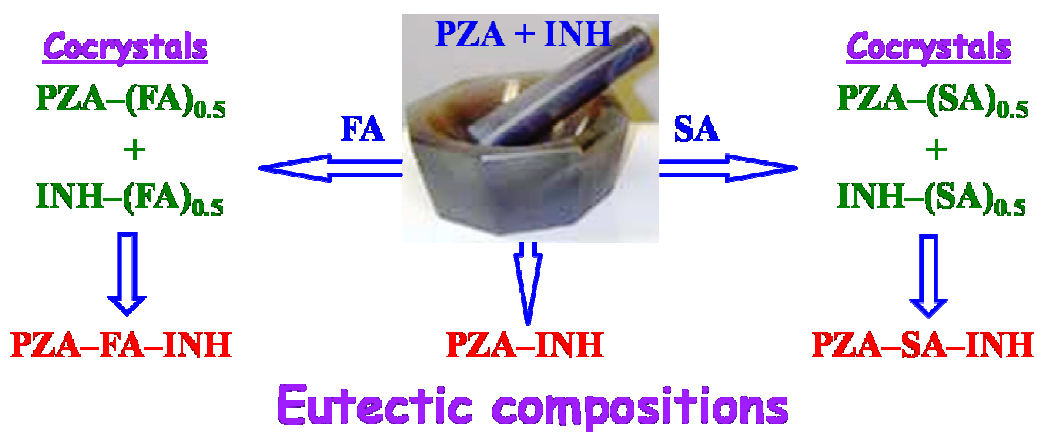
1. M. A. Miller-Hjelle, V. Somaraju and J. T. Hjelle, In *Modern pharmacology with clinical applications*, C. R. Craig and R. E. Stitzel, Eds., 5th ed., Little Brown & Company, Boston, 1997, pp 515–525.
2. WHO model list of Essential Medicines is available at http://www.who.int/selection_medicines/committees/expert/17/sixteenth_adult_list_en.pdf.
3. (a) P. V. Marshall and P. York, *Int. J. Pharm.*, 1989, **55**, 257; (b) M. Otsuka, R. Teraoka and Y. Matsuda, *Chem. Pharm. Bull.*, 1991, **39**, 2667.
4. (a) M. R. Caira, E. W. Pienaar and A. P. Lötter, *Mol. Cryst. Liq. Cryst.*, 1996, **279**, 241; (b) E. W. Pienaar, M. R. Caira and A. P. Lötter, *J. Crystallogr. Spectr. Res.*, 1993, **23**, 739–744 & 785–790.
5. F. Tian, H. Qu, M. Louhi-Kultanen and J. Rantanen, *J. Cryst. Growth*, 2009, **311**, 2580.
6. (a) R. K. Khankari and D. J. W. Grant, *Thermochim. Acta*, 1995, **248**, 61; (b) E. Shefter and T. Higuchi, *J. Pharm Sci.*, 1963, **52**, 781.
7. N. Sandler, J. Rantanen, J. Heinämäki, M. Römer, M. Marvola and J. Yliruusi, *AAPS Pharm. Sci. Tech.*, 2005, **6**, E174.
8. H. Wikström, J. Rantanen, A. D. Gift and L. S. Taylor, *Cryst. Growth Des.*, 2008, **8**, 2684.
9. N. A. Kasim, M. Whitehouse, C. Ramachandran, M. Bermejo, H. Lennernas, A. S. Hussain, H. E. Junginger, S. A. Stavchansky, K. K. Midha, V. P. Shah and G. L. Amidon, *Mol. Pharm.*, 2004, **1**, 85.

10. H. E. Paul, J. H. Kenyon, M. F. Paul and A. R. Borgmann, *J. Pharm. Sci.*, 1967, **56**, 882.
11. [http://www.betterhealth.vic.gov.au/bhcv2/bhcmcd.nsf/pages/pfcmacrc/\\$File/pfcmacrc.pdf](http://www.betterhealth.vic.gov.au/bhcv2/bhcmcd.nsf/pages/pfcmacrc/$File/pfcmacrc.pdf).
12. http://www.accessdata.fda.gov/drugsatfda_docs/label/2009/020064s019lbl.pdf.
13. V. Koradia, H. L. D. Diego, M. R. Elema and J. Rantanen, *J. Pharm. Sci.*, 2010, **99**, 3966.
14. M. Otsuka, R. Teraoka and Y. Matsuda, *Pharm. Res.*, 1992, **9**, 307.
15. G. Gever and J. G. Vincent, *GB Pat.*, 902692, *US Pat.*, 30078461962, 1962.
16. A. M. Deboeck, J. J. Fossion and R. R. Smolders, *Eur. Pat.*, 0066934, 1982.
17. (a) R. D. B. Walsh, M. W. Bradner, S. Fleischman, L. A. Morales LA, B. Moulton, N. Rodríguez-Hornedo and M. J. Zaworotko, *Chem. Commun.*, 2003, 186; (b) G. R. Desiraju, *Angew Chem. Int. Ed. Engl.*, 1995, **34**, 2311.
18. S. Cherukuvada, N. J. Babu and A. Nangia, *J. Pharm. Sci.*, 2011, **100**, 3233.
19. (a) V. R. Vangala, P. S. Chow and R. B. H. Tan, *Acta Crystallogr.*, 2011, **E67**, o550; (b) V. R. Vangala, P. S. Chow and R. B. H. Tan, *CrystEngComm*, 2011, **13**, 759; (c) M. Tutughamiarso, M. Bolte, G. Wagner and E. Egert, *Acta Crystallogr.*, 2011, **C67**, o18. (d) A. Alhalweh, S. George, S. Basavoju, S. L. Childs, S. A. A. Rizvi and S. Velaga, *CrystEngComm*, 2012, **14**, 5078.
20. (a) N. Shan, F. Toda and W. Jones, *Chem. Commun.*, 2002, 2372; (b) A. V. Trask, D. A. Haynes, W. D. S. Motherwell and W. Jones, *Chem. Commun.*, 2006, 51; (c) A. V. Trask, N. Shan, W. D. S. Motherwell, W. Jones, S. Feng,; R. B. H. Tan and K. J. Carpenter, *Chem. Commun.*, 2005, 880.
21. B. P. van Eijck and J. Kroon, *Acta Crystallogr.*, 2000, **B56**, 535.
22. S. R. Byrn, R. R. Pfeiffer and J. G. Stowell, *Solid-State Chemistry of Drugs*; SSCI, West Lafayette, IN, 1999.
23. (a) D. Martins, M. Sanselme, O. Houssin, V. Dupray, M. N. Petit, D. Pasquier, C. Diolez and G. Coquerel, *CrystEngComm*, 2012, **14**, 2507; (b) B. Samas, C. Seadeek, A. M. Campeta and B. P. Chekal, *J. Pharm. Sci.*, 2011, **100**, 186; (c) B. Nicolai, P. Espeau, R. Céolin, M. -A. Perrin, L. Zaske, J. Giovannini and F. Leveiller, *J. Ther. Anal. Cal.*, 2007, **90**, 337; (d) H. G. Brittain, Ed., *Polymorphism in Pharmaceutical Solids*, Informa Healthcare USA Inc., New York, 2009.

24. Y. Qiu; Y. Chen and G. G. Z. Zhang, Eds., *Developing Solid Oral Dosage Forms. Pharmaceutical Theory and Practice*, Academic Press, New York, 2009.
25. N. Blagden, M. de Matas, P. T. Gavan and P. York, *Adv. Drug Deliv. Rev.*, 2007, **59**, 617.
26. J. B. Dressman, G. L. Amidon, C. Reppas and V. P. Shah, *Pharm. Res.*, 1998, **15**, 11.
27. D. J. Good and N. Rodríguez-Hornedo, *Cryst. Growth Des.*, 2009, **9**, 2252.
28. *The Merck Index: An Encyclopedia of Chemicals, Drugs and Biologicals*, 14th ed., Merck Research Laboratories, 2006.
29. N. J. Babu and A. Nangia, *Cryst. Growth Des.*, 2011, **11**, 2662.
30. F.-M. Lee and L. E. Lathi, *J. Chem. Eng. Data*, 1972, **17**, 304.
31. *CRC Handbook of Chemistry and Physics*, ed. D. R. Lide, 90th ed., CD-ROM ver, CRC Press/Taylor & Francis, 2010.
32. N. Schultheiss and A. Newman, *Cryst. Growth Des.*, 2009, **9**, 2950.
33. GRAS/EAFUS (Everything Added to Food in the United States) substances list: <http://www.fda.gov/Food/FoodIngredientsPackaging/ucm115326.htm>.
34. A. Glomme, J. März and J. B. Dressman, *J. Pharm. Sci.*, 2005, **94**, 1.
35. L. X. Yu, A. S. Carlin, G. L. Amidon and A. S. Hussain, *Int. J. Pharmaceutics*, 2004, **270**, 221.
36. The International Pharmacopoeia, 3rd ed., WHO, Geneva, 2003.

CHAPTER FIVE

PYRAZINAMIDE AND ISONIAZID COCRYSTALS AND EUTECTICS



Solid state grinding of the two anti-tubercular drugs Pyrazinamide (PZA) and Isoniazid (INH) with Succinic acid (SA) and Fumaric acid (FA) gave the respective drug-(coformer)_{0.5} cocrystals which formed 1:1:1 ternary eutectic compositions, PZA-SA-INH and PZA-FA-INH, upon further grinding. Grinding of the pure drugs resulted in a 1:1 PZA-INH binary eutectic.

5.1 Introduction

Pyrazinamide (PZA) and Isoniazid (INH) are the first-line anti-tuberculosis drugs administered with Rifampicin and Ethambutol dihydrochloride in fixed dose combination (FDC).¹ All the four drugs are on the WHO Model List of Essential Medicines.² Multi-drug therapy is important for tuberculosis (TB), HIV, malaria and cardiovascular targets to treat the disease in a comprehensive way.³ Several combination formulations marketed as polypills are also on the WHO Model List of Essential Medicines² and combination drugs for multiple disease conditions are being studied.⁴ The advantages of combination drugs are better drug management, coping with drug resistance, as well as intellectual property reasons.³ However, on the down side, FDCs pose drug compatibility, dosage, and pharmacokinetic problems.⁵ A fall in the bioavailability of isoniazid and rifampicin due to drug–drug interactions in the anti-TB FDC products was noted.⁶ As a consequence, individual drugs of the anti-TB FDC formulations are separately coated with polymers to avoid mutual interaction and then blended to make up the final product formulation.⁷

The conventional approach in combination drug therapy is to physically blend the drugs as a solid mixture. Covalent joining of the drugs through a labile linker is a recent synthetic approach for drug combinations.^{4,8} The non-covalent approach (i.e. co-crystallization methodology that involves no making or breaking of covalent bonds)⁹ of combining the drugs was pursued in this study. Even as extensive literature is reported on drug cocrystals,¹⁰ mainly in the last decade,^{10c-m} drug–drug cocrystals¹¹ and drug–drug eutectics¹² are, as such, less explored. PZA and INH make a model system to study the potential of co-crystallization in physical property enhancement for combination drugs. Even though PZA and INH are not currently marketed as a two drug FDC formulation, their combination therapy was reported to be effective long ago.¹³

PZA is known to be tetramorphic¹⁴ but INH has no polymorphs so far. Both the drugs were reported to form cocrystals independently^{11a,b,15} but they did not co-crystallize into a drug–drug cocrystal.^{11a} In this work, attempts to make a binary cocrystal of PZA and INH by solution crystallization and by classical mechano-chemical grinding¹⁶ (solid state grinding technique – detailed in Experimental Section) were unsuccessful but led to a 1:1 binary eutectic PZA–INH¹⁷ (discussed later). Then, the classical and robust carboxylic acid–pyridine heterosynthon¹⁸ was thought of to build a ternary cocrystal

Solid state grinding of PZA and INH with the diacid (SA or FA) in 1:1:1 molar stoichiometry (detailed in Experimental Section) did not result in a new cocrystal phase. Instead 1:1:1 ternary eutectics of PZA and INH with SA (PZA–SA–INH) and FA (PZA–FA–INH) were obtained and each phase was characterized by DSC, PXRD, ss-NMR and FT-IR.¹⁷ These three component solid phases of fixed stoichiometry were found to be eutectic composition of their respective binary cocrystals (i.e. PZA–SA–INH is composed of PZA–(SA)_{0.5} and INH–(SA)_{0.5} and PZA–FA–INH is composed of PZA–(FA)_{0.5} and INH–(FA)_{0.5}). These ternary eutectics are the first examples of cocrystals making novel eutectic phases.¹⁷ Solubility and dissolution experiments on the novel phases showed that their intrinsic dissolution rates (IDRs) are in the order, PZA–SA–INH > INH > PZA–INH > PZA–FA–INH > PZA. Thus, all the new eutectics have faster dissolution than PZA and overall PZA–SA–INH ternary eutectic has faster dissolution than the parent drugs and also the binary cocrystals.¹⁷

5.2 Crystal structures of Binary Cocrystals

X-ray crystal structures of the newly obtained 1:0.5 binary PZA–SA, PZA–FA and INH–FA cocrystals were determined in this work. The INH–SA cocrystal reported by Lemmerer et al. (collected at 173 K)^{15d} was redetermined at 298 K.¹⁷ The nature of an adduct can be predicted, as being salt (ionic), cocrystal (neutral) or intermediate/mixed ionization complex, based on the ‘ ΔpK_a rule’ when the parent compounds are basic (here PZA and INH) and acidic (here SA and FA) in nature.²⁰ In this case, all the adducts are expected to be cocrystals (neutral species) since the ΔpK_a values are negative (Table 5.1). All the adducts, except INH–FA, are cocrystals and the latter is found to be a mixed ionic complex wherein the proton is shared between O (carboxylic acid of FA) and N (pyridine of INH) atoms¹⁷ (Figure 5.2d). Although an isolated case, this example demonstrates the difficulty in anticipating the nature of an adduct (whether ionic, neutral or mixed ionic) with respect to carboxylic acid–pyridine synthon from the ‘ ΔpK_a rule’.

Table 5.1 pK_a values and nature of O–H...N interaction in the molecular adducts.

S. No.	Drug	Coformer	pK_{a1} (base)	pK_{a1} (acid)	$\Delta pK_a =$ $pK_a \text{ (base)} - pK_a \text{ (acid)}$	O–H...N interaction
1	PZA ^a	SA ^b	0.5	4.21	–3.71	neutral
2	PZA	FA ^b	0.5	3.02	–2.52	neutral
3	INH ^c	SA	1.8	4.21	–2.41	neutral
4	INH	FA	1.8	3.02	–1.22	mixed ionic

^a Ref 21a; ^b Ref 21b; ^c Ref 21c.

In the crystal structures of the binary adducts, both the diacids, SA and FA, lie about an inversion centre. Thus, each half of the diacid molecule is connected to a full molecule of the drug such that each diacid molecule connects two drug molecules on either side through the carboxylic acid–pyridine synthon¹⁷ (Figure 5.2). Thus, the molar ratio of these binary adducts can be designated as ‘1:0.5’ or ‘2:1’ stoichiometry. X-ray crystallographic parameters are shown in Table 5.2 and hydrogen bonds in Table 5.3. PZA–SA and PZA–FA cocrystals are isomorphous²² (same space group and unit-cell dimensions, Table 5.2), as well as isostructural,²³ with a unit-cell similarity index (Π) of 0.0021. In both the structures, each of the diacid connects two PZA molecules on either side through acid–pyridine synthon to form a zigzag tape that propagates through PZA amide $R_2^2(8)$ dimers (Figure 5.3). Adjacent tapes are non-planar (each of which along (11–2) and (–112) planes make an angle of 22.1° in PZA–SA and 21.9° in PZA–FA) and form criss-cross structures through N–H···O and C–H···O interactions in 3D (Figure 5.3). Thus, the two cocrystals of their isomorphous nature can form solid solutions.

In INH–SA cocrystal, linear tapes are formed by INH N–H···O $R_2^2(10)$ dimers connected by carboxylic acid–pyridine synthon (Figure 5.4). Such linear tapes form a 2D sheet through INH hydrazide N–H···N $R_2^2(6)$ dimers and auxiliary C–H···O bonds (Figure 5.4). INH–FA is a sheet structure (Figure 5.5), similar to INH–SA cocrystal, but is formed by zigzag tapes contrast to linear tapes of the latter. The INH–FA adduct is an exceptional case which is found to violate the ‘ ΔpK_a rule’²⁰ by forming a mixed ionization complex. The ΔpK_a value is negative (–1.22, Table 5.1) and is expected to be a cocrystal just as the above three cases. But, surprisingly, there is a partial proton transfer from acid (FA) to pyridine (INH) resulting in O···H···N intermediate ionization state (Figure 5.2d). The shared proton is closer to the carboxyl O atom in the 298 K structure but moved closer to pyridine N atom in the 100 K structure (Table 5.3),¹⁷ which in agreement with several structures of this kind in the literature.^{11a,24} The salt–cocrystal continuum was well characterized by variable temperature diffraction studies,^{11a,24} which show that temperature affects the hydrogen location between the donor and acceptor and emphasizes that an ionization state cannot be categorically assigned in some cases. This illustrates the role of factors other than ΔpK_a , in these cases temperature, on proton location.^{20a} Examples of this kind play a crucial role in the ongoing exercise on the classification of multi-component crystalline solids.²⁵

Table 5.2 Crystallographic parameters.

Molecular adduct	PZA-SA	INH-SA	PZA-FA	INH-FA	INH-FA
empirical formula	C ₅ H ₅ N ₃ O– (C ₄ H ₆ O ₄) _{0.5}	C ₆ H ₇ N ₃ O– (C ₄ H ₆ O ₄) _{0.5}	C ₅ H ₅ N ₃ O– (C ₄ H ₄ O ₄) _{0.5}	(C ₆ H ₇ N ₃ O) ₂ –(C ₄ H ₄ O ₄)	(C ₆ H ₇ N ₃ O) ₂ –(C ₄ H ₄ O ₄)
formula weight	182.16	196.19	181.16	390.36	390.36
crystal system	monoclinic	monoclinic	monoclinic	monoclinic	monoclinic
space group	<i>P</i> 2 ₁ / <i>n</i>	<i>P</i> 2 ₁ / <i>n</i>	<i>P</i> 2 ₁ / <i>n</i>	<i>P</i> 2 ₁ / <i>n</i>	<i>P</i> 2 ₁ / <i>n</i>
<i>Z</i> ^a	6	6	6	6	6
<i>T</i> /K	298(2)	298(2)	298(2)	298(2)	100(2)
<i>a</i> /Å	3.8701(4)	6.971(6)	3.7408(7)	8.1339(3)	7.883(2)
<i>b</i> /Å	17.3536(18)	19.508(17)	17.352(2)	8.7424(4)	8.697(3)
<i>c</i> /Å	12.4978(13)	7.260(6)	12.558(2)	12.4779(5)	12.506(4)
α /°	90	90	90	90	90
β /°	95.859(2)	114.603(13)	95.760(16)	96.933(4)	97.74(3)
γ /°	90	90	90	90	90
<i>V</i> /Å ³	834.97(15)	897.7(13)	811.0(2)	880.81(6)	849.5(4)
<i>D</i> _{calc} /g cm ^{–3}	1.449	1.452	1.484	1.472	1.526
μ /mm ^{–1}	0.116	0.113	0.119	0.115	0.120
reflns collected	8467	9228	3083	3941	8546
unique reflns	1655	1784	1656	1794	1677
observed reflns	1433	1563	1194	1512	1557
<i>R</i> ₁ [<i>I</i> > 2σ(<i>I</i>)]	0.0424	0.0486	0.0520	0.0366	0.0397
<i>wR</i> ₂ [all]	0.1038	0.1301	0.1146	0.0897	0.0942
goodness-of-fit	1.056	1.085	1.040	1.052	1.114
diffractometer	Bruker Smart-Apex	Bruker Smart-Apex	Oxford Xcalibur Gemini	Oxford Xcalibur Gemini	Bruker Smart-Apex
CCDC no. ^b	849831	849829	849830	849828	849827

^a *Z* = *Z*' (no. of crystallographically non-equivalent molecules of any type in the asymmetric unit)²⁶ × no. of independent general positions of the space group; ^b Ref. 17.

Table 5.3 Hydrogen bonds in crystal structures of the adducts.

Interaction	H...A/Å	D...A/Å	∠D-H...A/°	Symmetry code
PZA-SA				
O2-H2...N3	1.80(2)	2.700(2)	174(2)	^a
N1-H1A...O2	2.31(2)	3.053(2)	140(2)	3/2-x, 1/2+y, 1/2-z
N1-H1B...O1	1.96(2)	2.910(2)	173(2)	1-x, 1-y, -z
N1-H1A...N2	2.30(2)	2.720(2)	108(1)	^b
C5-H5...O3	2.61	3.272(2)	128	^a
C3-H3...O3	2.53	3.438(2)	164	3/2+x, 1/2-y, 1/2+z
C4-H4...O1	2.39	3.304(2)	169	1/2+x, 1/2-y, 1/2+z
INH-SA				
O3-H3A...N3	1.66(3)	2.621(3)	171(3)	^a
N1-H1A...O1	2.24(3)	3.008(3)	146(2)	-x, -y, 1-z
N1-H1B...O3	2.29(3)	3.120(3)	152(2)	-x, -y, 1-z
N2-H2...N1	2.16(2)	2.940(3)	152(2)	1-x, -y, 1-z
C4-H4...O2	2.32	3.128(3)	144	-1/2+x, 1/2-y, -1/2+z
C5-H5...O2	2.72	3.339(3)	125	^a
PZA-FA				
O2-H2...N3	1.74(3)	2.686(2)	174(3)	^a
N1-H1A...O2	2.27(3)	3.073(3)	140(2)	1/2-x, -1/2+y, 1/2-z
N1-H1B...O1	1.93(3)	2.913(3)	172(2)	1-x, -y, 1-z
N1-H1A...N2	2.29(3)	2.726(3)	107(2)	^b
C5-H5...O3	2.56	3.224(2)	128	^a
C3-H3...O3	2.44	3.344(2)	163	-3/2+x, 1/2-y, -1/2+z
C4-H4...O1	2.38	3.304(3)	171	-1/2+x, 1/2-y, -1/2+z
INH-FA^c				
O3...H3A...N3	1.22(2), 1.33(3)	2.542(2)	172(2)	^a
N1-H1A...O1	2.30(2)	3.048(2)	142(2)	1/2+x, 3/2-y, -1/2+z
N1-H1B...O3	2.28(2)	3.047(2)	143(2)	3/2-x, 1/2+y, 3/2-z
N2-H2...O2	2.01(2)	2.873(2)	163(2)	x, -1+y, z
C4-H4...O2	2.86	3.439(2)	121	^a
C4-H4...N1	2.67	3.534(2)	155	x, -1+y, z
C5-H5...O1	2.61	3.500(2)	161	-1/2+x, 3/2-y, 1/2+z
C6-H6...O2	2.57	3.353(2)	142	x, 1+y, z
INH-FA^d				
O3...H3A...N3	1.30(3), 1.23(3)	2.523(2)	171(2)	^a
N1-H1A...O1	2.19(2)	3.015(2)	148(2)	-1/2-x, 3/2+y, 3/2-z
N1-H1B...O3	2.20(2)	2.987(2)	146(2)	-3/2+x, 5/2-y, 1/2+z
N2-H2...O2	2.00(2)	2.832(2)	163(2)	x, -1+y, z
C4-H4...O2	2.77	3.365(2)	121	^a
C4-H4...N1	2.62	3.503(2)	154	x, -1+y, z
C5-H5...O1	2.52	3.432(2)	162	-1/2+x, 3/2-y, 1/2+z
C6-H6...O2	2.55	3.341(2)	141	x, 1+y, z

^a Molecules in the same asymmetric unit; ^b Intramolecular hydrogen bond; ^c 298 K data;^d 100 K data.

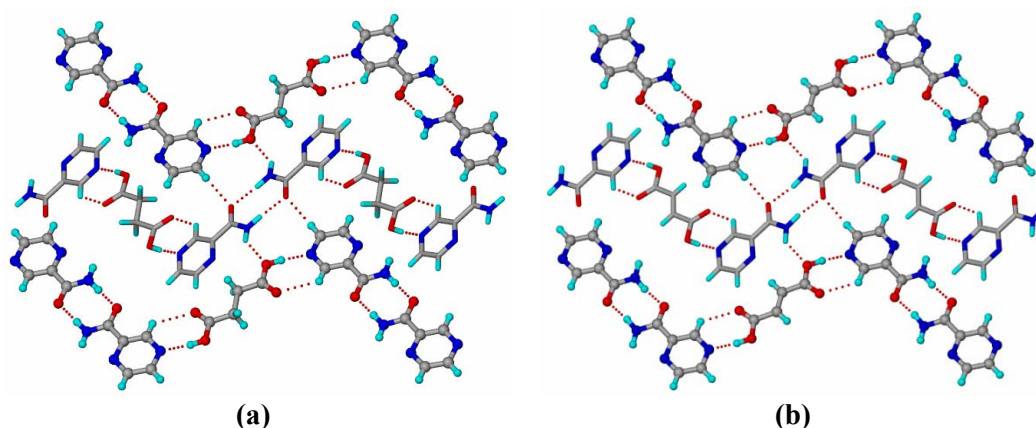


Figure 5.3 Isostructural cocrystals (a) PZA-SA and (b) PZA-FA are characterized by homologous crisscross structures formed by zigzag tapes (shown in ball-stick and capped-stick models for clarity) of acid-pyridine synthon connected amide dimer PZA molecules.

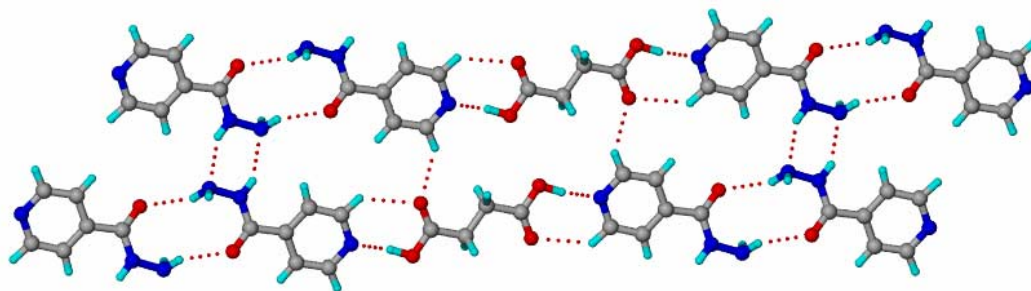


Figure 5.4 Linear tapes of acid-pyridine synthon connected N-H...O dimer INH molecules form a sheet structure through INH N-H...N dimers and auxiliary C-H...O interactions in INH-SA cocrystal.

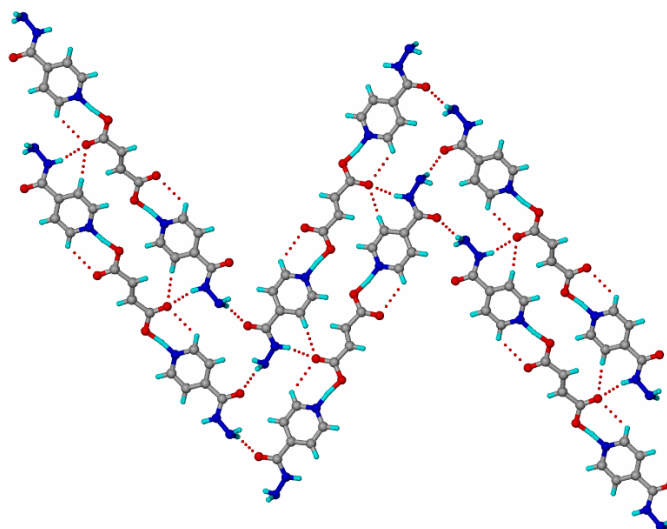


Figure 5.5 N-H...O bonded INH molecules form zigzag tapes through acid-pyridine synthon and make a sheet structure through N-H...O and C-H...O bonds in INH-FA mixed ionic complex.

5.3 Characterization of Eutectics of PZA–INH combination

As discussed in Chapter 1, a eutectic is ‘a conglomerate of solid solutions’ or ‘a conglomerate of lattice structures of two or more components’. A solid solution essentially retains the lattice structure of its parent components, as the inclusion of minor component happens substitutionally or interstitially in the lattice structure of the major component.²⁷ Hence, there will be no significant change in the bonding patterns and crystal packing arrangement in the overall parent lattice. As a result, no appreciable change can be observed in the diffraction and spectroscopic patterns of a solid solution or eutectic compared to its parent materials unlike other multi-component crystalline solids such as salts, cocrystals, complexes etc. In the latter cases, adhesive (hetero) interactions replace cohesive (homo/self) interactions and lead to distinct bonding interactions between the components and, thus, can direct the crystal packing such that their packing arrangement can be different from that of the parent components. Thus, these materials can exhibit characteristic diffraction and spectroscopic patterns. In contrast, a eutectic exhibits close diffraction and spectroscopic patterns to its component materials. The only unambiguous characterization of a eutectic, so far in published literature, is melting point analysis through a phase diagram²⁷ as discussed in Chapter 1. A eutectic exhibits characteristic low melting point compared to its components because of its excess thermodynamic functions (free energy, enthalpy and entropy)²⁸ originating from weak and imperfect interactions between the solid solution domains.²⁷ In this work, the ternary eutectics (PZA–diacid–INH), characterized by low melting points, were found to be composed of binary adducts (drug–(diacid)_{0.5}) but not the pure starting materials through X-ray diffraction and spectroscopic analysis.¹⁷ Thus, the diffraction and spectroscopic techniques are found to be useful in assessing the components of a eutectic, whether made up of pure starting materials or adducts.

5.3.1 X-ray diffraction analysis

Single crystal X-ray diffraction is the principal technique to characterize crystalline solids, more importantly multi component species since it reveals the identity and bonding interactions and structural organization of the components in the lattice. An adduct structure can be ascertained²⁰ as being a salt, cocrystal, complex or solid solution. Generating diffraction quality single crystals is central in this technique. Unlike other multi-component crystalline solids, eutectics are heterogeneous in nature (composed of

different solid solutions) and hence do not tend to afford single crystals. The inherent entropy/disorder between the component solid solution domains²⁷ seems not to aid the formation of diffraction quality single crystals. Apart from few inorganic materials (for e.g. Lead-Tin system),^{27a} eutectic microstructure is poorly understood in organic materials. The lack of crystal structure of a eutectic, despite its long history, emphasizes the difficulty in generating single crystals of a eutectic, otherwise its lattice structure would have been determined just like other crystalline solids. The current challenge is to dissect the organic eutectic materials into solid solutions and assess their domain structure as established for a few inorganic materials.

Mechano-chemical grinding is a well established technique for the synthesis of adducts such as salts and cocrystals.^{16,29} In this study, cocrystals were prepared by solid state grinding¹⁷ (detailed in Experimental Section). The sequence of establishing the adduct nature is as follows: (i) At first, the solid ground products of drug (PZA or INH) and coformer (SA or FA), in 1:0.5 stoichiometry, were assigned to be novel materials basing on their distinct diffraction and spectroscopic patterns and melting points compared to the parent materials, (ii) afterwards single crystals of these materials were grown and were found to be cocrystals (mixed ionic complex in case of INH-FA) through their X-ray crystal structures and (iii) finally the solid ground products were established as cocrystals by PXRD profile match with that of the calculated lines from the respective X-ray crystal structures.

In this work, the original goal was to make drug-drug cocrystals of PZA and INH with or without using a non-covalent linker.¹⁷ The same solid state grinding technique was applied to make a binary PZA-INH and ternary PZA-diacid-INH adducts (detailed in Experimental Section). But, surprisingly, despite the potential to form cocrystals through strong heteromolecular interactions, the solid ground materials did not exhibit any new diffraction peaks in the PXRD. The ground product of PZA and INH showed a PXRD pattern that matched with that of the pure drugs (Figure 5.6). In the latter cases (PZA-diacid-INH), the ground product showed a PXRD pattern that matched with peaks corresponding to the binary cocrystals but not the pure components (i.e. $\text{PZA-diacid-INH} = \text{PZA-(diacid)}_{0.5} + \text{INH-(diacid)}_{0.5}$ and not $\text{PZA} + \text{diacid} + \text{INH}$) (Figure 5.7). But, the ground products (PZA-INH and PZA diacid-INH) exhibited characteristic lower melting points than their components in the DSC (discussed next). Thus, PZA-INH and PZA-diacid-INH are inferred as eutectic compositions with the

latter composed of binary cocrystals and not pure components (i.e. PZA–SA–INH is composed of PZA–(SA)_{0.5} and INH–(SA)_{0.5} and PZA–FA–INH is composed of PZA–(FA)_{0.5} and INH–(FA)_{0.5}).¹⁷ Attempts to grow single crystals of the binary and ternary eutectics by using the ground products as seeds were unsuccessful by solution crystallization; the components precipitated or gave a mixture of compounds which can be due to solubility mismatch or inherent entropy of the eutectic. On the other hand, no attempts were made to ascertain the exact eutectic compositions through a phase diagram. For the ease of study and understanding, the components were taken in molar ratios (1:1 for binary and 1:1:1 for ternary) and ascertained as eutectic compositions in a broad sense.

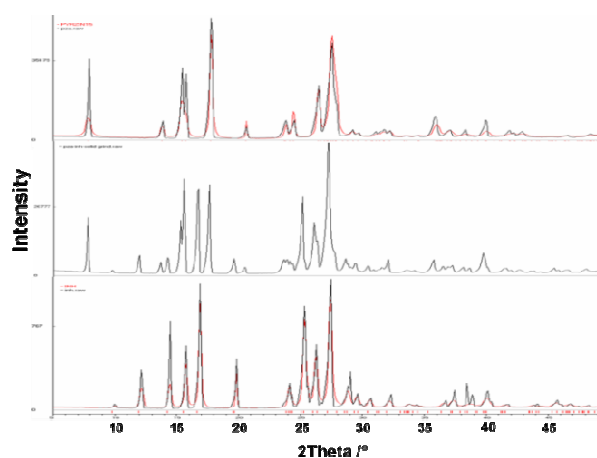


Figure 5.6 PXR D pattern of PZA–INH ground product (middle) matches with those of PZA (top) and INH (bottom). Experimental PXR D patterns (black) of the pure drugs overlay peak-to-peak on the calculated lines (red) from the crystal structures.

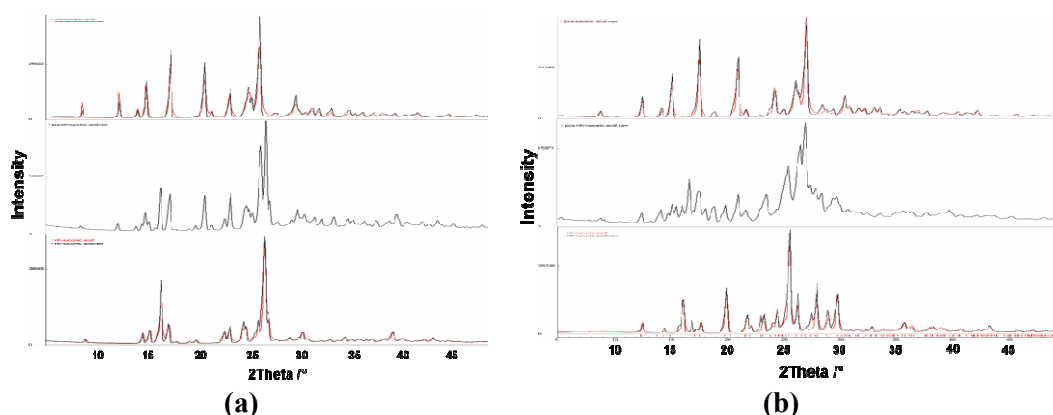


Figure 5.7 PXR D pattern of (a) PZA–SA–INH ground product (middle) matches with those of binary PZA–SA (top) and INH–SA (bottom) cocrystals. Similarly, (b) PZA–FA–INH ground product (middle) matches with those of PZA–FA (top) and INH–FA (bottom). Experimental PXR D patterns (black) of cocrystals overlay peak-to-peak on the calculated lines (red) from the crystal structures.

5.3.2 Thermal analysis

Eutectics are traditionally prepared by co-melting and solvent-mediated co-precipitation of the components.^{27b,30} These methods generally give rise to a precipitate-kind of material, which is characterized as a eutectic when the material exhibits characteristic lower melting point than that of the components. It is not clear whether co-precipitation can really result in eutectic formation, since a eutectic-forming physical mixture too upon heating results in a eutectic. A eutectic composition and a eutectic-forming physical mixture both exhibit close melting points, PXRD and spectroscopic patterns. As per conventional wisdom, a physical mixture has heterogeneous distribution and random interactions. Thus, subtle differences exist between pre-formed eutectic and eutectic-forming physical mixture with respect to their homogeneity and integrity. These differences were quantified by DSC with respect to peak broadness and offset of eutectic endotherm by Mingda Bi et al.³¹ They showed that compaction, a widely used technique in pharmaceutical manufacturing, can result in eutectic formation. With an increase in the compaction force, the intimate contact area between the components improved such that the compressed material showed lower melting temperature compared to a physical mixture.³¹ This means that a pre-formed eutectic (whether formed by co-melting or any other method) exhibits lower melting compared to a eutectic-forming physical mixture.

Grinding,¹⁶ a physical stress technique just like compaction, resulted in the formation of both cocrystals and eutectics in this study.¹⁷ It is understood that the weak interactions in a eutectic develop as a result of molecular mobility and reorganization during the heating process; similar interactions can possibly be induced by grinding. Generally, random interactions are characteristic of a physical mixture at ambient temperature. However, the physical mixture can attain non-random interactions through molecular mobility and reorganization at higher temperature and thus give rise to eutectics or adducts.^{10h,i} The same non-random interactions that can develop during grinding process to give a salt/cocrystal^{29,32} are perhaps giving the eutectic composition in these cases. When grinding results in the formation of salts/cocrystals (having strong interactions) it is not unusual that it can induce the formation of eutectic structures (with weak interactions) such that the components are accommodated in the lattice, if the process is entropically driven. Thus, grinding and compaction assume to be new techniques that can lead to an unambiguous formation of a eutectic as well as applicable

to heat-labile materials (since co-melting is not appropriate for such materials), with the former being a less expensive technique.

The ground product of PZA and INH showed a lower melting endotherm (142 °C) than the pure components (PZA 190 °C; INH 172 °C) in the DSC (Figure 5.8). Similarly, the ternary adducts PZA–diacid–INH exhibited lower melting points than the components (Figure 5.9). Whether the ternary product is a eutectic composition of the parent compounds or the binary cocrystals was differentiated by PXRD, which showed excellent match of diffraction peaks with those of the cocrystals (Figure 5.7). The lowering of melting point for both eutectic and cocrystal phases correlated with the melting point of the diacid, i.e. succinic acid adducts have lower melting point than their fumaric acid counterparts (Table 5.4). The characteristic sharp and lower melting endotherm for the pre-formed eutectic (obtained upon grinding in this work) with respect to a physical mixture was also observed in these cases (Figures 5.8 & 5.10). Based on the grinding and DSC studies, the sequence of eutectic formation appears to be: binary cocrystals are formed upon grinding/heating the components, which then lead to the ternary eutectic composition on further grinding/heating. Notably, the ternary products are eutectic composition of binary cocrystals and not the three compounds as discussed earlier. This was further supported by spectroscopic analysis discussed next.

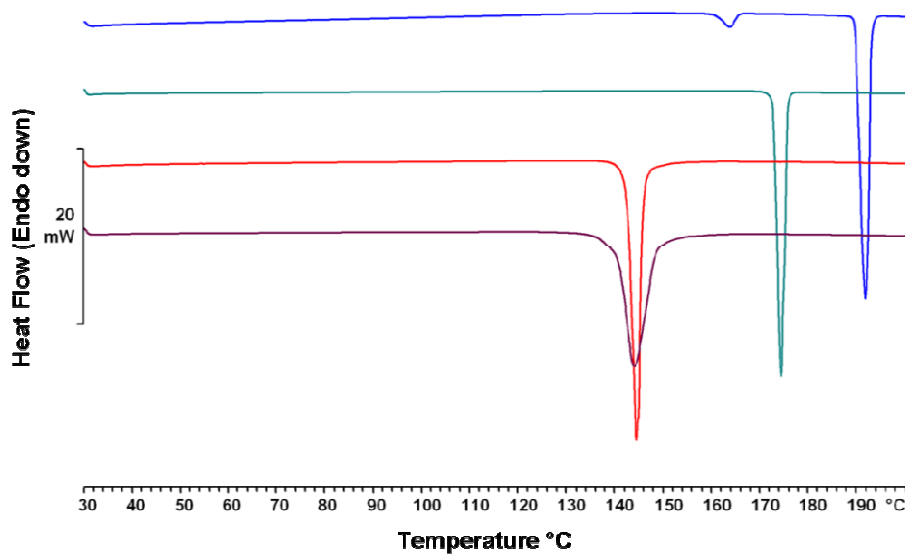


Figure 5.8 DSC of binary PZA–INH eutectic formed by grinding (red), an equimolar physical mixture of PZA and INH (brown), PZA (blue), and INH (green). The melting endotherm of grinding-induced eutectic is sharper than that of the eutectic-forming physical mixture. The small endotherm at about 160 °C in PZA (blue) is due to polymorphic transition from $\alpha \rightarrow \gamma$ polymorph of pyrazinamide.^{14c}

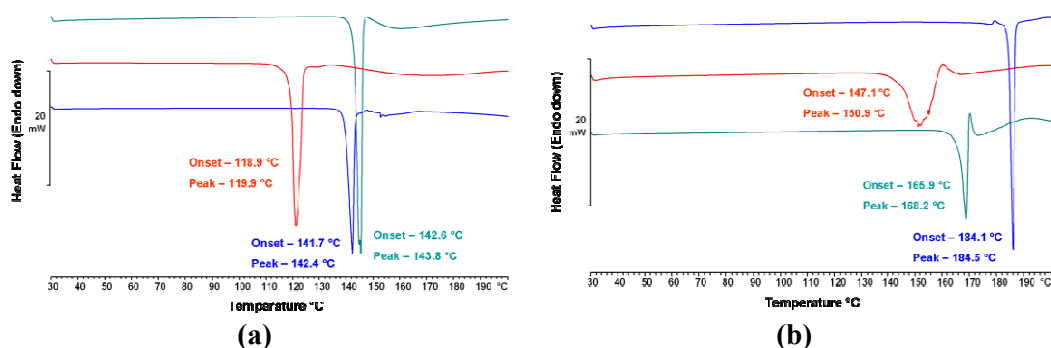


Figure 5.9 DSC of (a) ternary PZA-SA-INH eutectic formed by grinding (red), binary PZA-SA (blue) and INH-SA (green) cocrystals. (b) Thermograms for PZA-FA-INH (red), PZA-FA (blue) and INH-FA (green).

Table 5.4 Melting point (DSC) and solubility (water) and IDR (pH 1.2 HCl solution) of the compounds.

Compound	Melting point (°C)	Solubility (mg mL ⁻¹)	IDR (mg cm ⁻² min ⁻¹)
PZA	190	22 ^a	3.3
INH	172	125 ^b	12.9
PZA-INH	142	^c	8.3
SA	188 ^d	83 ^d	^e
FA	287 ^d	6 ^f	^e
PZA-SA	142	^c	4.6
INH-SA	144	155.8	18.2
PZA-SA-INH	120	^c	21.7
PZA-FA	184	8.7	1.9
INH-FA	168	49.5	7.9
PZA-FA-INH	150	^c	6.7

^a Ref 21a; ^b Ref 21c; ^c Dissociates in solution; ^d Ref 21b; ^e Not determined; ^f Ref 10c.

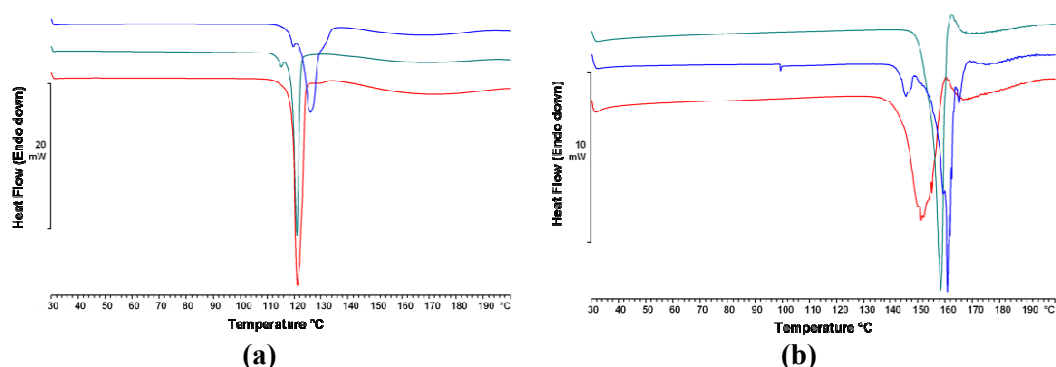


Figure 5.10 DSC of (a) ternary PZA-SA-INH eutectic formed by grinding (red), physical mixture of PZA-SA and INH-SA cocrystals (green), and physical mixture of pure compounds PZA, SA and INH (blue). (b) Thermograms for PZA-FA-INH system. The melting endotherm of grinding-induced eutectic is clean and lower than that of the eutectic-forming physical mixtures.

5.3.3 Spectroscopic analysis

Spectroscopy is known to complement X-ray diffraction in the characterization of solid forms and their bonding interactions and molecular organization.^{10a,20a,33} IR spectroscopy is generally used as a first-hand tool to characterize hydrogen bonded adducts.³⁴ Shifts in the vibrational frequencies with respect to the starting materials indicate the formation of an adduct. Since cohesive interactions dominate the adhesive interactions in a eutectic, as discussed earlier, there will be no appreciable change in the bond vibrations with respect to the components. Hence, FT-IR spectrum of binary PZA–INH eutectic was manifested as an admixture of the parent drugs (Figure 5.11, Table 5.5). But, in case of ternary eutectics, it is plausible that the components can be pure starting materials or binary cocrystals. Since the strong carboxylic acid–pyridine synthon is manifested in the binary cocrystals, a shift in the C=O, C–O and O–H vibrations was observed in their FT-IR spectra as expected (Table 5.5). The FT-IR spectra of ternary eutectics were found to be different from that of the pure starting materials but matched with that of the binary adducts (Table 5.5, Figures 5.12 & 5.13). In addition, broad bands around 2500 and 1900 cm^{-1} attributed to neutral intermolecular O–H \cdots N hydrogen bond³⁵ were observed in the binary cocrystals (except INH–FA which is a mixed-ionic complex) and ternary eutectics and not in the parent drugs (Figures 5.12 & 5.13). Thus, the IR spectra strengthen the integrity of the ternary eutectics as composed of their corresponding binary adducts.¹⁷

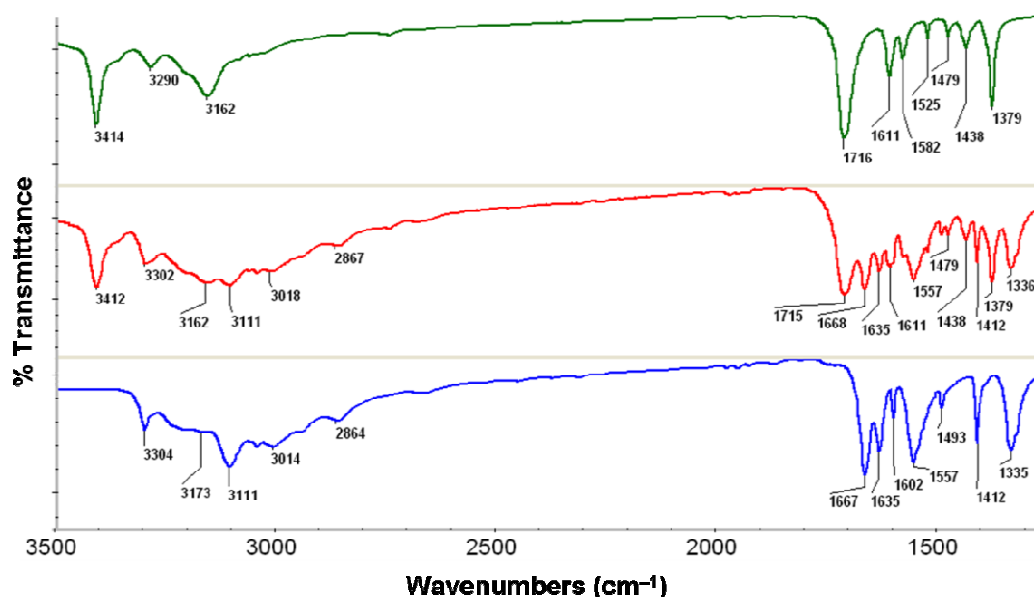
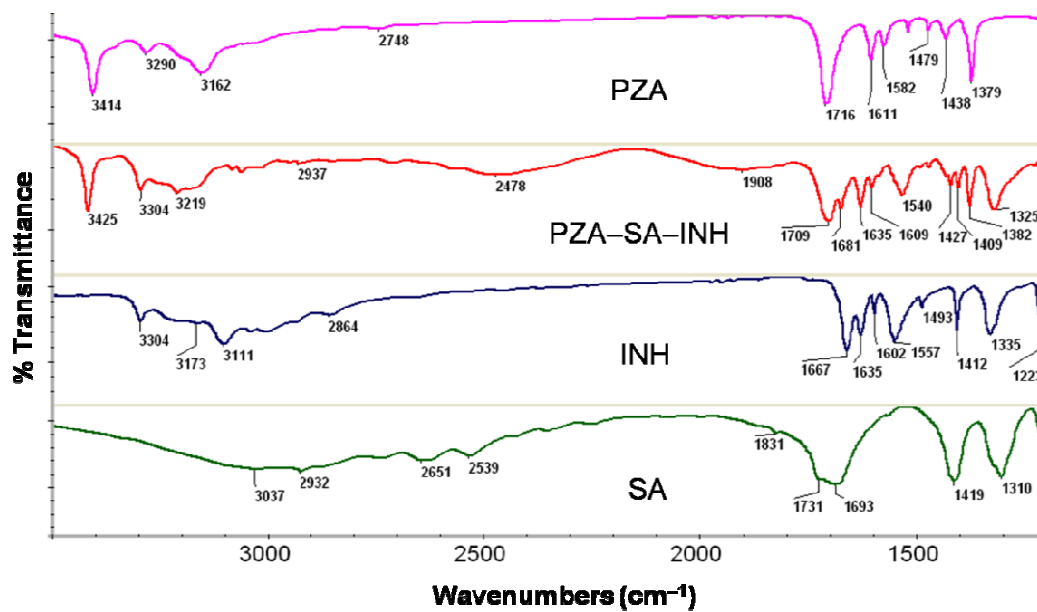


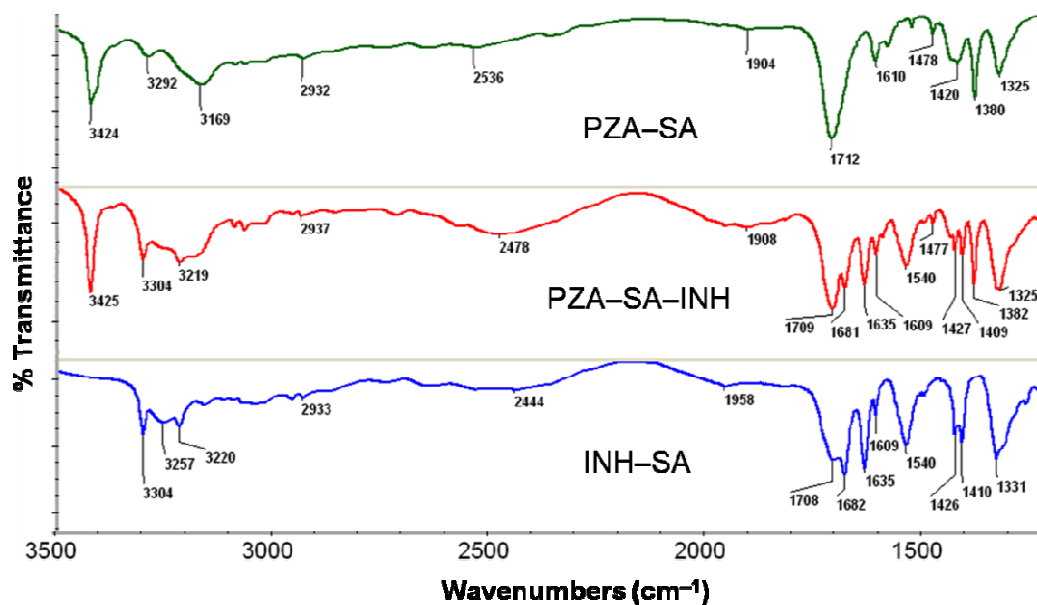
Figure 5.11 FT-IR spectrum of binary PZA–INH eutectic (red) compared with that of PZA (green) and INH (blue) shows no shift in the vibrational frequencies of eutectic compared to the pure drugs, thus, indicating no cocrystal formation.

Table 5.5 FT–IR spectral bands of compounds.

IR vibration	PZA (pure)	INH (pure)	SA (pure)	FA (pure)	PZA–INH (eutectic)	PZA–SA (cocrystal)	INH–SA (cocrystal)	PZA–SA–INH (eutectic)	PZA–FA (cocrystal)	INH–FA (cocrystal)	PZA–FA–INH (eutectic)
N–H (stretch)	3414, 3162	3304, 3111	---	---	3412, 3302, 3162, 3111	3424, 3169	3303, 3220	3425, 3304, 3219	3426, 3183	3323, 3166	3403, 3325, 3219
O–H (stretch)	---	---	3037	3083	---	2932	2933	2937	2810	2819	2810
C=O (stretch)	1716	1667	1731, 1693	1675	1715, 1668	1712	1708, 1682	1709, 1681	1710, 1693	1681	1712, 1682
N–H (bend)	1611	1635, 1602	---	---	1635, 1611	1610	1635, 1609	1635, 1609	1603	1637, 1581	1638
O–H (bend)	---	---	1419	1426	---	1420	1426	1427	1434	1414	1413
C–N (stretch)	1379	1412	---	---	1412, 1379	1380	1410	1409, 1382	1383	1323	1377
C–O (stretch)	---	---	1310	1320	---	1325	1331	1325	1313		1321

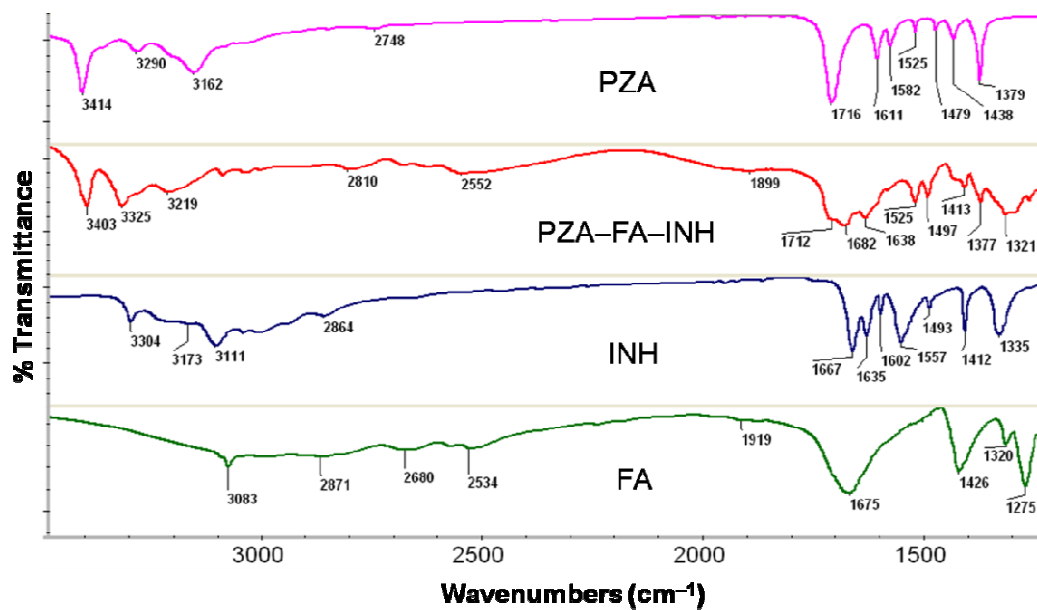


(a)

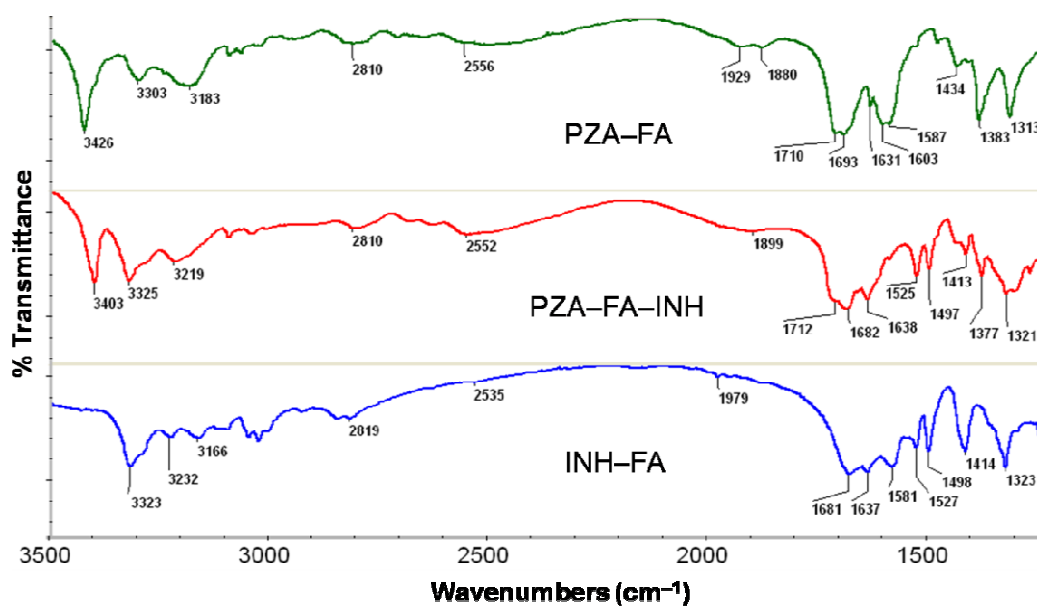


(b)

Figure 5.12 Comparison of FT-IR spectrum of (a) PZA-SA-INH eutectic (red) with that of PZA (magenta), INH (blue), and SA (green), and with (b) binary PZA-SA (green) and INH-SA (blue) cocrystals. The C=O, O-H, N-H and C-N vibrations in the ternary eutectic are different from those of the pure starting materials but match with the peaks for binary cocrystals. Broad peaks around 2500 and 1900 cm^{-1} attributed to neutral O-H \cdots N hydrogen bond were found in both cocrystals and the eutectic.



(a)



(b)

Figure 5.13 Comparison of FT-IR spectrum of (a) PZA-FA-INH eutectic (red) with that of PZA (magenta), INH (blue) and FA (green), and with (b) binary PZA-FA (green), and INH-FA (blue) adducts. The C=O, O-H, N-H and C-N vibrations in the ternary eutectic are different from those of the pure starting materials but match with the peaks for binary cocrystals. Weak peaks at 2535, 1979 cm^{-1} in INH-FA imply an intermediate/mixed ionic state of the $\text{O}\cdots\text{H}\cdots\text{N}$ synthon.

Similarly, ss-NMR spectroscopy was characteristic in establishing the integrity of obtained cocrystals and eutectics.¹⁷ Chemical shift values in ^{13}C ss-NMR (Figure 5.14, Table 5.6) and ^{15}N ss-NMR spectra (Table 5.7, Figure 5.15) of PZA–INH eutectic matched with that of PZA and INH. In case of ternary eutectics, their ^{13}C ss-NMR spectra matched with that of the binary cocrystals (Figure 5.16), but not the pure starting materials (Table 5.6). ^{15}N ss-NMR spectra resolved both the adducts and eutectics through significant chemical shifts with respect to starting materials. For a heterocyclic nitrogen, an upfield shift with respect to the parent compound is indicative of adduct formation (20–40 ppm for cocrystal; 40–80 ppm for mixed ionization complex; 80–120 ppm for salt)^{33a} as electron density on the nitrogen increases upon hydrogen bond formation. The pyridyl N peak (of acid–pyridine synthon) showed an upfield shift of 42.9 ppm in PZA–SA cocrystal and 50.2 ppm in INH–SA and similar shifts were observed for PZA–SA–INH eutectic (43.5, 49.0 ppm) (Table 5.7, Figure 5.17a). The pyridyl N peak (of acid–pyridine synthon) is shifted upfield by 79.3 ppm in INH–FA (Figure 5.17b) due to the intermediate H atom position (in between neutral and ionic state, $\text{O}\cdots\text{H}\cdots\text{N}$) observed in its crystal structure. The same peak was also found in PZA–FA–INH eutectic but pyrazine N peaks were not resolved as in PZA–FA cocrystal (Figure 5.17b). In all, both ^{13}C and ^{15}N ss-NMR spectra satisfactorily resolved the composition of ternary eutectics as comprised of their corresponding binary adducts.¹⁷

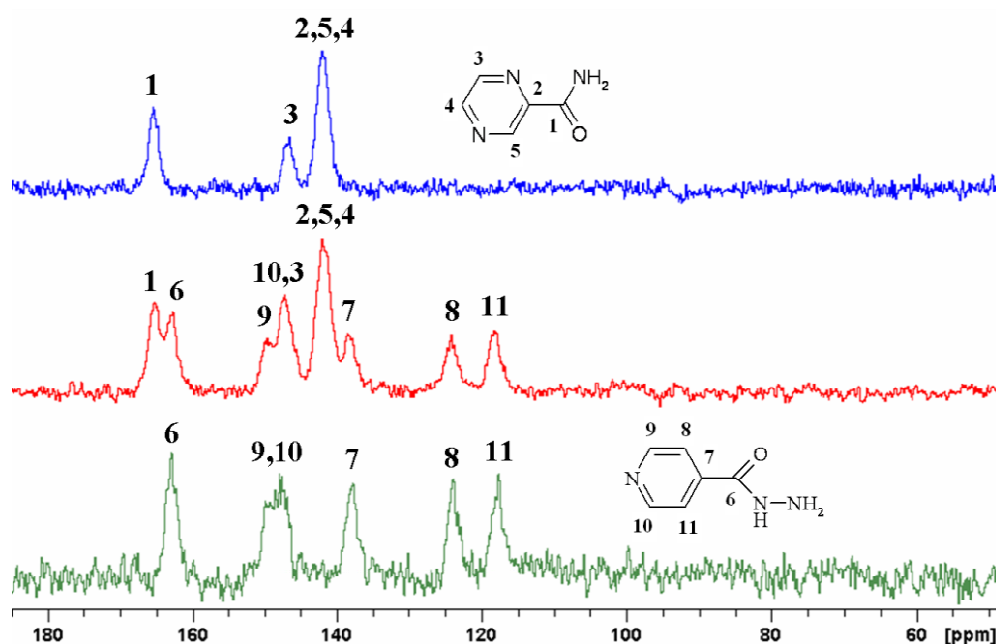


Figure 5.14 ^{13}C ss-NMR spectrum of PZA–INH eutectic (red) matches with the peaks of PZA (blue) and INH (green).

Table 5.6 ^{13}C ss-NMR chemical shifts (δ , ppm scale) of compounds.

PZA (pure)	INH (pure)	SA (pure)	FA (pure)	PZA–INH (eutectic)	PZA–SA (cocrystal)	INH–SA (cocrystal)	PZA–SA–INH (eutectic)	PZA–FA (cocrystal)	INA–FA (cocrystal)	PZA–FA–INH (eutectic)
166.8	164.3	180.1	172.1	166.7	174.4	175.3	174.3	166.7	169.5	170.0
147.9	151.4	28.2	136.1	164.1	167.1	166.3	166.6	146.1	165.0	167.1
143.3	149.4			151.1	145.5	149.3	149.5	144.8	146.1	165.4
	139.1			148.5	139.1	144.7	145.1	138.8	143.1	146.5
	125.3			143.4	29.8	140.9	141.3	135.1	136.4	143.4
	119.0			139.8		121.5	139.0		125.1	136.6
				125.6		29.6	121.7		122.4	125.5
				119.6			29.6			122.5

Table 5.7 ^{15}N SS-NMR chemical shifts (δ , ppm scale) of compounds.

PZA (pure)	INH (pure)	PZA–INH (eutectic)	PZA–SA (cocrystal)	INH–SA (cocrystal)	PZA–SA–INH (eutectic)	PZA–FA (cocrystal)	INH–FA (cocrystal)	PZA–FA–INH (eutectic)
–29.9 (N3-non intramolecular hydrogen bonded pyrazine N)	–42.1 (N6-pyridine N)	–251.9 (N5)	–72.8 (N3)	–92.3 (N6)	–73.4 (N3)	–280.2 (N1)	–121.4 (N6)	–121.4 (N6)
–279.1 (N1-Amide NH ₂)	–252.3 (N5-hydrazide secondary amine)	–279.2 (N1)	–280.2 (N1)	–253.9 (N5)	–91.1 (N6)		–250.4 (N5)	–250.0 (N5)
	–322.5 (N4-hydrazide primary amine)	–321.9 (N4)		–324.5 (N4)	–252.8 (N5)		–327.8 (N4)	–278.1 (N1)
					–280.4 (N1)			–327.0 (N4)
					–324.6 (N4)			

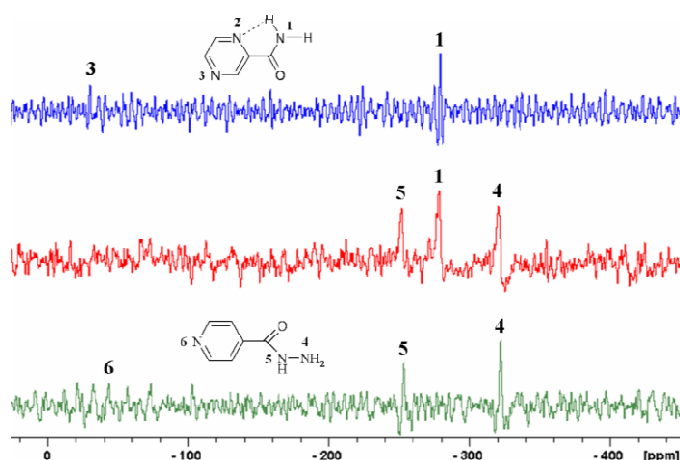


Figure 5.15 ^{15}N ss-NMR spectrum of PZA-INH eutectic (red) matches with the peaks of PZA (blue) and INH (green). The intramolecular hydrogen bonded pyrazine N of PZA could not be detected even after over 24 h of FID acquisition. Other nitrogens are weakly resolved but assigned with respect to side bands.

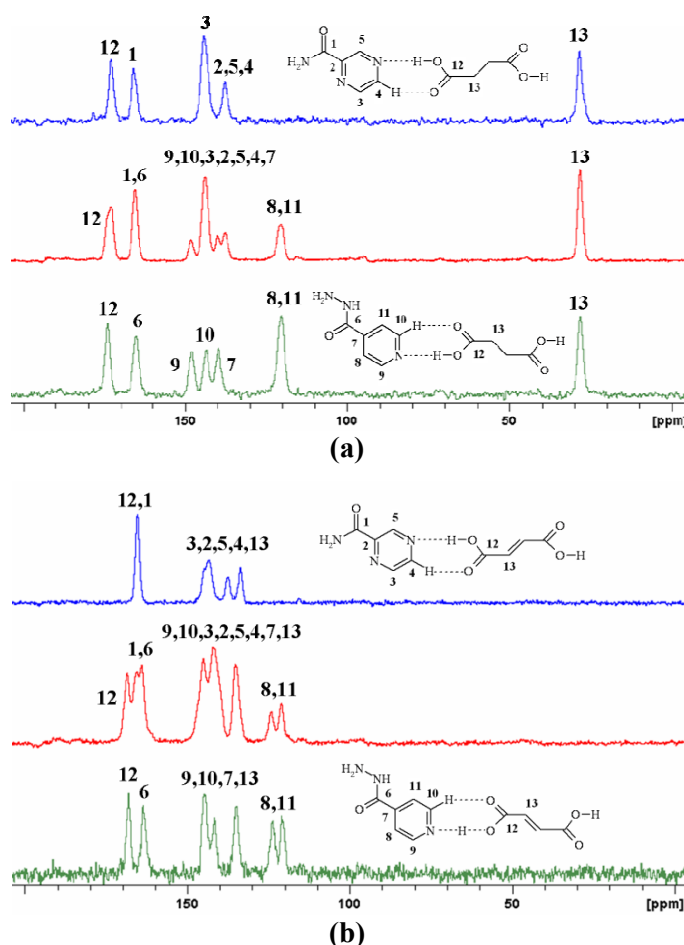


Figure 5.16 ^{13}C ss-NMR spectrum of (a) PZA-SA-INH eutectic (red) matches with binary PZA-SA (blue) and INH-SA (green) cocrystals. Similarly, (b) PZA-FA-INH eutectic (red) matches with binary PZA-FA (blue), and INH-FA (green) adducts.

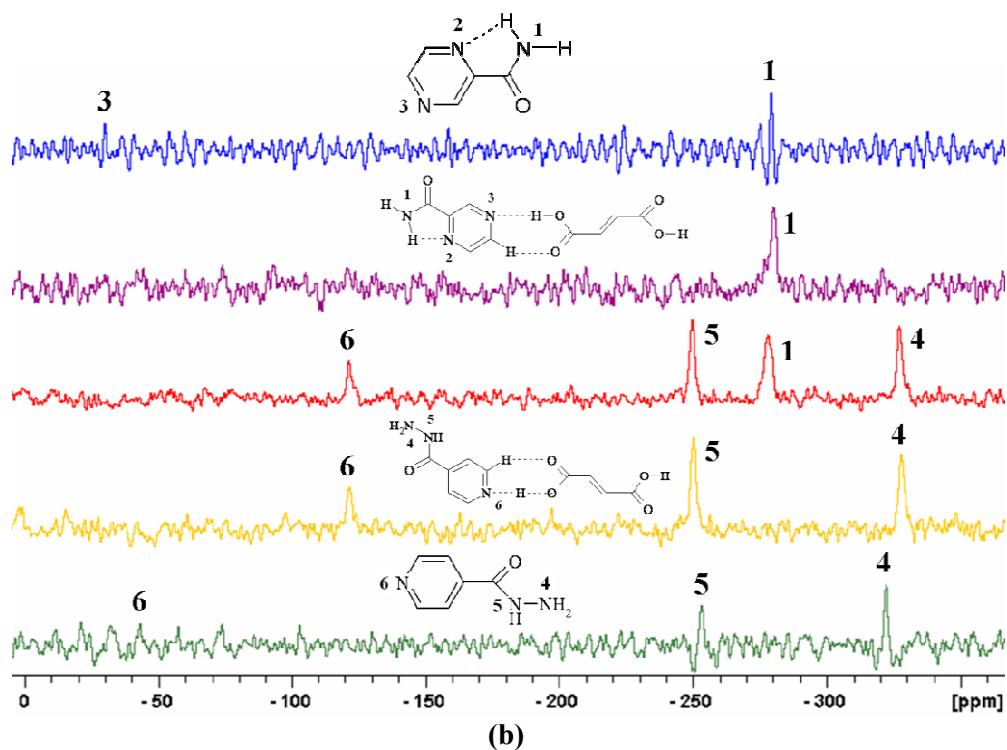
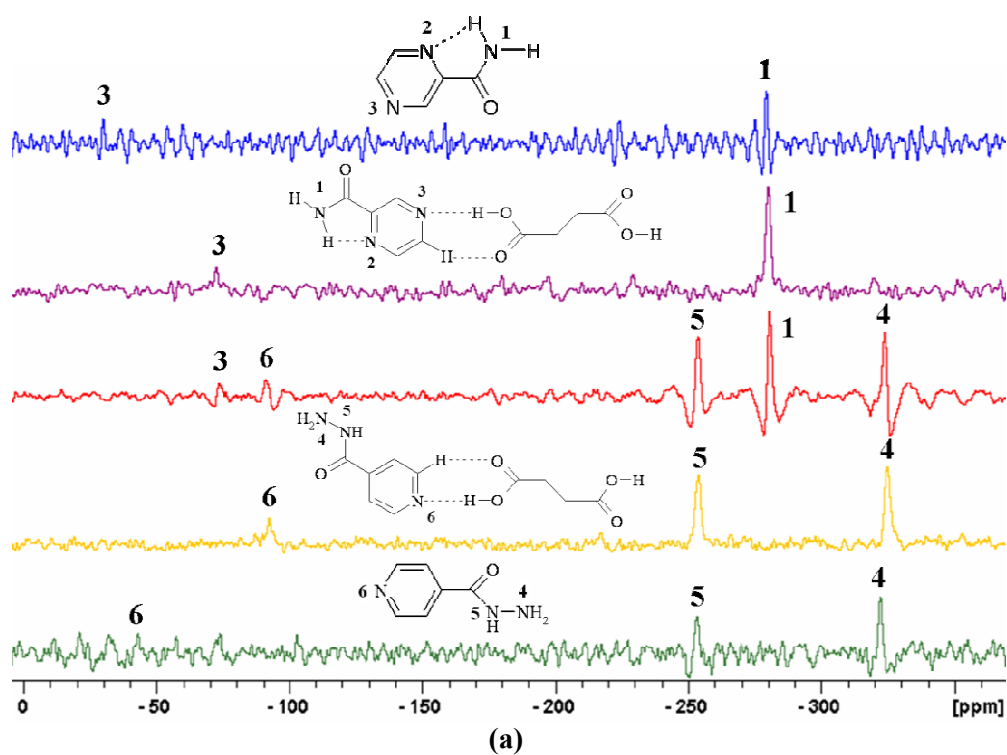


Figure 5.17 Comparison of ^{15}N ss-NMR spectrum of (a) PZA-SA-INH eutectic (red) with that of PZA (blue), PZA-SA (purple), INH-SA (yellow), and INH (green), and of (b) PZA-FA-INH eutectic (red) with that of PZA (blue), PZA-FA (purple), INH-FA (yellow), and INH (green). The upfield chemical shifts in binary adducts and eutectics match with each other.

5.4 Solubility and Dissolution study

Eutectics have excess thermodynamic functions (free energy, enthalpy and entropy) due to weak and imperfect intermolecular interactions²⁸ and, thus, these materials can confer higher solubility and faster dissolution rate compared to other crystalline modifications, akin to amorphous forms. Both PZA and INH are highly soluble and rapidly dissolving drugs.^{21a,c} In this work, the solubility and dissolution behavior of newly prepared cocrystals and eutectics was studied.¹⁷ Equilibrium solubility measurements in water (detailed in Experimental Section) were unsuccessful in four cases out of seven systems because they are incongruently dissolving,^{10k,1} i.e. the solubility of one component is much higher than the other. Solubilization of the more soluble component in water resulted in precipitation of the less soluble component of the adduct, and hence their solubility could not be determined. The binary cocrystal PZA–SA and eutectics PZA–INH, PZA–SA–INH and PZA–FA–INH are incongruently dissolving systems and dissociated in the aqueous slurry medium resulting in precipitation of the less soluble species. The solid residue at the end of the experiment was confirmed to be PZA (first three cases) and PZA–FA (last case) by PXRD. The aqueous solubility of PZA and fumaric acid is lower than that of INH and succinic acid (PZA 22 mg/mL,^{21a} FA 6 mg/mL,^{10c} INH 125 mg/mL,^{21c} SA 83 mg/mL^{21b}) (Table 5.4). The dissociated components resulted in the less soluble PZA–FA cocrystal in the last case. Equilibrium solubility for the other three binary adducts could be measured because of their stability (INH–SA 155.8 mg/mL, PZA–FA 8.7 mg/mL and INH–FA 49.5 mg/mL) (Table 5.4). The adducts follow the ‘coformer solubility rule’:³⁶ the more soluble succinic acid coformer improved the solubility of INH and the less soluble fumaric acid gave low solubility adducts (Table 5.4). The higher stability of INH–SA and PZA–FA cocrystals is possibly a result of closer solubility of the components. INH–FA is expected to be less stable because of large difference in the solubility of its components but the observed stability was ascribed to the partial ionic state in the crystal structure (salt like nature).

As discussed in Chapter 4, even though a solid form dissociates during equilibrium solubility conditions, the same material can still be useful if it facilitates drug release within a desirable time-frame before it is destabilized.^{10a,b} A dissolution study serves the purpose by evaluating the drug release from the formulation into the medium.³⁷ A biowaiver is recommended by the WHO to a solid oral dosage form in the Model List of Essential Medicines if its *in vitro* dissolution tests comply with *in vivo*

bioavailability specifications.³⁸ According to the WHO biowaiver dissolution criterion, an immediate release (IR) solid oral dosage form should exhibit ‘very rapid’ (no less than 85% of the drug must be dissolved in 15 minutes) or ‘rapid’ (no less than 85% of the drug must be dissolved in 30 minutes) *in vitro* dissolution kinetics. In this context, dissolution behavior of the adducts was compared with pure drugs in pH 1.2 HCl solution at 37 °C by rotating disk intrinsic dissolution rate (DIDR) method³⁹ (detailed in Experimental Section). The extent of solid form dissolved in 30 min was: INH–SA 94%, PZA–SA–INH 92%, INH 73%, PZA–INH 64%, INH–FA 62%, PZA–FA–INH 50%, PZA–SA 36%, PZA 25%, and PZA–FA 15% (Figure 5.18). Thus, INH–SA cocrystal and PZA–SA–INH eutectic qualified the criterion of ‘rapid’ dissolution, but pure drug forms did not clear the bar in the tested conditions.¹⁷ Dissolution of INH increased from 73% to 94% (in INH–SA cocrystal) and the two-drug combination of PZA and INH increased from 64% (in PZA–INH eutectic) to 92% in the ternary eutectic (PZA–SA–INH). PZA–SA–INH eutectic dissolved 3.7 times faster than PZA and 1.3 times faster than INH; PZA–INH and PZA–FA–INH eutectics dissolved 2.5 and 2.0 times faster than PZA respectively. The dissolution improvement for pure PZA in its SA cocrystal was moderate (25% to 36%). The ternary eutectic PZA–SA–INH exhibited faster dissolution for the first 15 min but dropped below INH–SA cocrystal between 15–30 min (Figure 5.18). Calculated IDR values followed the order: PZA–SA–INH ($21.7 \text{ mg cm}^{-2} \text{ min}^{-1}$) > INH–SA (18.2) > INH (12.9) > PZA–INH (8.3) > INH–FA (7.9) > PZA–FA–INH (6.7) > PZA–SA (4.6) > PZA (3.3) > PZA–FA ($1.9 \text{ mg cm}^{-2} \text{ min}^{-1}$).

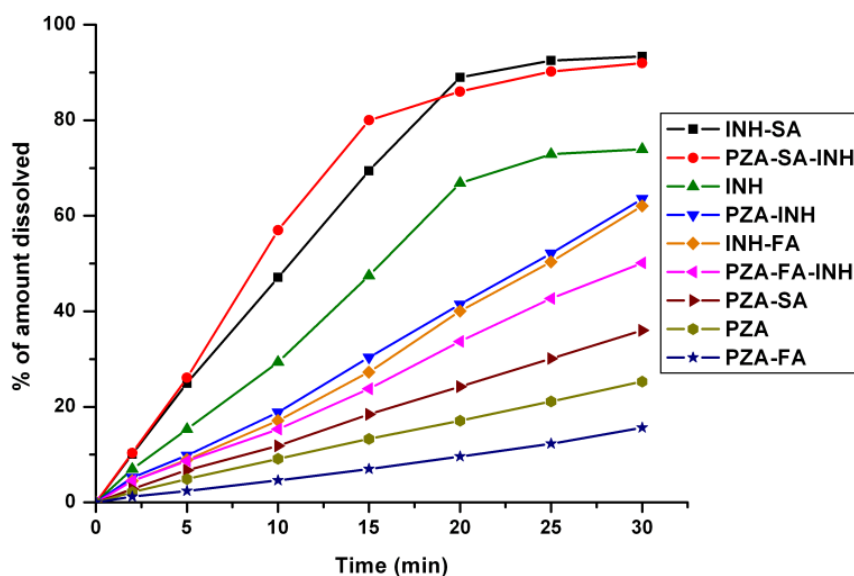


Figure 5.18 Dissolution curves of the compounds in pH 1.2 aq. HCl solution.

There is a semi-empirical inverse relationship between melting point and solubility,^{10c,40} and these systems showed mixed results.¹⁷ INH-SA cocrystal with lower melting point showed higher solubility with respect to INH following the inverse relation. But PZA-FA and INH-FA exhibited lower solubility though their melting point is lower than the parent compounds (Table 5.4). A similar effect of coformer solubility vs. melting point on the dissolution rates was observed in these systems.¹⁷ All the succinic acid adducts (PZA-SA, INH-SA and PZA-SA-INH) having lower melting points showed faster IDRs with respect to their parent drugs. However, fumaric acid adducts (PZA-FA, INH-FA) showed slower IDRs despite having lower melting points than the parent drugs (Table 5.4). On the other hand, IDRs of PZA-FA-INH and PZA-INH eutectics are in-between PZA and INH. It appears that the compensation of solubility of INH (high) and PZA (low) resulted in intermediate values for these cases. These results show that the coformer solubility (high/low) has a greater influence on solubility/dissolution (high/low) than melting point (low/high) for a multi component system as noted by Good et al.³⁶ Thus, the applicability of ‘coformer solubility rule’ was extended to IDRs of both cocrystals and eutectics in this study.¹⁷ The inclusion of high soluble succinic acid coformer facilitated faster dissolution for PZA and INH (in binary cocrystals) and PZA-INH combination (in ternary eutectic). The less soluble fumaric acid gave the opposite effect of decreasing dissolution rates of the adducts. Thus, a control over the solubility/dissolution of the drugs was achieved through cocrystals and eutectics in this study.

5.5 Conclusions

Co-crystallization of the two anti-tuberculosis drugs pyrazinamide and isoniazid gave surprising but important results.¹⁷ Co-grinding not only resulted in drug cocrystals but also drug eutectics. This study shows that grinding can produce long-range order (to give a cocrystal) or short range order (to give a eutectic) depending on whether adhesive or cohesive interactions dominate. Very often the products of co-grinding experiments are discarded without further analysis when no cocrystal formation is observed by diffraction and spectroscopy. This study suggests that even failed co-crystallization experiments should be ascertained for eutectic formation. On the other hand, reporting unsuccessful co-crystallization experiments will have broad implications in understanding co-crystallization processes and stimulates efforts to gain further insights into the design and

outcome of cocrystals.⁴¹ For example, the seemingly straightforward benzamide–benzoic acid cocrystal⁴² does not actually manifest due to the absence of auxiliary interactions⁴³ apart from the viable amide–acid heterosynthon⁴⁴ and thus the system makes a eutectic.^{28b} Eutectics are well studied in inorganic materials where asymmetry, mismatch and misfit between the components induce eutectic structures such that the components are accommodated in the lattice through weak interactions.²⁷ Thus, the factors of lack of auxiliary interactions, misfit and mismatch between the components appear to have resulted in eutectic compositions in this study. This study was started with the intent of making drug–drug cocrystals but the results were drug–drug eutectics.¹⁷ Though superficially it appears that the design aspect is lacking in the synthesis of eutectics unlike cocrystals, careful analysis of the plausible supra/hetero molecular interactions will give some lead whether or not the materials can form eutectics. Thus, the same cocrystallization experiment can result in the formation of cocrystals/eutectics depending on the interactions (adhesive or cohesive) that dominate, provided the process is entropically favorable; other the system will make a simple mixture. Further studies of these phenomena are needed to understand and predict cocrystal/eutectic formation.

For the first time, a control over the solubility/dissolution of drugs is achieved via cocrystals and eutectics through this study.¹⁷ The two ternary eutectics PZA–SA–INH and PZA–FA–INH were established to be eutectics of the corresponding binary cocrystals through X-ray diffraction and spectroscopy. All three eutectics (including PZA–INH binary eutectic) exhibited superior IDR than PZA (the less soluble drug) and were stable in laboratory storage conditions of ambient temperature (15–40 °C) and humidity (30–70% RH) in the investigated period of one year. PZA–SA–INH eutectic and INH–SA cocrystal conform to the WHO biowaiver dissolution criterion whereas pure INH and PZA did not qualify the criterion in the tested conditions.¹⁷ Thus, eutectics can confer dual advantages of solubility/dissolution (because of high thermodynamic functions) and stability (because of crystalline nature), which are the prime issues in drug research and development, in a novel drug formulation.

In addition to making ternary cocrystals^{20c,45} and drug–drug cocrystals,¹¹ the present approach of blending drugs into a eutectic composition (with or without a cofomer) can be utilized for combination drugs that fail to co-crystallize.¹⁷ Whether the drug material is amorphous, salt, cocrystal, eutectic or any complex, the objective is to develop a drug formulation with improved physico-chemical properties, and this end

goal was achieved, in part, in this study. Even though dosage aspects of the FDC formulation (PZA–INH in 5:1 ratio)^{1b,2} are still to be realized in PZA–INH drug eutectic (1:1 ratio), a practical approach of potential utility in pharmaceutical property management was demonstrated through eutectics in this study.

5.6 Experimental Section

Materials and Methods: PZA and INH were purchased from Acros Organics and used without further purification. All other chemicals were of analytical or chromatographic grade. Water purified from a deionizer cum mixed bed purification system was used for experiments.

Co-crystallization: Drug and coformer were taken in 1:0.5 molar stoichiometry (about 200 mg combined together) and subjected to solid state grinding using a mortar-pestle for 15 minutes. The resultant ground product was used for crystallization and scaled up for analytical characterization and experiments.

PZA–SA (C₇H₈N₃O₃): Solid ground mixture of PZA (24.6 mg, 0.2 mmol) and SA (11.8 mg, 0.1 mmol) was dissolved in 5 mL hot isopropanol and left for slow evaporation at room temperature. Colorless rod crystals were obtained after a few days upon solvent evaporation.

¹H NMR (DMSO-d₆): δ 2.40 (2H, s), 7.86 (1H, s), 8.27 (1H, s), 8.70 (1H, s), 8.84 (1H, s), 9.16 (1H, s). OH (succinic acid) exchange in solvent.

¹³C NMR (DMSO-d₆): δ 29.25, 143.86, 144.05, 145.50, 147.86, 165.57, 174.05.

INH–SA (C₈H₁₀N₃O₃): Solid ground mixture of INH (27.4 mg, 0.2 mmol) and SA (11.8 mg, 0.1 mmol) was dissolved in 4 mL hot acetonitrile and left for slow evaporation at room temperature. Colorless plate crystals were obtained after a few days upon solvent evaporation.

¹H NMR (DMSO-d₆): δ 2.40 (2H, s), 7.71 (2H, s), 8.69 (2H, s). OH (succinic acid) and NHs (INH) exchange in solvent.

¹³C NMR (DMSO-d₆): δ 29.83, 122.09 (2C), 141.34, 151.18 (2C), 165.02, 174.73.

PZA–FA (C₇H₇N₃O₃): Solid ground mixture of PZA (24.6 mg, 0.2 mmol) and FA (11.6 mg, 0.1 mmol) was dissolved in 5 mL hot methanol and left for slow evaporation at room temperature. Colorless plate crystals were obtained after a few days upon solvent evaporation.

^1H NMR (DMSO- d_6): δ 6.61 (1H, s), 7.85 (1H, s), 8.25 (1H, s), 8.70 (1H, s), 8.84 (1H, s), 9.17 (1H, s). OH (fumaric acid) exchange in solvent.

^{13}C NMR (DMSO- d_6): δ 134.45, 143.86, 144.07, 145.54, 147.86, 165.56, 166.45.

INH-FA ($\text{C}_8\text{H}_9\text{N}_3\text{O}_3$): Solid ground mixture of INH (27.4 mg, 0.2 mmol) and FA (11.6 mg, 0.1 mmol) was dissolved in 4 mL hot methanol and left for slow evaporation at room temperature. Colorless plate crystals were obtained after a few days upon solvent evaporation.

^1H NMR (DMSO- d_6): δ 6.61 (1H, s), 7.71 (2H, s), 8.70 (2H, s). OH (fumaric acid) and NHs (INH) exchange in solvent.

^{13}C NMR (DMSO- d_6): δ 121.47 (2C), 134.45, 140.72, 150.67 (2C), 164.36, 166.46.

Eutectic composition: Compounds were taken in equimolar ratio (about 200 mg combined together) and subjected to solid state grinding using a mortar-pestle for 15 minutes. The resultant ground product was scaled up and used for analytical characterization and experiments.

PZA-INH ($\text{C}_{11}\text{H}_{12}\text{N}_6\text{O}_2$)

^1H NMR (DMSO- d_6): δ 4.61 (2H, s), 7.70 (2H, s), 7.84 (1H, s), 8.26 (1H, s), 8.68 (3H, s), 8.83 (1H, s), 9.17 (1H, s), 10.01 (1H, s).

^{13}C NMR (DMSO- d_6): δ 121.48 (2C), 140.73, 143.86, 144.03, 145.49, 147.86, 150.65 (2C), 164.42, 165.61.

PZA-SA-INH ($\text{C}_{15}\text{H}_{18}\text{N}_6\text{O}_6$)

^1H NMR (DMSO- d_6): δ 2.40 (4H, s), 7.70 (2H, s), 7.86 (1H, s), 8.27 (1H, s), 8.70 (3H, s), 8.84 (1H, s), 9.17 (1H, s). OHs (Succinic acid) and NHs (INH) exchange in solvent.

^{13}C NMR (DMSO- d_6): δ 29.22 (2C), 121.46 (2C), 140.71 (1C), 143.86 (1C), 144.06 (1C), 145.53 (1C), 147.86 (1C), 150.67 (2C), 164.36 (1C), 165.56 (1C), 174.08 (2C).

PZA-FA-INH ($\text{C}_{15}\text{H}_{16}\text{N}_6\text{O}_6$)

^1H NMR (DMSO- d_6): δ 6.61 (2H, s), 7.71 (2H, s), 7.86 (1H, s), 8.27 (1H, s), 8.70 (3H, s), 8.84 (1H, s), 9.17 (1H, s). OHs (Fumaric acid) and NHs (INH) exchange in solvent.

^{13}C NMR (DMSO- d_6): δ 121.47 (2C), 134.45 (2C), 140.71 (1C), 143.86 (1C), 144.07 (1C), 145.54 (1C), 147.86 (1C), 150.67 (2C), 164.36 (1C), 165.55 (1C), 166.45 (2C).

X-ray Crystallography: X-ray reflections for PZA-SA, INH-SA and INH-FA (100 K) were collected on Bruker SMART-APEX CCD diffractometer equipped with a graphite

monochromator and Mo-K α fine-focus sealed tube ($\lambda = 0.71073 \text{ \AA}$). Data reduction was performed using Bruker SAINT software. Intensities were corrected for absorption using SADABS. Structures were solved and refined using SHELX-97. X-ray reflections for PZA-FA and INH-FA (298 K) were collected on an Oxford Xcalibur Gemini Eos CCD diffractometer using Mo-K α radiation. Data reduction was performed using CrysAlisPro (version 1.171.33.55). OLEX2-1.0 and SHELX-97 were used to solve and refine the structures. All non-hydrogen atoms were refined anisotropically. Hydrogen atoms on O and N were located from difference electron density maps and all C-H atoms were fixed geometrically using HFIX command in SHELX-TL. The final CIF files and hydrogen bond geometries were validated in PLATON. X-Seed was used to prepare packing diagrams.

Powder X-ray Diffraction: PXRD were recorded on Bruker D8 Advance diffractometer using Cu-K α X-radiation ($\lambda = 1.5406 \text{ \AA}$) at 40 kV and 30 mA. Diffraction patterns were collected over 2θ range of $5\text{--}50^\circ$ at scan rate of 1° min^{-1} . Powder Cell 2.4 was used to plot diffraction patterns.

Spectroscopy: IR spectra were recorded on samples dispersed in KBr pellets on a Nicolet 6700 FT-IR spectrometer. Solution and solid state NMR spectra were recorded on a Bruker Avance spectrometer at 400 MHz. SS-NMR spectra were recorded on a Bruker 4 mm double resonance CP-MAS probe in zirconia rotors at 5.0 kHz with a cross-polarization contact time of 2.5 ms and a recycle delay of 8 s. ^{13}C CP-MAS spectra were recorded at 100 MHz and referenced to the methylene carbon of glycine, and then the chemical shifts were recalibrated to the TMS scale ($\delta_{\text{glycine}} = 43.3 \text{ ppm}$). Likewise, ^{15}N CP-MAS spectra were recorded at 40 MHz and referenced to glycine N atom, and then the chemical shifts were recalibrated to nitromethane N ($\delta_{\text{glycine}} = -347.6 \text{ ppm}$). Additionally the identity and stoichiometry of the components in the eutectics and binary adducts was established through solution ^1H NMR integration and ^{13}C NMR spectra.

Thermal Analysis: DSC was performed on a Mettler Toledo DSC 822e module on a typical sample size of 3-5 mg in the temperature range $30\text{--}200^\circ\text{C}$ @ 5°C/min . Samples were placed in crimped but vented aluminum pans and purged by a stream of dry nitrogen flowing at 80 mL/min.

Equilibrium Solubility and Intrinsic Dissolution Measurements: Prior to solubility and dissolution measurements in the particular medium, standard curves of the

compounds were obtained and their molar extinction coefficients were determined spectrophotometrically on a Thermo Scientific Evolution 300 UV-Vis spectrometer based on the absorbance at 268 nm. The respective molar extinction coefficients of the compounds were used to estimate solubility (water: INH-SA 22.46, PZA-FA 46.08, INH-FA 23.73 mL mg⁻¹ cm⁻¹ respectively) and dissolution (pH 1.2 HCl solution: PZA 57.59, INH 36.45, PZA-INH 48.22, PZA-SA 43.06, INH-SA 27.21, PZA-SA-INH 34.23, PZA-FA 45.67, INH-FA 28.11, PZA-FA-INH 35.45 mL mg⁻¹ cm⁻¹ respectively) values. Equilibrium solubility was determined in water using the shake-flask method.⁴⁶ Excess amount of powdered compound was added to 5 mL water to result in a suspension which was stirred at room temperature for 24 h. The suspension was equilibrated for one hour and then filtered through 2.5 μ m Whatman filter paper. The concentration of the solution thus obtained was determined spectrophotometrically after appropriate dilution using the molar extinction coefficients of the respective compounds. IDR experiments in pH 1.2 HCl solution were carried on a USP certified Electrolab TDT-08L Dissolution Tester for one hour by the disk intrinsic dissolution rate (DIDR) method.³⁹ For IDR testing, 200 mg of the compound was taken in the intrinsic attachment and compressed to a 0.5 cm² disk using a hydraulic press at a pressure of 2.5 ton inch⁻² for 5 min. The intrinsic attachment was placed in a jar of 900 mL medium preheated to 37 °C and rotated at 75 rpm. Aliquots of 5 mL were collected at specific time intervals and concentration of the aliquots was determined spectrophotometrically. The linear region of the dissolution profile (regression > 0.99) was used to determine the IDR of the compound as [slope of the amount dissolved ÷ surface area of the disk] per unit time. There is no transformation of the compounds before (upon compression) and after the dissolution experiment as analyzed by IR and PXRD profiles.

5.7 References

1. (a) M. -T. Gutierrez-Lugo and C. A. Bewley, *J. Med. Chem.*, 2008, **51**, 2606; (b) E. Catalani, *Int. J. Tuberc. Lung Dis.*, 1999, **3**, S289.
2. WHO model list of Essential Medicines is available at http://www.who.int/selection_medicines/committees/expert/17/sixteenth_adult_list_en.pdf.
3. (a) B. Blomberg, S. Spinachi, B. Fourie and R. Laing, *Bull. World Health Organ.*, 2001, **79**, 61; (b) G. Sanz and V. Fuster, *Nat. Clin. Pract. Cardiovasc.*

- Med.*, 2009, **6**, 101; (c) A. I. Wertheimer and A. Morrison, *Pharm. Ther.*, 2002, **27**, 44;
- (d) <http://apps.who.int/medicinedocs/pdf/s6172e/s6172e.pdf>, WHO Report, 2003.
4. (a) C. H. Arnaud, *Chem. Eng. News*, 2011, **89**, 32; (b) A. L. Hopkins, J. S. Mason and J. P. Overington, *Curr. Opin. Struct. Bio.*, 2006, **16**, 127.
 5. S. Frantz, *Nat. Rev. Drug Discov.*, 2006, **5**, 881.
 6. (a) S. Singh and B. Mohan, *Int. J. Tuberc. Lung Dis.*, 2003, **7**, 298; (b) H. Bhutani, S. Singh, K. C. Jindal and A. K. Chakraborti, *J. Pharm. Biomed. Anal.*, 2005, **39**, 892.
 7. <http://apps.who.int/prequal/whopar/whoparproducts/TB168Part6v1.pdf>.
 8. (a) L. Petersen, P. T. Jørgensen, C. Nielsen, T. H. Hansen, J. Nielsen and E. B. Pedersen, *J. Med. Chem.*, 2005, **8**, 1211; (b) H. Matsumoto, T. Hamawaki, H. Ota, T. Kimura, T. Goto, K. Sano, Y. Hayashi and Y. Kiso, *Bioorg. Med. Chem. Lett.*, 2000, **10**, 1227.
 9. (a) Ö. Almarsson, M. J. Zaworotko, *Chem. Commun.*, 2004, 1889; (b) C. B. Aakeröy, J. Desper and J. F. Urbina, *Chem. Commun.*, 2005, 2820. (c) N. Shan and M. J. Zaworotko, *Drug Discov. Today*, 2008, **13**, 440.
 10. (a) N. J. Babu and A. Nangia, *Cryst. Growth Des.*, 2011, **11**, 2662; (b) S. Cherukuvada, N. J. Babu and A. Nangia, *J. Pharm. Sci.*, 2011, **100**, 3233; (c) N. Schultheiss and A. Newman, *Cryst. Growth Des.*, 2009, **9**, 2950; (d) A. V. Trask, *Mol. Pharmaceutics*, 2007, **4**, 301; (e) N. Blagden, M. de Matas, P. T. Gavan and P. York, *Adv. Drug Deliv. Rev.*, 2007, **59**, 617; (f) M. K. Stanton, R. C. Kelly, A. Colletti, Y.-H. Kiang, M. Langley, E. J. Munson, M. L. Peterson, J. Roberts and M. Wells, *J. Pharm. Sci.*, 2010, **99**, 3769; (g) S. Karki, T. Friščić, L. Fábíán, P. R. Laity, G. M. Day and W. Jones, *Adv. Mater.*, 2009, **21**, 3905; (h) E. Lu, N. Rodríguez-Hornedo and R. Suryanarayanan, *CrystEngComm*, 2008, **10**, 665; (i) D. P. McNamara, S. L. Childs, J. Giordano, A. Iaricchio, J. Cassidy, M. S. Shet, R. Mannion, E. O'Donnell and A. Park, *Pharm. Res.*, 2006, **23**, 1888; (j) C. B. Aakeröy, S. Forbes and J. Desper, *J. Am. Chem. Soc.*, 2009, **132**, 17048; (k) S. L. Childs, N. Rodríguez-Hornedo, L. S. Reddy, A. Jayasankar, C. Maheshwari, L. McCausland, R. Shipplett and B. C. Stahly, *CrystEngComm*, 2008, **10**, 856; (l) K. Guo, G. Sadiq, C. Seaton, R. Davey and Q. Yin, *Cryst. Growth Des.*, 2010, **10**, 268.

11. (a) P. Grobelny, A. Mukherjee and G. R. Desiraju, *CrystEngComm*, 2011, **13**, 4358; (b) A. O. L. Évora, R. A. E. Castro, T. M. R. Maria, M. T. S. Rosado, M. R. Silva, A. M. Beja, J. Canotilho and M. E. S. Eusébio, *Cryst. Growth Des.*, 2011, **11**, 4780; (c) M. L. Cheney, D. R. Weyna, N. Shan, M. Hanna, L. Wojtas and M. J. Zaworotko, *J. Pharm. Sci.*, 2011, **100**, 2172; (d) S. Aitipamula, P. S. Chow and R. B. H. Tan, *CrystEngComm*, 2009, **11**, 1823; (e) P. M. Bhatt, Y. Azim, T. S. Thakur and G. R. Desiraju, *Cryst. Growth Des.*, 2009, **9**, 951.
12. (a) A. Górniak, A. Wojakowska, B. Karolewicz and J. Pluta, *J. Ther. Anal. Calorim.*, 2011, **104**, 1195; (b) J. A. Rogers, *WO Pat.*, 2008/073324 A1, 2008; (c) Y. Sakata, E. Tanabe, T. Sumikawa, S. Shiraishi, Y. Tokudome and M. Otsuka, *Int. J. Pharmaceutics*, 2007, **335**, 12.
13. M. J. Small, *Chest*, 1959, **36**, 265.
14. (a) C. Tamura, H. Kuwano and Y. Sasada, *Acta Crystallogr.*, 1961, **14**, 693; (b) R. A. E. Castro, T. M. R. Maria, A. O. L. Évora, J. C. Feiteira, M. R. Silva, A. M. Beja, J. Canotilho and M. E. S. Eusébio, *Cryst. Growth Des.*, 2010, **10**, 274; (c) S. Cherukuvada, R. Thakuria and A. Nangia, *Cryst. Growth Des.*, 2010, **10**, 3931.
15. (a) C. B. Aakeröy, J. Desper and B. A. Helfrich, *CrystEngComm*, 2004, **6**, 19; (b) J. A. McMahon, J. A. Bis, P. Vishweshwar, T. R. Shattock, O. L. McLaughlin and M. J. Zaworotko, *Z. Crystallogr.*, 2005, **220**, 340; (c) Y. Simonov, V. Kravtsov, E. Ganin and T. Lis, *Acta Crystallogr. Sect. A: Found. Crystallogr.*, 2006, **62**, s219; (d) A. Lemmerer, J. Bernstein and V. Kahlenberg, *CrystEngComm*, 2010, **12**, 2856; (e) H. Abourahma, D. S. Cocuzza, J. Melendez and J. M. Urban, *CrystEngComm*, 2011, **13**, 6442; (f) A. Lemmerer and J. Bernstein, *J. Chem. Crystallogr.*, 2011, **41**, 991; (g) A. Lemmerer, *CrystEngComm*, 2012, **14**, 2465.
16. (a) M. C. Etter and G. M. Frankenbach, *Chem. Mater.*, 1989, **1**, 10; (b) A. V. Trask and W. Jones, *Top. Curr. Chem.*, 2005, **254**, 41; (c) G. Kaupp, *CrystEngComm*, 2009, **11**, 388; (d) A. Dilor, T. Friščić and W. Jones, *CrystEngComm*, 2012, **14**, 2350.
17. S. Cherukuvada and A. Nangia, *CrystEngComm*, 2012, **14**, 2579.
18. (a) R. D. B. Walsh, M. W. Bradner, S. Fleischman, L. A. Morales, B. Moulton, N. Rodríguez-Hornedo and M. J. Zaworotko, *Chem. Commun.*, 2003, 186; (b) B. R. Bhogala and A. Nangia, *Cryst. Growth Des.*, 2003, **3**, 547; (c) P.

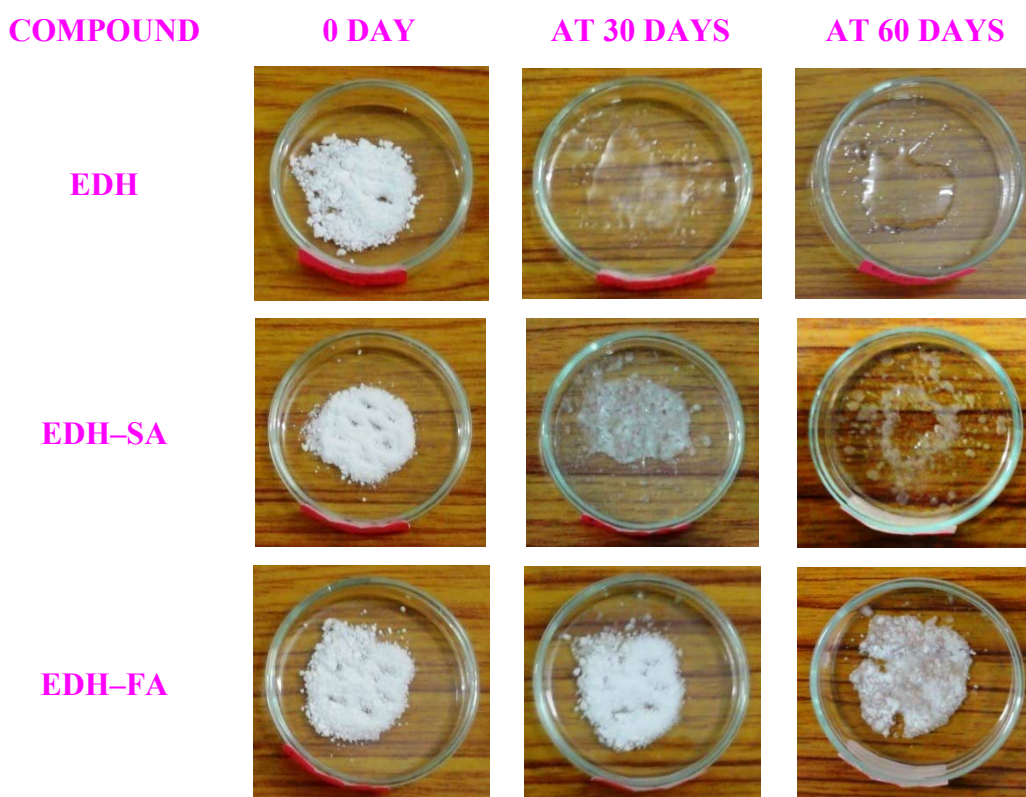
- Vishweshwar, A. Nangia and V. M. Lynch, *Cryst. Growth Des.*, 2003, **3**, 783;
- (d) S. Karki, T. Friščić and W. Jones, *CrystEngComm*, 2009, **11**, 470.
19. GRAS/EAFUS (Everything Added to Food in the United States) substances list:
<http://www.fda.gov/Food/FoodIngredientsPackaging/ucml15326.htm>.
20. (a) S. L. Childs, G. P. Stahly and A. Park, *Mol. Pharmaceutics*, 2007, **4**, 323; (b) *Handbook of Pharmaceutical Salts, Properties, Selection and Use*, ed. P. H. Stahl and C. G. Wermuth, Wiley-VCH, 2002; (c) B. R. Bhogala, S. Basavoju and A. Nangia, *CrystEngComm*, 2005, **7**, 551.
21. (a) C. Becker, J. B. Dressman, G. L. Amidon, H. E. Junginger, S. Kopp, K. K. Midha, V. P. Shah, S. Stavchansky and D. M. Barends, *J. Pharm. Sci.*, 2008, **97**, 3709; (b) *CRC Handbook of Chemistry and Physics*, ed. D. R. Lide, 90th ed., CD-ROM ver, CRC Press/Taylor & Francis, 2010; (c) 2010C. Becker, J. B. Dressman, G. L. Amidon, H. E. Junginger, S. Kopp, K. K. Midha, V. P. Shah, S. Stavchansky and D. M. Barends, *J. Pharm. Sci.*, 2007, **96**, 522.
22. (a) http://reference.iucr.org/dictionary/Isomorphous_crystals; (b) N. K. Nath, B. K. Saha and A. Nangia, *New J. Chem.*, 2008, **32**, 1693.
23. (a) http://reference.iucr.org/dictionary/Isostructural_crystals; (b) A. Kalman, L. Parkanyi and G. Argay, *Acta Crystallogr. Sect. B: Struct. Sci.*, 1993, **49**, 1039. (c) S. K. Chandran, R. Thakuria and A. Nangia, *CrystEngComm*, 2008, **10**, 1891.
24. (a) T. Steiner, I. Majerz and C. C. Wilson, *Angew. Chem. Int. Ed.*, 2001, **40**, 2651; (b) J. A. Cowan, J. A. Howard, G. J. McIntyre, S. M. Lo and I. D. Williams, *Acta Crystallogr. Sect. B: Struct. Sci.*, 2003, **59**, 794; (c) C. C. Wilson, *Acta Crystallogr. Sect. B: Struct. Sci.*, 2001, **57**, 435.
25. Polymorphs, Salts, and Cocrystals: What's in a Name?, *Cryst. Growth Des.*, 2012, **12**, 2147.
26. B. P. van Eijck and J. Kroon, *Acta Crystallogr.*, 2000, **B56**, 535.
27. (a) D. R. Askeland and P. P. Fulay, *Essentials of Materials Science and Engineering*, 2nd ed., Cengage Learning, 2009; (b) M. D. Moore and P. L. D. Wildfong, *J. Pharm. Innov.*, 2009, **4**, 36.
28. (a) S. S. Das, N. P. Singh, T. Agrawal, P. Gupta, S. N. Tiwari and N. B. Singh, *Mol. Cryst. Liq. Cryst.*, 2009, **501**, 107; (b) N. B. Singh, S. S. Das, N. P. Singh and T. Agrawal, *J. Cryst. Growth*, 2008, **310**, 2878; (c) N. B. Singh and P. Kumar, *J. Chem. Eng. Data*, 1989, **34**, 145.

29. A. V. Trask, D. A. Haynes, W. D. S. Motherwell and W. Jones, *Chem. Commun.*, 2006, 51.
30. (a) P. W. Scott, A. C. Williams and B. W. Barry, *J. Contr. Rel.*, 1998, **50**, 297; (b) P. W. Scott, A. C. Williams and B. W. Barry, *Int. J. Pharm.*, 2001, **219**, 161.
31. M. Bi, S. -J. Hwang and K. R. Morris, *Ther. Acta*, 2003, **404**, 213.
32. (a) K. Chadwick, R. Davey and W. Cross, *CrystEngComm*, 2007, **9**, 732; (b) T. Frišćić and W. Jones, *Cryst. Growth Des.*, 2009, **9**, 1621.
33. (a) Z. J. Li, Y. Abramov, J. Bordner, J. Leonard, A. Medek and A. V. Trask, *J. Am. Chem. Soc.*, 2006, **128**, 8199; (b) F. G. Vogt, J. S. Clawson, M. Strohmeier, A. J. Edwards, T. N. Pham and S. A. Watson, *Cryst. Growth Des.*, 2009, **9**, 921.
34. R. M. Silverstein, F. X. Webster and D. J. Kiemle, *Spectrometric Identification of Organic Compounds*, John Wiley & Sons, NJ, 2005.
35. (a) D. Hadzi and N. Kobilarov, *J. Chem. Soc. A*, 1966, 439. (b) J. P. Castaneda, G. S. Denisov, S. Yu. Kuchero, V. M. Schreiber and A. V. Shurukhina, *J. Mol. Struct.*, 2003, **660**, 25; (b) C. B. Aakeröy, J. Desper and M. E. Fasulo, *CrystEngComm.*, 2006, **8**, 586.
36. D. J. Good and N. Rodríguez-Hornedo, *Cryst. Growth Des.*, 2009, **9**, 2252.
37. (a) J. B. Dressman, G. L. Amidon, C. Reppas and V. P. Shah, *Pharm. Res.*, 1998, **15**, 11; (b) Y. Qiu; Y. Chen and G. G. Z. Zhang, Eds., *Developing Solid Oral Dosage Forms. Pharmaceutical Theory and Practice*, Academic Press, New York, 2009.
38. (a) WHO Technical Report Series No. 937, 40th Report, 2006: http://whqlibdoc.who.int/trs/who_trs_937_eng.pdf; (b) S. Strauch, E. Jantravid, M. Stahl, L. Rågo and J. B. Dressman, *J. Pharm. Sci.*, 2011, **100**, 822.
39. L. X. Yu, A. S. Carlin, G. L. Amidon and A. S. Hussain, *Int. J. Pharmaceutics*, 2004, **270**, 221.
40. M. K. Stanton and A. Bak, *Cryst. Growth Des.*, 2008, **8**, 3856.
41. (a) J. I. Arenas-Garcia, D. Herrera-Ruiz, K. Mondragón-Vásquez, H. Morales-Rojas and H. Höpfl, *Cryst. Growth Des.*, 2010, **10**, 3732; (b) J. I. Arenas-Garcia, D. Herrera-Ruiz, K. Mondragón-Vásquez, H. Morales-Rojas and H. Höpfl, *Cryst. Growth Des.*, 2012, **12**, 811; (c) A. Lemmerer, J. Bernstein and M. A. Spackman, *Chem. Commun.*, 2012, **48**, 1883.
42. H. G. Brittain, *Cryst. Growth Des.*, 2009, **9**, 2942.

43. (a) C. C. Seaton and A. Parkin, *Cryst. Growth Des.*, 2011, **11**, 1502; (b) L. S. Reddy, P. M. Bhatt, R. Banerjee, A. Nangia and G. J. Kruger, *Chem. Asian J.*, 2007, **2**, 505.
44. L. Leiserowitz and F. Nader, *Acta Crystallogr. Sect. B:Struct. Sci.*, 1977, **33**, 2719.
45. (a) L. H. Thomas, N. Blagden, M. J. Gutmann, A. A. Kallay, A. Parkin, C. C. Seaton and C. C. Wilson, *Cryst. Growth Des.*, 2010, **10**, 2770; (b) T. Friščić, A. V. Trask, W. Jones and W. D. S. Motherwell, *Angew. Chem. Int. Ed.*, 2006, **45**, 7546; (c) C. B. Aakeröy, A. M. Beatty and B. A. Helfrich, *Angew. Chem. Int. Ed.*, 2001, **40**, 3240.
46. A. Glomme, J. März and J. B. Dressman, *J. Pharm. Sci.*, 2005, **94**, 1.

CHAPTER SIX

ETHAMBUTOL DIHYDROCHLORIDE EUTECTICS



Snapshots of ethambutol dihydrochloride (EDH) and its eutectics viz. ethambutol dihydrochloride–succinic acid (EDH–SA) and ethambutol dihydrochloride–fumaric acid (EDH–FA), subjected to accelerated stability testing conditions of 40 °C and 75% RH (relative humidity) for two months. The eutectics exhibit greater hygroscopic stability compared to the parent drug.

6.1 Introduction

Tuberculosis (TB) is the second largest killer disease in the world after HIV/AIDS and is the top three causes of death for women in the age group 15 to 44.¹ In 2010, about 1.4 million people died from TB. BCG (Bacillus Calmette-Guérin) vaccine, the only licensed vaccine, is effective against childhood TB but its efficacy declines after 10-20 years.² Thus, chemotherapy forms the crucial mode of treatment for the disease but development of drug resistance warrants sound strategies to contain it. The World Health Organization (WHO), in 1995, developed a strategy called DOTS (Directly Observed Treatment, Short-course) to control TB and drug resistance due to monotherapy.^{1,3} According to this, a standard six-month course of four drugs namely Rifampicin, Isoniazid, Pyrazinamide and Ethambutol (dihydrochloride) in a fixed dose combination (FDC) formulation is administered to treat TB in a comprehensive way.³ Through this approach, even if tubercle bacteria develop resistance to one or more of these drugs, they will succumb to remaining drugs of the combination. Since 1995, an estimated 7 million lives were saved through the use of DOTS polytherapy.¹ However, multidrug-resistant strains evolved through the course of time leading to multidrug-resistant tuberculosis (MDR-TB).^{1,4} The primary causes of MDR-TB are incomplete/inadequate treatment, mismanagement of the course regimen and use of poor quality medicines.¹ Apart from nonadherence to the GMP (Good Manufacturing Practice) standards in the production of medicines,⁵ the inherent drug-drug interactions^{5b,6} and consequent degradation in the combination formulation was reported to be responsible for sub-standard or poor quality anti-TB FDC products. The hygroscopicity of ethambutol dihydrochloride (abbreviated as EDH), one of the components of the FDC, is found to catalyse the degradation of rifampicin and isoniazid in the formulation resulting in instability and loss of quality of the FDC products upon storage.⁷ As a consequence, individual drugs of the FDC formulation are separately coated with polymers to avoid mutual interaction and water uptake and then blended to make up the final product formulation.⁸ It seems by the time the quality problems of the anti-TB FDC formulations were realized, damage has been done due to inadequacy of drug dosage (because of decomposition upon storage) and thus leading to MDR-TB. Thus, new formulations that can minimize drug-drug interactions and sustain the potency of the drugs are the need of the hour. Therefore, controlling the hygroscopicity of ethambutol dihydrochloride can lead to quality sustenance of the anti-TB FDC formulations.

6.2 Solid form screening

Salt screening of ethambutol base (abbreviated as EMB) with the intent of obtaining less hygroscopic salts, and thus provide alternatives to the existing hydrochloride salt formulation, resulted in hygroscopic salts and ionic liquids (discussed in Chapter 3). Hence, the attention was turned to other solid forms that can solve the hygroscopicity problem of the drug. A scheme about the pros and cons of various solid forms was devised in this study (Table 6.1). Based on this, cocrystals and eutectics were pursued as they showed promising results in pharmaceutical property management of several drugs.⁹

Table 6.1 Scheme of solid formulation options to tackle the hygroscopicity problem of EDH.

API formulation	EMB (base)	EDH (salt)
Amorph	Not a viable option – because of its high thermodynamic functions, it can tend to be hygroscopic	Not a viable option – because of its high thermodynamic functions, it can tend to be hygroscopic
Salt	Viable option – but salt screening resulted in hygroscopic salts and ionic liquids (Chapter 3)	–
Cocrystal^a	Viable option	Viable option
Solid solution^b	Viable option – but needs isomorphous solids to form	Viable option – but needs isomorphous solids to form
Eutectic^c	Since it is a low melting compound (88 °C), making a eutectic with still lower m.p. is not a viable option	Though it has high thermodynamic functions, its crystalline nature makes it a viable option
Solid dispersion^d	Viable option – but there is no design aspect	Viable option – but there is no design aspect

^a A cocrystal is a stoichiometric multi-component crystalline solid.^{9a,10}

^b A solid solution is a variable stoichiometry multi-component crystalline solid.^{9f,10,11}

^c A eutectic is a conglomerate of solid solutions.¹⁰

^d A solid dispersion is a dispersion of two or more components in a solid matrix.^{9f,10,12}

In this study, cocrystallization trials with ethambutol base with several coformers that cannot result in salt formation such as urea, nicotinamide, glycine, cytosine etc. did not succeed. Attempts were not made to ascertain any eutectic formation, because a eutectic with still lower melting point will bring on production-related stability problems for this already low melting compound (Table 6.1). Then, cocrystallization of ethambutol dihydrochloride (EDH) salt was attempted. GRAS dicarboxylic acid coformers (fumaric

acid (FA), succinic acid (SA) and L-tartaric acid (TA)¹³; Figure 6.1) were selected based on the non-hygroscopic nature and lack of hydrates for FA and SA,^{14,15} though L-tartaric acid hydrates,¹⁵ its cocrystal with piracetam was shown to exhibit hygroscopic stability.¹⁶ The properties of partner molecules of cocrystals and eutectics are known to play a vital role in affecting their properties e.g. high soluble coformer can confer solubility/dissolution improvement to its cocrystal/eutectic.^{9a,e,17} Thus, these coformers can impart hygroscopic stability to their cocrystals/eutectics. Solid state grinding¹⁸ of EDH with FA/SA/TA in 1:1 ratio resulted in eutectic compositions (EDH-FA-G; EDH-SA-G; EDH-TA-G; 'G' represents ground product). In addition, the traditional method of, co-melting^{9f,19} (in 1:1 ratio) also gave the eutectics (EDH-FA-M; EDH-SA-M; 'M' represents molten product) except in case of L-tartaric acid where the molten material did not solidify (perhaps because of supercooling).²⁰ On the other hand, no attempts were made to ascertain the exact eutectic compositions through a phase diagram. For the ease of study and understanding, the components were taken in 1:1 molar ratio and ascertained as eutectic compositions in a broad sense. The novel eutectic compositions were found to exhibit greater hygroscopic stability compared to the parent drug (discussed later).

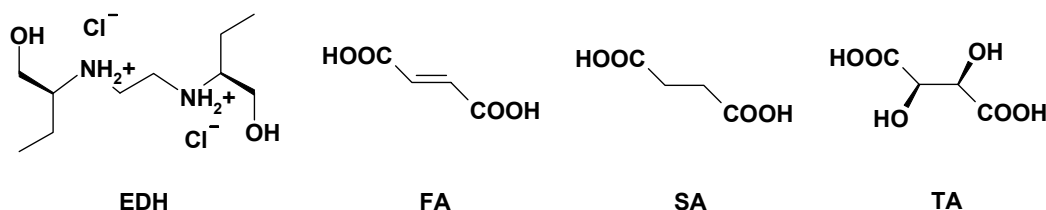
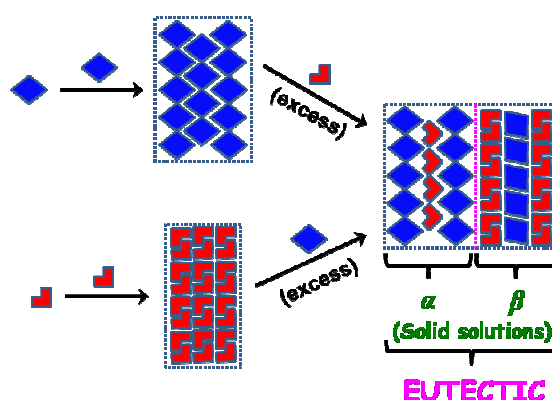


Figure 6.1 Molecular structures of the compounds of this study.

6.3 Characterization of the EDH eutectics

As discussed in Chapters 1 and 5, cocrystal/eutectic formation takes place depending on whether adhesive or cohesive interactions dominate between the components. The formation of eutectics of EDH with the dicarboxylic acid coformers (Figure 6.1) can be due to lack of strong heteromolecular interactions that can result in a cocrystal viz. (i) there are no viable acceptor groups in both the components to satisfy the strong hydrogen bond donor groups (carboxylic acid and hydroxyl) and (ii) no viable functional groups (such as amide and pyridine) that can break the acid dimer of the carboxylic acid, and (iii) more number of hydrogen bond donors (especially weak C–H donors) compared to acceptor groups. Hence, such a system will tend to form a eutectic. As per the Lead-Tin

system,²¹ it is hypothesized that EDH (major component) accommodates minor component FA/SA/TA in its crystal lattice up to the extent its lattice structure is not affected and thus forms a solid solution. When FA/SA/TA proportion goes beyond the threshold which EDH can accommodate, it can lead to strain and disorganization of the lattice. To conciliate, the system reorganizes into two phases (solid solutions - ' α ' and ' β ', Scheme 6.2) one with EDH as major component and other with EDH as minor component accommodated in the lattice structure of FA/SA/TA. The EDH rich and poor solid solutions make separate domains in the crystal lattice each with its parent lattice structures, i.e. the solid solution rich in EDH will have the lattice structure of EDH and the solid solution rich in dicarboxylic acid will have the lattice structure of diacid. The two solid solutions (domains) will be bound together through weak and imperfect interactions to result in a eutectic structure²¹ (Scheme 6.2). The poor inter-phase bonding leads to excess thermodynamic functions (free energy, enthalpy and entropy) of the eutectic with the result that it exhibits characteristic lower melting point than the components.^{9f,21,22} The high thermodynamic functions of the eutectics can result in solubility improvement of drugs similar to amorphous forms²³ and solid dispersions.^{9f,12} But, unlike solid dispersions which are largely amorphous in nature,^{9f} eutectics being crystalline have less free energy than amorphous materials and thus can confer stability advantage too. On this ground, the novel EDH eutectics were subjected to hygroscopic stability testing, which gave encouraging results (discussed later).



Scheme 6.2 When two elements/compounds lacking strong adhesive interactions are combined, they can give rise to 'eutectics' when a second (minor) component tries to accommodate in the lattice structure of the parent (major) component beyond its solubility limit. The mismatch and misfit between the components leads to segregation of the lattice structure into domains of solid solutions (α and β) each of which rich in a particular component. These domains (solid solutions) which sustain their parent lattice structures are held by weak and imperfect interactions (indicated by dotted magenta line) and result in the eutectic microstructure.

The melting points of the EDH eutectics are proportional to the melting point of the coformer (FA – 287, SA – 188, TA – 169 °C) with fumaric acid eutectic having the highest melting point (Figure 6.2). Slight differences in the melting points of the eutectics obtained by heating physical mixture, ground mixture and melt were observed in the DSC (Figure 6.3). The physical mixture has the highest eutectic endotherm followed by ground mixture and then by melts. Also the polymorphic transformation endotherm of EDH (form II \rightarrow form I, around 75 °C)²⁴ is found to diminish from physical mixture to molten eutectic (Figure 6.3). This shows that the intimate contact area in reorganization to result in a eutectic structure increased from physical mixture to ground mixture to molten material²⁵ i.e. the physical mixture with heterogeneous distribution and random interactions transformed into a homogeneous material with non-random interactions upon grinding or melting.^{9e} The PXRD patterns (Figure 6.4) and ¹³C ssNMR spectra (Figure 6.5) of the eutectics obtained through grinding and melting closely match with that of the components but were slightly different from one another. The diffraction peaks of the molten material were broad and showed lower intensity compared to ground material i.e. it was less crystalline. This indicates that the extent of reorganization in forming a eutectic structure is different upon melting compared to grinding. This is not unprecedented since reorganization of the components in the lattice takes place through a liquid phase upon melting which is not the case for grinding where reorganization happens only in solid state. Overall, the DSC (showing polymorphic transformation of EDH just like pure EDH), PXRD and spectroscopic patterns of the obtained eutectics (matching with that of the components) are in line with the eutectic microstructure as composed of the lattice structures of the components²¹ (Scheme 6.2).

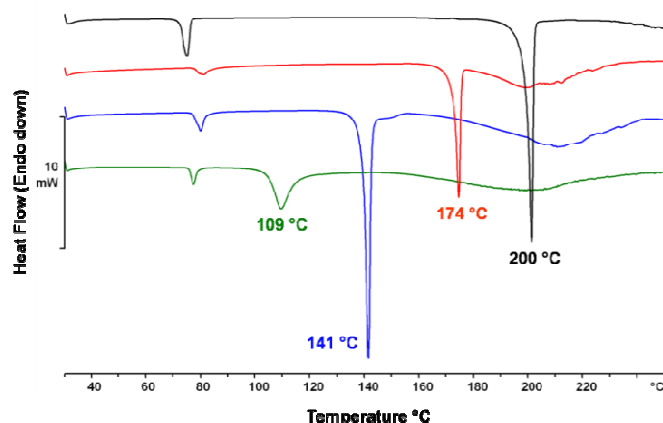


Figure 6.2 DSC of EDH (black), EDH–FA–G (red), EDH–SA–G (blue) and EDH–TA–G (green). The small endotherm around 75 °C pertaining to EDH polymorphic transformation (form II \rightarrow form I)²⁴ is observed in all three eutectic compositions.

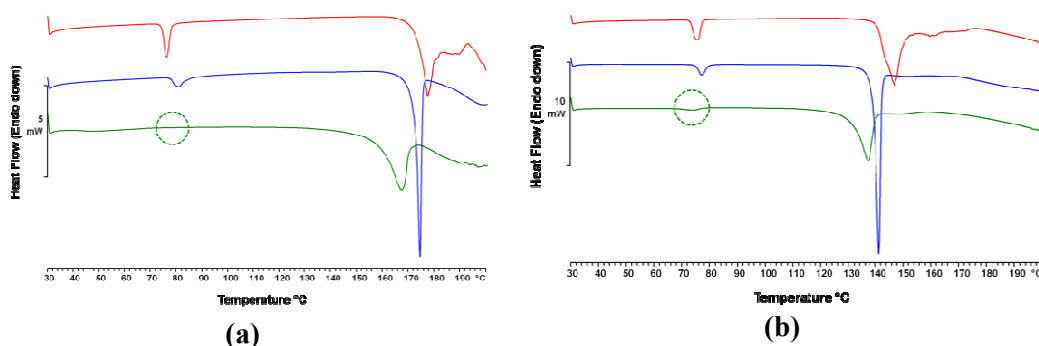
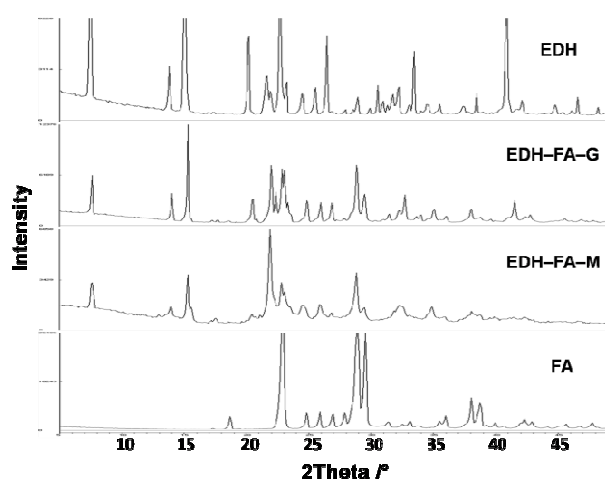
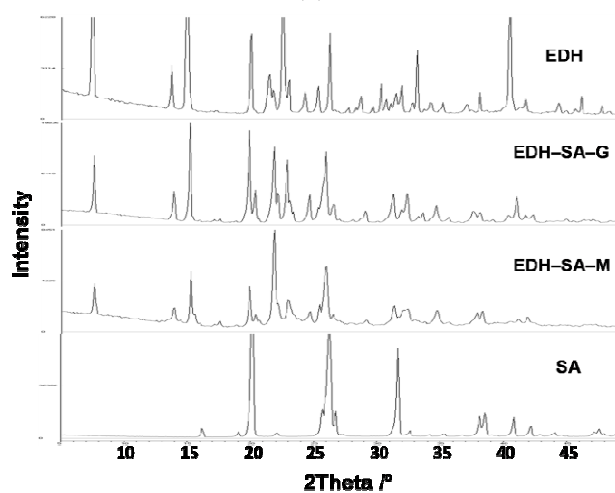


Figure 6.3 DSC of (a) EDH-FA (m.p. around 170 °C) and (b) EDH-SA (m.p. around 140 °C) systems to show lowering of eutectic endotherm and suppression of phase transition endotherm of EDH (form II \rightarrow form I around 75 °C)²⁴ from physical mixture (red) to melt (green) through ground material (blue).



(a)



(b)

Figure 6.4 PXRD patterns of (a) EDH-FA and (b) EDH-SA systems showing good match of diffraction lines between eutectics and the components. In addition, the eutectics obtained through grinding and melting exhibit slight differences with respect to peak broadening and intensity.

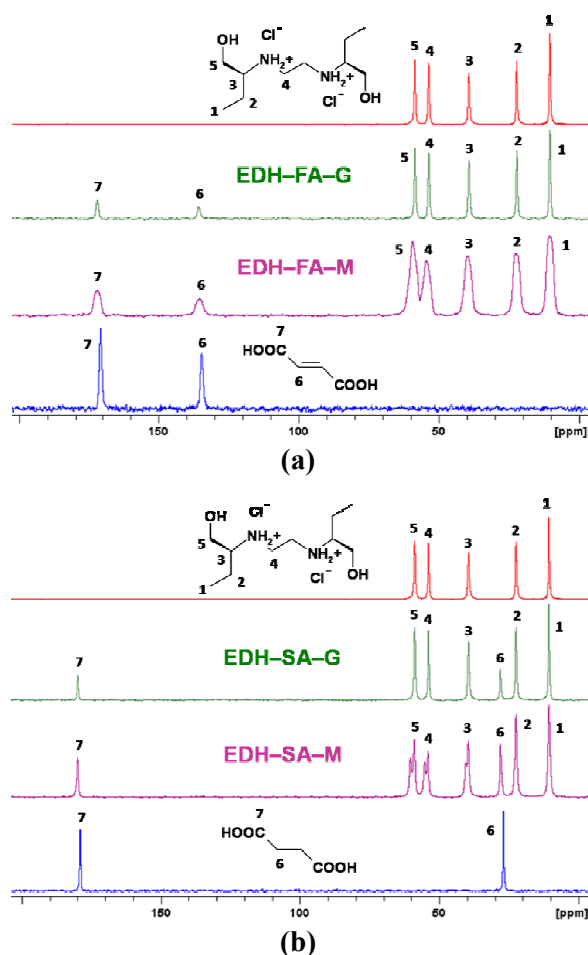


Figure 6.5 ^{13}C ssNMR spectra of (a) EDH-FA and (b) EDH-SA systems showing good match of chemical shifts between eutectics and the components. In addition, the eutectics obtained through grinding and melting exhibit differences with respect to peak broadening in the former and peak splitting in the latter which indicates slightly different crystalline environments in them.

6.4 Hygroscopicity study

The new EDH eutectics were tested for their hygroscopic stability, as per the WHO/ICH guidelines,²⁶ in accelerated stability testing conditions of 40 °C and 75% RH for two months and compared with EDH. Samples were analyzed for water uptake periodically at 15, 30 and 60 days through TGA and KF titration and the data are given in Table 6.2. Integrity of the samples was confirmed through NMR and PXRD (wherever possible) before and after the study. EDH salt looked slightly hygroscopic (upon visual inspection) and showed 5% water uptake by 15 days and became semisolid with 20% water uptake after 30 days and completely turned liquid after 60 days (Figure 6.6). There appears to be some correlation between melting point of the eutectic and its hygroscopic stability as

the hygroscopic stability behavior improved from L-tartaric acid eutectic to fumaric acid eutectic (Table 6.2). EDH-TA-G eutectic with lowest melting point of the EDH eutectics was found to liquefy within 15 days (by visual inspection) and showed highest water uptake of 55% at the end of two months (Table 6.2). The molten product of EDH-TA became semisolid upon cooling and hence not tested. On the other hand, differences in hygroscopic behavior between grinding-induced eutectic^{9e} (ground product) and heat-induced eutectic²⁵ (molten product) were observed in the cases of EDH-FA and EDH-SA systems. The heat-induced eutectics with less crystallinity compared to grinding-induced eutectics (PXRD in Figure 6.4) have less hygroscopic stability. EDH-SA-M eutectic became pasty after 15 days and completely turned liquid with 48% water uptake by 60 days, while EDH-SA-G showed only 14% water uptake after 60 days and was semisolid (Figure 6.6, Table 6.2). Similarly, EDH-FA eutectics showed differences in water uptake behavior with EDH-FA-M 13% and EDH-FA-G 3% after 60 days (Figure 6.6, Table 6.2). This indicates that there might be differences in the domain organization of grinding-induced and heat-induced eutectics with the result that they exhibited slightly different hygroscopic behavior. In all, both the EDH-FA eutectics and EDH-SA-G eutectic showed greater hygroscopic stability than EDH in the tested conditions.

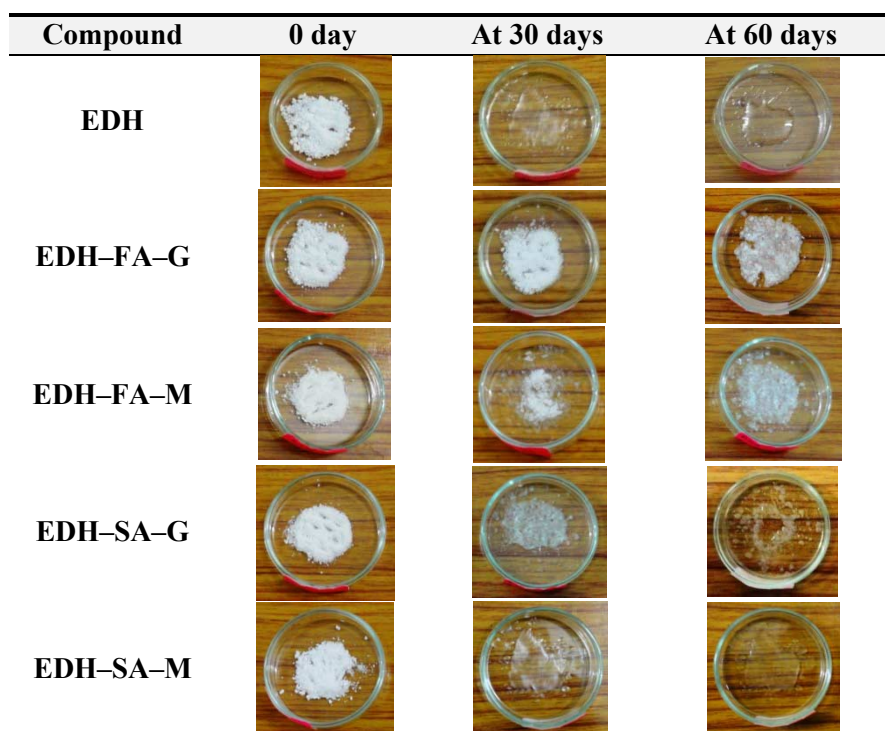


Figure 6.6 Snapshots of the compounds to show their relative hygroscopicity with EDH-FA-G eutectic showing higher stability towards the accelerated stability testing conditions of 40 °C and 75% RH for two months.

Table 6.2 Melting points and hygroscopic behavior of the compounds.

Compound	Melting point (°C)	% water uptake							
		0 day		At 15 days		At 30 days		At 60 days	
		TGA	KF	TGA	KF	TGA	KF	TGA	KF
EDH	200	0.2	0.3	5.2	5.4	20.2	19.3	45.6	45.8
EDH-FA-G ^a	174	0.2	0.2	0.2	0.2	0.5	0.4	2.9	3.0
EDH-FA-M ^b	167	0.2	0.2	4.4	4.6	9.1	10.1	13.1	13.3
EDH-SA-G ^a	141	0.2	0.2	1.3	0.9	5.9	5.8	13.7	13.8
EDH-SA-M ^b	137	0.2	0.2	15.7	15.9	30.6	30.3	48.2	48.3
EDH-TA-G ^a	109	0.2	0.2	19.5	19.3	38.5	38.6	54.5	54.6

^a eutectic obtained by grinding; ^b eutectic obtained by melting.

Hygroscopic stability testing of the eutectics was also carried out through a DVS (Dynamic Vapor Sorption) study. Samples were subjected to a 10-90-10% RH cycle at 40 °C (detailed in Experimental Section) and their water adsorption/desorption behavior was studied. EDH was found to adsorb 106% water at 90% RH and retain 37% water upon coming back to 10% RH (Figure 6.7). EDH-FA-G eutectic showed a maximum water uptake of 60% (at 90% RH) and retained only 14% water at the completion of the experiment (Figure 6.8a). EDH-FA-M eutectic, which showed a maximum water uptake of 72%, retained only 1% water after the experiment (Figure 6.8b). Similarly for EDH-SA system, grinding-induced eutectic showed comparatively lower water uptake (76%) than heat-induced eutectic (80%), but retained more water (23% vs. 4%) at the end of the experiment (Figure 6.9). The hygroscopic stability behavior of the eutectics in the DVS experiments is in line with the trend observed in accelerated stability testing conditions: (i) EDH being the most hygroscopic material, (ii) fumaric acid eutectics exhibiting greater hygroscopic stability than succinic acid eutectics as well as EDH and (iii) grinding-induced eutectics showing comparatively less water uptake than heat-induced eutectics. But, with respect to the desorption behavior in the DVS experiments, the heat-induced eutectics showed lesser water retention upon desorption than the grinding-induced eutectics, although they adsorbed more water at 90% RH (Figures 6.8 & 6.9). They were expected to be less prone to desorption and this behavior further demonstrates the differences in the domain organization of heat-induced and grinding-induced eutectics. In all, both fumaric acid and succinic acid eutectics (whether grinding-induced or heat-induced) displayed greater hygroscopic stability compared to EDH in the tested conditions. Importantly, the obtained results were in line with the proposition of stability advantage of eutectics and further demonstrated the utility of eutectics as novel solid

forms in solving stability problems of APIs. The potential of these eutectics as candidates for future anti-TB FDC formulations containing Ethambutol needs to be established by testing these eutectics in presence of other drugs of the FDC formulation.

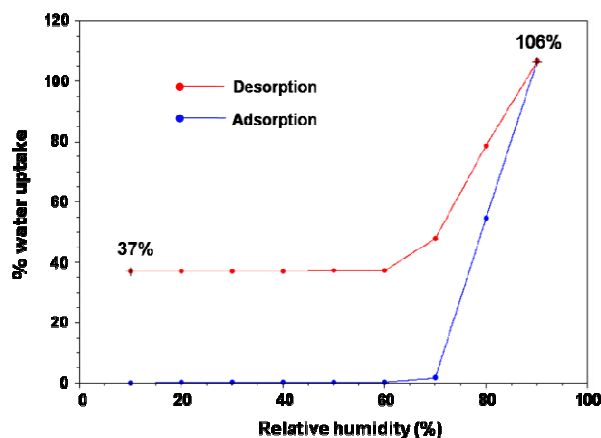


Figure 6.7 DVS gravimetry of ethambutol dihydrochloride shows 106% water uptake at 90% RH and 37% water retention after desorption.

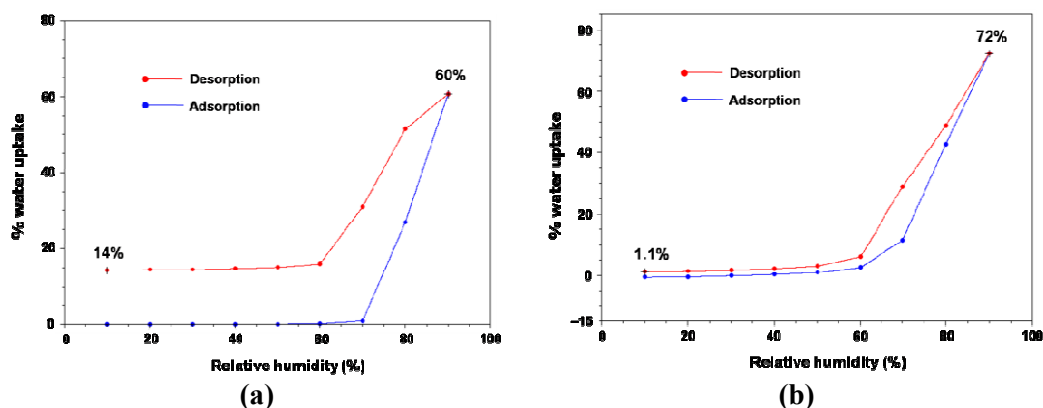


Figure 6.8 DVS gravimetry of (a) EDH-FA-G and (b) EDH-FA-M eutectics showing higher water uptake but lesser retention in the latter compared to the former.

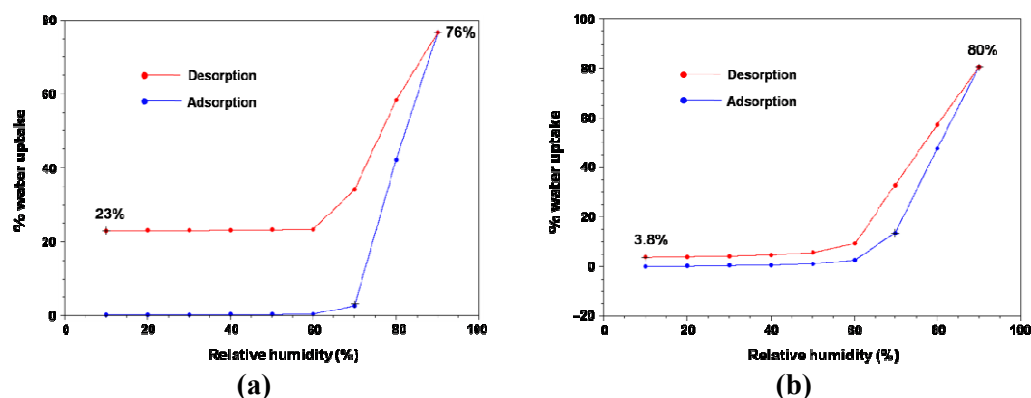


Figure 6.9 DVS gravimetry of (a) EDH-SA-G and (b) EDH-SA-M eutectics showing higher water uptake but lesser retention in the latter compared to the former.

6.5 Conclusions

In this study, dicarboxylic acid eutectics of ethambutol dihydrochloride, the marketed form of ethambutol drug, were obtained through co-grinding and co-melting techniques. In an analogy to cocrystals, this study was carried out on three propositions viz. (i) design aspect for eutectics or deliberate formation of eutectics, (ii) translating properties of a material to its eutectic and (iii) stability advantage of eutectics, and results are favorable. As per the understanding that materials with stronger adhesive (hetero) interactions can form cocrystals and those having stronger cohesive (homo) interactions can result in eutectics (discussed in Chapters 1 and 5), getting eutectics of EDH in this work is no surprise. The lack of potent functionalities in EDH that can break the strong acid homo dimer of carboxylic acids (FA/SA/TA) and the imbalance between donors and acceptors, understandably, minimized the possibility of heteromolecular interactions between the components and thus resulted in eutectics. It is not out of place to draw similarity between eutectics and ionic liquids (IL – salt with melting point less than 100 °C)^{20b,c,27} since both of them have a common feature of low melting point. The reasons of molecular asymmetry, charge delocalization and lack of strong heteromolecular interactions between the components to result in ILs^{20b,c,27} are more or less true for deep eutectic solvents (DESs),²⁸ a sub-category of eutectics, and happens to be the case for eutectics too. Also, supercooling or glass formation generally observed in ILs²⁰ is also found in one of the eutectics of this work.

A correlation between the melting point of the eutectic and its hygroscopic stability is also observed with high melting eutectics showing greater stability to hygroscopicity. The non-hygroscopic and high melting fumaric acid imparted its properties to the eutectics. The EDH–FA eutectics have higher melting points and exhibited less hygroscopicity than EDH and other eutectics in the accelerated stability testing conditions as well as DVS experiments. In the current scenario of rising MDR-TB,¹ new formulations with superior properties are the need of the hour. Thus, the EDH–FA eutectics become potential candidates for future anti-TB FDC formulations. In chapter 5, the solubility/dissolution advantage of eutectics was demonstrated and in this work the stability advantage was shown. Thus, the prime issues of solubility/dissolution and stability in drug research and development²⁹ were addressed through eutectics. In all, eutectics were established to be novel/alternate solid forms of APIs that deem to be explored to modulate physico-chemical properties of the drugs.

On the other hand, with the exception of melting point, eutectics cannot be characterized by routine analytical techniques of diffraction and spectroscopy used to characterize other multi-component crystalline solids (salts, cocrystals, complexes etc). This is because the inclusion of minor component happens substitutionally or interstitially in the major component thereby the lattice (domain) structure of each of the solid solutions in the eutectic material remains largely unaffected²¹ (Scheme 6.2). As a result, there will be no significant change in the diffraction and spectroscopic patterns of the eutectic compared to a physical mixture. Nevertheless, slight changes in these patterns can be characteristic of eutectics but this need to be established through statistical analysis on ample number of materials. Of late, the atomic pair distribution function (PDF) analysis, based on scattering and diffraction phenomena, which is known to appraise the local structure of crystalline and amorphous materials, has been proposed to be useful in understanding the eutectic microstructure.^{9f,30} Overall, the techniques for the characterization of eutectics need to be strengthened.

A descending trend in eutectic melting from physical mixture to ground mixture to melt was observed in this study and is consistent with the increase in the intimate contact area²⁵ from physical mixture to ground mixture to melt-crystallized material. As such, slight differences in the diffraction and spectroscopic patterns between grinding-induced and heat-induced eutectics of EDH were observed, which indicate differences in their domain organization. Also, these eutectics exhibited variations in their hygroscopic nature (in accelerated stability testing conditions) and desorption behavior (water retention in DVS experiments) which further demonstrates some kind of polymorphic behavior in them. But, as eutectic microstructure is poorly understood in organic materials, it is too hasty to arrive at polymorphism³¹ in eutectics. The current challenge is to dissect the organic eutectic materials into solid solutions and assess their domain structure as established for inorganic materials. Whether polymorphism in eutectics/solid solutions is probable or not will be a question for future studies.

6.6 Experimental Section

Materials and Methods: Ethambutol dihydrochloride (Lot#090M0189V) was purchased from Sigma Aldrich and used without further purification. All other chemicals were of analytical or chromatographic grade. Water purified from a deionizer cum mixed bed purification system was used for experiments.

Ethambutol dihydrochloride (C₁₀H₂₆Cl₂N₂O₂):

¹H NMR (DMSO-d₆): δ 0.92 (3H, t, *J* 8), 1.68 (2H, m), 3.06 (1H, m), 3.71 (2H, m), 5.40 (1H, s), 9.29 (2H, d, *J* 80 (N–H coupling)). Protons of –CH₂ group (attached to –NH₂⁺ group) merged with dissolved water peak of DMSO-d₆.

¹³C NMR (DMSO-d₆): δ 10.24, 20.78, 41.27, 57.99, 60.74.

Preparation of Eutectics

Co-grinding: EDH and diacid were taken in an equimolar ratio and subjected to neat grinding using a mortar-pestle for 15 min.

Co-melting: Co-ground mixtures were taken in a sublimation tube and heated in an oil/salt bath beyond 10 °C of their observed melting point in the DSC. The tube was held until a uniform liquid with no trace of solid material is formed and then kept aside for ambient cooling.

EDH–FA (C₁₄H₃₀N₂O₆): Both the eutectics obtained upon co-grinding and co-melting showed identical solution NMR spectra.

¹H NMR (DMSO-d₆): δ 0.90 (3H, t, *J* 8), 1.65 (2H, m), 3.10 (1H, m), 3.64 (2H, m), 5.40 (1H, s), 6.61 (1H, s), 9.27 (2H, s, *br*). Protons of –CH₂ group (attached to –NH₂⁺ group of EDH) merged with dissolved water peak of DMSO-d₆ and of carboxylic acid (FA) exchange in solvent.

¹³C NMR (DMSO-d₆): δ 10.22, 20.76, 41.25, 57.95, 60.72, 134.43, 166.40.

EDH–SA (C₁₄H₃₂N₂O₆): Both the eutectics obtained upon co-grinding and co-melting showed identical solution NMR spectra.

¹H NMR (DMSO-d₆): δ 0.90 (3H, t, *J* 8), 1.66 (2H, m), 2.39 (2H, s), 3.06 (1H, m), 3.65 (2H, m), 5.40 (1H, s), 9.28 (2H, s, *br*). Protons of –CH₂ group (attached to –NH₂⁺ group of EDH) merged with dissolved water peak of DMSO-d₆ and of carboxylic acid (SA) exchange in solvent.

¹³C NMR (DMSO-d₆): δ 10.22, 20.76, 29.23, 41.23, 57.93, 60.71, 174.05.

EDH–TA (C₁₄H₃₂N₂O₈): Both the eutectics obtained upon co-grinding and co-melting showed identical solution NMR spectra.

¹H NMR (DMSO-d₆): δ 0.92 (3H, t, *J* 8), 1.66 (2H, m), 3.07 (1H, m), 3.64 (2H, m), 4.30 (1H, s), 5.39 (1H, s), 9.10 (2H, s, *br*). Protons of –CH₂ group (attached to –NH₂⁺ group of EDH) merged with dissolved water peak of DMSO-d₆ and of carboxylic acid and hydroxyl groups (TA) exchange in solvent.

^{13}C NMR (DMSO- d_6): δ 10.21, 20.76, 41.26, 57.97, 60.76, 72.59, 173.54.

Powder X-ray Diffraction: PXRD were recorded on Bruker D8 Advance diffractometer using Cu-K α X-radiation ($\lambda = 1.5406 \text{ \AA}$) at 40 kV and 30 mA. Diffraction patterns were collected over 2θ range of $5\text{--}50^\circ$ at scan rate of 1° min^{-1} . Powder Cell 2.4 was used to plot the diffraction patterns.

NMR Spectroscopy: Solution and solid state NMR spectra were recorded on a Bruker Avance spectrometer at 400 MHz. SS-NMR spectra were recorded on a Bruker 4 mm double resonance CP-MAS probe in zirconia rotors at 5.0 kHz with a cross-polarization contact time of 2.5 ms and a recycle delay of 8 s. ^{13}C CP-MAS spectra were recorded at 100 MHz and referenced to the methylene carbon of glycine, and then the chemical shifts were recalibrated to the TMS scale ($\delta_{\text{glycine}} = 43.3 \text{ ppm}$). The identity and stoichiometry of the components in the eutectics was established through solution ^1H NMR integration and ^{13}C NMR spectra.

Thermal analysis: DSC was performed on a Mettler Toledo DSC 1 module calibrated with indium ($T_m = 156.60^\circ\text{C}$; $\Delta H_f = 28.45 \text{ J g}^{-1}$) and zinc ($T_m = 419.50^\circ\text{C}$; $\Delta H_f = 107.50 \text{ J g}^{-1}$) as per the manufacturer's specifications. TGA was performed on a Mettler Toledo TGA/SDTA 851e module calibrated with indium ($T_m = 156.60^\circ\text{C}$) and aluminium ($T_m = 660.30^\circ\text{C}$). The typical sample size is 3–5 mg for DSC and 6–8 mg for TGA and the temperature range used is $30\text{--}250^\circ\text{C}$ at 5°C min^{-1} . Samples were placed in crimped but vented aluminium pans for DSC and open alumina pans for TGA and were purged by a stream of dry nitrogen flowing at 50 mL min^{-1} .

Karl Fischer (KF) titration: Water content of the samples was determined using a Spectralab volumetric MA 101 C Karl Fischer titrator with KF reagent (single solution) as the titrant and anhydrous methanol as the solvent. About 50 mg of each sample was taken for analysis.

Hygroscopic stability testing

Accelerated stability testing: About 200 mg of each of the compounds were placed in a glass petri dish and stored without a lid in a Thermolab T-908 stability chamber pre-maintained at 40°C and 75% RH (as per the WHO/ICH guidelines)²⁶ for 2 months. Percentage water uptake of the samples was assessed periodically at 15, 30 and 60 days by TGA and KF titration. The integrity of the samples was established by NMR and PXRD (wherever possible) before and after the study.

Dynamic Vapor Sorption (DVS) study: DVS measurements were performed on a TA Vapor Sorption Analyzer (Model - Q5000SA) at 40 °C. About 5 mg of the sample was placed in a metallic-quartz sample pan and subjected to relative humidity (RH) flux from 10 to 90% and back to 10% RH with a step size of 10% RH. A dwell time of 60 min was used when % weight change is > 0.1% for adsorption/desorption in the particular RH.

6.7 References

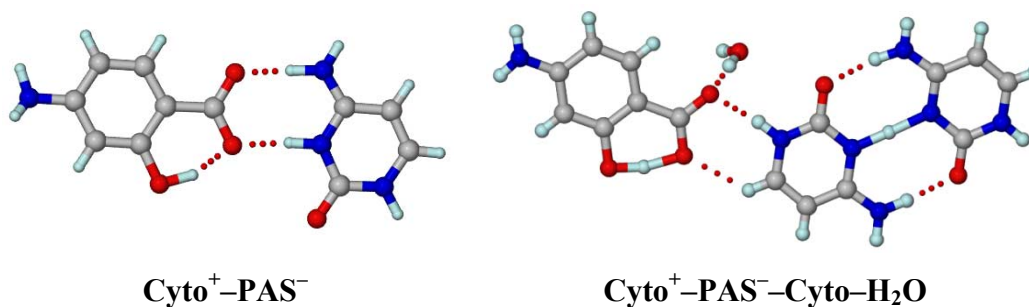
1. <http://www.who.int/mediacentre/factsheets/fs104/en/>.
2. (a) P. Andersen and T. M. Doherty, *Nat. Rev. Microbiol.*, 2005, **3**, 656; (b) Y. Hiraishi, S. Nandakumar, S.-O. Choi, J. W. Lee, Y.-C. Kim, J. E. Posey, S. B. Sable and M. R. Prausnitz, *Vaccine*, 2011, **29**, 2626.
3. http://whqlibdoc.who.int/publications/2010/9789241547833_eng.pdf.
4. M. D. Iseman, *New Engl. J. Med.*, 1993, **329**, 784.
5. (a) R. Laing, H. Vrakking and B. Fourie, *Int. J. Tuberc. Lung Dis.*, 2004, **8**, 1043; (b) S. Singh, H. Bhutani and T. T. Mariappan, *Ind. J. Tuberc.*, 2006, **53**, 201; (c) K. F. Laserson, A. S. Kenyon, T. A. Kenyon, T. Layloff and N. J. Binkin, *Int. J. Tuberc. Lung Dis.*, 2001, **5**, 448.
6. H. Bhutani, S. Singh and K. C. Jindal, *Pharm. Dev. Tech.*, 2005, **10**, 517.
7. (a) H. Bhutani, S. Singh, K. C. Jindal and A. K. Chakraborti, *J. Pharm. Biomed. Anal.*, 2005, **39**, 892; (b) S. Singh and B. Mohan, *Int. J. Tuberc. Lung Dis.*, 2003, **7**, 298.
8. <http://apps.who.int/prequal/whopar/whoparproducts/TB168Part6v1.pdf>.
9. (a) N. Schultheiss and A. Newman, *Cryst. Growth Des.*, 2009, **9**, 2950; (b) N. Shan and M. J. Zaworotko, *Drug Discov. Today*, 2008, **13**, 440; (c) J. A. Rogers, *WO Pat.*, 2008/073324 A1, 2008; (d) A. Górniak, A. Wojakowska, B. Karolewicz and J. Pluta, *J. Ther. Anal. Calorim.*, 2011, **104**, 1195; (e) S. Cherukuvada and A. Nangia, *CrystEngComm*, 2012, **14**, 2579; (f) M. D. Moore and P. L. D. Wildfong, *J. Pharm. Innov.*, 2009, **4**, 36.
10. New definition: discussed in Chapter 1.
11. A. I. Kitaigorodski, *Mixed Crystals*, Springer: Berlin, **1984**, 275.
12. (a) A. Sharma and C. P. Jain, *Int. J. Drug Deliv.*, 2011, **3**, 149; (b) S. R. Vippagunta, Z. Wang, S. Hornung and S. L. Krill, *J. Pharm. Sci.*, 2007, **96**, 294.
13. <http://www.fda.gov/Food/FoodIngredientsPackaging/ucm115326.htm>.

14. C. Peng, M. N. Chan and C. K. Chan, *Environ. Sci. Technol.*, 2001, **35**, 4495.
15. Cambridge Structural Database, ver. 5.33, ConQuest 1.14, November 2011 release, May 2012 update; www.ccdc.cam.ac.uk.
16. M. Viertelhaus, R. Hilfiker and F. Blatter, *Cryst. Growth Des.*, 2009, **9**, 2220.
17. (a) D. J. Good and N. Rodríguez-Hornedo, *Cryst. Growth Des.*, 2009, **9**, 2252; (b) C. B. Aakeröy, S. Forbes and J. Desper, *J. Am. Chem. Soc.*, 2009, **132**, 17048.
18. (a) A. V. Trask and W. Jones, *Top. Curr. Chem.*, 2005, **254**, 41; (b) N. Shan, F. Toda and W. Jones, *Chem. Commun.*, 2002, 2372.
19. P. W. Scott, A. C. Williams and B. W. Barry, *J. Contr. Rel.*, 1998, **50**, 297.
20. J. G. Huddleston, A. E. Visser, W. M. Riechert, H. D. Willauer, G. A. Broker and R. D. Rogers, *Green Chem.*, 2001, **3**, 156; (b) E. W. Castner, Jr., J. F. Wishart, *J. Chem. Phys.*, 2010, **132**, 120901; (c) P. M. Dean, J. Turanjanin, M. Y.-Fujita, D. R. MacFarlane and J. L. Scott, *Cryst. Growth Des.*, 2009, **9**, 1137.
21. D. R. Askeland and P. P. Fulay, *Essentials of Materials Science and Engineering*, 2nd ed., Cengage Learning, 2009.
22. (a) S. S. Das, N. P. Singh, T. Agrawal, P. Gupta, S. N. Tiwari and N. B. Singh, *Mol. Cryst. Liq. Cryst.*, 2009, **501**, 107; (b) N. B. Singh, S. S. Das, N. P. Singh and T. Agrawal, *J. Cryst. Growth*, 2008, **310**, 2878. (c) N. B. Singh and P. Kumar, *J. Chem. Eng. Data*, 1989, **34**, 145.
23. S. B. Murdande, M. J. Pikal, R. M. Shanker and R. H. Bogner, *J. Pharm. Sci.*, 2010, **99**, 1254.
24. J. M. Rubin-Preminger, J. Bernstein, R. K. Harris, I. R. Evans and P. Y. Ghi, *Cryst. Growth & Des.*, 2004, **4**, 431.
25. M. Bi, S. -J. Hwang and K. R. Morris, *Ther. Acta*, 2003, **404**, 213.
26. http://www.ich.org/fileadmin/Public_Web_Site/ICH_Products/Guidelines/Quality/Q1F/Stability_Guideline_WHO.pdf.
27. (a) K. Bica and R. D. Rogers, *Chem. Commun.*, 2010, **46**, 1215; (b) J. Stoimenovski, D. R. McFarlane, K. Bica and R. D. Rogers, *Pharm. Res.*, 2010, **27**, 521. (c) S. Cherukuvada and A. Nangia, *CrystEngComm*, 2012, DOI: 10.1039/c2ce25842k.
28. (a) A. P. Abbott, D. Boothby, G. Capper, D. L. Davies and R. K. Rasheed, *J. Am. Chem. Soc.*, 2004, **126**, 9142; (b) Z. Maugeri and P. D. de María, *RSC Adv.*, 2012, **2**, 421.

29. (a) A. M. Thayer, *Chem. Eng. News*, 2010, **88**, 13; (b) Y. Qiu; Y. Chen and G. Z. Zhang, Eds., *Developing Solid Oral Dosage Forms. Pharmaceutical Theory and Practice*, Academic Press, New York, 2009; (c) *Handbook of Pharmaceutical Salts, Properties, Selection and Use*, ed. P. H. Stahl and C. G. Wermuth, Wiley-VCH, 2002.
30. (a) T. Proffen, K. L. Page, S. E. McLain, B. Clausen, T. W. Darling, J. A. TenCate, S. -Y. Lee and E. Ustundag, *Z. Kristallogr.*, 2005, **220**, 1002; (b) V. Petkov, M. Gateshki, J. Choi, E. G. Gillan and Y. Ren, *J. Mater. Chem.*, 2005, **15**, 4654.
31. (a) J. Bernstein, *Polymorphism in Molecular Crystals*; Clarendon, Oxford, U. K., 2002. (f) S. Aitipamula and A. Nangia, In *Supramolecular Chemistry: From Molecules to Nanomaterials*, P. A. Gale and J. W. Steed, Eds., John Wiley & Sons Ltd, West Sussex, U. K., 2012, pp. 2957–2974.

CHAPTER SEVEN

4-AMINOSALICYLIC ACID ADDUCTS



Solution crystallization of p-aminosalicylic acid (PAS) and cytosine (Cyto) in 1:1 ratio resulted in two different stoichiometry adducts viz. a 1:1 salt ($\text{Cyto}^+ - \text{PAS}^-$) and a 1:1:1:1 salt cocystal hydrate ($\text{Cyto}^+ - \text{PAS}^- - \text{Cyto} - \text{H}_2\text{O}$). Carboxylate–aminopyrimidinium synthon is present in the former and carboxylate–pyrimidinium and cytosinium–cytosine in the latter.

7.1 Introduction

4-aminosalicylic acid, commonly known as *p*-aminosalicylic acid (abbreviated as PAS, Figure 7.1), is a second-line drug used in the treatment of multi-drug-resistant tuberculosis (MDR-TB)¹ and is on the WHO Model List of Essential Medicines.² It was also found to be effective towards ulcerative colitis³ and Crohn's disease,⁴ the potent drug being its isomer 5-aminosalicylic acid^{4,5} (5-ASA or Mesalazine, Figure 7.1). Both these aminosalicylic acids are amphoteric compounds and have no polymorphs so far. But, interestingly one exists in an unionized state (PAS: 4-NH₂C₆H₃(OH)COOH) and the other as a zwitterion/inner salt (5-ASA: 5-NH₃⁺C₆H₃(OH)COO⁻) in the solid state⁶ (Figure 7.1). In buffer solutions, PAS is found to exist as different ionic species (a) as a diprotic acid (NH₃⁺C₆H₃(OH)COOH) below its pK_{a1} (=1.79), (b) as a zwitterion (NH₃⁺C₆H₃(OH)COO⁻) at its isoelectric point (pI = 2.71) and (c) as a diprotic base (NH₂C₆H₃(OH)COO⁻) above its pK_{a2} (=3.63).⁷ PAS is found to decarboxylate to 3-aminophenol (NH₂C₆H₄OH) through the zwitterionic state⁷ and also upon melting.⁸ About 13-25% of PAS is estimated to decompose in the pH range 1.3-4.2 in 24 h with the highest percentage of decomposition at its isoelectric point.⁷ PAS is being used since 1940s,¹ but there is no study on the control of its decomposition in aqueous media. In the recent past, drug-drug cocrystals with Pyrazinamide, Isoniazid⁹ and Sulfadimidine¹⁰ were reported which can have applications in multi-drug therapy. An amorphous form,¹¹ several salts (sodium^{8b}, potassium, hydrochloride, sulfate, mesylate, ammonium etc.),¹² molecular salts¹³ (piperazinium, morpholinium) and a dioxane solvate¹⁴ of PAS were also reported by different groups, and among these ammonium salt is polymorphic.¹⁵ However, crystal structures of many of these salts are not reported. In this study, X-ray crystal structures of sodium dihydrate, sulfate and mesylate salts were determined. In addition, a salt and a salt cocrystal with cytosine and a nicotinamide cocrystal were newly obtained upon solid form screening and their crystal structures were determined.

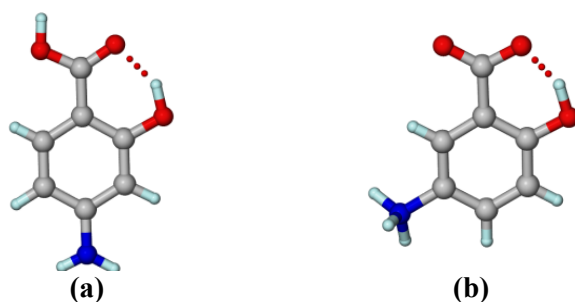


Figure 7.1 (a) 4-aminosalicylic acid exists in an unionized form and (b) 5-aminosalicylic acid exists as zwitterion in the solid state.

7.2 Crystal Structures of the Adducts

PAS of its rich functionalities (carboxylic acid, amine and phenol) can form a multitude of adducts¹⁶ with various coformers depending on the pK_a differences¹⁷ and thus becomes a model compound of study. The same solid form screening experiments can result in the crystallization of its zwitterionic form or a new polymorph, which can be important as a novel form.¹⁸ Two cytosine adducts (a salt CYT^+-PAS^- and a salt cocrystal hydrate $CYT^+-PAS^--CYT-H_2O$) and a nicotinamide cocrystal hydrate ($PAS-NAM-H_2O$) were obtained in this work. Further, the reported sodium dihydrate,^{8b} sulfate and mesylate salts¹² were reproduced, of which the anhydrate of sodium salt was newly isolated. Attempts to obtain zwitterionic form and polymorphs of PAS by different screening methods such as evaporative crystallization (in various solvents and different temperatures), sublimation,¹⁹ crystallization from aqueous HCl solutions of different pH and metathesis reactions using its adducts were unsuccessful. All the crystallization experiments are detailed in Experimental Section.

Sodium-4-Aminosalicylate dihydrate ($Na^+-PAS^--2H_2O$): When PAS was dissolved in NaOH solution and left for ambient crystallization, the salt dihydrate was obtained in the space group $P2_1/c$. X-ray crystallographic parameters are listed in Table 7.1 and hydrogen bonds in Table 7.2. It is a coordination compound wherein sodium (Na^I) is six-coordinated in a twisted-octahedral geometry. The six liganding positions are occupied by three PAS molecules (through COO^- , OH, NH_2 groups), one crystallographic unique water molecule and two waters which are also shared by neighbouring Na^I atom (Figure 7.2a). Na^I atoms form a tape with PAS and water molecules and connect to adjacent tapes through channel waters along the a -axis (Figure 7.2b).

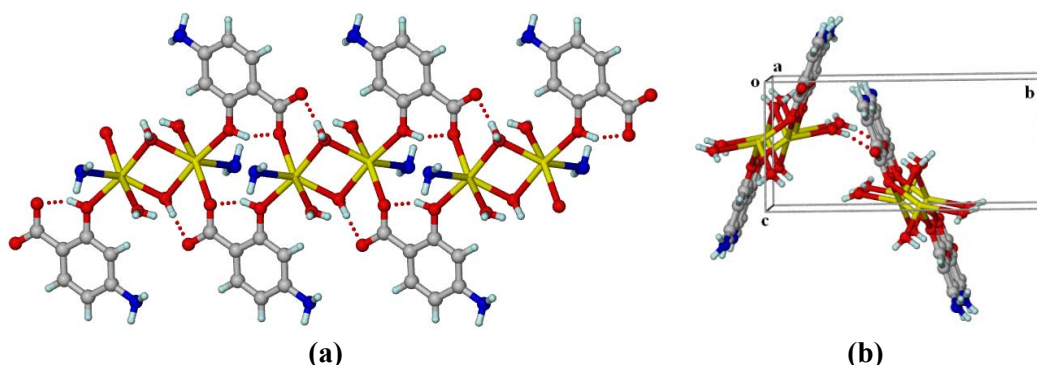


Figure 7.2 (a) Six-coordinated sodium forms a tape with PAS and water molecules. (b) Adjacent tapes connected by channel waters along the a -axis make an angle of 33.7° with each other.

Table 7.1 Crystallographic parameters.

Adduct	Na ⁺ –PAS [−] –2H ₂ O	2PAS ⁺ –SO ₄ ^{2−}	PAS ⁺ –CH ₃ SO ₃ [−]	Cyto ⁺ –PAS [−]	Cyto ⁺ –PAS [−] –Cyto–H ₂ O	PAS–NAM–H ₂ O
empirical formula	C ₇ H ₁₀ NNaO ₅	C ₁₄ H ₁₆ N ₂ O ₁₀ S	C ₈ H ₁₁ NO ₆ S	C ₁₁ H ₁₂ N ₄ O ₄	C ₁₅ H ₁₉ N ₇ O ₆	C ₁₃ H ₁₅ N ₃ O ₅
formula weight	211.15	404.35	249.24	264.25	393.37	293.28
crystal system	monoclinic	orthorhombic	monoclinic	monoclinic	monoclinic	triclinic
space group	<i>P</i> 2 ₁ / <i>c</i>	<i>Pba</i> 2	<i>P</i> 2 ₁ / <i>c</i>	<i>P</i> 2 ₁ / <i>c</i>	<i>P</i> 2 ₁ / <i>n</i>	<i>P</i> $\bar{1}$
<i>Z</i> *	16	12	8	16	16	6
<i>T</i> /K	298(2)	298(2)	298(2)	100(2)	298(2)	100(2)
<i>a</i> /Å	8.790(4)	15.7940(16)	5.3525(5)	12.6069(17)	7.4285(6)	6.750(2)
<i>b</i> /Å	14.615(7)	19.897(2)	17.8159(12)	13.6925(18)	22.0769(18)	7.060(2)
<i>c</i> /Å	6.955(3)	5.5179(6)	11.0537(10)	14.595(2)	10.9219(10)	14.809(4)
α /°	90	90	90	90	90	95.977(4)
β /°	97.799(8)	90	99.057(8)	110.973(3)	101.461(9)	97.899(5)
γ /°	90	90	90	90	90	104.722(4)
<i>V</i> /Å ³	885.3(8)	1734.0(3)	1040.93(15)	2352.5(5)	1755.5(3)	668.9(3)
<i>D</i> _{calc} /g cm ^{−3}	1.584	1.549	1.590	1.492	1.488	1.456
μ /mm ^{−1}	0.174	0.246	0.325	0.116	0.118	0.114
reflns collected	9005	3402	4343	24058	6349	5351
unique reflns	1749	3402	2132	4667	2992	2206
observed reflns	1558	3244	1420	3233	1367	1653
<i>R</i> ₁ [<i>I</i> > 2σ(<i>I</i>)]	0.0434	0.0443	0.0426	0.0856	0.0517	0.0400
<i>wR</i> ₂ [all]	0.1015	0.1110	0.0982	0.1405	0.0664	0.0967
goodness-of-fit	1.103	1.135	0.968	1.142	0.851	1.040
diffractometer	Bruker Smart-Apex	Bruker Smart-Apex	Oxford Xcalibur Gemini	Bruker Smart-Apex	Oxford Xcalibur Gemini	Bruker Smart-Apex

* *Z* = *Z*' (no. of crystallographically non-equivalent molecules of any type in the asymmetric unit)²⁰ × no. of independent general positions of the space group.

Table 7.2 Hydrogen bonds in crystal structures of the adducts.

Interaction	H...A/Å	D...A/Å	∠D-H...A/°	Symmetry code
Na⁺-PAS⁻-2H₂O				
O4-H4A...O2	2.12(3)	2.895(2)	163(3)	x, y, 1+z
O4-H4B...O2	1.82(3)	2.745(2)	178(3)	1-x, -y, 1-z
O3-H3...O1	1.69(4)	2.526(2)	156(3)	^a
O5-H5A...O2	2.49(4)	3.137(3)	146(4)	^b
O5-H5B...O2	2.06(4)	2.937(3)	176(3)	x, 1/2-y, 1/2+z
N1-H1A...O5	2.43(3)	3.234(4)	157(2)	1+x, 1/2-y, -1/2+z
2PAS⁺-SO₄²⁻				
O1-H1...O7	1.58(4)	2.578(3)	158(4)	^b
O4-H4A...O10	1.72(4)	2.619(3)	170(4)	^b
O3-H3...O1	1.68(4)	2.605(4)	136(3)	^a
O6-H6A...O5	1.90(5)	2.612(4)	143(4)	^a
N1-H1A...O9	1.85(3)	2.763(4)	174(3)	1/2-x, 1/2+y, z
N1-H1A...O10	2.57(4)	3.067(4)	115(3)	1/2-x, 1/2+y, z
N1-H1B...O5	1.96(3)	2.833(4)	162(3)	1/2-x, 1/2+y, z
N1-H3C...O10	1.99(4)	2.838(4)	155(3)	1/2-x, 1/2+y, -1+z
N2-H2A...O8	2.13(5)	2.817(4)	147(5)	1/2-x, 1/2+y, -1+z
N2-H2A...O9	2.56(5)	3.085(4)	126(4)	1/2-x, 1/2+y, z
N2-H2B...O7	1.85(5)	2.810(4)	171(4)	1/2+x, 1/2-y, -1+z
N2-H2C...O9	1.93(4)	2.867(4)	163(4)	1/2+x, 1/2-y, z
C4-H4...O8	2.67	3.364(4)	132	x, y, -1+z
C11-H11...O1	2.62	3.538(4)	169	^b
C14-H14...O3	2.36	3.278(4)	171	x, y, 1+z
PAS⁺-CH₃SO₃⁻				
O1-H1...O6	1.81(4)	2.649(3)	168(4)	1-x, -y, 1-z
O3-H3...O2	1.78(4)	2.595(3)	151(3)	^a
N1-H1A...O5	1.97(3)	2.818(3)	175(2)	^b
N1-H1B...O4	2.25(3)	3.045(3)	151(3)	1+x, y, z
N1-H1B...O5	2.41(3)	3.170(3)	147(3)	1+x, y, z
N1-H1C...O2	2.34(4)	2.764(3)	104(3)	1-x, 1/2+y, 3/2-z
N1-H1C...O4	2.14(4)	3.068(3)	152(3)	1+x, 1/2-y, 1/2+z
N1-H1C...O6	2.59(4)	3.116(3)	113(3)	1+x, 1/2-y, 1/2+z
C4-H4...O6	2.66	3.413(3)	159	^b
C6-H6...O5	2.68	3.568(3)	139	^b
C8-H8C...O3	2.55	3.460(4)	159	-x, 1/2+y, 3/2-z
Cyto⁺-PAS⁻				
O3-H3...O1	1.56(5)	2.497(4)	153(5)	^a
O6-H6A...O4	1.53(5)	2.539(4)	159(5)	^a
N1-H1A...O7	2.37(4)	3.123(5)	148(4)	x, 1/2-y, 1/2+z
N1-H1B...O6	2.45(4)	3.196(5)	136(3)	-x, -1/2+y, 1/2-z
N2-H2A...O8	2.22(5)	3.096(5)	158(4)	1-x, 1/2+y, 1/2-z
N2-H2B...O4	2.52(4)	3.247(5)	142(3)	-x, -1/2+y, 1/2-z
N3-H3A...O2	1.76(4)	2.707(5)	170(4)	^b
N4-H4A...O4	1.75(4)	2.726(4)	174(4)	1+x, -1+y, z
N5-H5A...O5	1.71(5)	2.707(5)	175(4)	1+x, -1+y, z

N5–H5B···O3	2.03(4)	2.895(5)	172(4)	$1+x, y, z$ _b
N6–H5B···O7	2.09(5)	2.862(5)	148(4)	
N7–H7A···O2	1.88(4)	2.801(5)	176(3)	$x, 1/2-y, 1/2+z$
N8–H8A···O1	1.69(5)	2.691(5)	173(4)	$x, 1/2-y, 1/2+z$
N8–H8B···O5	1.83(5)	2.737(5)	172(4)	$x, -1+y, z$
C4–H4···O6	2.45	3.286(5)	146	$-x, -1/2+y, 1/2-z$
C13–H13···O8	2.34	3.170(5)	146	$1-x, 1/2+y, 1/2-z$
C18–H18···O1	2.41	3.307(5)	157	$1-x, 1-y, -z$
C22–H22···N1	2.47	3.240(6)	138	$x, 1/2-y, -1/2+z$
Cyto⁺–PAS[−]–Cyto–H₂O				
O3–H1···O1	1.15(4)	2.482(3)	165(3)	_a
O6–H6A···O3	2.04(3)	2.831(4)	175(4)	_b
O6–H6B···O2	1.94(4)	2.823(4)	177(5)	$1/2+x, 1/2-y, 1/2+z$
N1–H1A···O1	2.28(3)	3.075(4)	150(3)	$-1/2+x, 1/2-y, 1/2+z$
N1–H1B···O3	2.56(2)	3.372(4)	158(3)	$-1+x, y, z$
N2–H2···O2	1.84(3)	2.767(4)	172(2)	$-1/2+x, 1/2-y, 1/2+z$
N3–H3···N6	1.52(4)	2.826(3)	177(3)	$-x, -y, -z$
N4–H4A···O4	2.06(3)	2.908(4)	150(3)	$1+x, y, z$
N4–H4B···O5	1.89(4)	2.841(4)	171(4)	$-x, -y, -z$
N5–H5···O6	1.88(4)	2.770(4)	164(4)	$-1+x, y, z$
N7–H7A···O5	2.17(3)	2.935(4)	149(3)	$1+x, y, z$
N7–H7B···O4	1.88(3)	2.857(4)	168(3)	$-x, -y, -z$
C6–H6···O1	2.55	3.401(4)	152	$-1+x, y, z$
C10–H10···O2	2.51	3.425(4)	170	$1/2+x, 1/2-y, 1/2+z$
C11–H11···O1	2.44	3.125(4)	131	$-1/2+x, 1/2-y, 1/2+z$
C14–H14···O6	2.70	3.582(4)	159	_b
PAS–NAM–H₂O				
O1–H1···N3	1.63(2)	2.6402(19)	177(2)	$1-x, 1-y, -z$
O3–H3···O2	1.69(2)	2.518(2)	156(2)	_a
O5–H5A···O3	2.03(2)	2.825(2)	158(2)	$-1+x, y, z$
O5–H5B···O4	1.99(3)	2.819(2)	178(3)	_b
N1–H1A···O5	2.14(2)	3.027(2)	168(2)	$1-x, 1-y, 1-z$
N1–H1B···O4	2.30(2)	3.042(2)	150(2)	$x, -1+y, z$
N2–H2A···O4	2.03(2)	2.923(2)	172(2)	$1-x, 1-y, 1-z$
N2–H2B···O5	2.00(2)	2.893(2)	158(2)	$x, -1+y, z$
C11–H11···O2	2.44	3.117(2)	128	$1-x, 1-y, -z$
C13–H13···O5	2.70	3.609(2)	161	_b

^a Intramolecular hydrogen bond; ^b Molecules/ions in the same asymmetric unit.

Bis-4-Ammonium salicylic acid sulfate (2PAS⁺–SO₄^{2−}): A 2:1 PAS sulfate salt was crystallized upon slow evaporation of a methanolic solution. The crystal structure was solved by removing vaguely resolved peaks possible of a solvent (detailed in Experimental Section). Each sulfate moiety connects the crystallographic unique PAS molecules through N⁺–H···O[−] and O–H···O bonds which make a zigzag chain (Figure

7.3a) along the *b*-axis. Such chains extend into a corrugated sheet-like structure through auxiliary interactions involving orthogonal oxygens of the sulfate group (Figure 7.3b).

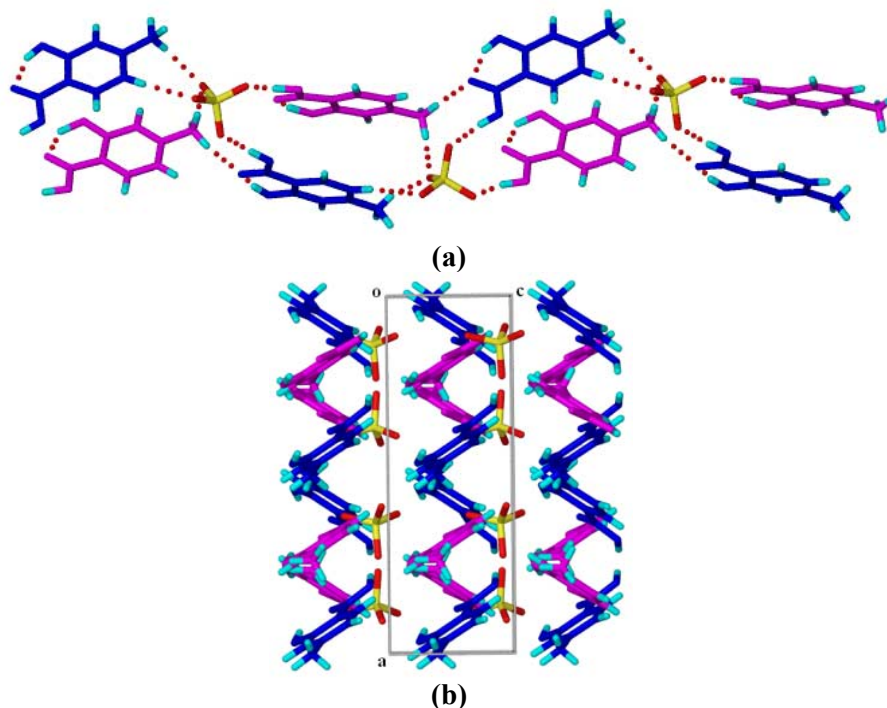


Figure 7.3 (a) Crystallographic unique PAS molecules (shown in different color) make zigzag chains through $\text{N}^+-\text{H}\cdots\text{O}^-$ and $\text{O}-\text{H}\cdots\text{O}$ bonds with sulfate groups. (b) Such chains form corrugated sheets along the *a*-axis.

4-Ammonium salicylic acid mesylate ($\text{PAS}^+-\text{CH}_3\text{SO}_3^-$): A 1:1 PAS mesylate salt was crystallized upon slow evaporation of a methanolic solution. Parallel tapes of $\text{N}^+-\text{H}\cdots\text{O}^-$ bonded PAS molecules are connected by mesylate molecules through $\text{N}^+-\text{H}\cdots\text{O}^-$, $\text{O}-\text{H}\cdots\text{O}$ and $\text{C}-\text{H}\cdots\text{O}$ interactions and extend into sheets (Figure 7.4) parallel to the (102) plane. Such sheets are connected by orthogonal oxygens of the mesylate moieties and lie at an interplanar separation of 3.53 Å.

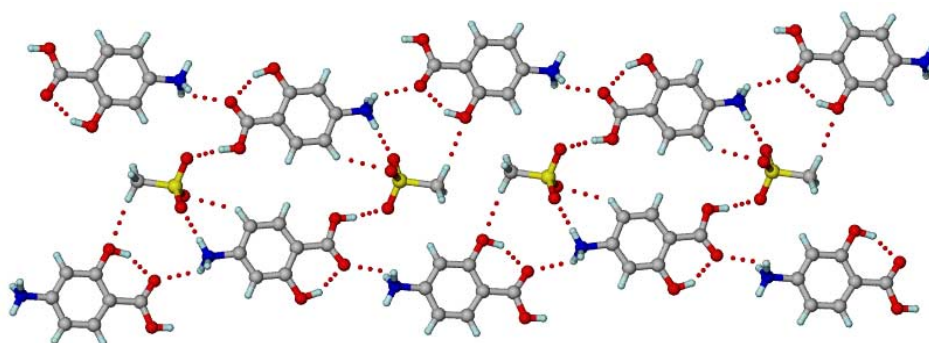


Figure 7.4 Parallel tapes of PAS molecules are connected by mesylate molecules through $\text{N}^+-\text{H}\cdots\text{O}^-$, $\text{O}-\text{H}\cdots\text{O}$ and $\text{C}-\text{H}\cdots\text{O}$ hydrogen bonds and make a sheet structure.

Cytosinium-4-Aminosalicylate (Cyto⁺-PAS⁻): Solution crystallization of PAS and cytosine in 1:1 ratio in methanol resulted in two different stoichiometry adducts viz. a 1:1 salt and a 1:1:1:1 salt cocrystal hydrate from different batches. In the crystal structure of the salt, each of the two symmetry independent PAS and cytosine molecules were present. PAS was found to donate its proton to the pyrimidine N that flanks the amino group of cytosine (Figure 7.5a). Thus, the crystallographic unique PAS anions and cytosinium cations form heterodimers of carboxylate–aminopyrimidinium synthon. These finite heterodimers propagate perpendicular to each other through N–H···O and C–H···O hydrogen bonds and make a maze-like structure in the 3D (Figure 7.5b).

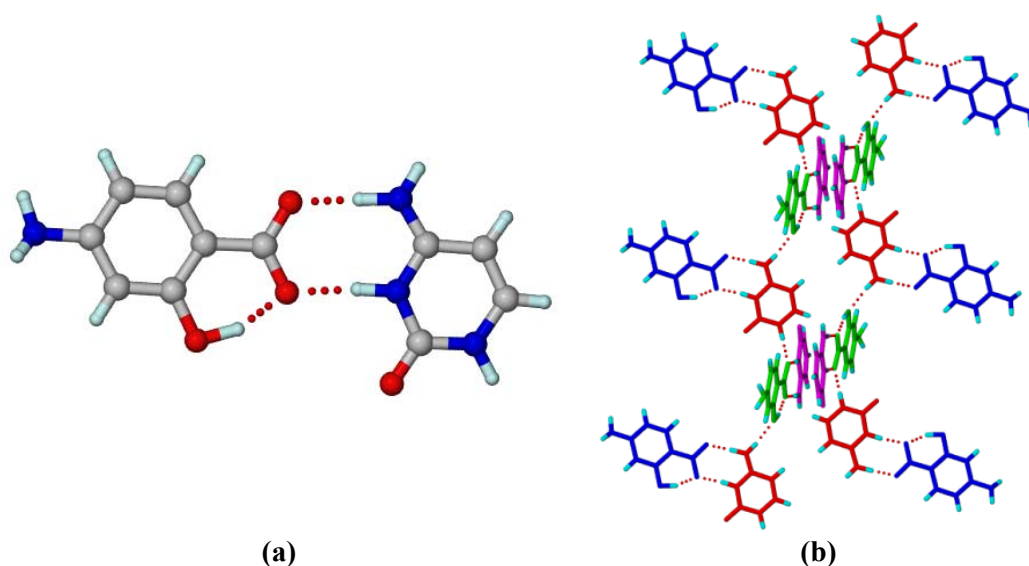


Figure 7.5 (a) Carboxylate–aminopyrimidinium synthon between PAS anion and cytosinium cation in the heterodimer. (b) These finite heterodimers exist between all the symmetry independent PAS and cytosine molecules (shown in different color) and propagate in a perpendicular fashion in the 3D.

Cytosinium-4-Aminosalicylate cytosine hydrate (Cyto⁺-PAS⁻-Cyto-H₂O): Crystal structure of this adduct shows a PAS anion, a cytosinium cation and cytosine and water molecules in the asymmetric unit. Thus, the adduct is a salt cocrystal since cytosine manifested both in unionized and ionized states in the crystal structure. Contrast to the salt structure, PAS anion makes a carboxylate–pyrimidinium synthon (Figure 7.6a) and not the carboxylate–aminopyrimidinium synthon with the cytosinium cation, though the proton was transferred to pyrimidine N that flanks the amino group. The aminopyrimidinium group of the cytosinium cation makes a 3-point synthon with unionized cytosine where the pyrimidinium N–H is shared between the two moieties (N–H distance: cytosinium cation = 1.31(4) Å; unionized cytosine = 1.52(4) Å). The 3-point

synthon flanked by PAS anions propagates into infinite tapes through $C(6)R_4^2(8)$ graph set²¹ pattern (Figure 7.6b). These tapes form a herringbone structure that makes channels for water inclusion parallel to the a -axis (Figure 7.6c). Very recently, Sridhar et al. observed that whenever the cytosine:acid ratio is 2:1, the 3-point cytosinium–cytosine synthon involving the aminopyrimidine group is preferred over the carboxylate–aminopyrimidinium synthon.²²

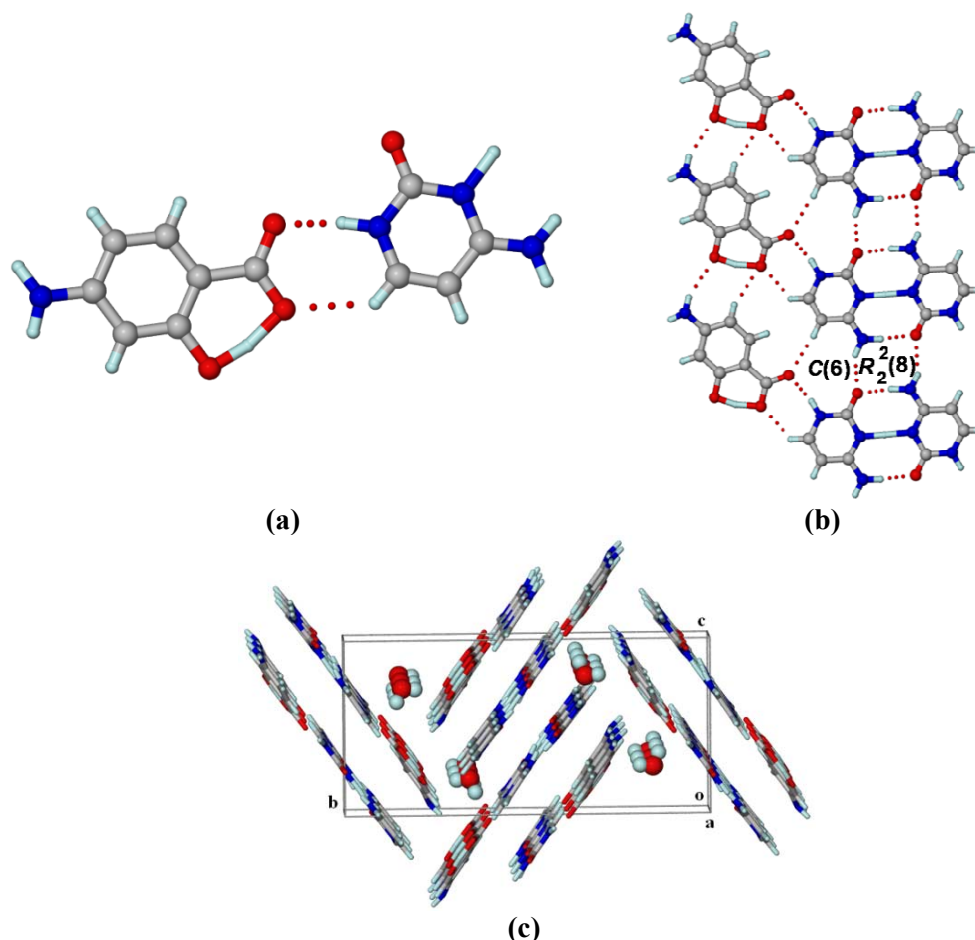


Figure 7.6 (a) Carboxylate–pyrimidinium synthon between PAS anion and cytosinium cation. (b) Cytosinium cation and cytosine are connected by 3-point synthon of N–H···O and N–H···N hydrogen bonds and extend into infinite tapes through $C(6)R_4^2(8)$ motif. (c) The tapes form a herringbone structure which makes water channels along the a -axis.

Generally, grinding technique (neat and/or liquid assisted) is employed to prepare macroscopic amounts of an adduct.²³ The cytosine salt and nicotinamide cocrystal hydrate (discussed next) were reproduced by using the technique, the former by ethanol-assisted and the latter by water-assisted grinding, but the cytosine salt cocrystal was not obtained. The PXRD of the ground material (of PAS and cytosine in 1:2 ratio

subjected to water assisted grinding) did not match with calculated powder pattern from the X-ray crystal structure. It is believed that the crystallization of this salt cocrystal is a kinetic effect. The pK_a difference between cytosine and PAS is less ($\Delta pK_a = 4.4$ (conjugate acid of pyrimidine base of cytosine)²⁴ – 3.63 (PAS carboxylic acid)⁷ = 0.77) and hence both ionized and unionized species can exist in solution to finally result in the crystallization of two different adducts (a salt and a salt cocrystal).

4-Aminosalicylic acid–Nicotinamide hydrate (PAS–NAM–H₂O): Similar to cytosine case, the pK_a difference between nicotinamide and PAS is less ($\Delta pK_a = 4.2$ (conjugate acid of pyridine base of nicotinamide)²⁵ – 3.63 (PAS carboxylic acid)⁷ = 0.57) and hence salt/cocrystal formation cannot be predicted. A 1:1:1 cocrystal hydrate of PAS and nicotinamide was obtained upon crystallization from a methanolic solution. PAS molecules connect the amide dimer nicotinamide molecules through acid–pyridine synthon and extend into zigzag tapes through water molecules (Figure 7.7). Such tapes extend into 2D sheets parallel to the (–211) plane which are separated by an interplanar distance of 3.26 Å. The water molecules form channels along the *a*-axis and connect the sheets through O–H···O hydrogen bonds. The same cocrystal hydrate was obtained upon water-assisted grinding of the components. Neat grinding of PAS and nicotinamide (to avoid water/moisture) did not afford any anhydrous cocrystal as monitored by PXRD. It seems that the adduct does not crystallize without a water of crystallization.

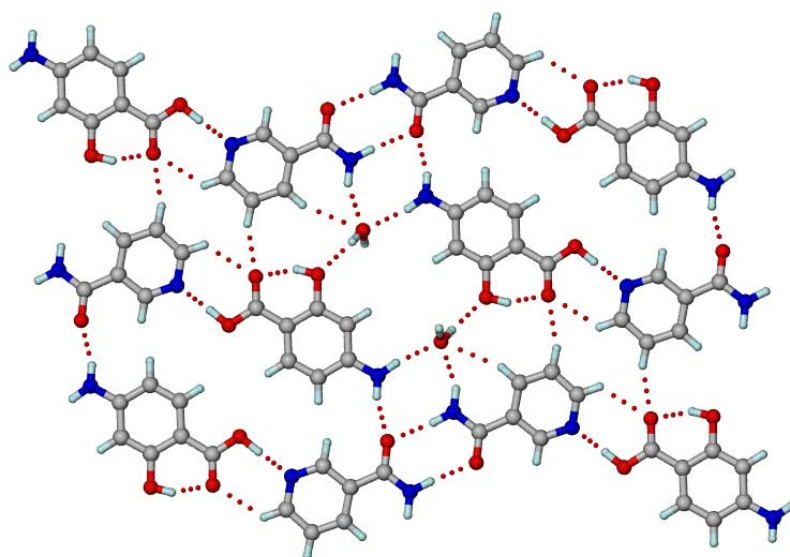


Figure 7.7 Zigzag tapes formed by amide dimer nicotinamide molecules connected through acid–pyridine synthon with PAS molecules extend into a sheet structure through water molecules.

7.3 Thermal analysis of the Adducts

All the adducts except PAS–cytosine salt cocrystal were obtained in bulk quantity and their integrity was confirmed by PXRD match (Figure 7.8). Sodium and sulfate salts were obtained from direct synthesis and nicotinamide cocrystal was prepared through water assisted grinding (detailed in Experimental Section). A solvent of crystallization is manifested in these adducts which is found to be water in sodium and nicotinamide cases but could not assigned in the sulfate case. Thus, the former two adducts may afford anhydrides. To attempt careful dehydration and obtain anhydrous adducts, DSC and TGA of adducts were done to obtain information of water loss upon heating. Nicotinamide cocrystal hydrate did not show any transition pertaining to water loss and melted abruptly (Figure 7.9) and hence cannot yield an anhydrate upon heating. The dihydrate sodium salt showed a transition in the temperature range 80–100 °C, prior to melting endotherm at 193 °C, in the DSC which corresponds to dehydration of the material as the weight loss in TGA in the same temperature range matched with two waters stoichiometry of the crystal structure (calc. 17.06%; obs. 16.43%) (Figure 7.10a). Controlled dehydration of the dihydrate salt at 110 °C for 30 minutes resulted in an anhydrous material as observed by DSC and TGA (Figure 7.10b). Water assisted grinding of the dehydrated salt again resulted in the original dihydrate salt and the hydrate ↔ anhydrate transformation was monitored by PXRD (Figure 7.11). Thus, the PAS-sodium salt was obtained both in hydrate and anhydrate forms in a controlled way.

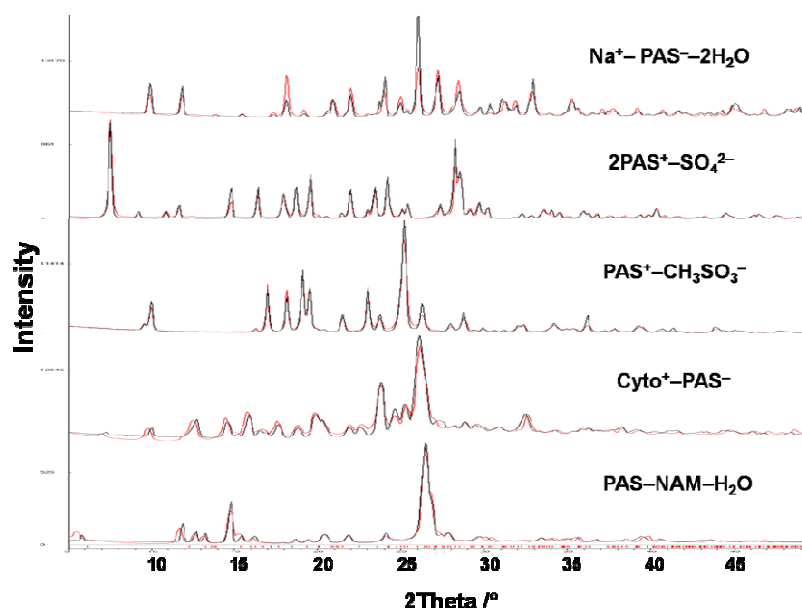


Figure 7.8 Overlay of the calculated lines from X-ray crystal structures (red) and experimental PXRD pattern (black) of PAS adducts show peak-to-peak match.

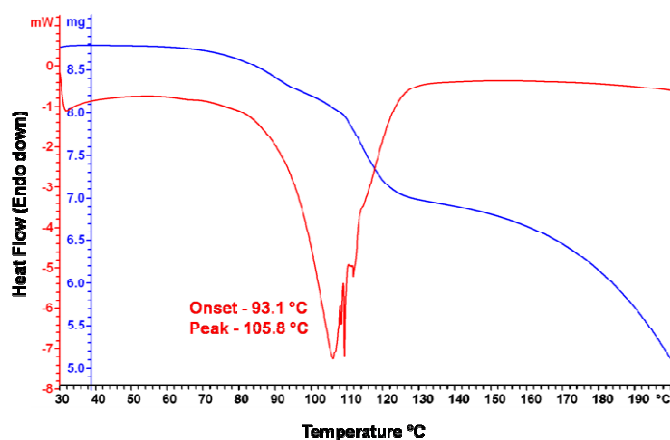


Figure 7.9 DSC (red) and TGA (blue) of PAS-NAM-H₂O.

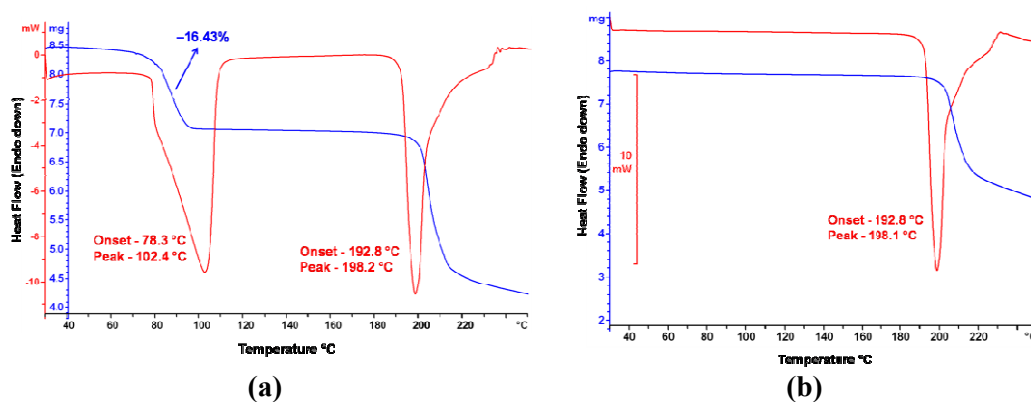


Figure 7.10 DSC (red) and TGA (blue) of (a) Sodium-4-Aminosalicylate dihydrate and (b) its anhydrate. The former shows water loss in the temperature range 80–100 °C before melting and the latter exhibits clean melting at 193 °C.

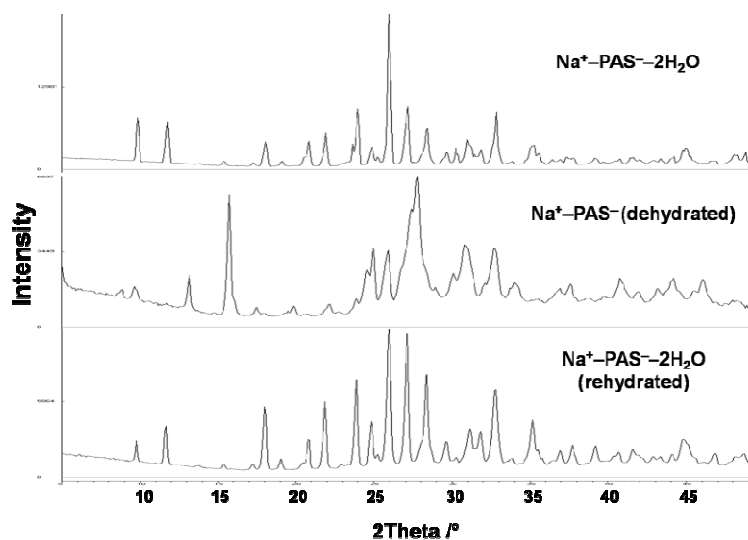


Figure 7.11 PXRD patterns of Sodium-4-Aminosalicylate dihydrate to show formation of an anhydrate upon dehydration and its conversion to the original dihydrate upon rehydration.

7.4 Conclusions

Solid form space of PAS was explored and variable stoichiometry adducts of PAS with cytosine (a salt and a salt cocrystal) and sodium (anhydrate and hydrate salts) were obtained in this study. In addition, a nicotinamide cocrystal hydrate was also obtained and X-ray crystal structures of few known salts were determined. PAS has the tendency to form solvates/hydrates in its adducts as observed in four (including sulfate structure though the solvent could not be resolved) out of six cases studied in this work. PAS-sodium salt was obtained both in hydrate and anhydrate forms in a controlled way. The ambiguity in the prediction of salt/cocrystal for the range $0 < \Delta pK_a < 3^{17}$ is observed in the cases of cytosine and nicotinamide adducts. The manifestation of 2-point (carboxylate–aminopyrimidinium) synthon in the 1:1 cytosine salt and 3-point (cytosinium–cytosine) synthon in the 2:1 cytosine salt cocrystal is in line with the Cambridge Structural Database analysis by Sridhar et al.²² But, only the former was reproducible by grinding technique and not the latter. This example demonstrates the complexity of crystallization phenomenon and warrants more studies to understand and control crystallization outcomes for scale-up purposes. On the other hand, examples of this kind play a crucial role in the ongoing exercise on the classification of multi-component crystalline solids.²⁶

7.5 Experimental Section

Materials and Methods: 4-aminosalicylic acid was purchased from Shanghai Xunxin Chemical Co., Ltd, China, and used without further purification. All other chemicals were of analytical or chromatographic grade. Water purified from a deionizer cum mixed bed purification system was used for experiments.

Synthesis of Adducts

a. Sodium-4-Aminosalicylate dihydrate ($\text{Na}^+ - \text{PAS}^- - 2\text{H}_2\text{O}$): 153 mg (1 mmol) PAS was dissolved in aqueous NaOH (40 mg or 1 mmol in 3 mL) solution and left for slow evaporation at room temperature. Brown colored crystals in plate morphology were formed after a few days.

b. Bis-4-Ammonium salicylic acid sulfate ($2\text{PAS}^+ - \text{SO}_4^{2-}$) and 4-Ammonium salicylic acid mesylate ($\text{PAS}^+ - \text{CH}_3\text{SO}_3^-$): PAS and acid (in 2:1 molar ratio for sulfuric acid and 1:1 for methanesulfonic acid) were separately dissolved in acetone and kept at -20°C for

10 minutes. After incubation, the two solutions were mixed and stirred for 5-10 minutes in an ice cold bath. Salt obtained as a grayish precipitate in solution was filtered on a 2.5 μm Whatman filter paper and washed with acetone and dried. Single crystals of sulfate salt as brownish needles were obtained, when 30 mg of the compound was crystallized from 5 mL warm methanol at room temperature. Similarly, the mesylate salt crystallized as brownish plates.

c. Cytosinium-4-Aminosalicylate ($\text{Cyto}^+ - \text{PAS}^-$) and Cytosinium-4-Aminosalicylate cytosine hydrate ($\text{Cyto}^+ - \text{PAS}^- - \text{Cyto} - \text{H}_2\text{O}$): 30 mg (0.2 mmol) PAS and 22 mg (0.2 mmol) cytosine were dissolved in 6-8 mL warm methanol and left for slow evaporation at room temperature. Two different stoichiometry adducts (1:1 and 2:1) both in brown color but the former in plate morphology and the latter in needle morphology were obtained from different batches.

d. 4-Aminosalicylic acid–Nicotinamide hydrate ($\text{PAS} - \text{NAM} - \text{H}_2\text{O}$): 30 mg (0.2 mmol) PAS and 24 mg (0.2 mmol) nicotinamide were dissolved in 6 mL warm ethanol and left for slow evaporation at room temperature. Brown colored crystals in plate morphology were formed after a few days.

Co-grinding: About 200 mg of the components, combined together as per the stoichiometric ratio in the crystal structure, was ground for 15-20 min using a mortar-pestle. 8-10 drops solvent was added during grinding in case of solvent-assisted grinding. PXRD of the ground material was recorded to confirm complete reaction of starting materials and formation of a new crystalline phase.

Polymorph screening experiments of PAS: PAS was crystallized from aqueous HCl solutions in the pH range 1.2–4.0 i.e. near its pK_a values⁷ with the intent of isolating its zwitterionic form. Also metathesis reaction of $\text{Cyto}^+ - \text{PAS}^-$ salt with PAS hydrochloride salt ($\text{PAS}^+ - \text{Cl}^-$, prepared as per the method by Forbes et al.),¹² was carried out by grinding to induce the crystallization of its zwitterion. Apart from evaporative crystallization in several solvents and sublimation, the above experiments did not result in any polymorph/zwitterion of PAS as monitored by PXRD.

X-ray Crystallography: X-ray reflections for sodium, sulfate and cytosine salts and nicotinamide cocrystal were collected on a Bruker SMART-APEX CCD diffractometer equipped with a graphite monochromator and Mo-K α fine-focus sealed tube ($\lambda = 0.71073 \text{ \AA}$). Data reduction was performed using Bruker SAINT software. Intensities

were corrected for absorption using SADABS. Structures were solved and refined using SHELX-97. The sulfate structure contained vaguely resolved peaks possible of a solvent which were removed by using ‘squeeze’ from Platon. X-ray reflections for mesylate salt and cytosine salt cocrystal were collected on an Oxford Xcalibur Gemini Eos CCD diffractometer using Cu-K α radiation ($\lambda = 1.5418 \text{ \AA}$). Data reduction was performed using CrysAlisPro (version 1.171.33.55) and OLEX2-1.0 was used to solve and refine the structure. All non-hydrogen atoms were refined anisotropically. Hydrogen atoms on heteroatoms were located from difference electron density maps and all C–H hydrogens were fixed geometrically. The final CIF files and hydrogen bond geometries were validated in PLATON. X-Seed was used to prepare packing diagrams.

Powder X-ray Diffraction: PXRD were recorded on Bruker D8 Advance diffractometer using Cu-K α X-radiation ($\lambda = 1.5406 \text{ \AA}$) at 40 kV and 30 mA. Diffraction patterns were collected over 2θ range of $5\text{--}50^\circ$ at scan rate of 1° min^{-1} . Powder cell 2.4 was used to plot the diffraction patterns.

Thermal analysis: DSC was performed on a Mettler Toledo DSC 1 module calibrated with indium ($T_m = 156.60^\circ\text{C}$; $\Delta H_f = 28.45 \text{ J g}^{-1}$) and zinc ($T_m = 419.50^\circ\text{C}$; $\Delta H_f = 107.50 \text{ J g}^{-1}$) as per the manufacturer’s specifications. TGA was performed on a Mettler Toledo TGA/SDTA 851e module calibrated with indium ($T_m = 156.60^\circ\text{C}$) and aluminium ($T_m = 660.30^\circ\text{C}$). The typical sample size is 3–5 mg for DSC and 8–10 mg for TGA. The temperature range used in both DSC and TGA is $30\text{--}250^\circ\text{C}$ at 5°C min^{-1} . Samples were placed in crimped but vented aluminium pans for DSC and open alumina pans for TGA and were purged by a stream of dry nitrogen flowing at 50 mL min^{-1} .

7.6 References

1. (a) Para-aminosalicylic acid monograph, *Tuberculosis*, 2008, **88**, 137; (b) M. -T. Gutierrez-Lugo and C. A. Bewley, *J. Med. Chem.*, 2008, **51**, 2606.
2. WHO model list of Essential Medicines is available at http://www.who.int/selection_medicines/committees/expert/17/sixteenth_adult_list_en.pdf.
3. L. J. D. O’Donnell, A. S. Arvind, P. Hoang, D. Cameron, I. C. Talbot, D. P. Jewell, J. E. Lennard-Jones and M. J. G. Farthing, *Gut*, 1992, **33**, 947.
4. S. Schreiber, S. Howaldt and A. Raedler, *Gut*, 1993, **34**, 1081.

5. W. J. Sandborn, B. G. Feagan and G. R. Lichtenstein, *Aliment. Pharmacol. Ther.*, 2007, **26**, 987.
6. Cambridge Structural Database, ver. 5.33, ConQuest 1.14, November 2011 release, May 2012 update; www.ccdc.cam.ac.uk.
7. R. F. Rekker and W. TH. Nauta, *J. Med. Pharm. Chem.*, 1960, **2**, 281.
8. (a) M. Wesalowski, *Ther. Acta*, 1977, **21**, 243; (b) M. K. Rotich, B. D. Glass and M. E. Brown, *J. Ther. Anal. Calor.*, 2001, **64**, 681.
9. P. Grobelny, A. Mukherjee and G. R. Desiraju, *CrystEngComm*, 2011, **13**, 4358.
10. M. R. Caira, *J. Cryst. Spec. Res.*, 1992, **22**, 193.
11. A. P. Centolella, *US Pat.*, 2844625, 1958.
12. R. T. Forbes, P. York and J. R. Davidson, *Int. J. Pharm.*, 1995, **126**, 199.
13. (a) D. Braga, L. Maini, G. de Sanctis, K. Rubini, F. Grepioni, M. R. Chierotti and R. Gobetto, *Chem.–Eur. J.*, 2003, **9**, 5538; (b) B. Sarma, N. K. Nath, B. R. Bhogala and A. Nangia, *Cryst. Growth Des.*, 2009, **9**, 1546; (c) S. N. Black, E. A. Collier, R. J. Davey and R. J. Roberts, *J. Pharm. Sci.*, 2007, **96**, 1053.
14. V. André, D. Braga, F. Grepioni and M. T. Duarte, *Cryst. Growth Des.*, 2009, **9**, 5108.
15. V. André, M. T. Duarte, D. Braga and F. Grepioni, *Cryst. Growth Des.*, 2012, **12**, 3082.
16. Y. Qiu; Y. Chen and G. G. Z. Zhang, Eds., *Developing Solid Oral Dosage Forms. Pharmaceutical Theory and Practice*, Academic Press, New York, 2009.
The word ‘adduct’ encompasses all multi-component systems whether ionic (salt), molecular (cocrystal) or ionic/molecular (salt cocrystal, salt solvate, cocrystal solvate etc.) in nature.
17. (a) S. L. Childs, G. P. Stahly and A. Park, *Mol. Pharmaceutics*, 2007, **4**, 323; (b) *Handbook of Pharmaceutical Salts, Properties, Selection and Use*, ed. P. H. Stahl and C. G. Wermuth, Wiley-VCH, 2002; (c) B. R. Bhogala, S. Basavoju and A. Nangia, *CrystEngComm*, 2005, **7**, 551.
18. N. K. Nath, S. S. Kumar and A. Nangia, *Cryst. Growth Des.*, 2011, **11**, 4594.
19. (a) N. K. Nath, H. Aggarwal and A. Nangia, *Cryst. Growth Des.*, 2011, **11**, 967; (b) B. Sarma, S. Roy and A. Nangia, *Chem. Commun.*, 2006, 4918; (c) R. A. E. Castro, T. M. R. Maria, A. O. L. Évora, J. C. Feiteira, M. R. Silva, A. M. Beja, J. Canotilho and M. E. S. Eusébio, *Cryst. Growth Des.*, 2010, **10**, 274; (d) J. L. Atwood, L. J. Barbour, A. Jerga and B. L. Schottel, *Science*, 2002, **298**, 1000.

20. B. P. van Eijck and J. Kroon, *Acta Crystallogr.*, 2000, **B56**, 535.
21. (a) M. C. Etter, J. C. MacDonald and J. Bernstein, *Acta Crystallogr.*, 1990, **B46**, 256. (b) J. Bernstein, R. E. Davis, L. Shimoni, N.-L. Chang, *Angew. Chem., Int. Ed.*, 1995, **34**, 1555.
22. B. Sridhar, J. B. Nanubolu and K. Ravikumar, *CrystEngComm*, 2012, DOI: 10.1039/C2CE26076J.
23. (a) A. Dilor, T. Friščić and W. Jones, *CrystEngComm*, 2012, **14**, 2350; (b) A. V. Trask and W. Jones, *Top. Curr. Chem.*, 2005, **254**, 41; (c) N. Shan, F. Toda and W. Jones, *Chem. Commun.*, 2002, 2372.
24. V. Verdolino, R. Cammi, B. H. Munk and H. B. Schlegel, *J. Phys. Chem. B*, 2008, **112**, 16860.
25. M. R. L. Stratford, M. F. Dennis, P. Hoskin, H. Phillips, R. J. Hodgkiss and A. Rojas, *Brit. J. Can.*, 1996, **74**, 16.
26. Polymorphs, Salts, and Cocrystals: What's in a Name?, *Cryst. Growth Des.*, 2012, **12**, 2147.

CHAPTER EIGHT

CONCLUSIONS AND FUTURE PROSPECTS

The nature and properties of pharmaceutical solids are central to advances in pharmaceutical chemistry. Optimization of the solid drug formulation is crucial not only in drug research and development but also for oral administration and usage. An understanding of the phenomena that govern the physico-chemical behavior of pharmaceutical solids will lead to better medicines and aid ‘pharmaceutical form development’ and ‘intellectual property management’, and also avoid pit-falls in drug commercialization.

Several aspects of the solid state such as polymorphism, amorphous forms, salts, cocrystals and solid solutions/eutectics were studied in relation to pharmaceuticals. New definitions are proposed for multi-component systems to correlate cocrystals with eutectics. The factors that influence the formation of cocrystals and eutectics were explored and their utility as novel pharmaceutical solids was investigated.

The eutectic microstructure is poorly understood in organic materials and the current challenge is to analyze the organic eutectic materials in detail and assess their domain structure as established for inorganic materials. Polymorphism of solid solutions/eutectics will be a new topic for further explorations. On the other hand, with the exception of melting point, eutectics cannot be characterized by routine analytical techniques of diffraction and spectroscopy used for multi-component crystalline solids (salts, cocrystals, complexes etc). Thus, new techniques for the characterization of eutectics need to be developed e.g. atomic pair distribution function (PDF) analysis.

An API can give rise to a multitude of crystal forms upon solid form screening viz. polymorphs of the API itself; salts, hydrates/solvates, cocrystals and their polymorphs, solid solutions and eutectics. The inherent differences among these

crystalline forms, by virtue of their uniqueness, result in their varied physico-chemical properties which in essence is important for optimal solid form selection and development. Thus, each of these solid forms can be advantageous for specific and desirable applications in different systems. Extensive studies on various solid forms such as polymorphs, salts, ionic liquids, cocrystals and eutectics of several APIs were carried out with the intent of understanding and solving the problems associated with these APIs.

In chapter 2, the importance of establishing the relative stability of drug polymorphs in the real world conditions is discussed through the anti-TB drug Pyrazinamide. A control over polymorph crystallization was achieved through seeding, grinding and solvent-mediated processes. In chapter 3, salt screening of another anti-TB drug Ethambutol resulted in both high melting and low melting (ionic liquid) salts. The first case of polymorphism in an API ionic liquid Ethambutol dibenzoate which will alert the pharmaceutical community about polymorphism issues in ionic liquids is discussed. Thus, a study on polymorphism in both single and multi-component APIs is covered in chapters 2 and 3.

In chapter 4, the advantage of cocrystals over a salt form was studied in the case of anti-bacterial drug Nitrofurantoin (NF). The first of its kind study of additive/coformer effect of *p*-aminobenzoic acid (PABA) in controlling the hydration tendency of Nitrofurantoin through their cocrystal formation was carried out. NF–PABA combination can be useful as a novel/alternate formulation that can control hydration and dissolution and consequently the absorption rate of the drug.

The first examples of drug cocrystals forming eutectics and the importance of cocrystals and eutectics in modulating the solubility/dissolution of two anti-TB drugs Pyrazinamide and Isoniazid are discussed in chapter 5. Mechano-chemical grinding technique resulted in the formation of both cocrystals and eutectics respectively. The pharmaceutical formulation scope of the anti-TB drugs Pyrazinamide, Isoniazid and Ethambutol is broadened to cocrystals, eutectics and ionic liquids.

In chapter 6, in an analogy to cocrystals, the structure-property relationship in eutectics was studied with respect to (i) design aspect for eutectics or deliberate formation of eutectics, (ii) translating properties of a material to its eutectic and (iii)

stability advantage of eutectics, and results were favorable. This first of its kind study resulted in eutectics of the anti-TB drug Ethambutol dihydrochloride in the expected lines and the novel eutectics were found to control the hygroscopicity of the drug. Study on the effect of these eutectics in stabilizing the anti-TB FDC formulation of Rifampicin, Isoniazid and Pyrazinamide in accelerated stability testing conditions is ongoing.

In chapter 7, solid form screening of anti-TB drug 4-aminosalicylic acid resulted in various adducts such as salt, salt cocrystal, cocrystal, complex etc. and their crystal structures were determined. Since 4-aminosalicylic acid is found to partially decompose (to 3-aminophenol) in the pH range 1.3-4.2, a study on the effect of these adducts in controlling its decomposition can lead to a better formulation of the drug.

To conclude, physico-chemical properties of some important drugs were improved by new solid form modifications.

ABOUT THE AUTHOR

Cherukuvada Suryanarayan, eldest son of Mr. C. Mahajan and Mrs. C. Ramalakshmi, was born in 1980 at Kakinada, East Godavari District, Andhra Pradesh, India. He received primary education at Holy Cross Primary School, Hyderabad, and studied secondary education (VI to IX Std.) in Mansas High School, Vizianagaram. He obtained SSC from Nava Bharat Public High School, Kakinada, and completed Intermediate (Bi. P. C.) at Ideal Junior College, Kakinada. He pursued B. Sc. (B. Z. C.) in P. R. Govt. Degree College, Kakinada, affiliated to Andhra University. After obtaining M. Sc. (Biochemistry) from T. J. P. S. College, Guntur, affiliated to Acharya Nagarjuna University, he studied B. Ed. (Biological Sciences & English) at Gandhi Centenary College, Kakinada, affiliated to Andhra University. In 2007, he was awarded 'Junior Research Fellowship' (JRF) by Indian Council of Medical Research (ICMR), New Delhi, upon qualifying ICMR-JRF National Entrance Examination. He, then, joined Prof. Ashwini Nangia's Research Group, School of Chemistry, University of Hyderabad, as a PhD Student and was upgraded as a 'Senior Research Fellow' (SRF) in 2009.

LIST OF PUBLICATIONS

1. N–H . .N(pyridyl) and N–H . .O(urea) hydrogen bonding and molecular conformation of N-aryl-N'-pyridylureas.

Sreekanth K. Chandran, Naba K. Nath, **Suryanarayan Cherukuvada** and Ashwini Nangia

J. Mol. Struct., 2010, **968**, 99–107.

2. Conformational and Synthron Polymorphism in Furosemide (Lasix).

N. Jagadeesh Babu, **Suryanarayan Cherukuvada**, Ranjit Thakuria and Ashwini Nangia

Cryst. Growth Des., 2010, **10**, 1979–1989.

3. Pyrazinamide Polymorphs: Relative Stability and Vibrational Spectroscopy.

Suryanarayan Cherukuvada, Ranjit Thakuria and Ashwini Nangia

Cryst. Growth Des., 2010, **10**, 3931–3941.

4. Nitrofurantoin–*p*-Aminobenzoic Acid Cocrystal: Hydration Stability and Dissolution Rate Studies.

Suryanarayan Cherukuvada, N. Jagadeesh Babu and Ashwini Nangia

J. Pharm. Sci., 2011, **100**, 3233–3244.

5. Blonanserine HCl salt and its monohydrate.

D. Maddileti, Ranjit Thakuria, **Suryanarayan Cherukuvada** and Ashwini Nangia

CrystEngComm, 2012, **14**, 2367–2372.

6. Fast dissolving eutectic compositions of two anti-tubercular drugs.

Suryanarayan Cherukuvada and Ashwini Nangia

CrystEngComm, 2012, **14**, 2579–2588.

7. Crystal Structures of Pyrogallol, Its Hydrate, and Stable Multiple *Z'* Cocrystals with N-Heterocycles Containing Metastable Conformers of Pyrogallol.

Ranjit Thakuria, **Suryanarayan Cherukuvada** and Ashwini Nangia

Cryst. Growth Des., 2012, **12**, 3944–3953.

8. Polymorphism in an API ionic liquid: ethambutol dibenzoate trimorphs.

Suryanarayan Cherukuvada and Ashwini Nangia

CrystEngComm, 2012, DOI: 10.1039/c2ce25842k.

9. Crystal Structures of Pyridine Sulfonamides and Sulfonic Acids.

Kalyanachakravarthi Akiri, **Suryanarayan Cherukuvada**, Soumendra Rana and Ashwini Nangia

Cryst. Growth Des., 2012, DOI: 10.1021/cg3007603.

10. Salts and Ionic Liquids of Ethambutol.

Suryanarayan Cherukuvada and Ashwini Nangia (Manuscript under preparation)

11. Hygroscopic Stable Eutectics of Ethambutol Dihydrochloride.

Suryanarayan Cherukuvada and Ashwini Nangia (Manuscript under preparation)

12. Variable Stoichiometry Adducts of 4-Aminosalicylic Acid.

Suryanarayan Cherukuvada, Geetha Bolla, Kanishka Sikhligar and Ashwini Nangia
(Manuscript under preparation)

PARTICIPATION IN SYMPOSIA & CONFERENCES

1. Participated in the **Indo-US Bilateral Workshop on Pharmaceutical Cocrystals and Polymorphs** held at Hotel Regaalis, Mysore, India, during February 8-11, 2009.
2. Participated in the **38th National Seminar on Crystallography** held at University of Mysore, Mysore, India, during February 11-13, 2009.
3. Participated in **MEDCHEM 2009 – Conference cum Workshop on Current Trends in Medicinal Chemistry** held at IIT Madras, Chennai, during April 2-4, 2009.
4. Presented a poster entitled “**Nitrofurantoin-*p*-Aminobenzoic Acid Cocrystal: Hydration Stability and Dissolution Rate Studies**” at the **International Symposium on Facets of Weak Interactions in Chemistry** held at University of Calcutta, Kolkata, India, during January 13-15, 2011.
5. Presented a poster entitled “**Nitrofurantoin-*p*-Aminobenzoic Acid Cocrystal. Hydration stability and Dissolution Rate Studies**” at the **6th Junior National Organic Symposium Trust (J-NOST) Conference** held at University of Hyderabad, Hyderabad, India, during January 28-31, 2011.
6. Delivered an oral presentation entitled “**A Novel Ternary Cocrystal involving Two Antitubercular Drugs**” at the **Chemfest 2011** held at University of Hyderabad, Hyderabad, India, during February 25-26, 2011.
7. Presented a poster entitled “**A Novel Ternary Complex involving Two Antitubercular Drugs**” at the **International Conference on the Chemistry of Organic Solid state (ICCOSS) XX** held at Indian Institute of Science, Bengaluru, India, during June 26-30, 2011.
8. Presented a poster entitled “**A Novel Ternary Eutectic involving Two Antitubercular Drugs**” at the **XXII International Union of Crystallography Congress and General Assembly** held in Madrid, Spain, during August 22-30, 2011. Published as **Suryanarayan Cherukuvada** and **Ashwini Nangia**, *Acta Cryst.*, 2011, **A67**, C565.